

Electroactive Polymers for Corrosion Control

September 2, 2012 | <http://pubs.acs.org>
Publication Date: February 28, 2003 | doi: 10.1021/bk-2003-0843.fw001

ACS SYMPOSIUM SERIES **843**

Electroactive Polymers for Corrosion Control

Peter Zarras, Editor
Department of the Navy

John D. Stenger-Smith, Editor
Department of the Navy

Yen Wei, Editor
Drexel University



American Chemical Society, Washington, DC

In *Electroactive Polymers for Corrosion Control*; Zarras, P., et al.;
ACS Symposium Series; American Chemical Society: Washington, DC, 2003.



Library of Congress Cataloging-in-Publication Data

Electroactive polymers for corrosion control / Peter Zarras, editor, John D. Stenger-Smith, editor, Yen Wei, editor.

p. cm.—(ACS symposium series ; 843)

Includes bibliographical references and index.

ISBN 0-8412-3790-5

1. Conducting polymers—Congresses. 2. Corrosion and anti-corrosives—Congresses.

I. Zarras, Peter, 1961- II. Stenger-Smith, John D., 1961- III. Wei, Yen, 1957- IV. Series.

TA455.P58 .E395 2003

620.1'1223—dc21

2002035848

The paper used in this publication meets the minimum requirements of American National Standard for Information Sciences—Permanence of Paper for Printed Library Materials, ANSI Z39.48-1984.

Copyright © 2003 American Chemical Society

Distributed by Oxford University Press

All Rights Reserved. Reprographic copying beyond that permitted by Sections 107 or 108 of the U.S. Copyright Act is allowed for internal use only, provided that a per-chapter fee of \$24.75 plus \$0.75 per page is paid to the Copyright Clearance Center, Inc., 222 Rosewood Drive, Danvers, MA 01923, USA. Republication or reproduction for sale of pages in this book is permitted only under license from ACS. Direct these and other permission requests to ACS Copyright Office, Publications Division, 1155 16th St., N.W., Washington, DC 20036.

The citation of trade names and/or names of manufacturers in this publication is not to be construed as an endorsement or as approval by ACS of the commercial products or services referenced herein; nor should the mere reference herein to any drawing, specification, chemical process, or other data be regarded as a license or as a conveyance of any right or permission to the holder, reader, or any other person or corporation, to manufacture, reproduce, use, or sell any patented invention or copyrighted work that may in any way be related thereto. Registered names, trademarks, etc., used in this publication, even without specific indication thereof, are not to be considered unprotected by law.

TA 455 .P58E395 2003 c. 1

PRINTED IN THE

Electroactive polymers for
corrosion control

American Chemical Society
Library
1155 16th St.
Washington, DC 20036

Foreword

The ACS Symposium Series was first published in 1974 to provide a mechanism for publishing symposia quickly in book form. The purpose of the series is to publish timely, comprehensive books developed from ACS sponsored symposia based on current scientific research. Occasionally, books are developed from symposia sponsored by other organizations when the topic is of keen interest to the chemistry audience.

Before agreeing to publish a book, the proposed table of contents is reviewed for appropriate and comprehensive coverage and for interest to the audience. Some papers may be excluded to better focus the book; others may be added to provide comprehensiveness. When appropriate, overview or introductory chapters are added. Drafts of chapters are peer-reviewed prior to final acceptance or rejection, and manuscripts are prepared in camera-ready format.

As a rule, only original research papers and original review papers are included in the volumes. Verbatim reproductions of previously published papers are not accepted.

ACS Books Department

Preface

*Science is people,
—And a stimulating intellectual environment,
—And research money.
—We are entering the highly technologically focused 21st Century!
—What are we doing about it?*

The above thoughts jumped to my mind when I accepted the invitation from the editors to write a preface to this book on electroactive polymers for corrosion control—an important emerging technology derived from basic research on conducting polymers, also known as synthetic metals. The basic scientific research of today is the technology of tomorrow, upon which the material standard of living of our children and grandchildren will be based—bearing in mind at all times that the overall quality of life is not necessarily directly related to our standard of living as judged by our food, clothing, shelter, education, or even life expectancy—but advanced technology is certainly a most important parameter to be considered in our planning not only for the future, but for controllably shaping the future.

The enormous interdependency of today's science and tomorrow's technology (in every country of the world) on the policy of individual funding agencies or broad company policy is usually recognized and is taken as a self-obvious "truism," but what is not generally recognized is the critical importance of the implementation of that policy by individuals—the people who sit at an office desk and decide which specific research or possible R&D proposals will be funded, or to which referees a given proposal will be sent for evaluation, or who will select a panel or committee that will decide on the funding of a specific proposal. At a British Broadcasting Company television program produced during the Nobel week ceremonies in December 2000, in Stockholm, Sweden, in which all thirteen Nobel Laureates of 2000 were present, it was noteworthy that it was generally agreed by most that

much of what each Laureate considered to be some of his/her chief scientific contributions came from “moonlighting” (i.e., strictly “illegal” research, funded from a grant or contract not specifically directed to that topic)!

Dr. Kenneth J. Wynne, formerly of the U.S. Office of Naval Research, is an excellent example of such a person who shapes our technological futures! He was the first person worldwide to fund research 25 years ago in the now well established field of electronic “conducting” polymers. It takes an especially foolish or far-sighted project officer to fund a proposal to study a polymer, polyacetylene, $(CH)_x$, primarily because I, an organometallic chemist, had never seen a silvery polymer before! The very modest initial funding was primarily to provide the postdoctoral salary of Hideki Shirakawa, the polymer chemist who discovered (by accident!) this silvery form of polyacetylene. This funding was later extended by the Office of Naval Research and other funding agencies to promote collaborative studies—preliminary studies of Hideki Shirakawa, Alan Heeger (an experimental physicist at Penn) and myself on polyacetylene. This collaborative research on which the Nobel Prize in chemistry was jointly awarded to the three of us is often used as a classical example of the importance of interdisciplinary research in recent decades. It is universally recognized today that interdisciplinary research will play an increasingly important role in future scientific–technological developments.

The very existence of this book on *Electroactive Polymers for Corrosion Control* stems initially from:

1. The collaborative research of the three of us,
2. The decision by Ken Wynne to take the epic-making step to fund the initial work in the field of electroactive polymers (although undoubtedly some person on some future occasion would have decided to fund research in this area),
3. The countless thousands of dedicated scientists worldwide who put the flesh on our skeletal studies of 25 years ago—without whose blood, sweat, and tears (with the input of appropriate far-sighted funding agency–company personnel) the field could never have developed to what it is today.

The corrosion of iron and its alloys results in a loss of billions of dollars each year. This staggering amount is increased even more when the corrosion of other metals is included. Corrosion under common

environmental conditions results from the reaction of air and/or water alone, or in combination with substances suspended in air or water, or with gases present in air, such as sulfur dioxide or carbon dioxide, etc., or substances dissolved in water, such as sodium chloride, etc., as in seawater.

Prevention of or reduction in the rate of corrosion may be accomplished by mechanical methods such as use of a “passive” film or common paint as barrier coatings to prevent contact of the metal with its corrosive surroundings and/or by electrochemical methods. The use of a passive film is well exemplified by aluminum metal. Aluminum is so electropositive that, thermodynamically, it might at first sight be surprising that we have aluminum pots and pans in the kitchen! The *kinetic* stability of aluminum objects to corrosion in air is due to the fact that aluminum metal is coated with a very thin film of aluminum oxide, which serves as an excellent mechanical barrier to prevent air–water from reaching the aluminum surface. Removal of the film by scratching results in the immediate re-formation of a new protective layer of aluminum oxide by the instantaneous reaction of the newly exposed aluminum surface to air. This is well-illustrated by the well-known freshman chemistry experiment in which aluminum foil is wetted with a solution of mercuric chloride, which immediately reacts to produce aluminum chloride and mercury, the mercury immediately forming an amalgam with the aluminum surface, preventing the formation of the mechanically protective aluminum oxide “skin.” Copious quantities of fluffy aluminum oxide powder are formed immediately and the aluminum foil becomes hot to the touch due to the very rapid reaction of the exposed aluminum metal with air.

“Galvanized iron,” steel coated with a thin layer of zinc metal, serves as a good, common example of a sacrificial, non-passive coating, the zinc being corroded preferentially to the iron. It is more electropositive than the iron, loses its electrons more readily, and hence is more readily oxidized, “corroded.” However, if some of the zinc is removed, as by a scratch, to expose the iron surface beneath it, the exposed iron does not corrode, instead the zinc is corroded. The zinc (and its electrons), which is more electropositive than iron, is in electrical contact (i.e., is in electronic equilibrium with the iron and its electrons). When electrons are lost from this equilibrium system, to react with oxygen, etc., the source of the electrons is the more electropositive zinc (i.e., the zinc loses its electrons) “corrodes” in preference to the iron.

An obvious electrochemical method for reducing the rate of corrosion of a metal can be seen by the anodic protection of steel. The

metal is connected to the positive terminal of a low voltage DC power supply. At first sight, this may appear strange because the removal of electrons from the iron by the anode promotes conversion of iron to its positive ions (i.e., would appear to increase the rate of corrosion). However, the iron cations rapidly react with nearby anions, oxygen, carbon dioxide, etc. (promoted by electrons from the cathode) to form a thin mechanically sound layer of iron oxides, hydroxides, and the like, which mechanically inhibits passage of further corrosive materials to the surface of the iron. In some ways the phenomenon is somewhat similar to the protection of aluminum metal by the thin layer of aluminum oxide described above.

The conducting polymer, polyaniline (*1*) as can be seen from the contents of this volume, has attracted, together with the many other interesting and important materials, considerable attention in its ability to reduce the rate of corrosion of iron under certain conditions. According to one concept, in addition to acting as a “passive paint,” it can offer anodic protection when in electrical contact with certain iron alloys (*2*). The polyaniline, in an appropriate oxidation state, when in contact with steel of an appropriate redox potential, attracts electrons away from the iron (*2,3*). It acts somewhat similarly to the anodic protection of iron described above and probably results in the formation of a mechanically sound barrier of iron oxides, etc., which reduces access of the corrosive environment to the steel surface. The polyaniline is reduced by this process but, it is exposed to air, it is spontaneously re-oxidized (regenerated) by the air (*1–3*). Because polyaniline is an electronic conductor, a whole unitary piece must have the same oxidation state throughout at equilibrium (i.e., that portion which is exposed to the air re-oxidizes the portion not exposed to the air). If, for example, part of a polyaniline film coating steel is removed as by a scratch, the rate of corrosion of the exposed iron surface is reduced (*2*). The polyaniline, in effect, acts as a “catalyst” for initially increasing the rate of reaction of the iron with its corrosive environment to form the protective iron oxide, etc., film. In the case of reaction of aluminum with air, no such “catalyst” is, of course, necessary.

Frequently, there appears to be some confusion as to what given species the term “polyaniline” refers. Polyaniline can be synthesized in its base form in three different, discrete oxidation states: leucoemeraldine base (completely reduced form); pernigraniline base (completely oxidized form); and emeraldine base (partly oxidized, less reduced form intermediate between the two extreme oxidation states) (*1*). It can also be

isolated in forms of varying degrees of oxidation intermediate between the leucoemeraldine and emeraldine or between the emeraldine and pernigraniline oxidation states. All the above forms have a low conductivity in the semiconductor–insulator range (1).

We have recently pointed out that *there are as many different types of polyaniline as there are people who synthesize it* (4). In many studies involving polyaniline, it appears that investigators believed a polyaniline was in its emeraldine oxidation state; however, it is not generally recognized that unless sufficient time is used for its synthesis (5) (or the synthesis of its derivatives (6)) by the chemical oxidation of the monomer that the polymer may be in an oxidation state considerably higher than that of the presumed emeraldine oxidation state. To complicate matters even further, the composition, conductivity and redox potential of oxidation states close to that of the emeraldine oxidation state is changed greatly by the pH of the environment (1). Hence, when polyaniline is used in corrosion prevention, it is extremely important to know the pH of the environment to which polyaniline is exposed because this will significantly affect the conductivity, redox potential, and electrochemical properties of the polyaniline.

Furthermore, experimental evidence suggests that polyaniline in its emeraldine oxidation state is a “dynamic block copolymer” and that the nature of solid polyaniline in its emeraldine oxidation state can depend critically on how the solid polymer is formed from solution (7). It is important to note that the effectiveness and mechanism of an oligomer of a substance in the inhibition of corrosion of metals may be significantly different from that of the polymer of the same substance due to the well-recognized difference in redox potentials, which may exist between an oligomer of a given molecular weight and the polymers. The same argument also applies to differences in redox potential caused by chemical modification of a material in its derivatives. Both the oligomeric and derivative approaches could lead to new technologies on the basis of the established fundamental concepts of conducting polymers.

The discovery that organic polymers have specific, characteristic electrochemical properties presents new opportunities of exploration in many different areas. Electroactive polymers (“synthetic metals,” “conducting polymers”), as can be seen by the many elegant studies presented in this book, offer a new approach to the study of inhibition of corrosion of metals.

References

1. MacDiarmid, A.G. *Angew. Chem. Int. Ed.* **2001**, *40*, 2581.
2. Ahmad, N.; MacDiarmid, A.G. *Synth. Met.* **1996**, *78*, 103.
3. MacDiarmid, A.G.; Zheng, W. *Mater. Res. Soc. Bulletin* **1997**, *22(6)*, 24.
4. MacDiarmid, A.G.; Jones, Jr., W.E.; Norris, I.D.; Gao, J.; Johnson, Jr., A.T.; Pinto, N.J.; Hone, J.; Han, B.; Ko, F.; Okuzaki, H.; Llangune, M. *Synth. Met.* **2001**, *119*, 27.
5. Manohar, S.K.; MacDiarmid, A.G.; Epstein, A.J. *Synth. Met.* **1991**, *41-43*, 711.
6. Mattoso, L.H.C.; MacDiarmid, A.G.; Epstein, A.J. *J. Polym. Sci.: Part A: Polym. Chem.* **1995**, *33*, 1227.
7. Shimano, J.Y.; MacDiarmid, A.G. *Synth. Met.* **2001**, *123(2)*, 251.

Alan G. MacDiarmid

Blanchard Professor of Chemistry
Department of Chemistry
University of Pennsylvania
231 South 34th Street
Philadelphia, PA 19104

Chapter 1

An Introduction to Corrosion Protection Using Electroactive Polymers

P. Zarras and J. D. Stenger-Smith

Naval Air Warfare Center Weapons Division, Department of the Navy,
Code 4T4220D, 1 Administration Circle, China Lake, CA 93555

An introduction to the chemistry and corrosion properties of electroactive polymers (EAPs) will be presented. This chapter will focus on both the synthesis of several classes of EAPs and the processes by which the insulating form is converted to the conducting form. The book chapter will present a compelling argument for the use of EAPs as corrosion protecting materials for metals in both acidic and alkaline aqueous environments. The corrosion inhibiting properties of EAPs and the proposed mechanisms by which EAPs perform will also be discussed.

Introduction

Polymers were originally thought of as electrical insulators, not electrical conductors. However, in the early 1960s Pohl, Katon and others synthesized and characterized polymers (some conjugated) with conductivities in the semiconductor range (1-4). Ultimately, the belief that polymers are all poor conductors was shattered by the discovery that iodine-doped polyacetylene exhibited electrical conductivity many orders of magnitude higher than neutral polyacetylene. This discovery was made in 1976 by Hideki Shirakawa, Alan MacDiarmid and Alan Heeger; they received the 2000 Nobel Prize in Chemistry for their work (5,6). The discovery of electrically conducting polymers triggered the development of a new multidisciplinary field known as "synthetic metals" (7). Since this early pioneering work of Shirakawa, MacDiarmid and Heeger, numerous additional developments and discoveries in conductive polymers have occurred. As a result, the field of polymeric electronics and photonics has

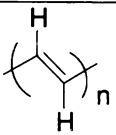
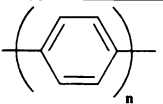
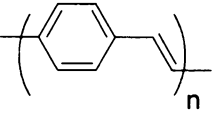
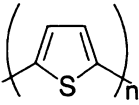
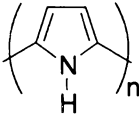
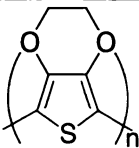
matured to offer the promise of a wide range of novel applications exploiting the unique chemical, physical, and electrical properties of conductive polymers.

Electroactive polymers (EAPs) are composed of conjugated chains containing π -electrons delocalized along the polymer backbone. In their neutral form, EAPs are semiconductive polymers that can be doped and converted into electrically conductive forms. The doping process can occur either by oxidative or reductive reactions, though oxidative reactions are more common. The conductivity is electronic in nature and does not involve concurrent ion migration in the solid polymer form. Some doping processes are reversible, with typical conductivities switching between those of insulators ($<10^{-10}$ S/cm) to those of metals (10^5 S/cm) (8).

Electroactive polymers comprise a broad range of materials which are characterized by conjugated repeat units (9). This conjugation is responsible for the unique electronic and optical properties of EAPs ranging from low oxidation potential to third order optical nonlinear properties. Researchers have exploited these unique materials to synthesize a variety of EAPs. These polymers exhibit a broad range of conductivities (10^{-4} to 10^3 S/cm) in their doped (oxidized) states. Most EAPs fall under the following classes: polyacetylenes, poly(*p*-phenylene)s, polyheterocycles, poly(phenylene vinylene)s, polyanilines and conjugated ladder polymers (Table 1). EAPs can be synthesized both chemically and electrochemically. There are three conducting states of EAPs: neutral (uncharged), where EAPs are insulators or semiconductors; oxidized (*p*-doped) where electrons are removed from the backbone, and the reduced (*n*-doped) (least common), where electrons are added to the backbone of the neutral polymer. The ability to control the level of conductivity in polymers has given researchers the tools to tailor properties to specific needs and devices. EAPs have potential applications in such diverse areas as actuators (10), supercapacitors/batteries (11), molecular electronics (12), electrochromic windows/displays (13), transistors (14), photovoltaics (15), bio/chemical sensors (16) and corrosion protection (17).

Corrosion protection using electroactive polymers was first suggested by MacDiarmid in 1985 (18). The usefulness of EAPs rests on the ability of researchers to tailor properties for specific applications. This process has been applied to EAPs extensively to allow the use of these materials for anti-corrosion coatings. It has been observed that most EAPs can be electrochemically produced by anodic oxidation (19), enabling one to obtain a conducting film directly on a surface. This fact has led researchers into the field of anti-corrosives (20). EAPs can go from the insulating to the conducting state through several doping techniques such as (1) chemical doping by charge transfer, (2) electrochemical doping, (3) doping of PANI by acid-base chemistry, (4) photodoping and (5) charge injection at a metal-semiconducting polymer interface. The doping techniques used influences the potential application of the EAPs. This paper will review the chemical, electrochemical and acid-base chemistry doping of PANI and other EAPs.

Table 1: Structures of EAPs and Conductivities (8)

Polymer	Structure	Conductivity [Doped form] (S/cm)
Polyacetylene (PA)		10^3-10^5
Poly(<i>para</i> -phenylene) (PPP)		10^2-10^3
Poly(<i>para</i> -phenylene vinylene) (PPV)		10^3-10^4
Poly(thiophene) (PT)		10^2
Poly(pyrrole) PPy		10^2-10^3
Poly(3,4-ethylenedioxythiophene) PEDOT		10^2

Synthesis of EAPs

In order to understand the chemistry of EAPs used in corrosion protection it is necessary to start with the synthesis of EAPs. There are currently several classes of EAPs which can exhibit conductivities (in the doped state) ranging from those of semiconductors to those of metals. These EAPs comprise the polyacetylenes (PA), poly(*para*-phenylenes) (PPP), polyheterocycles such as polythiophenes (PT), poly(phenylenes vinylenes) (PPV), polyanilines (PANI) and conjugated ladder polymers. Of these, the polyheterocycles, PPVs, and PANIs have been studied for corrosion protection (21), largely because poor stability, processability have limited the use of the other classes of EAPs.

The most widely studied of the EAPs for corrosion protection has been PANI. PANI has several advantages over most current EAPs, including easy chemical and electrochemical polymerization of monomer; doping and dedoping proceeds easily by treatment with standard aqueous acid and base and it is highly resistant to environmental degradation (22). PANI is a quite old material having been prepared in the 19th Century by H. Letheby (23). Clearly, at this time the polymeric nature of PANI was not understood; the material was called "aniline black" and was used in textiles as dyes and in printing. The preparation of PANI is accomplished by oxidation under mild conditions (24). However during the 1960s this material gained interest due to its unusual electrical properties (25). Since the 1980's and 90's this material has been extensively studied (26).

PANI is commonly prepared by polymerization of the aniline monomer using $(\text{NH}_4)_2\text{S}_2\text{O}_8$ in hydrogen chloride solution (27,28). The polymer can also be prepared by electropolymerization of the monomer (29). PANI is a difficult material to process under normal conditions. Several methods now exist for improving the processability and solubility of PANI. These methods include modification of the polymer backbone by introducing various functional groups such as alkoxy, amino, alkyl, aryl and sulfonyl (30), or by using novel acids such as camphor sulfonic acid to obtain a soluble form of the conducting version of PANI (31). The PANI that is produced from both chemical and electrochemical processes can exist in four different oxidation states: leucoemeraldine; pernigraniline, emeraldine base (intermediate form) and emeraldine salt (conductive form) (Figure 1) (32,33).

PANI is prepared as the emeraldine salt (ES) from both chemical and electrochemical polymerization techniques and then treated with base to give the emeraldine base (EB). This form (EB) is soluble in common organic solvents such as N,N-dimethylformamide, N,N-dimethylacetamide and 1-methyl-2-pyrrolidinone. Upon film formation or other casting technique, the emeraldine base can then be treated with acids (sometimes called protonic acid doping) to regenerate the conductive form, the emeraldine salt (Figure 2). The process to increase the electrical conductivity of PANI by protonation and decrease by deprotonation is sometimes referred to as compensation (4).

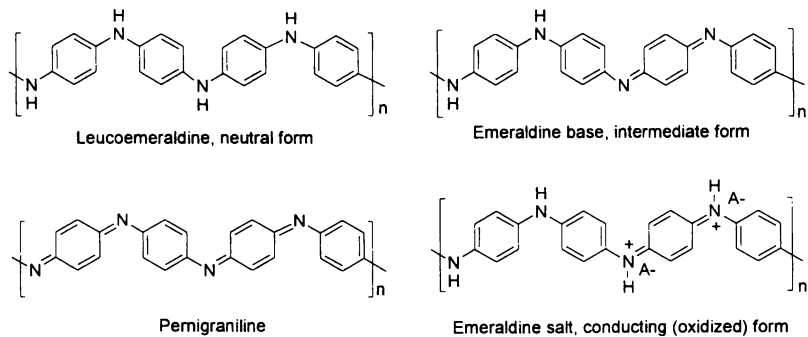


Figure 1: Four Forms of PANI

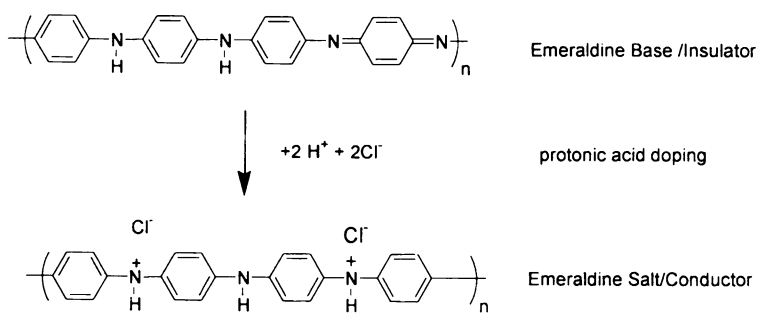
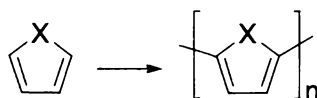


Figure 2. Protonic Acid Doping.

The heterocyclic monomers represented in Figure 3 are a class of monomers that can be polymerized to form fully conjugated polymers (34). The most common of these is pyrrole (X=NH), which has been recently investigated for corrosion protection (35). The thiophenes (X=S) have also been studied extensively for their electronic, electro-optical and corrosion properties; whereas the furans (X=O) have not been studied as well due to their high oxidation potential (>1.7V vs. Ag/Ag+), which results in very poor quality materials (36).



where X = O, NH, S

Figure 3. Heterocyclic structure.

Polypyrrole (PPy) and polythiophene (PT) can be doped to give moderate to high conductivities. They have been polymerized using both chemical and electrochemical methods. The resulting polymers are electron-rich materials that are easily oxidized and are therefore stable in the oxidized form. Polypyrrole and polythiophene have received considerable attention due to their high stabilities and ease of structural modification for improved processability. Both PPy and PT have been investigated for their corrosion properties (37).

Polypyrrole (PPy) was first reported in 1916 (38). Polypyrrole was prepared by the chemical oxidation of pyrrole using hydrogen peroxide and called "pyrrole black." Unmodified PPy and PT are both insoluble in common organic solvents and unprocessable. Chemical polymerization remains the simplest route, but electrochemical polymerization is the most important and versatile method, producing high quality films and high conductivities (10^2 S/cm) (39).

The polymerization of thiophenes includes chemical oxidative couplings of thiophenes (40), cross-coupling of Grignard reagents of dihalothiophenes (41), and electrochemical polymerization (42). PTs obtained from these methods are infusible and unprocessable. In order to improve solubility and processability of PTs, synthetic methods were developed to incorporate functional groups such as n-alkyl groups on the 3-position to improve processability without sacrificing electrical conductivity.

The synthesis of poly(3-alkylthiophene)s (P3ATs) has been accomplished by Kumada cross-coupling (37), and oxidative polymerization (39). Regiospecific synthetic techniques have been developed to obtain regioregular P3ATs (44).

Poly(phenylene vinylene)s (PPV) was first synthesized in 1960 by McDonald and Campbell (45). Efforts at improving the solubility and

processability of PPVs has led to the development of several precursor routes. The most widely used precursor route is that developed by Wessling and Zimmerman (Figure 4) (46,47). This process involves the synthesis of the bis-sulfonium salt of 1,4-bis(chloromethyl)benzene, followed by sodium hydroxide elimination and polymerization at low temperature to give an aqueous solution of a precursor polymer. The soluble precursor polymer can be processed into films, foams or fibers and converted to PPV by thermal elimination. There are several alternative approaches to Wessling and Zimmerman's sulfonium precursor methods, including the Gilch route (48) and Heck polymerization (49). These alternative routes are similar in utility to the Wessling and Zimmerman route. As with PANI and polyheterocycles, PPVs have been modified to improve solubility and processability (34).

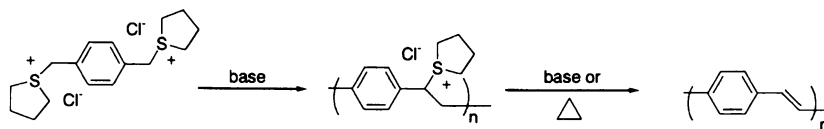


Figure 4. PPV synthesis

Corrosion Processes

Along with a knowledge of the different types of EAPs, their synthesis and doping processes, a fundamental understanding of the corrosion process affecting metals is needed. Corrosion is the destructive result of chemical reactions that occur between a metal or a metal alloy and its environment (50). Corrosion impacts many aspects of our daily lives, and various estimates put the costs to the US economy between 100–300 billion dollars annually (51-54). The most striking features of the corrosion process are the immense variety of conditions under which it occurs and the large number of forms in which it appears (54). Corrosion affects all structural materials and infrastructure of society to cause in many cases grave economic consequences or life-threatening situations. Infrastructure items that can be significantly damaged and eventually destroyed by corrosion include pipelines, bridges, automobiles, storage tanks, airplanes and ships (both military and commercial). All of these structures can be affected by corrosion and have been documented in the press as being the cause of several catastrophic events.

The most common environments for corrosion to occur are in natural waters, atmospheric moisture, rain and man-made solutions (such as storage tanks) (55). The ionic conductivity of an aqueous corrosive environment creates electrochemical reactions (56). These reactions are strongly influenced by the surface potential and acidity or basicity of the environment. These factors allow

electrochemical reactions to take place on a metal surface which is therefore changed from the metallic state to a non-metallic state. The products of corrosion can be dissolved species or solid corrosion products. No matter what the scenario, the energy of the system is lowered as the metal converts to a lower-energy form. The most studied example of this phenomenon is the rusting of iron. The metal (iron) is converted into the corrosion product, the non-metallic form (rust or iron oxides). The difficulty in preventing corrosion from occurring is both a scientific and engineering problem. Corrosion science is the study of the electrochemical processes and metallurgical processes that occur during corrosion in various environments. Corrosion engineering, on the other hand, is the design of methods and materials to prevent corrosion. An understanding of both disciplines is essential to prevent corrosion from affecting infrastructure.

There are generally several forms of corrosion that affect infrastructure. These corrosion forms are classified as (1) uniform or general corrosion, (2) galvanic corrosion, (3) pitting corrosion, (4) environmentally induced cracking, (5) hydrogen damage, (6) intergranular corrosion, (7) dealloying and (8) erosion corrosion (57). There are several corrosion-preventing barriers: anodic oxides, organic coatings, ceramics, inorganic coatings, phosphate and other conversion coatings (58). These coatings provide a barrier that resists penetration by aggressive environmental constituents. The goal of these coatings is to prevent the cathodic reaction ($2 \text{H}_2\text{O} + \text{O}_2 + 4\text{e}^- \rightarrow 4\text{OH}^-$) from taking place beneath the coating.

These coatings work well, but over time the barrier coating can fail due to prolonged exposure to the environment. The organic coatings can develop what is called "under coating corrosion" which initiates from weak spots and develops into blisters and filiform threads leading to corrosion failure (59). The organic protective coating (barrier coating) fails by separation at the coating/ substrate interface (60,61). The separation process is known as *delamination*. In time, delamination results in underfilm corrosion and eventual loss of the barrier properties of the coating. The corrosion-induced delamination occurs as a direct consequence of the electrochemical mechanism of corrosion (56). The anodic (electron generating) and the cathodic (electron-consuming) reactions occur at the sites where delamination has occurred. The kinetic barriers are at a minimum due to the high electrical conductivity of the metal, which provides an easy pathway for electrons between the anodic and cathodic sites.

Metal pretreatments have been used to extend the lifetimes of barrier coatings. These pretreatments are normally composed of phosphates, chromates and oxides, which contain a variety of metal cations. These processes are well established industrially and prolong the lifetimes of barrier coatings through better adhesion of the coatings onto the metal substrate. The pretreatments and primers that are used for corrosion protection--specifically chromate conversion coatings (CCC) and chromate containing primers--have come under increased

scrutiny and regulation from governmental agencies. The hexavalent chromium used in CCC and primers is a known human carcinogen (62) and is highly regulated (63). Alternative approaches are needed to replace barrier coatings that give limited lifetimes for corrosion protection. Ideally the material should not only provide the benefits of barrier coatings but also passivate the metal allowing the corrosion current to shift to the noble metal region (64).

Corrosion Protection with EAPs

Over the past 15 years, published evidence that an EAP, specifically polyaniline could inhibit corrosion has come from Mengoli et al. (65), DeBerry (66), and Ahmand and MacDiarmid (67). These results showed that PANI electrodeposited on passivated steel in a strong acid environment enhanced corrosion protection of the metal (21).

The most extensively studied of the EAPs for corrosion prevention has been PANI (68,69). At the Los Alamos National Laboratory (LANL) and the John F. Kennedy Space Center (KSC), researchers demonstrated that doped PANI coatings inhibited corrosion of carbon steel (70). Their approach was based on earlier work suggesting that the interfacial contact between the metal and a doped EAP would generate an electric field that would restrict the flow of electrons from the metal to an outside oxidizing species, thus preventing and/or reducing corrosion (71). The LANL-KSC tests were conducted in a 3.5wt % NaCl/0.1 M HCl environment using ca. 0.005 cm thick films of PANI doped with *p*-toluenesulfonic acid on carbon steel; the PANI was covered with an epoxy topcoat. The PANI/epoxy coating performed significantly better than the epoxy topcoat alone. These initial results were used by researchers at LANL-KSC to develop EAP coatings to resist the corrosive effects of acid vapor generated during space shuttle launches. The ground support equipment and structures at the KSC were susceptible to the severe environmental conditions. The environment around the launch site consists of marine, severe solar, and intermittent high levels of acid vapors (hydrochloric acid), as well as elevated temperatures.

There have been numerous reports in the literature regarding the use of EAPs in retarding corrosion on steel alloys (72). Elsenbaumer et al. (73), showed that PANI coated mild steel samples exposed to artificial brine and dilute HCl exhibited several times more corrosion protection than an epoxy barrier paint when scratched to expose precise areas of bare metal. Their results showed that the enhanced corrosion protection was a result of a passivating iron oxide layer formed even for the exposed bare steel metal. Wessling has demonstrated through several experimental techniques (including SEM and XPS) that dispersed PANI (CORRPASSIVTM) containing paints can induce the passivation

effect as a corrosion prevention primer (74). Wessling has proposed a mechanism to explain the corrosion protection of EAPs (75). He claims that the protection of steel by PANI is attributed to an increase in the corrosion potential and the redox catalytic activity of the PANI in the formation of a passive layer of metal oxide.

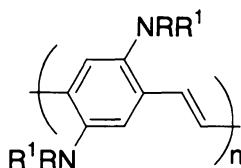
There is still debate over whether the emeraldine salt (ES) or emeraldine base (EB) form of PANI provides the best corrosion protection; several reports have shown that the EB form of PANI can perform as well as or better than the ES form of PANI (76,77). Epstein et al.⁷⁸ showed that the EB form of PANI coated onto cold rolled steel and iron samples inhibited corrosion when exposed to humidity chambers from one to seven days. X-ray photoelectron spectroscopy (XPS) depth profiling showed anodic protection for their samples. In addition to the polyaniline, oligomers of aniline have been used to retard against corrosion and to provide better solubility for casting films onto metal substrates (79,80). Wei et al. (81,82), have demonstrated that aniline oligomers, particularly the trimers, are effective anti-corrosion materials.

While there is general agreement that PANI performs well in retarding corrosion on carbon steel, the mechanism for this process is still under investigation. There have been several techniques used both to test EAP coatings for corrosion resistance and to evaluate the mechanism. The normal evaluation of such coatings is accelerated weathering tests in a laboratory setting to examine the likely performance of a coating. These tests mimic outdoor exposure to determine the effects of acid, neutral and/or alkaline spray (ASTM B117), sulfur dioxide spray, and ultra-violet light exposure. The tests compare the physical appearance of the coating to a known standard coating. To further evaluate the corrosion properties of a coating, electrochemical impedance spectroscopy (EIS) can be used (83). This ac technique measures adhesion and barrier properties of coatings and can give mechanistic data that traditional dc techniques cannot provide (84,85).

Several hypotheses are suggested for the mechanism of corrosion protection using EAPs, specifically PANI: (a) PANI contributes to the formation of an electric field at the metal surface, restricting the flow of electrons from metal to oxidant, (b) PANI forms a dense, strong adherent, low-porosity film similar to a barrier coating and (c) PANI causes the formation of protective layers of metal oxides on a metal surface (21)

While PANI has been extensively studied for corrosion control, its major drawback is its pH dependence. It works very well in acidic environments due to the formation of the conductive ES form, but at higher pH (>7), the non-conductive EB is formed (see Figure 1), and the material no longer provides adequate protection against corrosion. Thus, its use in a marine environment (pH ~8) is limited. In marine applications, pH-stable EAPs must be employed; several have been investigated. Double-stranded PANI has been coated onto

2024 T3 Al alloys (86); immersion tests in simulated seawater showed improved corrosion resistance as compared to control epoxy coating (87). Recently, a new polymer, poly(bis-dialkylamino)phenylene vinylene) (BAM-PPV) (Figure 5) was shown to adhere to 2024 T3 Al alloy in an immersion test using simulated seawater (pH ~8) and to retard corrosion (88-90). Constant current (galvanostatic) and constant potential (potentiostatic) method were used to investigate the corrosion protection of BAM-PPV on Al alloy plates. Quantitative evidence was obtained from these results to show corrosion inhibition was obtained without the loss of adhesion and no pH dependency was observed. These tests were run against control samples (non-coated Al alloys) and the coated coupons out performed the non-coated coupons. Visual inspection of the coupons showed significant pitting in the non-coated as compared to the coated (BAM-PPV) samples.



where R= methyl and R¹=hexyl

Figure 5. BAM-PPV

Several additional EAPs have been studied for their corrosion protective properties. Polypyrrole (PPy) has recently been examined for its anti-corrosion properties (91,92). PPy normally has poor solubility and mechanical properties, preventing its use in corrosion studies. Recent advances in improving its solubility and mechanical properties have been accomplished by adding functional groups to the pyrrole ring (93). Corrosion studies based on poly(3-octyl pyrrole) (94) have shown that these polymers can inhibit and delay the onset of corrosion for Al alloy 2024-T3. Poly (3-methylthiophene) was electropolymerized onto 430 stainless steel, which showed corrosion protection in both air and nitrogen saturated 1N sulfuric acid solutions (95). Polythiophene has been electrodeposited onto mild steel surfaces to provide corrosion protection in 3.5 % aqueous sodium chloride solution as determined by polarization and EIS analysis (96). Enhanced corrosion protection was found with a polyaniline-layered montmorillonite (clay) nanocomposite system as compared to polyaniline (97). The experiments were carried out in 5 wt% NaCl and showed better performance than conventional PANI by electrochemical measurements. Lignosulfonic acid-doped polyaniline (Ligno-PANI) has been investigated for its corrosion properties (98). Ligno-PANI has shown improved processability as compared to conventional PANI; it is water dispersible and

soluble in organic solvent such as DMSO and THF. The improved processability and reduced cost for this material makes it highly attractive for corrosion protection. Corrosion prevention has been demonstrated for Lingo-PANI and is found to be significant.

Conclusions

Electroactive polymers have been shown to offer many potential advantages as corrosion inhibiting coatings. More work is definitely needed to understand the mechanism by which EAPs can inhibit corrosion and to help investigators tailor materials to retard corrosion and prolong the lifetimes of coatings. To this end, researchers are investigating the mechanism of how EAPs work in corrosive environments. Several chapters in this book provide a basis for understanding this process and devising strategies to improve existing materials. This book is intended to provide the reader with an appreciation of the complexities of this problem and some possible solutions. Eventually, there will come a time when corrosion can be controlled and costs can be minimized with environmentally friendly materials.

Acknowledgements

Financial support is greatly appreciated through ONR (A. J. Sedriks), SERDP (C. Pellerin) and NAVAIR (J. W. Fischer).

References

1. Pohl, H.A., Bornmann, J. A., and Itoh, W., *Am. Chem. Soc. Poly. Chem. Preprints* **1961**, 2(1), 211.
2. Pohl, H.A., *Chem. Eng.* **1961**, 68(22), 105.
3. Katon, J. E., Wildi, B. S., *J. Chem. Phys.* **1964**, 40(10), 2977.
4. Pohl, H. A., and Engelhardt, E. H., *J. Phys. Chem.*, **1962**, 66, 2085.
5. Shirakawa, H., Louis, E., MacDiarmid A. and A. Heeger, *Chem. Commun.*, **1977**, 578.
6. MacDiarmid, A. G. and Heeger, A. J., *Synth. Met.*, **1978**, 1, 1013.
7. Bredas, J. L., Marder S. R. and Salaneck, W. R., *Macromolecules*, **2002**, 35(4), 1.
8. Epstein, A. J., *MRS Bulletin*, **1997**, 22(6), 16.
9. Smilowitz, L., *IEEE Circuits and Devices*, p. 19, January 1994.

10. Baughman, R. H., *Synth. Met.*, **1996**, 78, 339.
11. Ferraris, J. P., Brotherston, I. D., Loveday, D.C., Mudigonda, D. S.K., and Li, L., *Proc-Electrochem. Soc.*, **1999**, 98-115, 671.
12. Tour, J. M., *Polymer News*, **2000**, **25**, 329.
13. Sonmez, G., Schottland, P., Zong, K. and Reynolds, J. R., *J. Mater. Chem.*, **2001**, 11, 289.
14. Lovinger, A. J., Bao, Z., Katz, H. E. and Dodabalpur, A., *Polym. Mater. Sci. Eng.*, **1999**, **81**, 234 (1999).
15. Gratzel, M., *Pure Appl. Chem.*, **2001**, 73, 459.
16. McQuade, D. T., Pullen, A. E., and Swager, T.M., *Chem Rev. (Washington, DC)*, **2000**, 100, 2537.
17. Wessling, B., *Chemical Innovation*, p. 35 January 2001.
18. MacDiarmid, A. G., *Short Course on Conductive Polymers*, SUNY, New Platz, N.Y. 1985.
19. Heinze, J., *Topics in Current Chemistry*, **1990**, 152, 1.
20. Audebert, P., Bidan, G., Lapkowski, M., *J. J. Chem. Soc. Chem. Commun.*, **1986**, 887.
21. McAndrew, T. P., *TRI*, **1997**, 5(1), 7.
22. Huang, W. S., Humphrey, B. D., and MacDiarmid, A. G., *J. Chem. Soc., Faraday Trans*, **1986**, 1 (82), 2385.
23. Letheby, H., *J. Chem. Soc.*, **1862**, 15, 161.
24. Keifer, D. M., *Today's Chemist at Work*, **1996**, 5, 88.
25. Jozefowicz, M., Yu, L. T., Perichon, J., and Buvet, R., *J. Polym. Sci., Part C Polym. Symp.*, **1969**, 22, 1187.
26. Huang, W. S., Humphrey, B. D., and MacDiarmid, A.G., *J. Chem. Soc., Faraday Trans.*, **1986**, 1 82, 2385.
27. MacDiarmid, A. G., Chiang, J-C., Richter, A. E., Somaisiri, N. L. D., and Epstein, A. J., in L. Alcacer, ed., *Conducting Polymers*, Riedel, Dordrecht, Holland, 1987, p. 105.
28. Cao, Y., Andretta, A., Heeger, A. J., and Smith, P., *Polymer*, **1989**, 30(12), 2305.
29. Iroh, J. O. and Rajagopalan, R. R., *J. Appl. Polym. Sci.*, **2000**, 76, 1503.
30. Conklin, J. A., Huang S. C., Huang, S. M., Wen, T., and Kanar, R. B., *Macromolecules*, **1995**, 28, 6522.
31. Cao, Y., Smith, P., and Heeger, A. J., *Synth. Met.*, **1992**, 48, 91.
32. Kumar, D., and Sharma, R. C., *Eur. Polym. J.*, **1997**, 34(8), 1053.
33. Kumar, D., Sharma, R. C., Ram, M. K., Dhawan, S.K., and Chandra, S., *Ind. J. Chem.*, **1997**, 36A, 14.
34. McCullough, R. D., and Ewbank, P. C., *Regioregular, Head-to-Tail Coupled Poly(3-alkylthiophene) and Its Derivatives*, in Handbook of Conducting Polymers eds., T. A. Skotheim, R. L. Elsenbaumer and J. R. Reynolds, 1998, Marcel Dekker Inc. New York, p. 225.

35. Gelling, V. J., Tallman, D. E., Bierwagen, G. P., and Wallace, G. G., *Polymer Preprints*, **2000**, 41(2), 1770.
36. Reynolds, J. R., Child, A. D., Ruiz, J. P. Hong, S. Y., and Marynick, D. S., *Macromolecules*, **1993**, 26, 2095.
37. Troch-Nagels, G., Winand, R., Weymeersch, A., and Renard, L., *J. Appl. Electrochem.*, **1992**, 22, 756.
38. Angeli, A., *Gazz. Chim. Ital.*, **1916**, 46, 279.
39. Zhou, Z., and Heinze, J., *J. Phys. Chem.,B*, **1999**, 103, 8443.
40. Toshima, N., and Hara, S., *Prog. Polym. Sci.*, **1995**, 20, 155.
41. Kobayashi, M., Chen, J., Chung, T-C., Mores, F., Heeger, A. J., and Wudl, F., *Synth. Met.*, **1984**, 9, 77.
42. Pomerantz, M., Tseng, J. J., Zhu, H., Sproull, S. J., Reynolds, J. M., Uitz, R., and Arnott, H. J., *Synth. Met.*, **1991**, 41-43, 825.
43. McClain, M. D., Whittington, D. A., Mitchell, D. J., and Curtis, M. D., *J. Am. Chem. Soc.*, **1995**, 117, 3887.
44. Loewe, R. S., Ewbank, P. C., Liu, J., Zhai, L., and McCullough R. D., *Macromolecules*, **2001**, 34, 4324.
45. McDonald, R. N., and Campbell, T. W., *J. Am. Chem. Soc.*, **1960**, 82, 4669.
46. Wessling, R. A., *J. Polym. Sci. Polym. Sym.*, **1985**, 72, 55.
47. Lenz, R. W., Han, C-C., Stenger-Smith, J., and Karasz, *J. Polym. Sci.: Part A: Polym. Chem.*, **1988**, 26, 3241.
48. Gilch, H. G. and Whellwright, W. L., *J. Polym. Sci., Part A: Polym. Chem.*, **1966**, 4, 1337.
49. Pan, M., Bao, Z., and Yu, L., *Macromolecules*, **1995**, 28, 5151.
50. Marek, M. I., *Thermodynamics of Aqueous Corrosion*, in ASM Handbook, ed., J. R. Davis., et. al., Vol.13, Corrosion, ASM International, 1987, p. 18.
51. Lu, W-K., Basak, S., and Elsenbaumer, R. L., *Corrosion Inhibition of Metals by Conductive Polymers*, in Handbook of Conducting Polymers, eds., T. A. Skotheim, R. L. Elsenbaumer and J. R. Reynolds, Marcel Dekker, New York, 1998, p. 881.
52. Kuruvilla, A. K., *AMPITAC Newsletter*, **1998**, 2(2), 1.
53. Brumbaugh, D., *AMPITAC Newsletter*, **1999**, 3(1), 1.
54. Uhling, H. H., and Reive, R. W., *Corrosion and Corrosion Control*, Wiley, New York, 1985.
55. Fontana, M. G., *Corrosion Engineering*, McGraw Hill, New York, 1986.
56. Leidheiser, H., Jr., *Fundamentals of Corrosion Protection in Aqueous Solutions*, in ASM Handbook, ed., J. R. Davis., et. al., Vol. 13, Corrosion, ASM International, 1987, p. 377.
57. Marek, M. I., *Thermodynamics of Aqueous Corrosion*, in ASM Handbook, ed., J. R. Davis., et. al., Vol. 13, Corrosion, ASM International, 1987, p. 19.
58. Townsend, H. E., and Hart, R. G., *J. Electrochem. Soc.*, **1984**, 131, 1345.

59. McSweeney, E. E., in W. Von Fischer, E. G. Bobalek (eds), *Organic Protective Coatings*, Reinhold Publishing Corporation, New York, 1953 p. 305.
60. Fernandes, E. G., *Ind. Eng. Chem. Prod. Res. Dev.*, **1985**, 24, 353.
61. Leidheiser, H. Jr., *Ind. Eng. Chem. Prod. Res. Dev.*, **1981**, 20, 547.
62. Blasiak, J., and Kowalik, J., *Mutation Research*, **2000**, 469, 135.
63. National Emissions Standards for Chromium Emissions from Hard and Decorative Chromium Electroplating and Chromium Anodizing Tanks, Environmental Protection Agency, *Federal Register*, RIN 2060-AC14, January 25, 1995.
64. Wessling, B., and Posdorfer, J., *Electrochimica Acta*, **1999**, 44, 2139.
65. Mengoli, G., Munari, M. T., Bianco, P., and Musiana, M.M., *J. Appl. Polym. Sci.*, **1981**, 26, 4247.
66. DeBerry, D. W., *J. Electrochem. Soc.*, **1985**, 132, 1022.
67. Ahmand, N., and MacDiarmid, A. G., *Bull. Am. Phys. Soc.*, **1987**, 32, 548.
68. Thompson, K. G., Byran, C. J., Benicewicz, B. C., and Wroblewski, D. A., *Los Alamos National Laboratory Report*, LA-UR-92-360 (1991).
69. Wroblewski, D. A., Benicewicz, B. C., Thompson, K. G., and Byran, B. J., *Polym. Prepr.*, **1994**, 35(1), 265.
70. Phillips, M. A., *New Sci.*, **1994**, 144, 24.
71. Jain, F. C., Rosato, J. J., Laonia, and Agarwala, V. S., *Corrosion*, **1986**, 42, 700.
72. Sekine, I., Kohara, K., Sugiyama, T., and Yuasa, M., *J. Electrochem. Soc.*, **1992**, 22, 756.
73. Lu, W-K, Elsenbaumer, R. L., and Wessling, B., *Synth. Met.*, **1995**, 71, 2163.
74. Wessling, B., *Synth. Met.*, **1998**, 93, 143.
75. Wessling, B., *Adv. Mater.*, **1994**, 6(3), 226.
76. Jasty, S., and Epstein, A. J., *Poly. Mater.:Sci. Eng.*, **1995**, 72, 565.
77. Wei, Y., Wang, J., Jia, X., Yeh, J. M., and Spellane, P., *Polymer*, **1995**, 36, 4535.
78. Fahlman, M., Jastyt, S., and Epstein, A. J., *Synth. Met.*, **1997**, 85, 1323.
79. Sein, L. T., Jr., Wei, Y., and Jansen, S. A., *Polym. Prepr.*, **2000**, 41(2), 1741.
80. MacDiarmid, A. G., Zhou, Y., and Feng, J., *Synth. Met.*, **1999**, 100, 131.
81. Sein, L. T., Jr., Wei, Y., and Jansen, S., *J. Phys. Chem. A.*, **2000**, 104, 11371.
82. Jansen, S. A., Duong, T., Major, A. Wei., Y., and Sien, L. T., Jr., *Synth. Met.*, **1999**, 105, 107.
83. Menges, G., and Schnieder, W., *Kunststofftechnik*, **1973**, 12, 265.
84. Fedrizzi, L., Deflorian, F., Bonora, P. L., *Electrochim. Acta.*, **1997**, 42, 969.

85. Mansfeld, F., *Reviews of Appl. Electrochem.*, **1995**, 25, 187.
86. Sun, L., Liu, H., Clark, R., and Yang, S. C., *Synth. Met.*, **1997**, 85, 67.
87. Yang, S. C., Brown, R., Racicot, R., Lin, Y., and McClaraon, F., *Polym. Prepr.*, **2000**, 41(2), 1776.
88. Zarras, P. Stenger-Smith, J. D., and Miles, M. H., *Polym. Mat.: Sci. Eng. Preprints*, **1997**, 76, 589.
89. Zarras, P., Stenger-Smith, J. D., Ostrom, G. S., and Miles, M. H., in B. R. Hsieh and Y. Wei., eds., ACS Symposium Series, 735: *Semiconducting Polymers: Applications, Properties and Synthesis*, ACS Washington, DC 1999, p. 280.
90. Anderson, N., Irvin, D. J., Webber, C., Stenger-Smith, J. D., and Zarras, P., *Polym. Mater.: Sci. Eng.* **2002**, 86, 6.
91. Haase, V., and Beck, F., *Electrochimica. Acta.*, **1994**, 39(8/9), 1195.
92. Tallman, D. E., Pae, Y., and Bierwagen, G. P., *Corrosion*, **2000**, 56, 401.
93. Ashraf, S. A., Chen, F., Too, C. O., and Wallace, G. G., *Polymer*, **1996**, 37, 2811.
94. Gelling, V. J., Tallman, D. E., Bierwagen, G. P., and Wallace, G. G., *Polym. Prepr.*, **2000**, 41(2), 1770.
95. Ren, S., and Barkey, D., *J. Electrochem. Soc.*, **1992**, 139(4), 1021.
96. Kousik, G., Pitchumani, S., and Reganathan, N. G., *Prog. Org. Coat.*, **2001**, 43, 286.
97. Yeh, J-M., Liou, S-J., Lai, C-Y., Wu, P-C., and Tsai, T-Y., *Chem. Mater.*, **2001**, 13, 1131.
98. Berry, B. C., Shaikh A. U., and Viswanathan, T., *Polym. Prepr.*, **2000**, 41(2), 1739.

Chapter 2

Corrosion-Protective Coatings from Electroactive Polymers

Karen Gebert Thompson¹ and Brian C. Benicewicz^{2,3}

¹National Aeronautics and Space Administration,
John F. Kennedy Space Center, FL 32899

²Los Alamos National Laboratory, Los Alamos, NM 87545

³NYS Center for Polymer Synthesis and Department of Chemistry,
Rensselaer Polytechnic Institute, Troy, NY 12180-3590

In a research effort involving the National Aeronautics and Space Administration's John F. Kennedy Space Center and the Department of Energy's Los Alamos National Laboratory, electroactive polymers were developed as corrosion-protective coatings for metal surfaces. At the Kennedy Space Center, the launch environment consists of marine, severe solar, and intermittent high acid/elevated temperature conditions. Electroactive polymer coatings have been developed which impart corrosion resistance on mild steel surfaces, even when scratches exist in the protective coating. Such coatings appear promising for many commercial applications.

Until recently, the field of electroactive polymers comprised materials with virtually no processability. In the last few years, however, it was discovered that monomers based upon aniline, thiophenes, and pyrroles can be synthesized and polymerized to high molecular weight materials. Through proper control of substituents and synthesis conditions, polymers have been made that are both soluble in common organic solvents and melt processable below decomposition temperatures. Such breakthroughs demonstrate the potential of producing processable electroactive polymers.

Environmental and health concerns necessitate the development of coatings that provide alternatives to the excellent corrosion protection offered by chromate-containing coatings. Previous work in the 1980's (1-3) explored the concept of using electrically active coatings for corrosion protection. In 1988 we began work that took this concept further by developing processable coatings of electrically active polymers exhibiting corrosion resistance for steel substrates (4-7).

A coating with resistance to hydrochloric acid and corrosion is needed for ground support equipment and structures at the John F. Kennedy Space Center (KSC). The launch environment of the Space Transportation System Orbiter (commonly known as the Space Shuttle) consists of a marine, severe solar, and intermittent high acid/elevated temperature environment. The current zinc-rich coatings used on launch structures provide excellent protection except they are rapidly attacked by the high concentrations of hydrochloric acid released during a Space Shuttle launch. The KSC and Los Alamos National Laboratory (LANL) research effort involved the synthesis of electrically active polymers, formulation of such polymers into coatings, and subsequent environmental and physical testing of steel specimens coated with these materials. The objective of the study was to formulate these organic coatings to provide easy application, repair, and long term resistance to the KSC launch environment. This paper provides an historical review on the development and testing of these coatings.

Experimental

Polymer Selection

The research team synthesized several conducting polymers and prepared solutions of suitable viscosity for casting films. Solvents, casting techniques, and drying conditions were developed for coating metal coupons with pinhole-free films. For a material to qualify as a candidate for a corrosion-protective coating, selection criteria included ease of preparation and processing, dopability (i.e., increasing conductivity by additives serving as electron donors or acceptors), electrical conductivity, environmental stability, mechanical integrity of film, adhesion to steel, and low cost.

Several conducting polymers were synthesized during the research effort. In some cases specialized monomers were synthesized before subsequent polymerization; in other cases monomers were obtained commercially. Many polymers were eliminated from the study based upon the qualification criteria. For example, some polymers requiring specialized monomer synthesis were eliminated due to high production cost. Methods were developed for coating metal coupons with pinhole-free films of the following pi-conjugated polymers

and shown in Figure 1: polyaniline, poly(3-hexyl thiophene), poly(3-octyl thiophene), poly(3-thienylmethylacetate), and poly(3-thienylethylacetate).

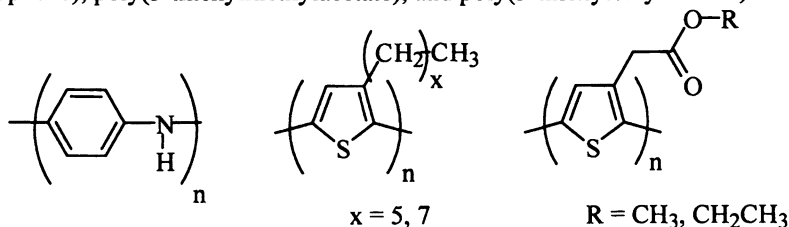


Figure 1. Polymers subjected to initial screening.

Adhesion to mild steel was an important consideration in the study. Adhesion problems were solved for many of the polymers through attaining appropriate blends of conductive polymer and epoxy and by applying undoped, chemically-prepared polymer to the surface of the steel and subsequently doping the coated surface to the conducting state. The protocol for surface preparation at KSC uses a relatively coarse bead or sand blasting to remove surface oxidation and impurities. The surface roughness created by the surface preparation techniques improved the adhesion of polymer films to the metal substrate. After steel samples were coated with candidate materials, the samples were tested by exposing them to salt water and to 0.1 M hydrochloric acid (HCl) solutions. Results of such adhesion studies concentrated the work effort on polyaniline coatings, which were clearly superior to others tested.

Polyaniline

The emeraldine form of polyaniline was prepared through standard methods by oxidation of aniline in HCl using ammonium persulfate as the oxidizing agent (8). The polyaniline powder was converted to the nonconducting emeraldine base by stirring in an ammonium hydroxide solution. Slight modifications in the published procedures produced high (up to 97%) yields of polymer with inherent viscosities (IV's) in the range of 0.5 to 0.7 dL/g (0.1% w/v in conc. H₂SO₄ at 30°C, Ubbelohde viscometer).

The emeraldine base of polyaniline can be easily dissolved in organic solvents with suitable stabilizers for application to steel substrates. Upon doping with many dopants, the solubility of polyaniline becomes limited in many common organic solvents. Consequently, the surfaces of the mild steel samples were initially coated with the undoped, chemically-prepared polyaniline. This coating of the mild steel coupons was accomplished using solutions of polyaniline in 1-methyl-2-pyrrolidinone (NMP). Dip-coating methods as well as a spray method were used for applying the polyaniline/NMP solutions to the steel. Both methods provided good coverage and good adhesion of the

polyaniline to the steel. Upon drying, the coatings were 1-2 mils (0.03-0.05 mm) thick.

Once dry, the undoped polyaniline coating was doped to the conducting state. By increasing the electrical conductivity of the polymer, dopants provide the proper electronic environment to impart corrosion resistance and acid resistance to the film. Over thirty different dopants were evaluated during the study. Three dopants were selected from the representative groups of protonic acid, Lewis acid, and charge-transfer compounds for further evaluation (p-toluene sulfonic acid, zinc nitrate, and tetracyanoethylene, TCNE). When films are used in acidic environments, the acid present in the environment also acts to dope the films even if the coatings are not doped in a separate processing step.

After the coating was doped to a conducting state, a topcoat of cross-linked epoxy or urethane was applied to the samples in order to impart improved abrasion resistance and other desirable properties to the coating. The epoxy topcoat used on the samples discussed in this chapter was Ciba-Geigy Bisphenol A GY 2600 resin cured with a cycloaliphatic/aliphatic amine hardener XU265. The resultant two-layer coating was designed to provide the proper electronic environment as well as coating toughness and resistance to harsh environmental conditions.

Corrosion Testing

Polymer-coated steel coupons were tested in the laboratory for corrosion resistance in two different environments via gas/liquid cells. One environment consisted of placing each coupon in an individual vial containing enough 3.5% NaCl solution to cover the coated portion of the coupon. All vials were capped with a rubber septum into which air was bubbled to ensure oxygenation of the solution. In the second environment, a 0.1M HCl solution was used in place of a saline solution. Photographs were taken of the samples before exposure to the above environments as well as throughout the testing. In some cases, the tests were carried out for twelve weeks.

Control samples of mild steel coated solely with the epoxy coating were tested to establish a baseline of the corrosion resistance of the conductive polymer-coated samples. The Ciba Geigy epoxy material was chosen because of its use in power plants for coating interior surfaces of industrial effluent stacks emitting sulfur dioxide. The material is reported to exhibit excellent acid resistance (9). The control samples were tested concurrently with the conductive polymer samples in the corrosion tests.

Beach exposure testing was carried out at the KSC Beach Corrosion Test Site, which is located on the Atlantic Ocean approximately one mile south of Launch Complex 39A at KSC. The test site is approximately 100 feet from the mean high tide line, with the orientation of the samples facing east toward the ocean at a 45 degree angle to receive the full extent of sun, rain and sea spray. The beach exposure test procedure is based on the test method described by

ASTM G50 (10), with the addition of an acid spray. Every two weeks, the specimens were sprayed with a 1.0M HCl/alumina powder slurry, which thoroughly wets the surface of the specimen and was allowed to remain on the surface of the specimen until dry or rinsed off by rain. The samples were visually inspected and photographed on a periodic basis.

Results and Discussion

Polyaniline synthesis and characterization

Polyaniline was prepared in accordance with published procedures (8). In our laboratory, a slight modification was developed that produced soluble polyaniline in high yields and reproducible IV's. This modification involved an increase in the molar ratio of ammonium persulfate to aniline to a higher value (1.5:1) than usually used in the literature. An aqueous 2.0M HCl/1.0M aniline solution was prepared and about half of a 1.5 M ammonium persulfate solution was added to the HCl/aniline solution. After a short induction time, the temperature of the reaction increased from 0°C to nearly 20°C. The remaining oxidant was added after the exothermic peak in the temperature profile. The polymerization temperature was kept near 0°C, and the polymerization time was usually 3-6 hours. The polymer was isolated as the emeraldine base and washed to remove low molecular weight oligomers. This general procedure produced high yields (~90%) and IV's in the range 0.5-0.7 dL/g. These IV's were found to be suitable for preparing and spray coating polyaniline solutions. Our initial molecular weight characterization by gel permeation chromatography (GPC) was conducted in N,N-dimethylformamide (DMF). As seen in Table 1, only lower molecular weight polyaniline is soluble in DMF. At higher molecular weights, dissolution of samples essentially fractionated the polymer by

Table 1. GPC of polyaniline.

<i>IV</i> , dL/g ¹	<i>M_n</i>	<i>M_w</i>	<i>PDI</i>
0.550	23,900	43,300	1.8
0.594	25,500	41,300	1.6
0.653	22,200 ²	42,600	1.9
0.686	24,200 ²	37,900	1.6
0.738	25,700 ²	40,500	1.6
1.13	42,400 ²	59,800	1.4

¹IV's were measured in conc. H₂SO₄ at 0.1% concentration at 30.0°C.

²Incomplete dissolution in DMF, high mw gel particles removed by filtration.

dissolving only the lower molecular weight species and narrowing the polydispersity. More recent studies have been conducted in DMAc/LiCl which appears to be a more suitable solvent for GPC studies (11).

Doping studies

A large number of dopants were screened for their ability to increase the conductivity of polyaniline. In general, three categories of possible dopants were analyzed: protonic acids, Lewis acids and charge transfer compounds. No attempts were made to optimize the contact time or selection of solvent. Table 2 shows the results of the screening process. These studies were performed on 2 x 3 cm films of emeraldine base form of polyaniline. The films were placed in vials of 0.25 M solutions with the indicated solvents for 2-24 hours. The films were removed from the solutions, rinsed with solvent, and dried. The conductivities were measured using the four-point probe method. The most surprising result of this study was the large number of materials that were effective in increasing the conductivity of polyaniline. Higher conductivities may be possible with these dopants under different doping conditions. Of course, many of the materials would not be suitable for general applications due to their hazardous nature or lack of stability in outdoor environments. However, this screening study provided the initial data to select dopants from each category for further testing.

Laboratory Corrosion Testing in Gas/Liquid Cells

Laboratory corrosion testing was performed on small samples (2.5 x 1.9 cm) that were dipcoated from polyaniline solutions and subsequently doped by submersion in the dopant solutions. The samples were then topcoated with a durable polymer coating for additional abrasion resistance. Control samples without the polyaniline undercoat were also tested. Some samples were scribed to expose bare metal substrate on the test article. Figure 2 shows photographs of samples before and after eight weeks of exposure to an aerated 0.1M HCl solution. The photograph on the top left shows mild steel coated only with epoxy before exposure. The sample shown on the top right was coated with undoped polyaniline in NMP, then doped with TCNE, followed by application of an epoxy topcoat. The sample shown on the bottom left is an epoxy control sample after eight weeks exposure to the acid solution. Corrosion was evident with the control sample, with pitting throughout the sample and mass loss from the exposed areas of the steel sample. The sample on the bottom right is a polyaniline/epoxy sample. No evidence of corrosion was seen, with the scribed surface still shiny and the exposed areas of the sample still intact and showing no mass loss. The solutions containing the scribed samples without the polyaniline undercoat turned rust-colored within a short period of time in both saline and acid test solutions. Remarkably, the solutions containing the scribed samples with the polyaniline undercoat did not turn rust-colored, indicating that very little corrosion was occurring even though bare metal was exposed to the

Table 2. Polyaniline film doping.

<i>Dopant</i>	<i>Solvent</i>	<i>Exposure time</i> <i>h</i>	<i>Conductivity</i> <i>S/cm</i>
HCl	Water	2	5
H ₂ SO ₄	Water	2	4
CH ₃ SO ₃ H	Water	2	2
DBSA	CH ₃ CN	24	2
CF ₃ CO ₂ H	Water	2	1
H ₃ PO ₄	Water	2	1
HBr	Water	2	6 x 10 ⁻¹
BF ₃	MeOH	24	3 x 10 ⁻¹
TCBQ	CH ₃ CN	24	2 x 10 ⁻¹
BF ₃ (g)	----	2	1 x 10 ⁻¹
PTSA	Water	24	8 x 10 ⁻²
PCl ₅	CH ₃ CN	24	7 x 10 ⁻²
AlCl ₃	CH ₃ CN	24	4 x 10 ⁻²
HClO ₄	Water	2	4 x 10 ⁻²
SnCl ₄	CH ₃ CN	24	4 x 10 ⁻²
Zn(NO ₃) ₂	CH ₃ CN	24	2 x 10 ⁻²
HF	Water	24	9 x 10 ⁻³
TCNE	CH ₃ CN	24	6 x 10 ⁻³
HCO ₂ H	Water	2	5 x 10 ⁻³
WCl ₆	CH ₃ CN	24	3 x 10 ⁻³
FeCl ₃	CH ₃ CN	24	1 x 10 ⁻³
TiCl ₄	CH ₃ CN	24	8 x 10 ⁻⁴
U(NO ₃) ₆	CH ₃ CN	24	3 x 10 ⁻⁴
Pb(NO ₃) ₂	Water	24	2 x 10 ⁻⁴
NiCl ₂	CH ₃ CN	24	2 x 10 ⁻⁴
CSA	CH ₃ CN	24	2 x 10 ⁻⁴
CuCl ₂	CH ₃ CN	24	1 x 10 ⁻⁴
I ₂	Water	24	1 x 10 ⁻⁴
AgNO ₃	CH ₃ CN	24	4 x 10 ⁻⁵
NiCl ₂	Water	24	2 x 10 ⁻⁵
CoCl ₂	CH ₃ CN	24	< 10 ⁻⁷
Cr ₂ O ₃	Water	24	< 10 ⁻⁷
DDQ	CH ₃ CN	24	< 10 ⁻⁷
TBBQ	CH ₃ CN	24	< 10 ⁻⁷

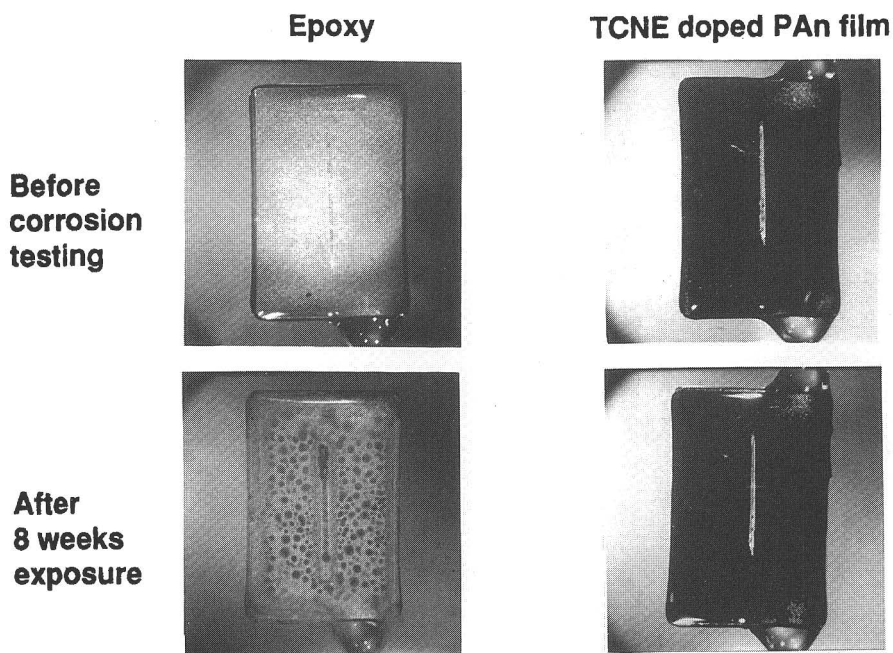


Figure 2. Laboratory corrosion testing of scribed samples in 0.1M HCl solutions

corrosive solutions. Since the polyaniline is dark in color, the coating was scraped off to verify that no corrosion was present. In fact, the polyaniline coating adhered to the substrate so tenaciously that it was difficult to scrape the coating from the steel. Similar tests were conducted in aerated 3.5% NaCl solutions with similar results.

Spray coating

For larger scale testing, application of polyaniline coatings via a spray coating technique was desirable. However, one of the major difficulties in processing polyaniline solutions is that these solutions tend to gel over periods from several minutes to several hours. Many workers have observed this behavior for solutions of the emeraldine base of polyaniline in NMP and have proposed that this gelling process was due to crosslinking of the polymer chains. Such crosslinking has been attributed to formation of physical crystalline regions (8) or to the formation of chemically bonded regions through oxidative processes (12).

Our initial experiments examined the relationship between polyaniline molecular weight and gel time. We noted that 5 wt% solutions of NMP could be prepared with a polyaniline IV of less than 0.65 dL/g which would remain fluid for several hours. However, solutions prepared with higher IV polymers gelled within a few minutes. Figure 3 shows the results of a study which examined the

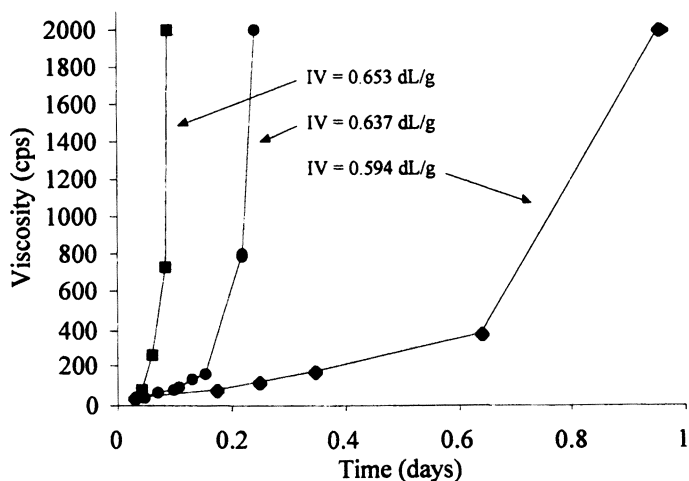


Figure 3. Gelation of polyaniline solutions (5 wt% in NMP).

effect of polymer IV on the gelation of polyaniline solutions. The molecular weight and polymer concentration both affected the gelation time of these

solutions. At 5 wt%, there was a critical IV when gelation proceeded rapidly. We analyzed a wide variety of additives to stabilize the solutions against gelation and found that amine additives (hindered amine light stabilizers, HALS) were particularly efficient for the application. Figures 4 and 5 show the

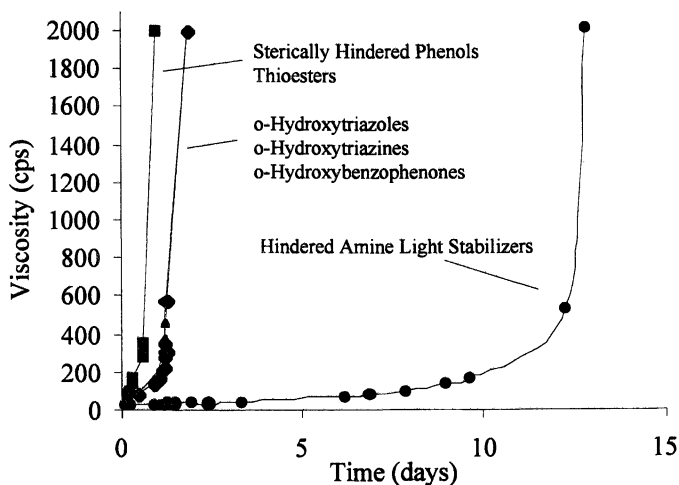


Figure 4. Gelation of polyaniline solutions with additives (5 wt% polymer solutions in NMP, polymer IV = 0.594 dL/g).

effects of amine additives versus other classes of additives and the effect of additive concentration on solution stabilization. Results from other researchers on solution gelation indicate that this is a general phenomenon of basic amines (13). In order to demonstrate that this is a physical gelation phenomenon, we allowed a solution without additives to form a gelled mass. The addition of a small amount of additive solution and mixing with a spatula for a few minutes re-dissolved the polymer and formed a solution suitable for spray coating. Spray coating was conducted using 5 wt% polymer solutions in NMP with 2% amine additive (based on polyaniline). The solutions were pumped through a sintered stainless steel 60 micron filter and fed to an industrial spray gun. This was done on a 1-2 liter batch size for multiple panel spray trials. Analysis of spray coated films by SEM showed a featureless, smooth, pinhole-free coatings. WAXS of free standing films made by spray coating onto non-stick surfaces displayed a broad peak indicating that the films were mostly amorphous.

Additional Environmental and Physical Testing

Testing was performed at the KSC Beach Corrosion Test Site located near Launch Complex 39A on the shore of the Atlantic Ocean. In addition to the

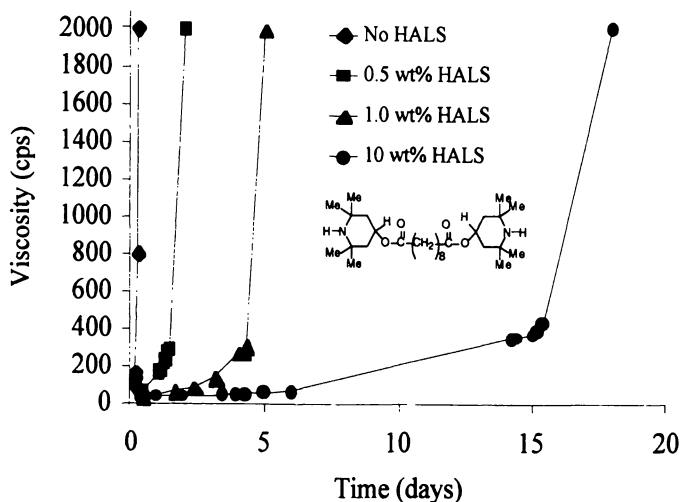


Figure 5. Effect of additive concentration on gelation (5 wt% polymer solutions in NMP, polymer IV = 0.637 dL/g, Tinuvin 770 wt% based on weight of polymer).

close proximity to salt spray from the ocean, seven Shuttle launches occurred in the first seven months of exposure. Twelve samples were prepared on carbon steel grit-blasted to a 0.076 mm profile. Six of these were coated with polyaniline that was doped with TCNE and six with polyaniline doped with p-toluenesulfonic acid. The samples were topcoated with polyurethane. Once coated, low-power optical microscopy revealed incomplete coating in areas that are difficult to coat, such as edges of the panel, in the area of the stamped sample numbers and inside the holes in the top portion of each sample. Two samples coated only with the polyurethane (as controls) were mounted on the same rack.

The samples were mounted on a stainless steel rack and placed outside at the KSC Beach Corrosion Test Site. Figure 6 presents typical samples after seven months of exposure. There was a noticeable difference between the samples with and without the polyaniline primer coating at this early time. Figure 7 shows typical samples after sixteen months of exposure. There was still a marked contrast between the samples with and without polyaniline primer coating. Figure 8 shows the same panels after 28 months. The harsh environment had a severe effect on the panels without the polyaniline primer coat. Some corrosion can be seen on the polyaniline panels around the edges, stamped numbers and holes. However, the corrosion in these incompletely coated areas is very slow and the development of the corrosion appears to be significantly delayed on this group of panels.

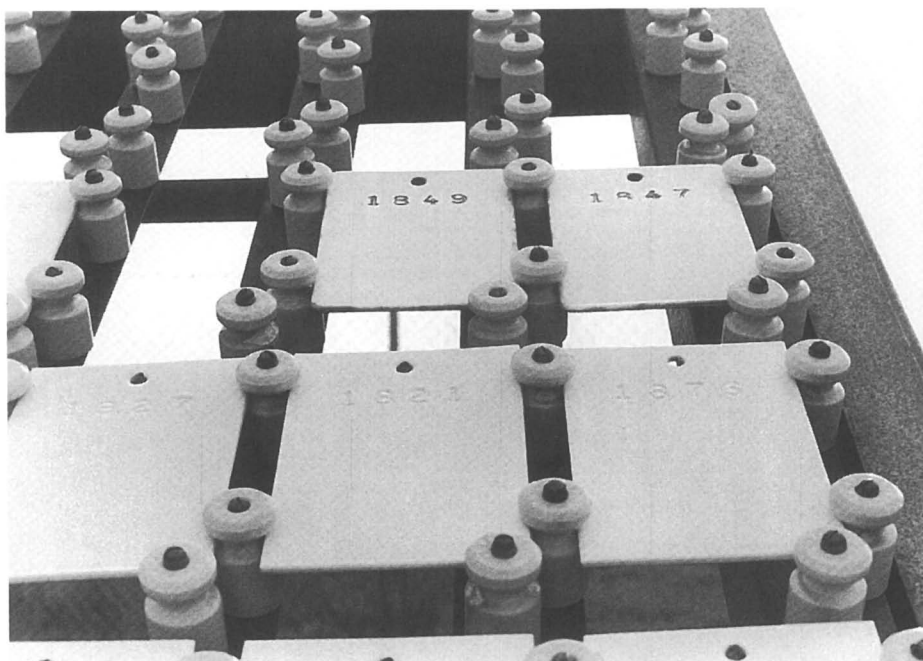


Figure 6. Outdoor corrosion testing at KSC Beach Corrosion Test Site after 7 months exposure. Upper two panels were coated with topcoat only, remaining panels included a polyaniline primer coat. Corrosion along the edges and inside the indentations of the sample numbers can be seen in the samples without the polyaniline primer.

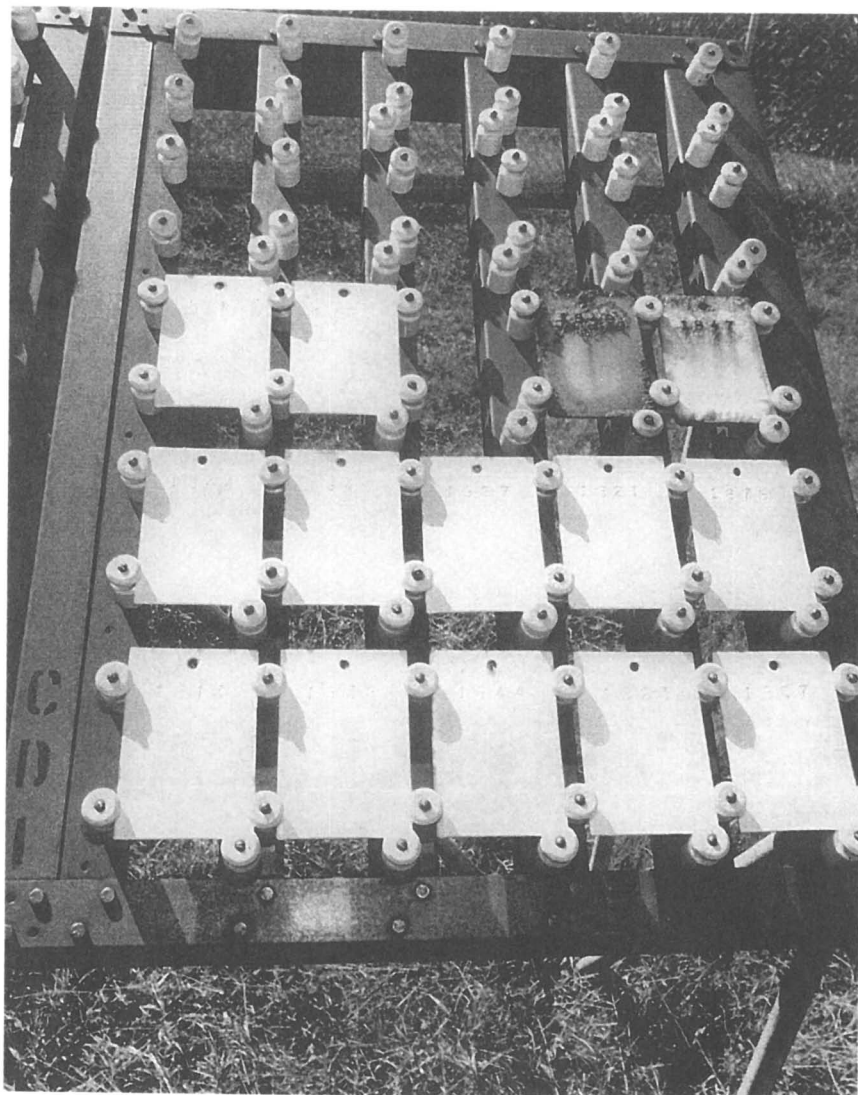


Figure 7. Outdoor testing after 16 months exposure showing complete sample set. Advance corrosion can be seen in the two control samples in the upper right that do not contain a polyaniline primer.

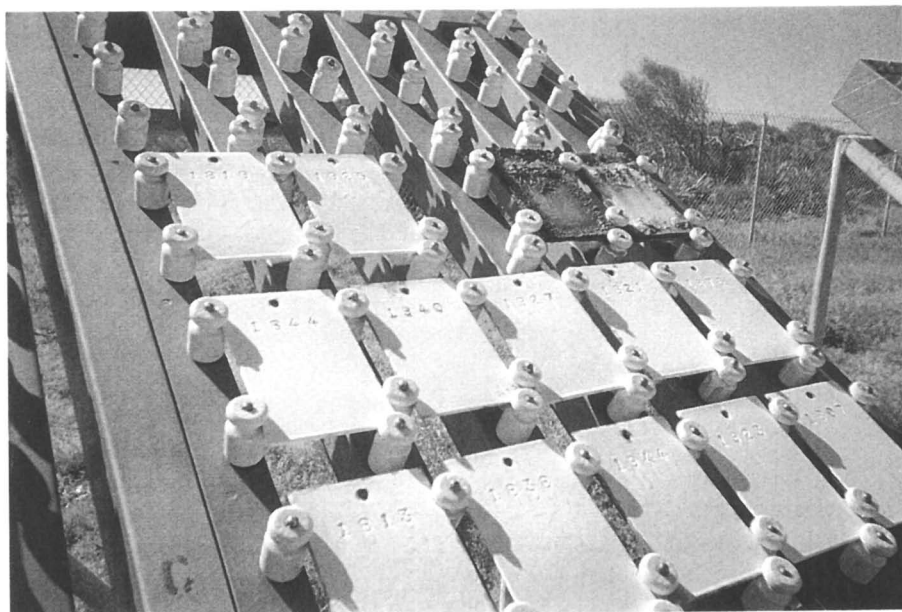


Figure 8. Outdoor testing after 28 months exposure.

Conclusions

This work demonstrated that in both laboratory and harsh outdoor corrosion-testing environments electrically active polymers provide corrosion protection to steel substrates. Samples that were solution coated with polyaniline that was subsequently doped and topcoated showed excellent to remarkable resistance to salt water or to aqueous HCl. Extensive environmental tests wherein the samples were exposed to sea spray as well as to occasional HCl have shown the long-term effectiveness of doped polyaniline primer coats in resisting that exposure. There is still strong interest in this technology area and multiple international companies are still actively involved in its further development.

Acknowledgements

Financial support from NASA is gratefully appreciated. The authors would also like to acknowledge their many co-workers at the Kennedy Space Center and Los Alamos National Laboratory for their significant contributions.

References

- (1) Mengoli, G.; Munari, M.T.; Bianco, P.; Musiani, M.M. *J. Appl. Polym. Sci.* **1981**, *26*, 4247-4257.
- (2) DeBerry, D.W. *J. Electrochem. Soc.* **1985**, *132*, 1022-1026.
- (3) Jain, F.C.; Rosato, J.J.; Kalonia, K.S.; Agarwala, V.S. *Corrosion* **1986**, *42*, 700-707.
- (4) Benicewicz, B.C.; Wroblewski, D.A.; Thompson, K.G.; Bryan, C.J. *U. S. Patent 5,658,649* August 19, 1997.
- (5) Thompson, K.G.; Bryan C.J.; Benicewicz, B.C.; Wroblewski, D.A. *Proceedings of Technology 2001, The Second National Technology Transfer Conference and Exposition*, NASA Conf. Pub. 3136, vol. 1, December, **1991**, 339-347.
- (6) Wroblewski, D.A.; Benicewicz, B.C.; Thompson, K.G.; Bryan, C.J. *Polym. Prepr.* **1994**, *35(1)*, 265-6.
- (7) Wroblewski, D.A.; Benicewicz, B.C. *Polym. Prepr.* **1994**, *35(1)*, 267-8.
- (8) Cao, Y.; Andreatta, A.; Heeger, A.J.; Smith, P. *Polymer* **1989**, *30(12)*, 2305-11.
- (9) Leidheiser, H.; White, M.L.; Mills, D.J. *Electric Power Institute Report #CS-5449, Research Project 1871-5*, October 1987.
- (10) ASTM G50-76, *Annual Book of ASTM Methods*, ASTM, Philadelphia, PA, **1986**, vol. 03.02.

- (11) Angelopoulos, M.; Liao, Y.-H.; Furman, B.; Graham, T. *Macromolecules* **1996**, *29*, 3046-3049.
- (12) Oh, E.J.; Min, Y.; Wiesinger, J.M.; Manohar, S.K.; Scherr, E.M.; Preist, P.J.; MacDiarmid, A.G.; Epstein, A.J. *Synthetic Metals* **1993**, *55-57*, 977-982.
- (13) Cohen, J.D.; Tietz, R.F. *U.S.P. 5,135,682* August 4, 1992.

Chapter 3

Effective Corrosion Protection with the Organic Metal Polyaniline: Basic Principles and Recent Progress

Bernhard Wessling

Ormecon Chemie, Ferdinand-Harten-Strasse 7, D-22949 Ammersbek,
Germany

After an introduction into the basic principles of corrosion protection with the Organic Metal Polyaniline, the method of assessing corrosion protection efficiency quantitatively will be described. It will be shown that polyaniline coatings are powerful anti-corrosion coatings, out-performing conventional coatings. The limits of improving Organic Metal coatings are not reached yet, as new formulations with even better performance are showing.

Historical Background

The seminal publication¹ in 1977* by MacDiarmid, Heeger and Shirakawa - describing the synthesis of electrically conductive polymers, focused my interest on this area of research. This work has led to the development of a new type of corrosion resistant coating.

Their paper (-published in *Chemical Communications*-) showed that the reaction of iodine with polyacetylene (PAC) resulted in a new polymeric compound, a radical-cation salt, which had a conductivity much higher than the original neutral PAC. However, these polymers were insoluble and unmoldable (and unstable). Our approach to solving this problem was to make them dispersible.

It took more than 5 years to prepare the first dispersion of PAC, which was based on the discovery that the conducting polymers are composed primarily not by fibrillar structures but by even smaller globular particles.² It was discovered in later years, that the primary particles - the smallest

* who have been honoured with the Nobel Price in Chemistry in 2000

entities that display all the properties seen in macroscopic conductive polymers - range from 10 - 15 nm in size. They form all kinds of agglomerates and aggregates, including fibrils, in a precise morphological hierarchy³.

Discovery of the „Organic Metal“ State in Dispersion

One of the most challenging questions arising from this work has been to understand, why dispersed PANi as well as PAc and other conducting polymers still show conductivity after a certain critical polymer concentration. Very complex network structures of the globular particles are formed above this concentration.⁴ For there lies no polymer matrix between the particles to prevent electron flow, the dispersion is conducting. Surprisingly the conductivity of certain dispersions was even higher than in the original PANi. This was the first conducting polymer to cross the boundary between insulators and metals - to become a true Organic Metal.⁵

These studies, which were done together with scientists from the universities of Cologne (Germany), Wellington (New Zealand) and Madras (India), also showed that the electrons were not mainly transported along the polymer chain. Rather, they were forming a ‘cloud’ of electrons, throughout the whole ‘metallic’ core of a primary particle, and then tunnelling from particle to particle.⁶

Apart from this basic scientific work, we were interested in possible commercial applications⁷: The attention was focused on all different kinds of dispersions: in polymer matrices, in solvents, in paints, and even in water.⁸ One of the areas of interest was corrosion protection.

First Corrosion Protection Work

The research in this area started in 1986 and we prepared the first dispersed polyaniline (PANi) containing coating in 1987.⁹ The aim was to find out, if corrosion protection was possible on just normal steel, without any pretreatment, especially without previous passivation in acid or under electrochemical conditions. We wanted to know, if corrosion protection was feasible using a PANi dispersion in a coating, hence without any electrochemical deposition of PANi. The research was motivated by the publication of deBerry in 1985¹⁰ according to which polyaniline, electrochemically deposited on pre-passivated stainless steel in strong acid environment, was enhancing the corrosion protection of this metal. Similar observations, however with a composition not identical with polyaniline, had previously been made by Mengoli et al¹¹. Both authors favoured the conclusion, that PANi, if electro-deposited on pre-passivated steel, was capable of maintaining the passive state.

Our proprietary knowledge at that time was how to disperse polyaniline, although still at a relatively low performance level, as we succeeded in first

dispersions of polyaniline only some years before. It was completely unknown, if a PANi dispersion coating would have any effect. If yes, what would the effect be based on, and if not, how to make it an anti-corrosion coating. Nothing at all was known about any anti-corrosion effect of PANi, if applied non-electrochemically and on a non pre-passivated steel surface, and nothing at all was to be expected in this direction at that time.

In 1987, corrosion protection was observed for the first time (see Ref. 9), and, moreover, that an oxide was formed, but this could have been any oxide or hydroxide, or even a first sign of rust. At this point, there was no evident improvement over state-of-the-art coatings (and it appeared as a brown, although dense and well adhering layer).

At that time, it was completely unclear, which mechanism was responsible for the corrosion protection, as we were not using stainless steel in the passive state, and polyaniline was not electrochemically formed and coated over it, but we used simple mild steel, and polyaniline was deposited from a dispersion, in an electroless process.

Ennobling and Passivation by the Organic Metal

In 1993, two phenomena responsible for the new corrosion protection principle were discovered: 1) a shift of the corrosion potential of the metal surface about 800 mV to the more noble range and 2) a new type of passivation (the formation of a stoichiometric iron(II) oxide)¹². For basic studies, pure polyaniline dispersions have been used, as well as polyaniline dispersion coatings which were deposited on untreated metals like normal iron, stainless steel, copper and aluminum.

The corrosion current was significantly reduced or even completely eliminated at comparable potentials (Figure 1). Investigations with SEM revealed that an oxide layer was formed between PANi coating and the metal surface. In cooperation with R. Elsenbaumer, we found that it is mainly composed by Fe_2O_3 (with an underlayer of Fe_3O_4)¹³. The study was repeated with a steel surface more clean to start with by XPS¹⁴ (Figure 2a and b) showing that there was no Fe_3O_4 , but only a clean $\gamma\text{-Fe}_2\text{O}_3$. (This does not exclude, that Fe_3O_4 might also occur in real situations, but it shows that $\gamma\text{-Fe}_2\text{O}_3$ is the passivating layer composition formed by PANi, which has independently been confirmed by R. Elsenbaumer¹⁵ and T. Schauer et al.¹⁶, although there is some dispute if it is the α - or the γ - form which is formed).

It is of basic interest that an oxide like this has not been observed or analyzed before for the „passive“ state of stainless steel or simple steel. Conventional passive stage is not a stable property: after removing the steel from the passivating medium, its passivity gets completely lost. In contrast, A.-M. LeGoff et al. have published, that the nature of the passive layer is FeOOH ¹⁷. In conclusion, our technology seems to be the first one which allows to produce Fe_2O_3 as a passivating oxide layer.¹⁸

Research together with G. Nimtz et al.¹⁹ and A. Kaiser et al.²⁰ lead - by using microwave and thermopower measurements - to the discovery, that

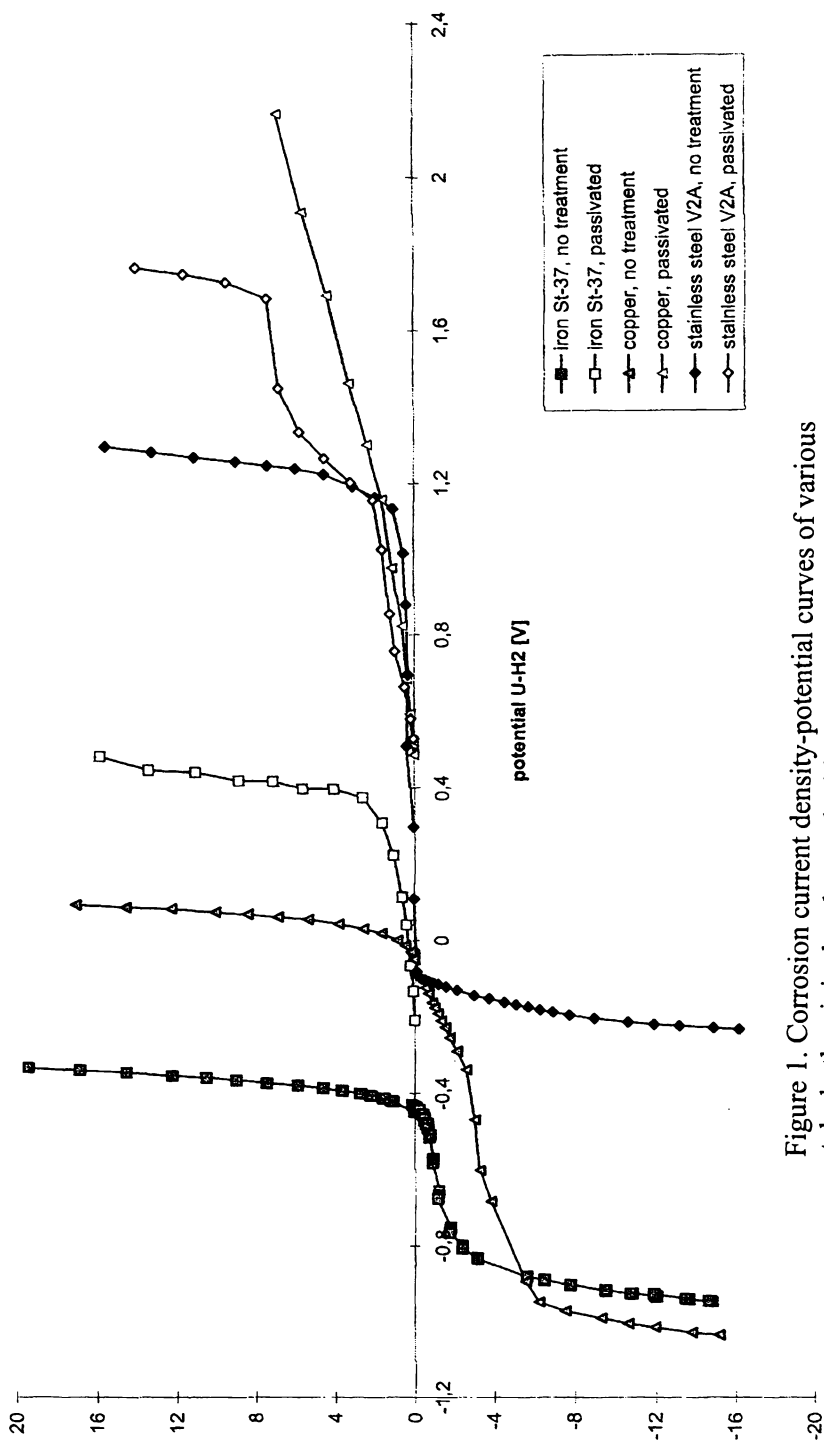


Figure 1. Corrosion current density-potential curves of various metals, both original and coated with polyaniline (Reproduced with permission from reference 12b)

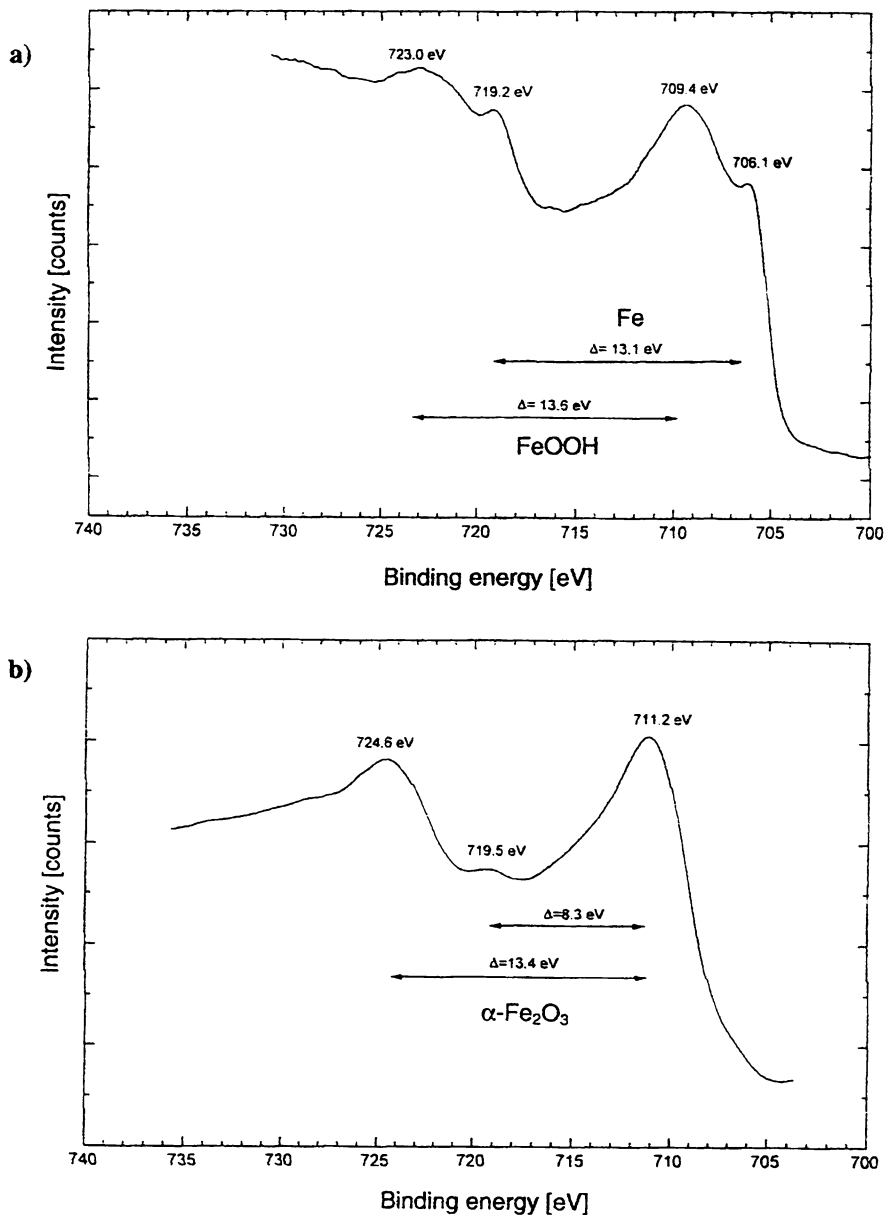


Figure 2. XPS analysis of passive iron oxide layers
a) untreated with Fe and FeOOH signal
b) in the presence of polyaniline with pure Fe_2O_3 signal (Reproduced with permission from reference 14)

polyaniline is not only a conductive polymer, but a true, though „mesoscopic“ metal, and hence can be considered as an „Organic Metal“. The ennobling was possible due to its metallic property, as it is situated slightly less noble than silver in the galvanic serie²¹.

Our group later succeeded in improving the dispersed PANi containing paints and coating systems (primer + top coat)²² which are capable of inducing the same passivation effect, but are moreover industrially applicable and effective as corrosion prevention coating systems (CORRPASSIVTM). They perform significantly better than anti-corrosion coating systems composed by zinc rich epoxy primers and epoxy top coats²³.

The reaction sequence which is responsible for the passivation (oxide layer formation) and the corrosion protection induced by the PANi layer was discovered at that period as well. Figure 3 shows an improved version of the reaction scheme²⁴. It involves Fe-oxidation by PANi (the more noble metal, emeraldine salt ES), which is thereby reduced to leucoemeraldine base (LE)²⁵. Further oxidation of Fe (II) to Fe (III) and reoxidation of LE to PANi (ES) via the emeraldine base EB occur both by oxygen; and Fe₂O₃ deposition by resulting OH. This scheme furthermore shows, that the Organic Metal acts as a catalyst, and that the full catalytic cycle (ES → LE → EB and back to ES) will only take place, if the necessary H⁺ will not be removed by the surrounding medium, i.e. only, if the acidic pH will be maintained within the primer, e.g. due to the barrier property of the top coat.

Evaluation of the Passive Oxide Formation Process

The reaction mechanism has been evaluated experimentally using many different approaches, which have been published earlier (24). A PANi dispersion was brought into contact with iron powder, or a film coated with PANi and iron powder was immersed into an electrolyte. The reaction progress was followed by UV-VIS spectroscopy.

The colour changes from green to yellowish green and later to pale yellow (reduction step, Figure 4a and b) which later turns back to green (back-reaction, Figure 5a and b). In neutral environment, the green gets a more bluish hue (Figure 5b), in contrast to an acid electrolyte which leads to the original nice PANi green (Figure 5a). Without iron powder there is no change of colour to be seen (Figure 6a and b). Figure 4a and 4b are showing the change of the spectrum of polyaniline with suspended iron powder in pTs and NaCl solution, Figure 5a and 5b show the back reaction in the period of one day.

A calibration showed that 90 % PANi has been reduced during the first 5 minutes, with a subsequent loss of extinction during the following 2 hours (in pTs, Figure 4a) or 10 min. (in NaCl, Figure 4b) with no further spectral change in the following 2 hours. All leucoemeraldine has reacted back to PANi during the next 24 hours.

For a better understanding of the back reaction two key experiments have been made:

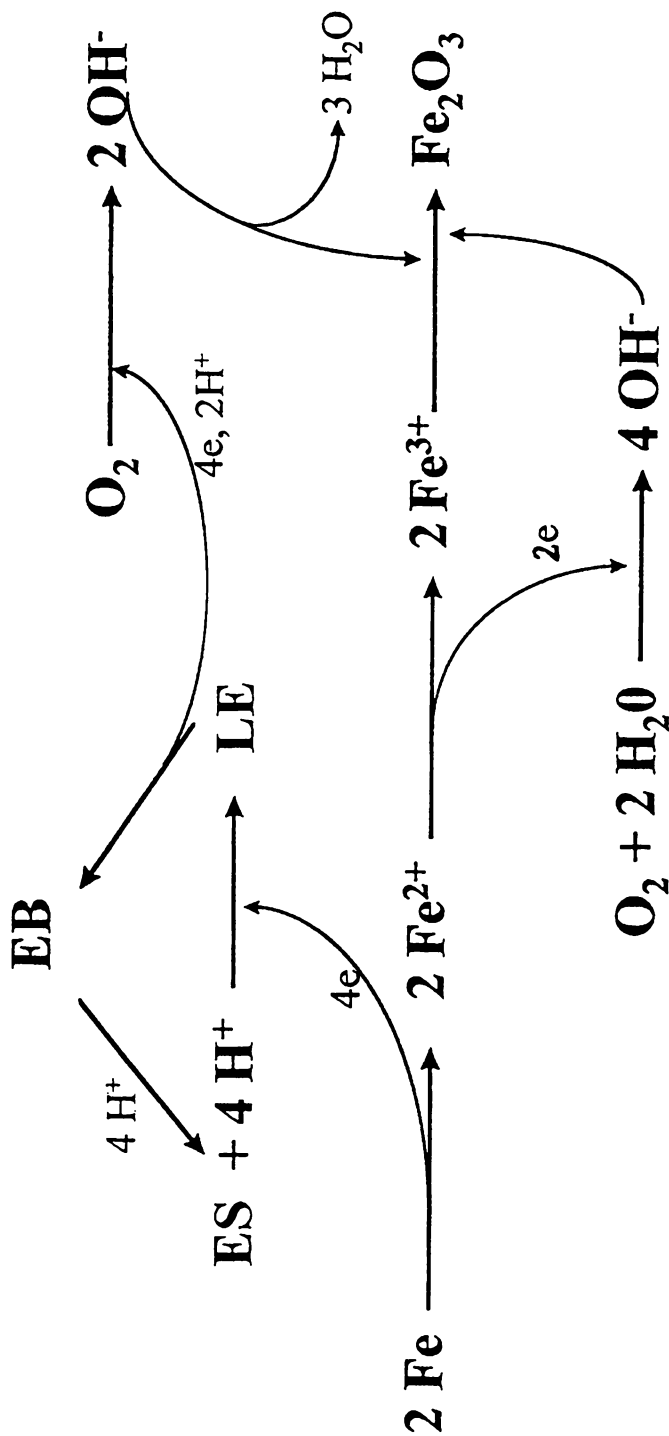


Figure 3. Reaction scheme

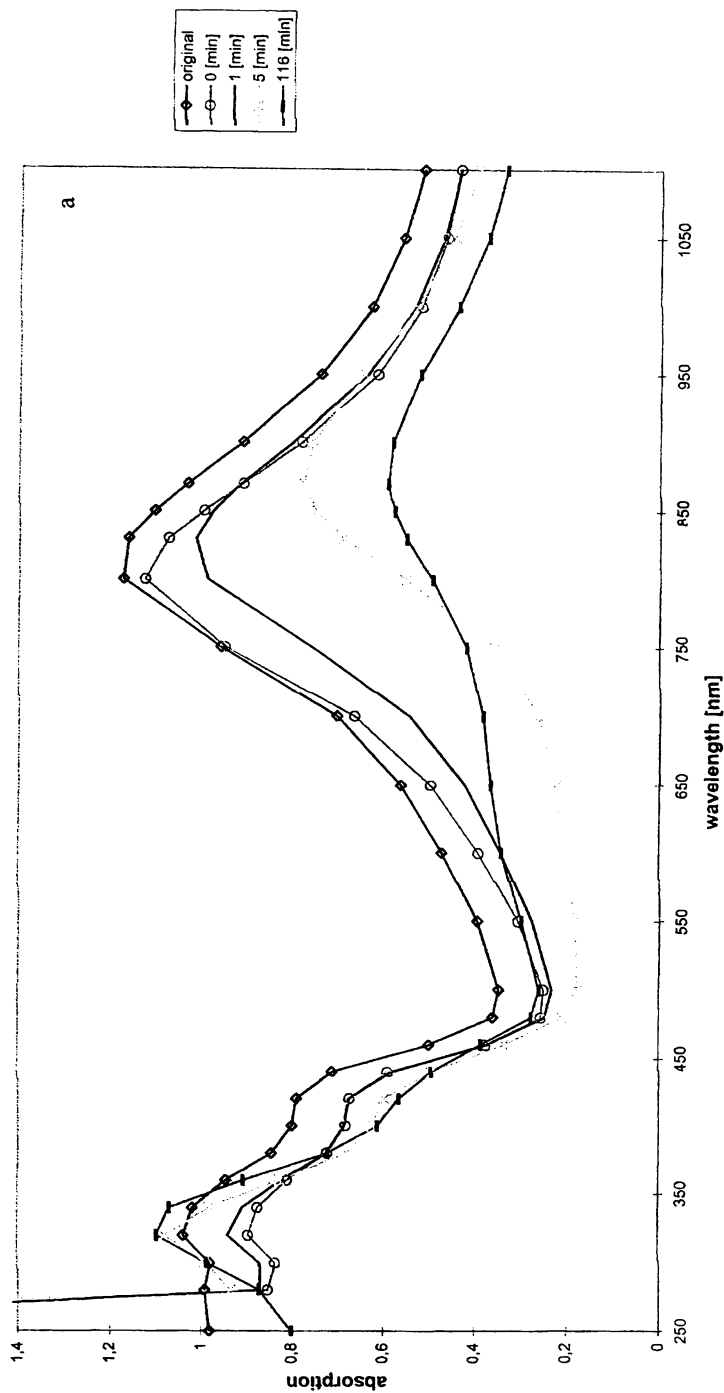


Figure 4. Spectral change of PANi on PP film with suspended iron (reduction step) a) measured in 0.1 M pTS b) measured in 1 M NaCl (Reproduced with permission from reference 24)
Continued on next page.

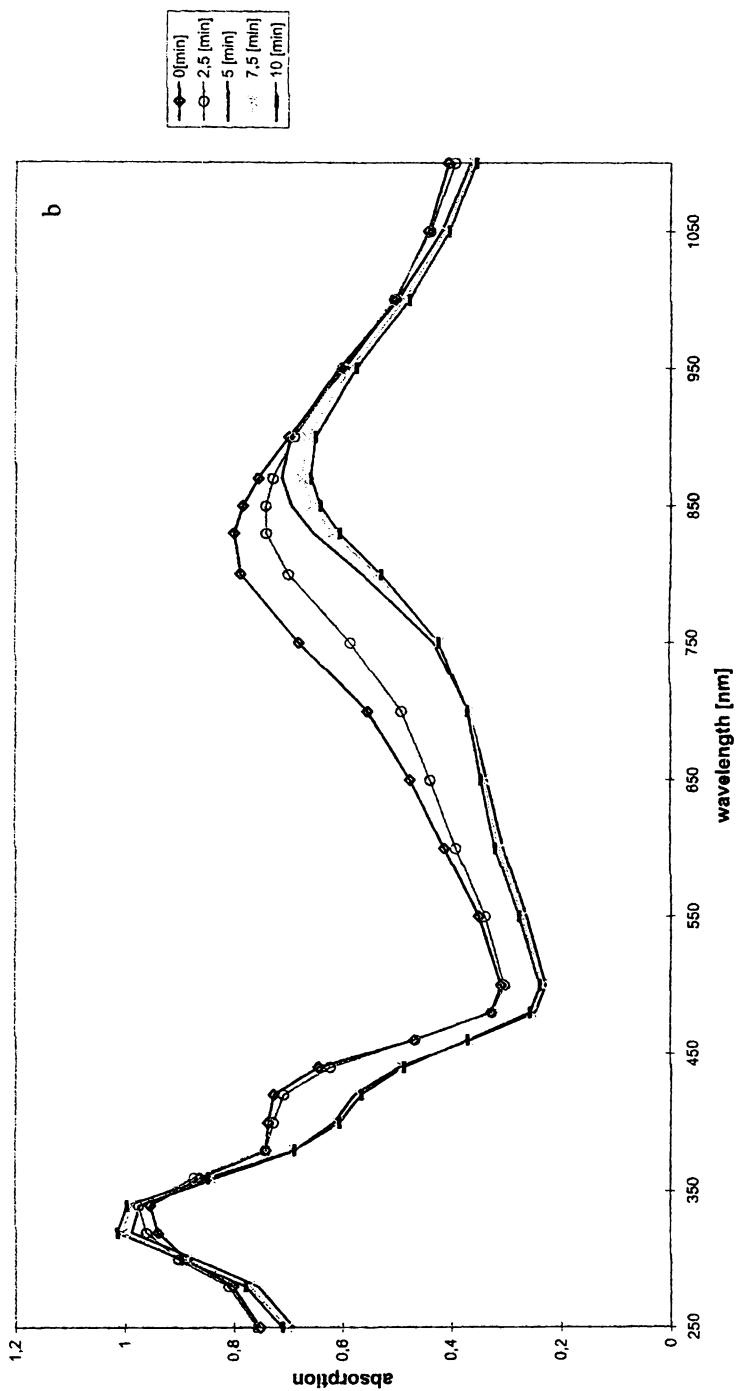


Figure 4. Continued.

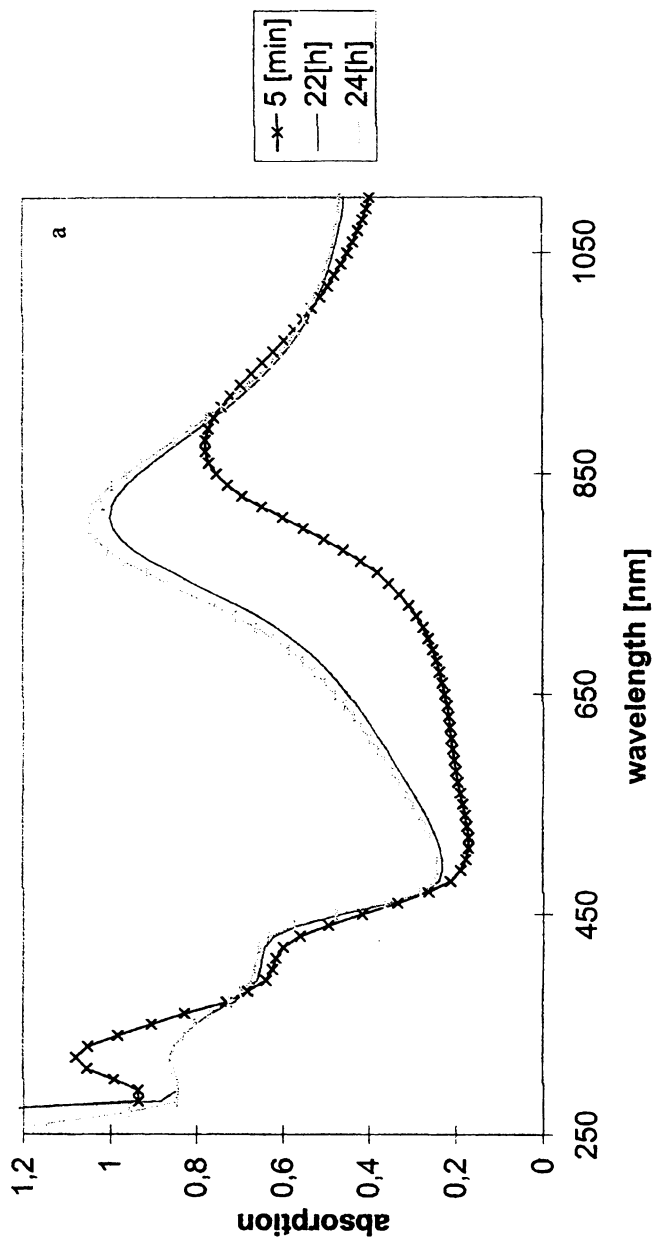


Figure 5. Spectral change of PANi on PP film with suspended iron (back reaction)

a) measured in 0.1 M pTS

b) measured in 1 M NaCl

(Reproduced with permission from reference 24) Continued on next page.

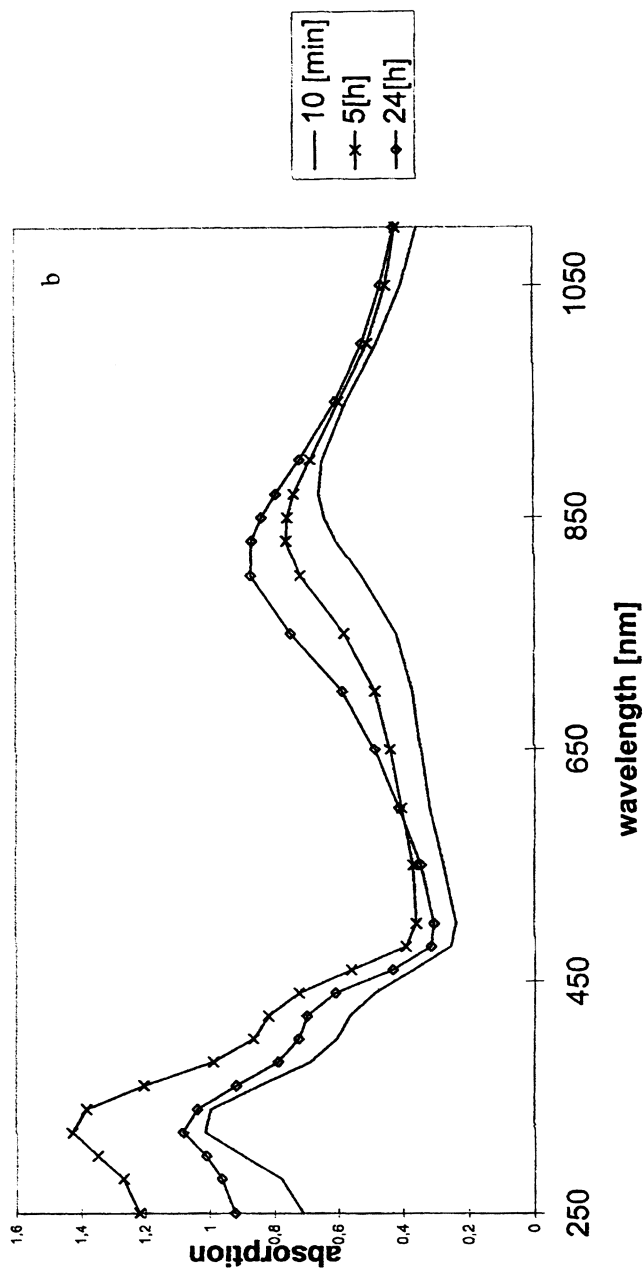


Figure 5. Continued.

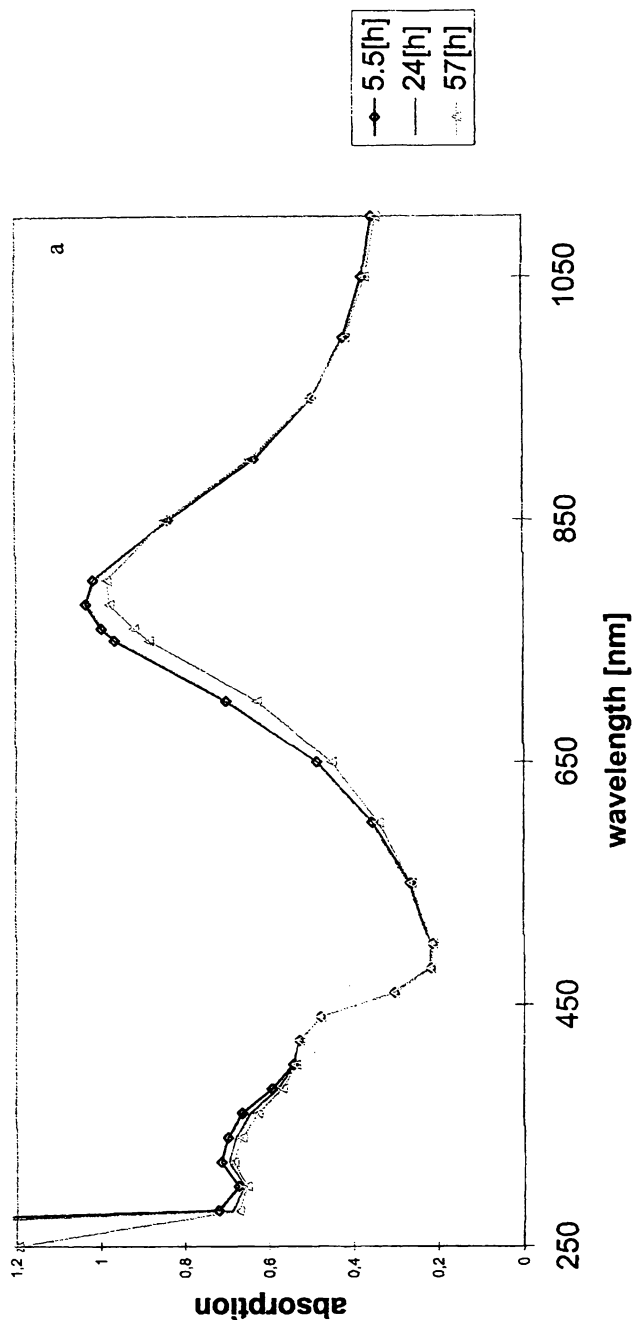


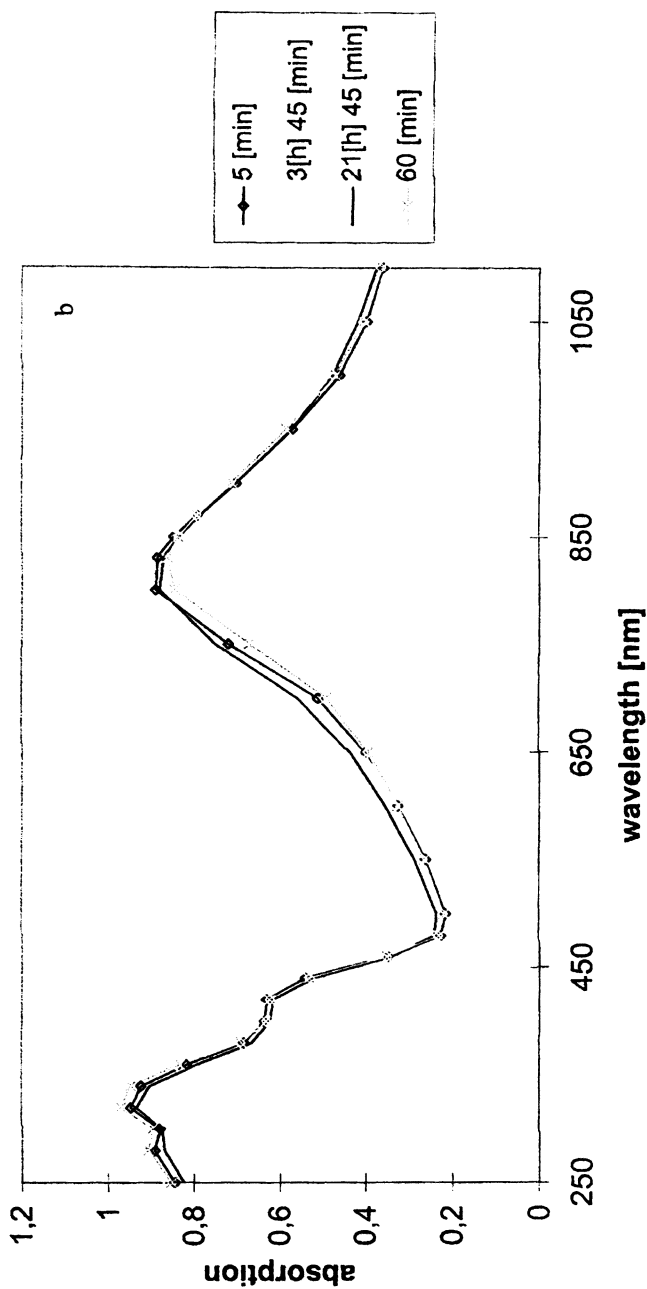
Figure 6. Spectral change of PANi on PP film without iron

a) measured in 0.1 M pTS

b) measured in 1 M NaCl

(Reproduced with permission from reference 24)

Continued on next page.

Figure 6. *Continued.*

- a) with the use of additional oxygen in the electrolyte
- b) using degassed solutions

during spectroscopy.

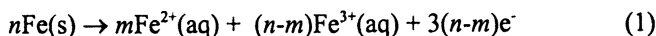
These experiments have shown, that oxygen is responsible for transforming Fe^{2+} to Fe^{3+} , as well as in the re-oxidation of the Leuco-PAni to the original (green) PAni salt.

The reaction scheme shown in Figure 3 is describing the whole passivation reaction sequence of polyaniline on the iron surface: polyaniline is acting as a redox catalyst and as a noble metal with respect to iron (or copper, stainless steel, aluminum, zinc and others).

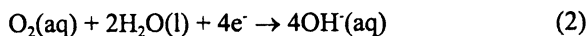
Difference between „Corrosion“ and „Passivation“

The formation of oxides during the corrosion process is completely different to the passivation described before.

Corrosion occurs in the presence of water, salt and oxygen, during which iron or steel undergo an electrochemical process in which different locations of the iron surface act as electrodes. At the local anode, iron is oxidized to soluble Fe^{2+} and Fe^{3+} ions:



At the local cathode, hydroxide ions are formed:



Rust, which forms subsequently, is composed of FeO , Fe_2O_3 , Fe_3O_4 and other mixed oxides, $\text{Fe}(\text{OH})_x$, and Fe^{2+} salts (chlorides, sulfates etc.). This highly irreproducible and irregular composition opens up new surfaces for self-catalytic growth - mainly Fe^{3+} salts acting as rust formation catalysts.

In the presence of the organic metal coating, a completely different galvanic process occurs, in which PAni is the cathode and iron the anode. This arrangement seems to be distributed evenly over the entire surface. The surface potential is shifted from formerly -400 mV (approx.) to +250 to 400 mV.

Now, the reaction as described above is taking place finally leading to Fe_2O_3 . Fe_2O_3 adheres very well and provides a barrier to further rust formation.

Optimal Polyaniline Formulation Required

It should be noted, that the new ennobling and passivation technology is only optimal and well reproducible with the advanced Organic Metal (PAni) dispersions in specially composed coating formulations. The particle size of PAni in the dispersion is about 70 nm. At such a small particle size level, the dispersed Organic Metal phase will form the necessary network of flocculation structures at very low concentrations²⁶ (we are using only about 2% PAni in our liquid coatings).

Other PAni formulations like „soluble polyaniline“²⁷ do not offer any corrosion prevention effect. It is important to know, that the sample mentioned in Table 4 in Ref. 27 is the Ormecon PAni dispersion (in other publications P. Kinlen referred to it as „PAni/thermoplastic“), which was transferred by us to Monsanto for their comparison tests. It performed as well as like a zinc-rich primer with an epoxy topcoat²⁸. The samples „PAni/Phenoxy“ and „PAni/Acrylic“ are PANDA products, which do not show any interesting anti-corrosion effect²⁹. Maybe this is due to the special structure of PANDA, which is called a „solution“, but is in fact a fine dispersion with a (mainly insulating) dispersion stabilization layer adsorbed on the particle surface³⁰.

Other approaches like neutral PAni dispersions in NMP (wrongly been assigned as „solutions“) to be doped after application on the metal³¹ are not only not effective, but also not practical³².

N-PAni (the emeraldine base, „undoped“) is also contributing some anti-corrosion effect, but by a factor of 100 to 1000 smaller (see Ref. 13); this effect is probably due to its amine groups and could therefore be attributed to a pure inhibition mechanism.

Development of Polyaniline Primers with a New Scientific Strategy

Starting the development of primers and coating systems, three problems had to be faced with: a) we had no practical experience in corrosion phenomena, and even less in coatings; b) experts in the field of corrosion and coatings disregarded of our discovery; c) as a newcomer in this field, Ormecon had to act promptly in at developing and testing the new coatings.

Soon (cf. Ref 12c, 22) it turned out, that a polyaniline containing primer only was not sufficient as a practically convincing coating system, but that it needed a top coat. This top coat (or possibly an intercoat between primer and final top coat) had to fulfill certain requirements in order to be compatible with the primer. The primer itself had to meet the following demands:

- the full metallic (ennobling) and catalytic (passivating) properties
- good adhesion to the metal substrate (in dry stage, as well as during the

corrosion attack / dry and wet adhesion)

- good overcoating ability
- practical application demands (viscosity, drying time, ...)
- The top coat (or the intercoat, resp.) had to offer a good (chemical and physical) compatibility with the primer³³
- sufficient „sealing“ properties
- all necessary weatherability and other surface properties needed (colour, gloss, mechanical or chemical and UV resistance, ...).

„Scientific Engineering“: a new Research and Development Tool for Anti-Corrosion Coatings

The concept is based on the idea to directly probe or measure the key parameters for an optimal anti-corrosion performance:

1. open circuit potential measurement (to measure the potential shift)
2. scratch test (to probe the range at which the potential shift extends to uncoated areas)
3. Scanning Kelvin potential measurement (SKP), evaluating the delamination
4. electrochemical impedance spectroscopy (EIS), using a new FFT technique to measure the diffusion of ionic species through the coating,-

all of it over a certain time with the progress of corrosion attack.

Measurement 1 and test 2 are used as a first screening. Measurement 3 and 4 are used for advanced screening of the samples, before they were combined with an immersion cycling, cycling climate test or salt spray test for those systems which pass the advanced screening successfully.

Open Circuit Potential Measurement

This routine measurement can be performed under various well-known conditions (see Refs. 12b, 13, 15) which does not require any further description. Schauer et al. (16) have confirmed the range of the high potential shift found by us earlier (cf. Ref. 12). Our internal specification is a potential shift to at least +100mV and a long term stability of it.

Ormecon Scratch Test

This test can be performed in two ways, (a) by coating half of a panel with CORRPASSIV™ primer, the other half with a conventional epoxy primer, then applying a top coat (e.g. 2-C EP) on both primers, or (b) by coating a panel completely with the coating system to be tested.

The coating is then injured with scratches 1 mm wide and 50 mm long, down to the metal. The panels are immersed in 10% salt containing water. After 1 night and after 100 and 300 hours, the panels are checked with respect to rust formation in the scratch: only those systems will be accepted to become commercial CORRPASSIV™ products, where no rust will be formed within the open scratch during this time (Figure 7). Conventional systems, also the very good ones, will develop rust in the open scratch, because the area there is not protected. They also develop rust under the coating, propagating at various velocities.

The protection and the ennobling provided by CORRPASSIV™, however is a far-reaching effect because of its metallic nature. We are assuming furthermore, that it is not only the ennobling which provides protection for open scratches of this size, but also the passivation by Fe₂O₃ formation: this oxide can be found up to about 400 μm away from the coating edge as seen by XPS³⁴.

This protection can be effective more than 1 mm away from a coating edge, which makes anti-corrosion systems based on the Organic Metal a powerful edge corrosion protection technology. Even much bigger areas being protected have been found even after removal of the coatings³⁵.

Scanning Volta Potential Measurements (Kelvin Probe)

The Volta potential measured with a Kelvin sensor is suitable for non-contact measurements of surface potentials even under undamaged surface coatings^{36,37}. The function principle and experimental set-up is shown in Figure 8a/b. The measurement object, the working electrode, and the reference electrode of the Kelvin probe form a capacitor, due to the small gap between them. Between those two electrodes a potential is developed, the amplitude of which gives a measure of the chemical nature of the material on the surface of the metal. A periodic variation in separation by means of an actuator built into the sensor changes the capacitance of the set-up. The resulting signal is converted to a measurement signal by means of a lock-in amplifier³⁸.

The resulting data is a scan of the surface Volta potential of the metal under the coating, which can - under certain conditions - be related with the corrosion potential. The parameters needed for this method³⁹ are the values of the different potentials, (a) between various sites, i.e. between the open scratch and the not injured areas of the coating (b) with the change in immersion time.

With this technique, adhesion (or delamination) of the coating under corrosive attack is monitored. The underfilm corrosion propagation velocity (more precise: the corrosion potential propagation velocity, due to the first delamination of the coating before even first corrosion occurs) can be quantitatively measured.

Figure 9 is showing a development of the Volta potentials in the open scratch and in the neighbourhood under the coating with time (CORRPASSIV™ primer plus top coat). The potential change during the first

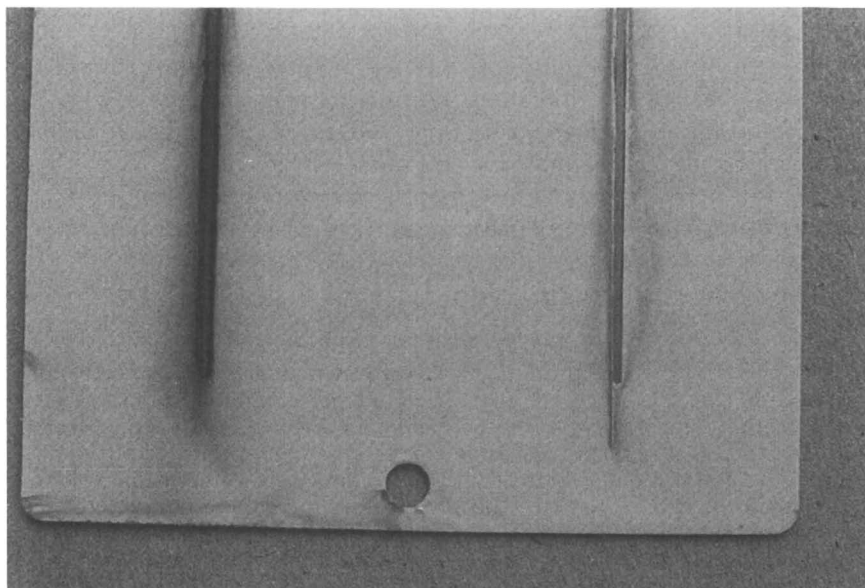


Figure 7. St-14 panel after 300 hours in permanent immersion test (DIN 50905 T4) in 3% NaCl solution

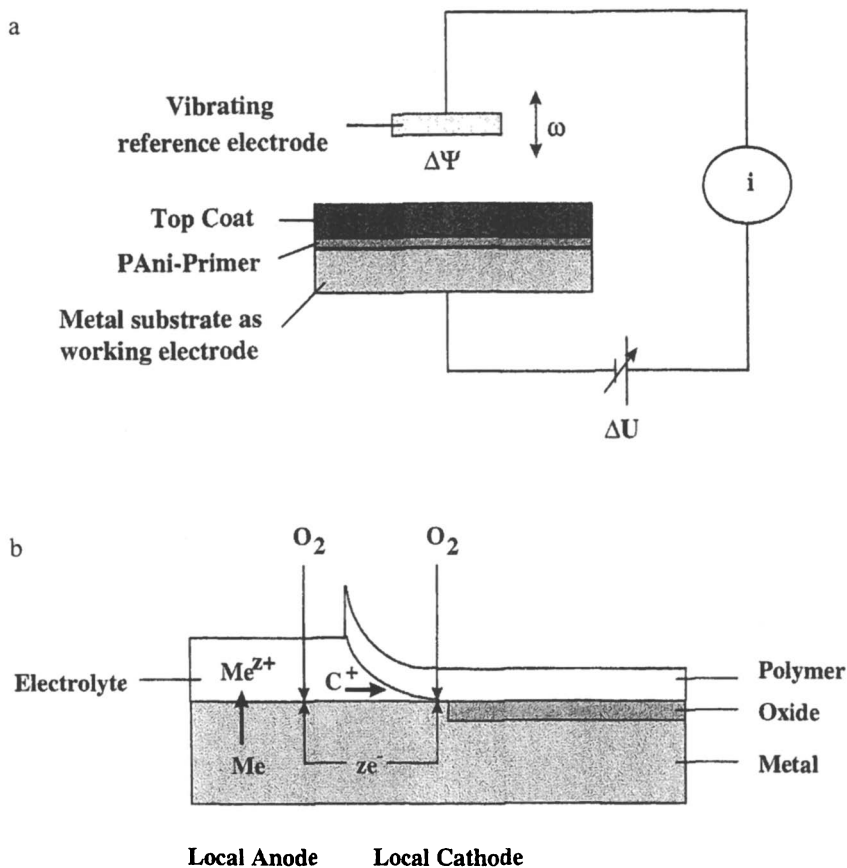


Figure 8. Function principle of corrosion potential measurements using a scanning Kelvin-probe

(a) function principle and

(b) galvanic element forming under delaminated metal/coating interface (Reproduced with permission from reference 42)

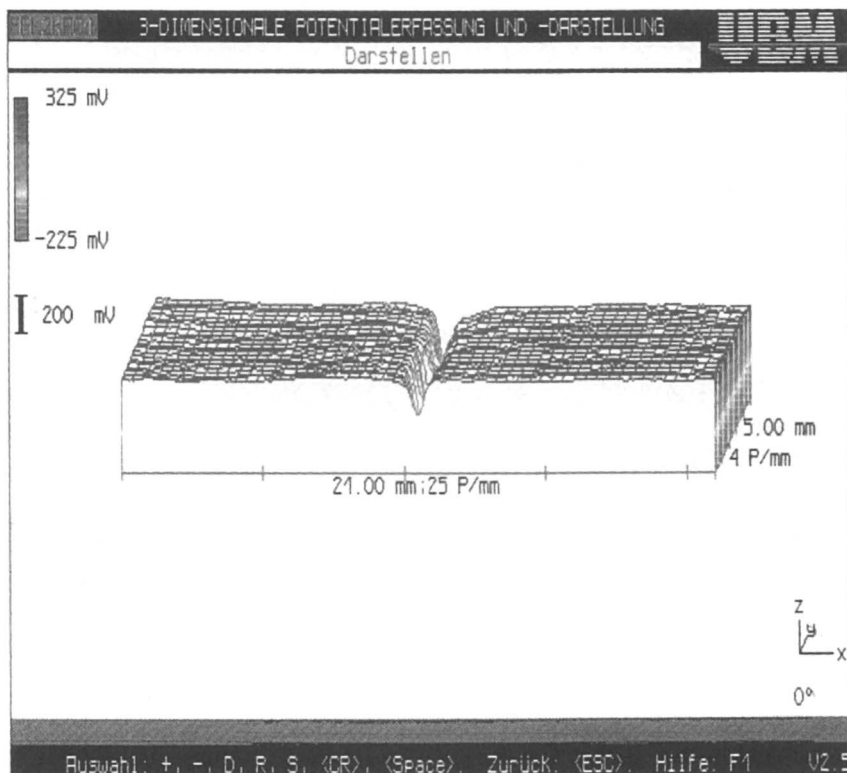
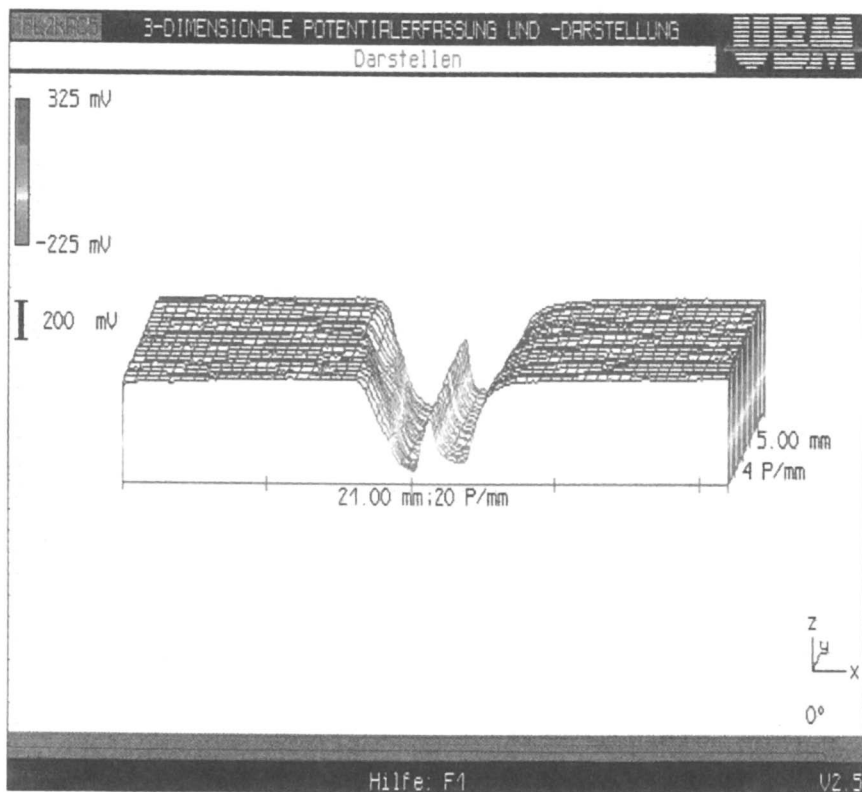


Figure 9. 3D-plots of the potential development in the scratch and under the coating; top $t=0$, bottom $t=24$ hours of immersion, for sample #2, cf Figure 10
Continued on next page.

Figure 9. *Continued.*

24 hours of immersion in salt water (after usual conditioning in humid atmosphere) is examined. The best system, forms „W“ form of the potential distribution, with no potential approaching strong enough negative values (Figure 10), to allow corrosion. Only, when the bottom of the „W“ form reaches values of -200mV or lower, a delamination (the prerequisite for corrosion) can be observed and corrosion may start. The delamination velocity is estimated with widening of the negative corrosion potential „W“ valley, if it occurs at all (Figure 11).

In contrast, scratches in coatings without Organic Metal primer have a big potential difference, a broad and deep valley, resulting in a high underrusting propagation velocity (Table I). In the middle of the scratch the potential is strongly increasing very quickly as the sign of rust formation.

Table I. Summary of SKP Results for Various Coating Systems

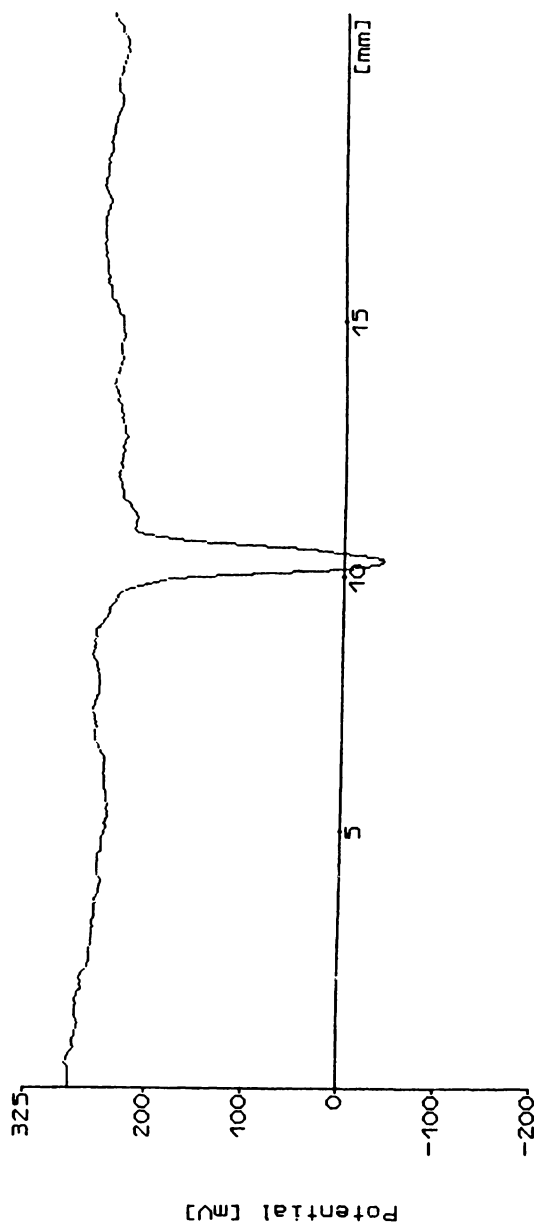
#	sample primer/topcoat	delamina- tion speed [$\mu\text{m}/\text{h}$]	potential E [mV] under coating	potential E [mV] in the scratch
1	„Corrpassiv“/2-C EP	0 (-3)	0 to 150	100 to 150 (no rust)
2	„Corrpassiv“/2-C AY	12 - 30	150 to 300	-100 to -300
3	„Corrpassiv“/1-C AY	35 - 80	150 to 300	-50 to -300
4	primer like in # 1 without OM/2-C EP	20 - 40	-200 to -100	-200 to +100 (rust)
5	EP/2-C EP	50 - 60	-200 to -100	50 to 250 (rust)
6	Zn-EP/2-C EP	30 -35	-150 to 0	-700 to -800

SOURCE: Ormecon Chemie GmbH & Co. KG

Three systems, each built up on the same primer, but top coated with different paints, have all passed the scratch test but were different in their Open Circuit Potential (OCP). The question to be evaluated was: Is there a difference in the delamination velocity? Table 1 shows the answer „Yes“: after 24 hours, significant differences can be noticed.

Note, that the performance order is in parallel with all other results. Primer formulations (same basis) without polyaniline under even the best top coats show 5-10 times quicker delamination. The best top coat on CORRPASSIV™ primer alone (on epoxy primer or even on Zn-rich epoxy primer) does not perform comparably well at all. It is the most important conclusion, that underrusting or persistent passivation, resp., is also strongly influenced by the top coat, a conclusion which is not at all self-explanatory, but can be understood in view of (Refs. 24, 14) and Figure 1.

The internal specification was set as an underfilm corrosion propagation velocity of between 3 and 5 $\mu\text{m}/\text{h}$ or less. Epoxy coating systems (primer plus top coat) are generally showing a velocity of around 20 to 60 $\mu\text{m}/\text{h}$, a factor of 10 or more faster than CORRPASSIV™ systems.



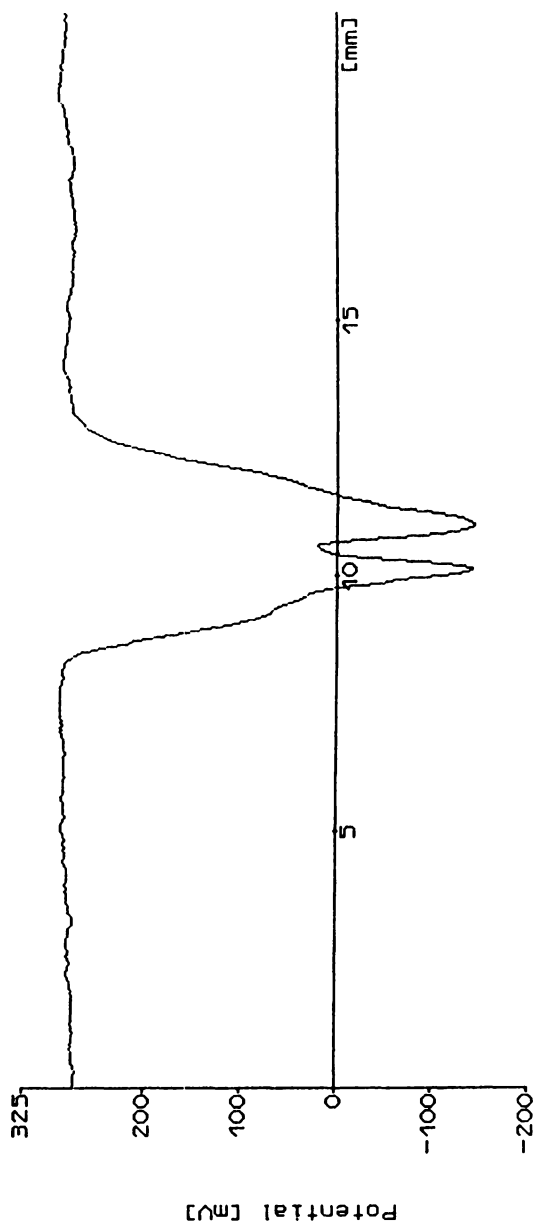


Figure 10. Development of a deep „W“ corrosion potential valley in a coating system (#2) not meeting the specifications: at (top) $t=0$, (middle) $t=12$, (bottom) $t=24$ hours immersion time, reaching the corrosion potential around -200mV and showing underrusting ($12\text{-}30\ \mu\text{m/h}$) *Continued on next page.*

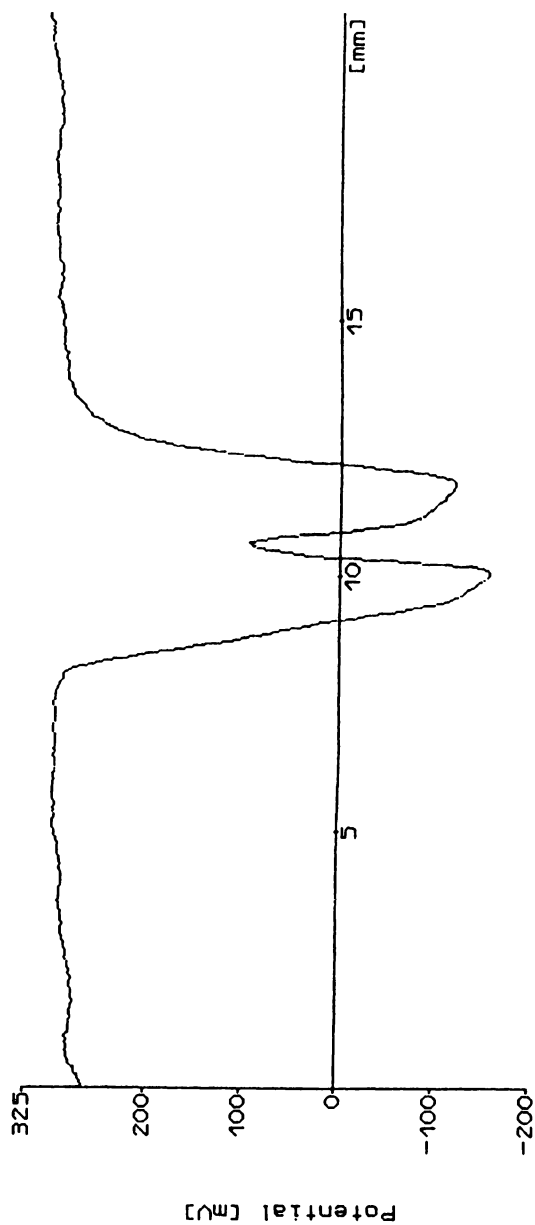


Figure 10. *Continued.*

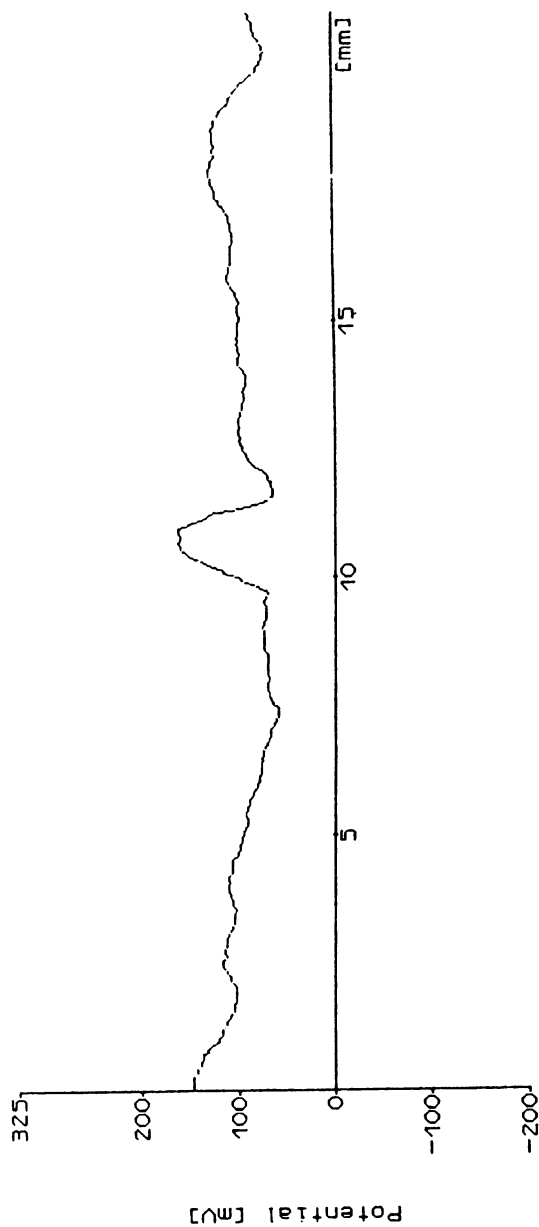
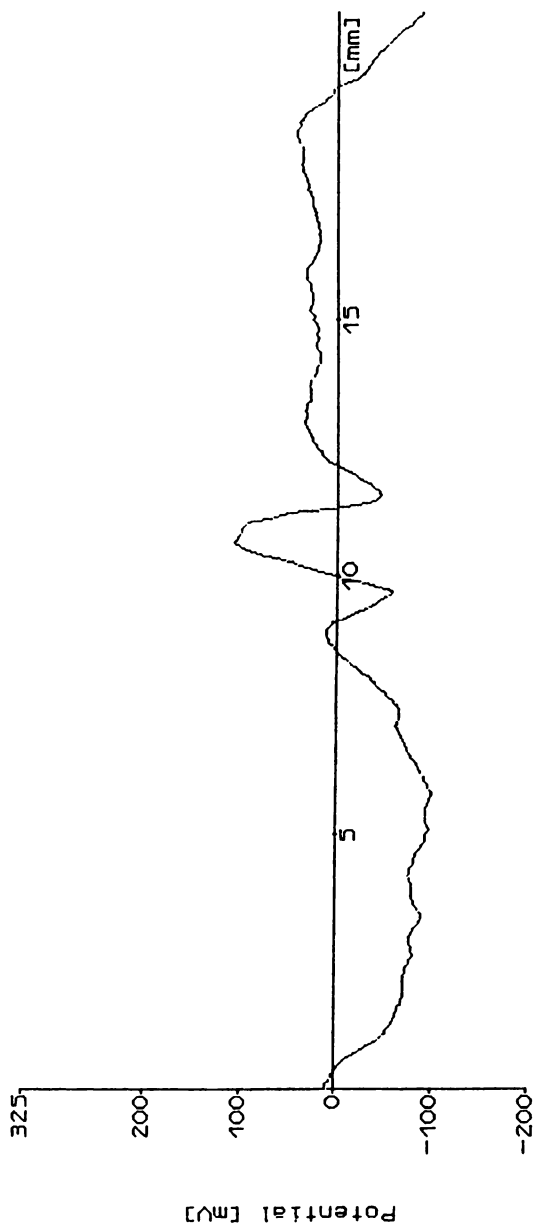


Figure 11. Development of a shallow „w“ potential distribution at elevated (passivation) level in the best performing coating system: (#1) at (top) $t=0$, (middle) $t=12$, (bottom) $t=24$ hours of immersion: no corrosion, no underrusting *Continued on next page.*



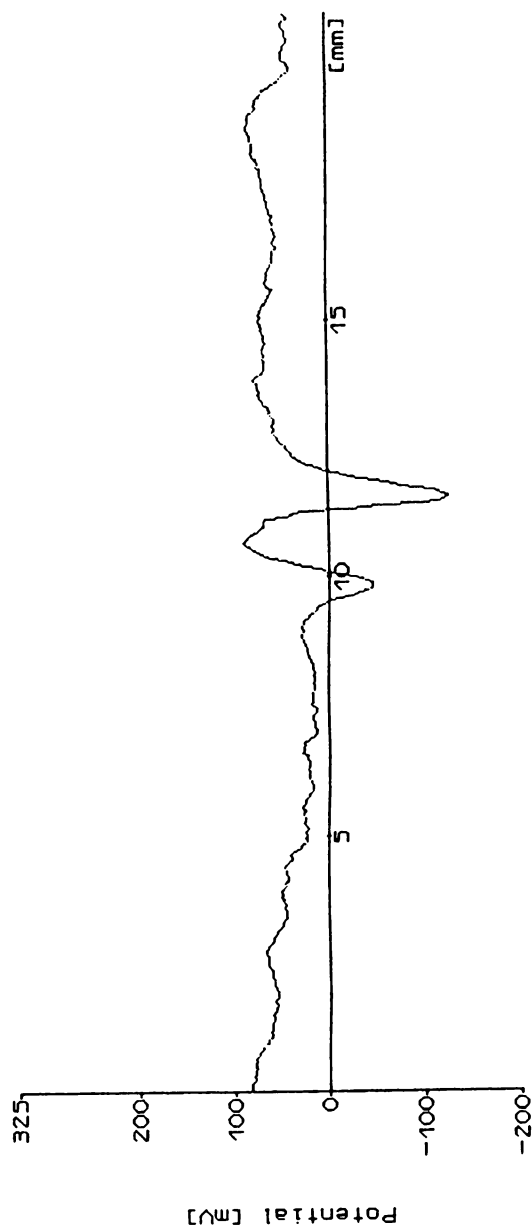


Figure 11. *Continued.*

Zn-rich epoxy primers (with epoxy top coat) do even show much quicker underfilm propagation, at least in the first 1-2 days. Such systems are not scratch-tolerant, they perform very well only with intact coatings. In comparison to that, the systems based on Organic Metals are performing extremely well both with and without scratches.

Only the best cathaphoretic coatings on Zn-Phosphate electrochemically pretreated steel in car manufacturing are showing figures of 3-5 $\mu\text{m/h}$ comparable with CORRPASSIVTM (0 - 5 $\mu\text{m/h}$).

Electrochemical Impedance Spectroscopy (EIS)

EIS is used to predict the performance of the entire primer / top coat (or eventually including an intercoat) system. This technique has been developed together with G. Popkirov based on his new FFT-EIS technique⁴⁰. Measurements are carried out with a three-electrode system using a cell as described in⁴¹. The experimental set-up for this Fourier Transformation Electrochemical Impedance Spectrometer is given in⁴². A frequency-rich perturbation signal with a small amplitude is applied to the electrochemical cell controlled by an EG&G Princeton Research potentiostat Model 263A. In the present investigation a computer programmed sum of 42 sine waves distributed over 4 decades was used to synthesize the perturbation signal of a home-built signal generator. The peak-to-peak amplitude of the perturbation voltage was usually 20 mV. The perturbation and the response signal are amplified and filtered by a Stanford Research Systems Inc. Model SR 640 Dual Channel Low-Pass filter. A/D and D/A conversion, timing and controlling were carried out by a 16-bit, 100 kHz transient recorder PC-card from United Electronic Industries, Inc. Model Win- 30/3016. Impedance spectra were evaluated by Fourier transformation of the perturbation and the response signal (cf Fig. 2 in Ref. 42). The data analysis was carried out using a simple $R_E (R_C C_C)$ equivalent circuit, where R_E is the electrolyte resistance, R_C is the resistance of the coating and C_C is the capacitance of the coating.

For the experiments describing the procedure and representative examples, lacquer systems were used on CORRPASSIVTM primer as follows:

1. two-component epoxy top coat - amine hardened = 2-C EP
2. two-component acrylic top coat = 2-C AY
3. one-component acrylic top coat = 1-C AY

The recording of impedance data takes about 20 seconds, Nyquist and Bode plots are available for interpretation after another 15 seconds. The bottleneck for measuring more samples is only the number of available immersion cells, as the samples are placed and immersed in the same cell for the measurement. As not all of the systems under development get

measured, but only those which have passed the first screening, this is not a practically important limitation.

The performance of the complete system under evaluation can be assessed after 2 to 4 weeks. If the impedance spectrum does not change significantly during this time (as shown by sample #1) a very good long-term corrosion protection performance can be expected.

Systems, which fail, are losing their resistance during the first weeks or even quicker. It can be seen, that the stability of the EIS spectra or loss of the pure capacitance behavior - parallel to the results found in VDA cycling test - is showing good or bad performance.

It should be noted, that systems (samples #5 and #6) composed by a pure epoxy primer or a Zn-rich epoxy primer top coated with the same EP top coat as in CORRPASSIV™/2-C EP (sample #1) again perform worse.

The experimental EIS data for three different top coated steel panels as a function of immersion time have been observed between 50 mHz and 1 kHz immediately on immersion and after 24, 48 and 140 h of testing in 5% NaCl. EIS data for polymer coated metals are usually determined at the corrosion potential E_{corr} ⁴³. Since for very protective coatings E_{corr} cannot be measured, a potential which is close to that for bare metals is reasonable. For substrates in aerated NaCl a value of -560 mV vs. Ag/AgCl was applied.

Under corrosive conditions the coatings of 2-C epoxy and 2-C acrylic top coat behaved similar at first, showing a coating resistance of 1.4 to 1.6 M Ω /cm² and a coating capacitance of about 50 pF/cm². During an immersion of 6 days changes occur for the 2-C acrylic coated sample. The capacity increased to 170 pF/cm² and the resistance decreased to 200 k Ω /cm² while they did not change for the epoxy during the test duration. In contrast to these coatings for the 1-C acrylic top coat the capacity and the resistance changed drastically in a duration of only 1 day to a resistance of 50 k Ω /cm² and a capacitance of 90 pF/cm².

For a better comparison, also changes in the systems using none or a zinc-rich primer with the same 2-C EP top coat were determined. During the first 70 h the systems seemed to behave similar to the corresponding CORRPASSIV™/2-C EP system, but after 140 h changes occurred.

The resistance decreased to values of 100 and 10 k Ω /cm² and the capacitance increased to values of 90 and 100 pF/cm², respectively (42). Only for the CORRPASSIV™/2-C EP system the coating resistance and capacity remains constant. For all other systems, including the 2-CP EP top coat without primer, the resistance decreases by a factor of 10 and the coating capacity rises by a factor of about 2. For the Zn-EP/2-C EP system the resistance changes by a factor of 100. The changes cannot only be explained by water absorption of the top coats. Compared with the systems 2-C EP and Zn-EP/2-C EP using the same top coat the CORRPASSIV™/2-C EP system should change as well. Thus the changes may have to be explained by changed ion concentrations in the coatings, i.e. iron, zinc and hydroxide ions. According to these findings a corrosion protective effect can be assigned to the CORRPASSIV™ primer.

These results demonstrate that EIS is capable of detecting localized corrosion phenomena such as disbonding of the coating and initiation of corrosion at the metal/coating interface as well as deterioration of the polymer coating and loss of its protective properties in an early stage.

For intact coatings the major deterioration mechanism is the transport of electrolyte solutions to the interface between the steel substrate and the coating. This transport results from the equalization of concentration and temperature differences. Water molecules disrupt the bonding and polar interactions which are responsible for a good adhesion at the interface⁴⁴. Due to the loss of adhesion underfilm corrosion gets possible.

Climate cycling test (VDA) / Salt Spray Test

This test is used only after successful basic and advanced screening (see sub-sections before).

The systems described above (scratched panels) have been subjected to these accelerated corrosion tests for comparison of these test results with our 4-step method⁴⁵.

The tests showed that all three coating systems provide highly efficient corrosion protection and complete suppression of underfilm corrosion over a period of more than 1000 h; especially with top coat 2-C EP no change at all was found even after 1000 h. The other top coats allow some blistering. None of the systems are really failing, but they are slightly different in their overall acceptable performance.

The 4-step „Scientific Engineering“ test method allows to differentiate much quicker and much more sensitively than the generally accepted accelerated corrosion tests do.

Recent Progress

The performance of our coatings is still far from the end of their optimization potential, but commercial applications realized in the last 5 years show that they improve the anti-corrosion capacity of conventional coatings by a factor of two to more than 10. These Organic Metal coatings are already proving their capabilities in marine environments, waste water treatment, chemical plants, coal mines and in public constructions in towns, parks and sport arenas⁴⁶. Conventional pumps, transporting highly corrosive waters in underground mining operations have to be replaced every 8-12 weeks. Since more than 3 years, such pumps are in use with polyaniline coatings - and their life-span does not seem to end soon: an enhancement of usage time by a factor of far more than 15.

Ormecon was initially forced to develop such paints, because paint manufacturers were reluctant to work with this new technology. However, now that such products have shown first commercial success, several independent companies have begun developing their own paints based on

this technology. A first system supplied by an independent paint manufacturer using the Organic Metal is HAKUDUR OM*. Ormecon's coating systems are continuously under improvement.

The earlier standard CORRPASSIV 4900 formulation has always shown a relatively weak wet adhesion (Gt 5). In most cases, this is not critical, but some customers request for better wet adhesion. Therefore a new primer was formulated, and with apparently only minor changes, the wet adhesion improved drastically to Gt 0.

The „minor changes“ were focused on the interfaces between polyaniline and the primer matrix, and a further reduction of the Organic Metal concentration by 30%. This resulted in a more than 30% improvement of the corrosion protection performance (undercutting, delamination velocity), besides the improvement in wet adhesion. All other properties remained the same positive.

A new primer based on polyester has been developed which is thermally curing. This primer is commercially used in a waste water filter system and has shown an extraordinary performance. The filter is internally and externally coated with the primer, then cured, and coated with a top coat (2-C-EP). This system has proven to outperform all other conventional coating systems tested under comparable practical conditions. The extraordinary result was, that the customer can now use cast iron for producing this filter, instead of stainless steel, which results in an incredible cost advantage at even better corrosion resistance.

Another new development is the first commercially useful 2-component epoxy primer containing dispersed Organic Metal. This primer is curing at room temperature. In contrast to other CORRPASSIV primers, it will be applied at 60 μm layer thickness, a requirement expressed by industrial coating companies, especially for rougher steel surfaces. Also, coaters have expressed a demand for 2-C-EP primers as an alternative for curable primers, where the first primer generation only consisted of physically drying, not chemically curing ones.

No negative observation (rust, blisters, ...) have been made after salt spray test, the wet adhesion is optimal (Gt 0), and the scanning Kelvin probe shows only 50% of the delamination velocity ($0.15 \text{ mm} / \text{h}^{1/2}$) compared to the standard CORRPASSIV 4900.

Moreover, it is very positive, that this primer can be directly top-coated with PU, which was not possible with the first generation of primers. This allows to have weatherable coating systems consisting of only 2 layers (compared to 3 layers, the intermediate being an epoxy layer).

EIS and SKP results for this new system in comparison with conventional corrosion tests will be published⁴⁷.

Moreover, it should be mentioned that there is significant progress in the development of water based polyaniline primers. Conventional water based anti-corrosion coatings have been outperformed with presently

* supplied by Chemische Werke Kluthe, Heidelberg, Germany, cf www.kluthe.de

available formulations, however, we do not want to commercialize our systems before they are not equal to the internal benchmark CORRPASSIV 4900.

Passivation of Copper

A completely different field, but no less interesting from the standpoint of Organic Metal - conventional metal interactions, is the passivation of copper by polyaniline.

During storage, unprotected copper surfaces get oxidized, leading to the formation of Cu_2O and later to a mixture of Cu_2O and CuO . By coating copper with organic agents (imidazole, benzotriazole or PANi) the surface can be protected⁴⁸. When treated with a dispersion of PANi, copper is covered with a thin film and the corrosion rate of the metal is reduced⁴⁹. Upon aging at high temperatures, various colors are developing. We studied the mechanism of PANi-Cu interaction. Results are presented on the formation of Cu(I)-complexes, Cu(I) and Cu(II)-oxides with polyaniline and without any surface protection.

Experimental

The copper foil (99.999% Goodfellow) used was polished using 6 μm , 3 μm and 1 μm diamond paste. It was rinsed with ethanol and cut into 1.5 x 1.5 cm pieces. Copper was etched for 1 min in 1 molar sulfuric acid, rinsed with de-ionized water and a) air dried or b) pretreated by immersion in a water dispersion of OM (0.01% and 3% PANi, Ormecon) for 1 min, rinsed with water and air dried. They were annealed in a convection oven (Nabertherm) at 155°C for different hours.

Electrochemical experiments were performed using a potentiostat/galvanostat (EG&G, model 263A) computer controlled by an IEEE-488 GPIB interface board. For chronopotentiometric reduction of copper oxide films a current of -100 $\mu\text{A}/\text{cm}^2$ was applied. The electrochemical reduction was performed in a borate buffer at a pH of 8.5 in a 50 ml glass cell with three 14.5/23 standard tapers. The copper foil served as working electrode, a platinum wire as counter electrode and a Ag/AgCl (3 mol/l KCl) as reference electrode, all mounted with taper joints.

Surface morphology and appearance were determined by scanning electron microscopy using a Philips XL30 SEM.

Results and discussion

Aging of copper pretreated with the OM dispersion in comparison with sulfuric acid etched plates causes the color to change with annealing time from various violet and bluish tones into silver and bright golden. This is

due to interference of light between the upper and lower thin oxide layers. Varying oxide layer thickness causes different colors. The copper oxide thickness was measured by sequential electrochemical reduction⁵⁰. The electric current applied is directly proportional to the oxide mass, provided the reduction current and the depleted area remain constant.

A relationship between color and oxide layer thickness was found. The change of oxide layer thickness for Cu₂O and CuO is shown in Figure 12.

The growth of copper oxides on surfaces etched with acids is proportional to time as expected for oxidation of metals in the gas phase. The PANi pretreated surface behaves different. The formation of CuO is proportional to \sqrt{t} while Cu₂O decreases exponentially to a minimum of 0.6 nm. From the slope of a CuO thickness vs. \sqrt{t} plot, the rate constant for the formation of CuO was calculated.

Rate constants at different temperatures were determined for both sample sets, summarized in Table II. The slope of an Arrhenius plot of rate constant vs. $1/T$ gives an activation energy of 35 kJ/mol for CuO formation. Without PANi an activation energy of 50 kJ/mol was calculated.

Table II. Rate constants for CuO formation with and without OM (PANi).

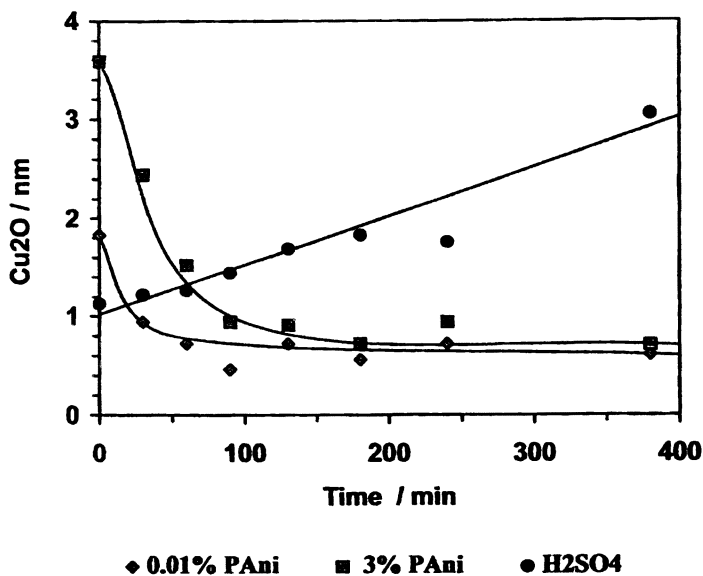
<i>T</i> [°C]	<i>With PANi</i>	<i>Without PANi</i>
	<i>k</i> [nm s ^{-1/2}]	<i>k</i> [nm s ⁻¹]
100	0.044	0.00012
125	0.199	0.00095
155	0.363	0.00175
175	0.428	0.00223
200	0.537	0.00507

SOURCE: Reproduced from Reference⁵¹. Copyright 2001 Elsevier Science

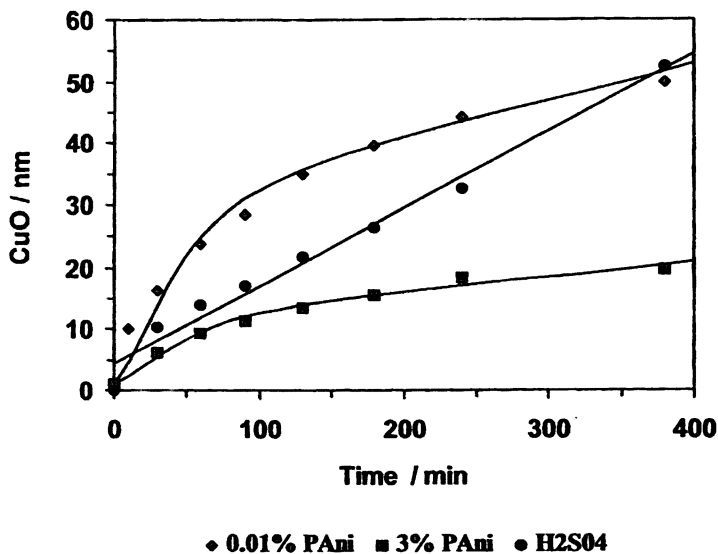
The \sqrt{t} dependence occurs because the formation of CuO is a diffusion limited reaction: copper is oxidized by PANi, the copper ions are transported through the film and form a Cu(I)-PANi complex; by diffusion Cu(I) ions are transported to the film-gas interface undergoing partial oxidation to Cu(II) easily because of the lower activation energy.

Analysis of the surface morphology and appearance by using SEM shows that an uniform copper oxide layer is formed on the PANi treated sample (Figure 13). The untreated copper is very rough (Figure 14).

During immersion of Cu in a dispersion of PANi a Cu(I)-PANi complex forms on the surface which determines the oxidation of the copper and the passivation of the surface. A Cu₂O layer with almost constant thickness is formed, the growth of the CuO layer is proportional to \sqrt{t} of aging.



Formation of Cu(I) oxide layer depending on aging time.



Formation of Cu(II) oxide layer depending on aging time.

Figure 12. Formation of Cu oxide layers depending on aging time.
(Reproduced with permission from reference 51)

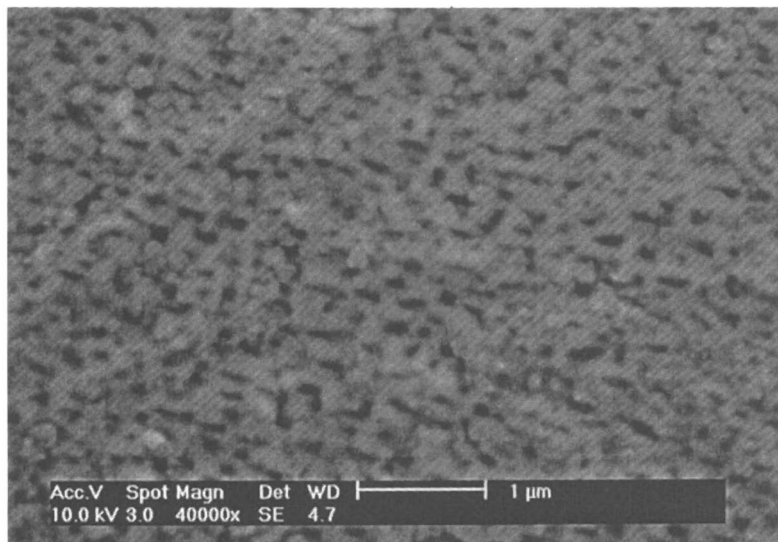


Figure 13. SEM image of golden copper/Pani surface after 2h at 155° C. (Reproduced with permission from reference 51)

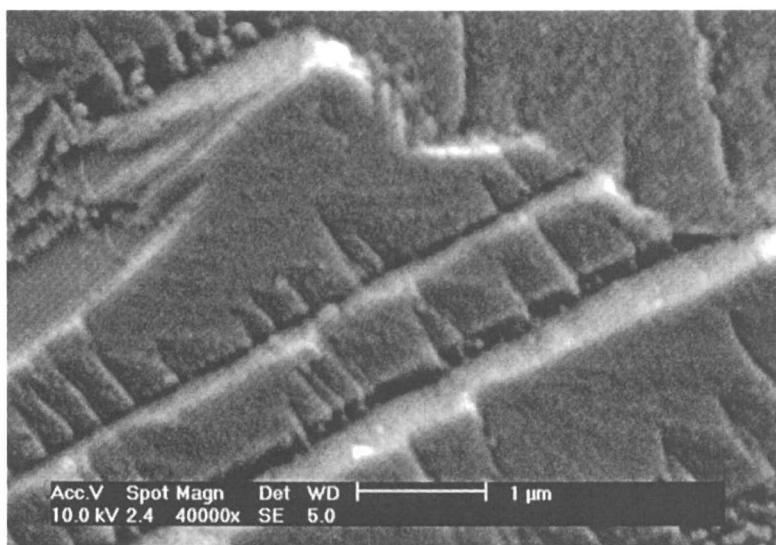


Figure 14. SEM image of copper oxidized by annealing at 155° C for 2 h. (Reproduced with permission from reference 51)

Summary

When applied in its Organic Metal state, well dispersed and in appropriate binder formulations, eventually coated with compatible top coats, polyaniline can provide a superior corrosion protection. Practical laboratory standard tests and a new electrochemical evaluation strategy show extraordinary corrosion protection abilities of such systems, outperforming state-of-the-art coatings. This is also observable for copper (and other metals like aluminum). Practical commercial applications do in fact reproduce the laboratory results, and are showing partially even incredible lifetime enhancements in very corrosive environments. Reference objects are publicly available for independent evaluation of the technology's capabilities.

References

- ¹ Shirakawa, H.; Louis, E.; MacDiarmid, A.; Chiang, C.; Heeger, A. *JCS, Chem. Commun.* **1977**, 578,
- ² Wessling, B. *Makromol. Chem.* **1984**, 185, 1265-1275
- ³ Wessling, B. *Chemical Innovation* **2001**, 1, 34-40
- ⁴ Wessling, B. *Zeitschrift f. Physikal. Chemie* **1995**, 191, 119-135
- ⁵ Wessling, B.; Srinivasan, D.; Rangarajan, G.; Mietzner, T.; Lennartz, W. *Eur. Phys. J. E* **2000**, 2, 207-120
- ⁶ 'Organic Metal' is a registered trademark to Zipperling Kessler
- ⁶ Pelster, R.; Nimtz, G.; Wessling, B. *Phys. Rev. B* **1994**, 49, No. 18, 12718-12723
- ⁷ Wessling, B. In *Handbook of Nanostructured Materials and Nanotechnology*; Nalwa, H.S.; Ed., Academic Press, 1999, Vol. 5, Chapter 10, pp 501-576
- ⁸ Wessling, B.; *Synth. Met.* **1998**, 93, 143-154
- ⁹ Wessling, B.; German Patent P 37 29 566.7, Zipperling Kessler & Co. 1987
- ¹⁰ DeBerry, D. W. *J. Electrochem. Soc.* **1985**, 132, 1022
- ¹¹ Mengoli, G.; Munari, M.; Bianco, P.; Musiani, M. *J. Appl. Polym. Sci.* **1981**, 26, 4247-4257
- ¹² a) Wessling, B. DE 43 34 628 A1, Zipperling Kessler & Co., 1993
b) Wessling, B. *Adv. Mater.* **1994**, 6, No. 3, 226-228
c) Wessling, B. PCT WO 95/00678, Zipperling Kessler & Co., 1993
- ¹³ Lu, W.-K.; Elsenbaumer, R.; Wessling, B. *Synth. Met.* **1995**, 71, 2163-2166
- ¹⁴ Wessling, B. *Synth. Met.* **1997**, 85, 1313-1318
- ¹⁵ Lu, W.-K.; Basak, S.; Elsenbaumer, R. In: *Handbook of Conducting Polymers, 2nd Ed.*, Skotheim, T.A.; Elsenbaumer, R.; Reynolds, J.R. Editors, M. Dekker: , 1998, pp 881-920

- ¹⁶ Schauer, T.; Joos, A.; Dulog, L.; Eisenbach, C.D. *Progress in Organic Coatings* **1998**, 33, 20-27
- ¹⁷ a) Hugot-Le Goff, A.-M.; Palotta, C. *J. Electrochem. Soc.* **1985**, 132, No. 11, 2805-2806
 b) Boucherit, N.; Delichere, P.; Joirot, S.; Hugot-Le Goff, A.-M. *Mat. Sci. Forum* **1989**, 44&45, 51-62
- ¹⁸ in case of copper, the oxide is Cu₂O (Wessling, B.; Posdorfer, J.; Strunskus, W. *Synth. Met.* **2001** 121, 1317-1318
- ¹⁹ a) Nimtz, G.; Enders, A.; Marquardt, P.; Pelster, R.; Wessling, B. *Synth. Met.* **1991**, 45, 197-201
 b) Pelster, R.; Nimtz, G.; Wessling, B. *Phys. Rev. B* **1994**, 49, No. 18, 12718-12723
- ²⁰ a) Subramaniam, C.K.; Kaiser, A.B.; Gilberd, P.W.; Wessling, B. *Journal of Polym. Sci., Part B: Polym. Phys.* **1993**, 31, 1425-1430
 b) Kaiser, A.B.; Subramaniam, C.K.; Gilberd, P.W.; Wessling, B. *Synth. Met.* **1995**, 69 197-200
 c) Subramaniam, C.K.; Kaiser, A.B.; Gilberd, P.W.; Liu, C.J.; Wessling, B. *Solid State Commun.* **1996**, 97, No.3, 235-238
- ²¹ our own unpublished measurements
- ²² Ormecon Chemie, Ammersbek (Germany) technical information (previously published by Zipperling Kessler & Co., Ormecon's holding)
- ²³ Test Report of DECHEMA (D-Frankfurt), „Tests on ‘passivated’ steel specimens. Scope of order: Corrosion test program for crevice and pitting corrosion and galvanic corrosion of various pre-treated steel specimens , 1994
- ²⁴ Wessling, B. (together with Schröder, S.; Gleeson, S.; Merkle, H.; Baron, F. *Materials and Corrosion* **1996**, 47, 439-445
- ²⁵ note: our Organic Metal is the first metal which can be reduced (2e⁻ and 2 H⁺ per dimer)
- ²⁶ The structures are comparable to those described in:
 a) Wessling, B. *Polym. Eng. & Sci.* **1991**, 31, No.16, 1200-1206
 The thermodynamic reasons for the structure formation are explained by non-equilibrium thermodynamics, cf.:
 b) Wessling, B. *Synth. Met.* **1991**, 45, 119-149
 c) Wessling, B. *Zeitschrift f. Physikalische Chemie* **1995**, 191, 119-135
 For more recent overviews about flocculation in dispersions, their thermodynamical basis and relationship with properties see:
 d) Wessling, B. In: *Handbook of Conducting Polymers*, Skotheim, T.A., Elsenbaumer, R.; Reynolds, J. Ed.; M Dekker 1998, pp 467-530
 e) Wessling, B. In: *Handbook of Organic Conductive Molecules and Polymers*, Nalwa, H.S., Ed., Wiley, 1997, Vol. 3, pp 497-632
- ²⁷ „PANDA“, a product developed by Monsanto, cf. Kinlen, P.; Silverman, D.; Jeffreys, C. *Synth. Met.* **1997**, 85, 1327-1332
- ²⁸ in fact, CORRPASSIV™ generally outperforms zinc-rich epoxies, and this even at significantly lower coating thickness (20 μm vs. 60-80 μm).
- ²⁹ we have also tested PANDA in direct comparison with CORRPASSIV

and standard corrosion prevention coatings and found no anti-corrosion effect at all, a fact which was later confirmed by other independent studies, too.

- 30 cf: Wessling, B. „Conducting Polymer / Solvent Systems: Solutions or Dispersions?“ 1996
- a) Proceedings of SEAM (Search for Electroactive Materials), workshop at Brooklyn Polytechnic Institute, NY., Dec. 1996
- b) Proceedings of 3rd BPS (Bayreuth Polymer & Materials Research Symposium), Bayreuth (Germany) April 1997; manuscript available at: <http://www.ornecon.de/Research/soludisp>
- see especially ch. 2.5 and 3 and Figure 13
- 31 Wroblewski, D.; Bencewicz, B.; Thompson, K.; Bryan, C. *Polym. Prepr.* **1994**, 35, Vol. 1, 265-266
- 32 a) R. Racicot, T. Brown, S.C. Yang, *Synth.Met.* **85** (1997) 1263
- b) M. Fahlmann, S. Jasty, A. Epstein, *Synth. Met.* **85** (1997) 1323-1326
- 33 there are several incompatibility phenomena which may occur: (a) insufficient wetting or interlayer adhesion (b) insufficient curing of the top coat due to the chemical properties of the primer, as the primer contains an acid salt and provides an acid environment, which cannot be tolerated by all top coat systems
- 34 unpublished results
- 35 cf. „Industrial reference objects“ / Reports Ormecon Chemie, here: „Skippers CORRPASSIV“ and „Protection of cattle barn steel plates“
- 36 Stratmann, M.; Streckel, H.; Feser, R. *Corros. Sci.* **1991**, 32, 467
- 37 Stratmann, M.; Feser, R.; Leng, A. *farbe und lacke* **1994**, 100, Vol 2, 93
- 38 Technical Information UBM („Measuring instrument for measuring corrosion potential with a Kelvin probe“, UBM Messtechnik GmbH, Ottostr. 2, D-76275Ettlingen)
- 39 we prefer to measure the corrosion potential and its shift during ennobling with the open circuit potential technique as described in 4.1, which is more realistic in relation to the corrosion process
- 40 Popkirov, G.S.; Schindler, R.N. *Electrochim. Acta* **1994**, 39, 2025; we are now using a principally comparable, but more modern and commercially useful apparatus
- 41 Rammelt, U.; Reinhard, G. *farbe und lacke* **1992**, 98, 4, 261
- 42 Wessling, B., Posdorfer, J. *Electrochim. Acta* **1999**, 44, 2139-2147
- 43 Wagner, C.; Traud, W. *Z. Elektrochem.* **1938**, 44, 391
- 44 Funke, W. In *Corrosion Control by Organic Coatings*, Leidheiser, H., Ed., Houston: National Association of Corrosion Engineers, NACE, 1981, 97 - 102
- 45 Schauer, T.; Joos, A.; Praschak, E. in Investigation of the compatibility of selected top coats with primer 900226/32, test report on behalf of Zipperling Kessler & Co (Ormecon Chemie), Forschungsinstitut für Pigmente und Lacke e.V., Stuttgart, 1996
- 46 see: www.ornecon.de

- ⁴⁷ Posdorfer, J.; Brueggen, L.; Wessling, B., to be published (Proc. of „I. Electrochemical Impedance Symposium EIS 2001“, Marilleva, Trento/Italy, June 2001)
- ⁴⁸ a) Putilova, I. N.; Balezin, S.A.; Barannik, V.P. *Metallic Corrosion Inhibitors*, Pergamon, New York, 1969
b) Poling, G.W. *Corros. Sci.* **1970**, 10, 359
c) Roberts, R. F. *J. Electron Spectrosc. Relat. Phenom.* 1974, 4, 273
- ⁴⁹ a) Wessling, B. *Adv. Mater.* 1994, 6, 226
b) Brusic, V.; Angelopoulos, M.; Graham, T. *J. Electrochem. Soc.* **1997**, 144, 436.
c) Wessling, B. *Circuit World* 25/4, 1999, p 8.
- ⁵⁰ a) Andrä, K. *Metalloberfläche* 50/3, 1996, p 176.
b) Bratin, P.; Pavlov, M.; Chalyt, G. *Printed Circuit Fabrication* 22/5, 1999, p 30.
c) Tench, M.; Kendig, M.W.; Anderson, D.P.; Hillman, D.D.; Lucey, G. K.; Gher, T.J. *Soldering Surf. Mount Technol.* 13/46, 1993, p 18.
- ⁵¹ Posdorfer, J.; Wessling, B. *Synth. Met.* **2001**, 119, 363-364

Chapter 4

Iron–Polyaniline Interfaces: Implications for Corrosion Protection

M. Fahlman¹, X. Crispin², J. A. O. Smallfield³, R. Lazzaroni⁵,
J. L. Brédas⁴, S. Li⁵, Y. Wei⁵, and A. J. Epstein³

¹Department of Science and Technology, Linköping University, SE–60174
Norrköping, Sweden

²Department of Physics, Linköping University, SE–58183 Linköping,
Sweden

³Department of Physics, The Ohio State University, Columbus, OH 43210

⁴Service de Chimie des Matériaux Nouveaux, Université de Mons-Hainaut,
Belgium

⁵Department of Chemistry, Drexel University, Philadelphia, PA 19104

Abstract

The early stages of interface formation between iron and a three-ring model molecule (trimer) of emeraldine base form of polyaniline (EB) were investigated using theoretical (DFT) and experimental (XPS) methods. Iron atoms were sputter-deposited in ultra high vacuum onto thin oligomer films, with X-ray photoelectron spectroscopy (XPS) core level spectra taken after each deposition. Similar studies were carried out for Fe sputter-deposited on EB polymer films as well. Based on the chemical shifts of the core level peaks and the theoretical results, iron was determined to donate charge (e^-) into the trimer and EB films. The reverse case where thin films of trimer and EB were deposited on iron also was studied. The C(1s) core level shake up spectra show that the π -electronic structure is modified for trimer and EB coatings on iron as compared to coatings on gold.

Introduction

Metal/conjugated polymer interfaces are of increased interest because of their role in light emitting devices (LEDs) (1-3), transistors (4-7) and photovoltaic cells (8-10). Though the chemistry and purity of the polymer materials are of obvious importance, the nature of the metal/polymer contact has been shown to have a critical role in device performance (11,12). Hence, a large number of studies on metal/polymer interfaces are available in literature (13-20). Another area of potential use for this class of polymers is in corrosion protection of metals, particularly steel. Chromate- and zinc-containing paints are commonly used today to prevent corrosion of steel (21). It is likely, however, that environmental concerns might reduce or even rule out the use of chromate based paints in the future. Hence the need for new corrosion protecting materials that are dispersible in paints. Conjugated polymers is one such class of materials that is being proposed as an alternative (22). Polyaniline (22-29) and polypyrrole (22,30) coatings are presently being considered and other electroactive polymers also may prove to be effective. So far, most of the emphasis has been placed on studying the corrosion protecting capabilities of doped polyaniline, *i.e.*, emeraldine salt (22-25,27,29). The emeraldine base (EB) form of polyaniline, however, also offers some corrosion protecting capabilities for iron (26), cold rolled steel (CRS) (31), and stainless steel (32).

We present here results of X-ray photoelectron spectroscopy studies on the interface between iron and EB, in polymer as well as three ringed model molecule form (hereafter referred to as 'trimer'), in order to elucidate the mechanism for the corrosion reducing effects provided by these organic coatings. We compare the experimental results with quantum chemical calculations. Together these data demonstrate that there is substantial electron transfer from the metal to EB and trimer as detected by the chemical shifts of the core level peaks (C 1s, N 1s and Fe(2p)).

Experimental Methodology

A VG Scientific ESCALAB MkII XPS spectrometer with Mg K_{α} X-rays (1253.6 eV) was used in these studies. Sputtering was carried out using 5.5 keV Ar-ions. Thin films (<100 Å) of EB (33) or trimer (34), depicted in Fig. 1, were deposited onto gold substrates through spin coating in air from 12 mg/ml N-methylpyrrolidinone (NMP) solutions. The EB material was extensively washed

with water and NH_4OH prior to being dissolved in NMP, yielding a chlorine content of $\sim 0.019\%$ as measured by the Schwarzkopf Microanalytical Laboratory in Woodside, NY.

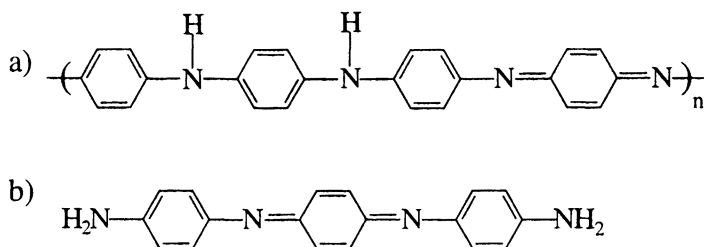


Figure 1. Geometrical structures of (a) emeraldine base polyaniline (EB) and (b) a three-ring model molecule of emeraldine base polyaniline (trimer).

Thin films of iron were then sputter deposited *in situ* ($p_{\text{sputter}} \sim 10^{-7}$ mbar, $p_{\text{base}} \sim 10^{-9}$ mbar) from a sputter-cleaned CRS target with XPS core level spectra being taken after each deposition. The Au(4f) core level peaks visible from the underlying gold substrate were used as a binding energy reference. The deconvolution of the N(1s) core level peak was done using a mixed Gaussian-Lorentzian function:

$$I(E) = I_0(m \cdot \exp(-4x^2 \ln 2) + (1-m)/(1+4x^2)), \quad x = (E - E_0)/(\text{FWHM}) \quad (1)$$

where m = mixing ratio, E = binding energy, I_0 = intensity at peak center, E_0 = binding energy at peak center, FWHM = full width at half maximum, $I(E)$ = peak intensity at binding energy E (35).

Thin films ($< 100 \text{ \AA}$) of EB and trimer were spun on iron and gold substrates and C(1s) shake up spectra were taken at the synchrotron radiation facility Max-lab in Lund, Sweden.

Theoretical Methodology

Theoretical modeling are used to investigate the nature of the interfacial interactions at the iron/emeraldine base and the iron/trimer interfaces. The first stage of iron deposition on EB and trimer films is simulated with organometallic

complexes composed of one iron atom interacting with each of the quinoidic and aromatic segments present in the emeraldine chain or the trimer: phenyl-capped p-phenylenediamine (ϕ -NH- ϕ -NH- ϕ , PC-PPDA) and phenyl-capped benzoquinodiiimine (ϕ -N- ϕ -N- ϕ , PC-BQD). In spite of the simplicity of these models, some features of the metal-polymer interfaces can be obtained, as shown previously for the interface created by sputtered aluminum deposited on emeraldine (36).

The calculations are performed in the framework of the density functional theory (DFT) (37). This method is a nonempirical approach, alternative to Hartree-Fock-based theories; it presently finds wider applications to chemical problems due to the possibility of including a significant part of electron correlation energy at a relatively low computational cost. The electron correlation is essential for a correct description of transition metal atoms, such as iron. The DFT technique has proven effective at modeling electronic and chemical properties of polyaniline model systems (38,39).

All the calculations are performed using the DMol program (40) with the DNP (double zeta numeric with polarization) basis set (all 3d, 4s, and 4p atomic orbitals of Fe included in the basis set). The core orbitals are frozen during the SCF iterations and a "FINE" mesh size is chosen for the calculations (41). During the geometry optimizations, the calculations are performed within the local spin density approximation (LSD) with the Vosko-Wilk-Nusair exchange-correlation potential (42), since it gives appropriate geometries for a reasonable computational cost. When discussing bond formation energies (noted abusively ΔH , in order to avoid any confusion with the XPS binding energy), basis-set superposition errors (BSSE) should be estimated; an advantage of the DMol numeric basis sets is their low BSSE values. For transition metal complexes, the BSSE was estimated to be significantly less than 5 kcal/mol (43). Although the LSD approximation is known to overestimate the bond formation energies, we don't discuss the absolute value of those energies but rather use it as a qualitative guidance helping to understand the XPS results. The charge analysis used in this work comes from the Hirshfeld scheme, which is directly based on the electronic density (44).

In the case of the transition metal atoms with partially filled 3d levels, the Self-Consistent Field (SCF) procedure, used to minimize the ground-state energy, shows strong oscillations in electron density and total energy. This oscillation problem is well-known in systems having a vanishing HOMO-LUMO gap due to the symmetry of the system or to d molecular orbitals very close to each other. In order to overcome the oscillation problem, we have followed the method proposed by Rabuck, *et al.*, (45): to reach convergence, one allows molecular orbitals to be

fractionally occupied. Here, the valence electrons are spread over a range of molecular orbital energies broader than that given by a Fermi-Dirac distribution at 0K. A non-zero temperature in the Fermi-Dirac distribution is used to spread the electron charge within a window of energy. The calculations have been performed in several steps. At each step, the SCF convergence is reached; then, the size of the window is reduced. Finally, the last step corresponds to zero temperature and gives integer orbital occupations at convergence.

Results and Discussions

The steel/EB interface was studied by sputter-depositing atoms (>99.2% Fe) from a sputter-cleaned CRS source onto EB/Au films in UHV, taking XPS core level spectra after each deposition. We expect that the sputtered iron atoms or small iron clusters deposited on the emeraldine and trimer films have high enough mobility over the surface to reach the more stable adsorption site on the organic surface. At higher iron coverage, less stable adsorption sites may be reached. The early stages of the resulting Fe/EB interface formation are shown in Fig. 2 (31).

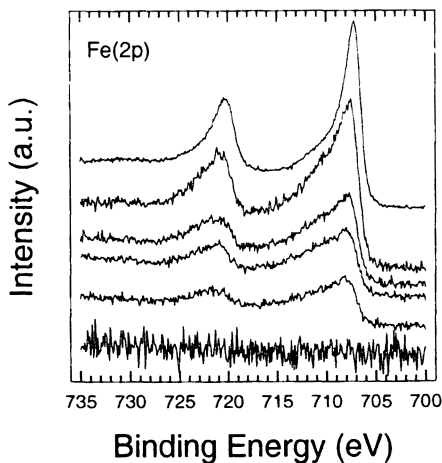


Figure 2. Fe 2p core level evolution during the early stages of iron/EB interface formation. From the bottom, Fe over layers of approximate average thickness: 0 Å, 0.2 Å, 0.4 Å, 0.8 Å, 1.6 Å, and 16.5 Å.

At low levels of coverage, the Fe($2p_{3/2}$) peak is shifted towards higher binding energy, 708.2 eV, as compared to 706.7 eV for metallic iron, signifying charge donation from the iron into the EB film. At higher levels of coverage, the iron peak becomes more metallic (707.2 eV), but still shows a slight shift towards higher binding energies as compared to bulk Fe metal. Sputter-deposited iron on Au substrates showed a shift of the Fe($2p_{3/2}$) binding energy to 707.5-707.6 eV at the early stages of interface formation, significantly less than the shift for Fe/EB, demonstrating that the binding energy shift detected for the Fe/EB system is not due to cluster effects. Iron particles supported on a ternary organic compound ($KC_{24}(DME)_{1.35}$) was found to have a binding energy of 707.4 eV (46), also supporting our claim of charge transfer between iron and EB.

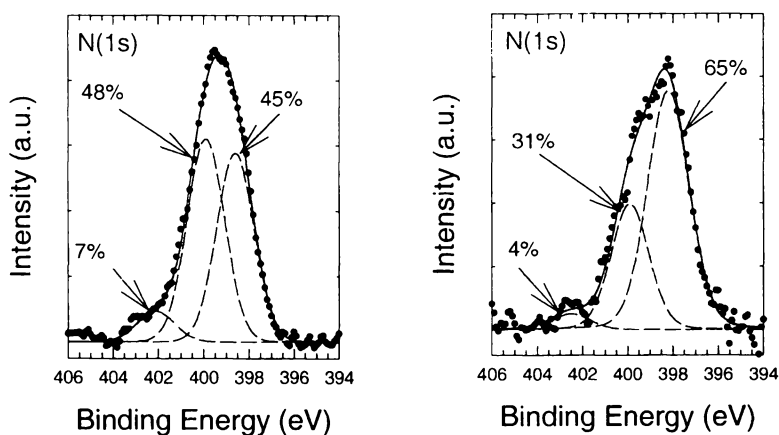


Figure 3. $N(1s)$ core level spectra (a, left) of pristine EB and (b, right) EB at high Fe coverage (10 \AA), deconvoluted with mixed Gaussian-Lorentzian function (dashed lines).

At low levels of iron coverage, the $N(1s)$ core level retains its roughly 1 to 1 ratio of amine ($\sim 399.9 \text{ eV}$) and imine ($\sim 398.6 \text{ eV}$) nitrogen, as depicted for pristine EB in Fig. 3a (31). The third feature of pristine EB at $\sim 402.1 \text{ eV}$ is assigned as a shake up peak originating from the imine nitrogen (36,47,48). The relative intensities of the three peaks for pristine EB are 45%, 48% and 7%, for the imine, amine and shake up respectively. For low coverage, no significant binding energy shifts in the $N(1s)$ core level peak are detected, though the intensity of the shake up peak at $\sim 402 \text{ eV}$ is decreased. This is similar to the initial interface formed for Al

on EB, where no significant shift is seen for the imine peak at low coverage ($< 3 \text{ \AA}$) (36,48). At high coverage ($\sim 10 \text{ \AA}$), shown in Fig. 3b (31), the relative intensities of the amine and shake up features are decreased to 31% and 4%, respectively, and an increase to 65%, in the relative intensity of the imine feature is detected. The imine peak is now slightly shifted to a lower binding energy, 398.2 eV, and there also is a slight broadening of this peak, 2.15 eV (FWHM) as compared to 1.97 eV for the amine peak. The initial shift of the Fe(2p) core level and the decrease in imine shake up feature of the N(1s) core level at low coverage is proposed to be indicative of iron preferentially reacting with the imine nitrogen of the EB films, possibly forming covalent bonds. The lack of a significant shift in the imine peak position are attributed to the accepted charge being spread out over the imine-quinoid-imine unit, as was the case for Al on EB (36,48).

The broadening observed for the low binding energy peak (398.2 eV) of the N(1s) core level at high iron coverage is suggested to be caused by iron reacting with amine nitrogen, moving the iron-amine feature of the N(1s) spectrum to lower binding energies due to charge transfer. The shift is large enough to place the iron-amine peak close to that of the imine and iron-imine features, thus causing the broadening and slight shift of the low binding energy peak of the N(1s) spectrum. This also explains the observed increase of the low binding energy peak intensity and drop of the amine peak intensity at high levels of coverage. This result is similar to the case of amine nitrogen of EB reacting with aluminum, where a shift towards lower binding energy by 1.7 eV was found to occur [Lazzaroni, 1992 #43; Calderone, 1994 #1].

At low levels of coverage, no shift in the C(1s) core level spectrum (not shown) is detected, as is expected if the accepted charge is spread out over the phenyl ring carbons and imine-quinoid-imine carbons. At high levels of coverage, a new feature appears as a low binding energy shoulder, suggesting that iron has 'saturated' the carbon sites on the rings, breaking the π -delocalization which causes most of the accepted charge to be localized on the carbon atoms. Thus, the model of initial interface formation between iron and imine (and possibly phenyl or quinoid carbons) then followed by the less favorable iron-amine reactions also is supported by the C(1s) core level spectra.

The evolution of the Fe(2p) core level spectra during the early stages of interface formation of sputter-deposited iron onto trimer films is depicted in Fig. 4. The Fe(2p_{3/2}) binding energy is shifted to $\sim 710.4 - 710.1$ eV for low coverage, signifying charge transfer (e^-) from the iron atoms into the trimer film, larger than is the case for iron deposited on EB.

The binding energy of ~ 710 eV suggests that the trimer molecules accept more charge than EB, i.e., the covalent bonding between the iron atoms and the trimer is

stronger. As the iron film thickness increases, the Fe(2p_{3/2}) peak is shifted towards more metallic binding energies, 707.3 eV at the highest coverage.

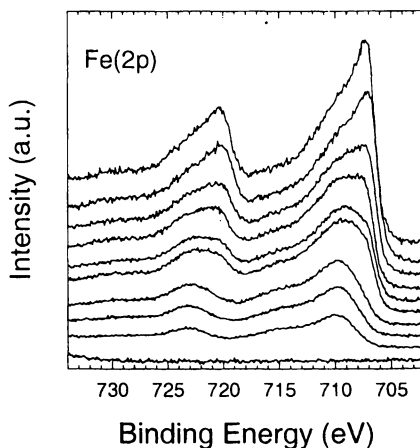


Figure 4. Fe(2p) core level evolution during the early stages of iron/trimer interface formation. From the bottom, Fe over layers of approximate average thickness: 0 Å, 0.2 Å, 0.4 Å, 0.6 Å, 0.8 Å, 1.0 Å, 1.2 Å, 1.4 Å, 1.6 Å and 2.1 Å..

A deconvolution of the N(1s) peak of pristine trimer is shown in Fig. 5a. The three components are imine nitrogen at 398.9 eV, amine nitrogen at 399.7 eV and an imine shake up feature at 402.0 eV. Ideally, there should be a 1:1 ratio between the amine and imine peaks. However, the relative intensity is only 41% for the imine feature as compared to 52% for the amine peak. This suggests that for some of the trimer molecules, the imine nitrogen have been protonated.

At extended coverage of Fe on trimer, Fig. 5b, the relative intensity of the amine peak has been decreased (43%) and the imine peak has undergone a slight shift towards lower binding energy, 398.4 eV, while having an increased relative intensity, 53%. Here too, there is a slight broadening of the imine peak, 2.28 eV (FWHM) as compared to 2.1 eV, suggesting a mix of chemical states, both iron-imine and iron-amine complexes. The increase in relative intensity of the peak at 398.4 eV is not due to deprotonation of the previous protonated imine sites, since the imine shake up peak at 402.0 eV is *decreased* in relative intensity, 4% vs. 7% for

the pristine case. The increase in the intensity of the low binding energy feature is proposed as due to amine nitrogen having formed bonds with iron atoms, receiving charge (e^-). The decrease in shake up intensity suggests that imine nitrogen also have reacted with iron, but due to the imine-quinoid-imine structure, the accepted charge is spread out, resulting in a much smaller shift of the imine nitrogen peak than would otherwise been the case. Thus, thin films of trimer interact with iron in much the same way as EB does, accepting charge (e^-) and forming bonds preferentially at the imine sites and possibly with phenyl or quinoid carbon, then amine sites at higher coverage.

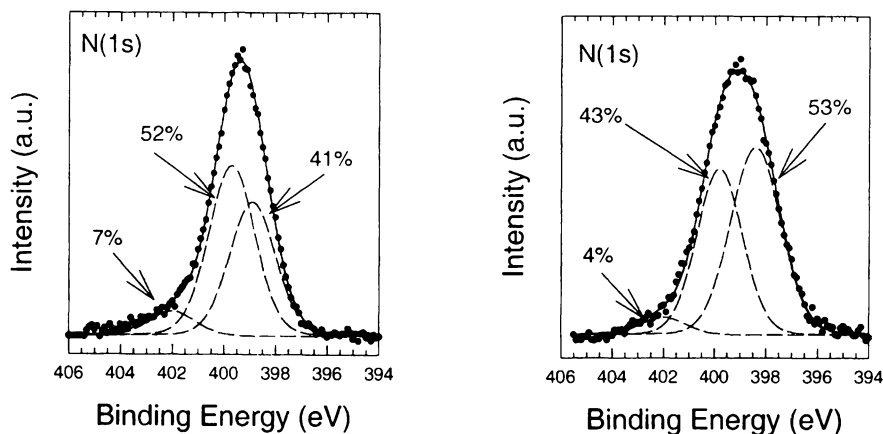


Figure 5. *N(1s)* core level spectra (a, left) of pristine trimer and (b, right) trimer at high average Fe coverage (2.1 \AA), deconvoluted with mixed Gaussian-Lorentzian function (dashed lines).

In Fig. 6. are displayed C(1s) shake up spectra of thin films of (a) EB on gold and iron substrates and (b) trimer on gold and iron substrates. The main shake up feature centered at $\sim 289 \text{ eV}$ is derived from excitations confined mainly to the phenylene rings (47). (A shake-up feature originating from excitations confined mainly on the quinoid rings would reside at $\sim 287 \text{ eV}$ (47), but this feature is not resolvable from the slope of the main peak at 285.0 eV). The thinness of the films allow us to 'see through' the film and probe the interface, though part of the signal comes from material away from the interface that may not have interacted with the substrate. (Inelastic scattering of electrons prevent probing depths of more than $\sim 100 \text{ \AA}$). If charge transfer takes place at the iron or gold interface, the π -electronic

structure of the EB or the trimer will be affected and hence also the shake up features. The strong modification of the shake-up features of both EB and trimer on iron as compared to films on gold suggests that the iron substrate has interacted with the organic films donating (or accepting) charge.

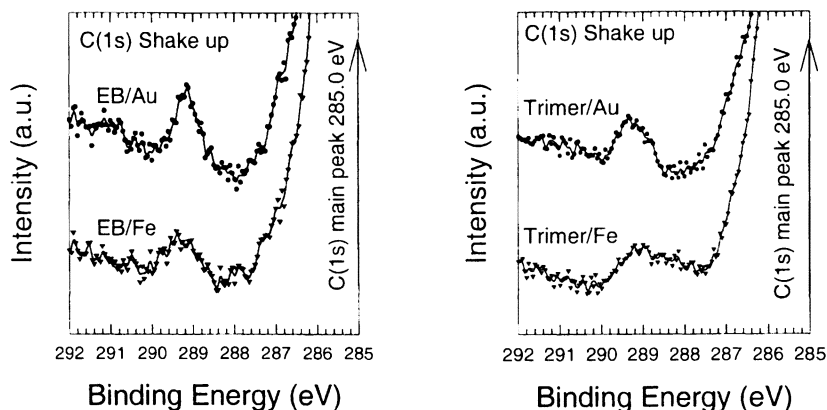


Figure 6. *C(1s)* shake up spectra of (a) EB on Au (circles) and EB on Fe (triangles); (b) Trimer on Au (circles) and trimer on Fe (triangles).

The DFT calculations support the experimental results while providing more detail into the bond formations. Here, the stability of the interaction between an iron atom and different sites of the organic films is estimated from the models described previously. For one iron atom, four different adsorption sites can be envisaged: above the aromatic ring (Fig. 7a) or close to the amine nitrogen (Fig. 7b), these adsorption sites are simulated with PC-PPDA; above the quinoid ring (Fig. 7c) or close to the nitrogen imine (Fig. 7d) present in the PC-BQD model molecule.

For each adsorption site, the structure optimization indicates that the iron atom is covalently bound to the organic molecule, with carbon-iron interatomic distances around 2.0 Å and nitrogen-iron interatomic distances between 1.8 Å and 2.2 Å. Moreover, the iron atom carries a positive charge in each complex.

The calculated bond formation energies indicate that the iron atoms prefer to interact with the aromatic ring ($\Delta H = 63$ kcal/mol), the quinoid ring ($\Delta H = 68$ kcal/mol), and the imine nitrogen ($\Delta H = 55$ kcal/mol). In contrast, the iron atom does not interact strongly with the amine nitrogen ($\Delta H = 24$ kcal/mol). Interestingly, the

iron atomic charge follows the trend in stability. The iron atom interacting with the three most stable adsorption sites carries a high positive charge $Q(\text{Fe})$: $+0.25|e|$ for the aromatic ring, $+0.36|e|$ for the quinoid ring, and $+0.39|e|$ for the imine nitrogen site, while the iron atom bound to the amine nitrogen carries only a charge of $+0.06|e|$. Those results suggest that the first stage of the deposition of sputtered iron atoms on the emeraldine or trimer films should be characterized by a high core-electron binding energy for these iron atoms, since they carry a partial positive charge. This prediction is in good agreement with the XPS results at low levels of coverage: the $\text{Fe}(2p_{3/2})$ binding energy is shifted towards higher binding energy, 710.4–710.1 eV, compared to 707.3 eV for a thick iron film (trimer).

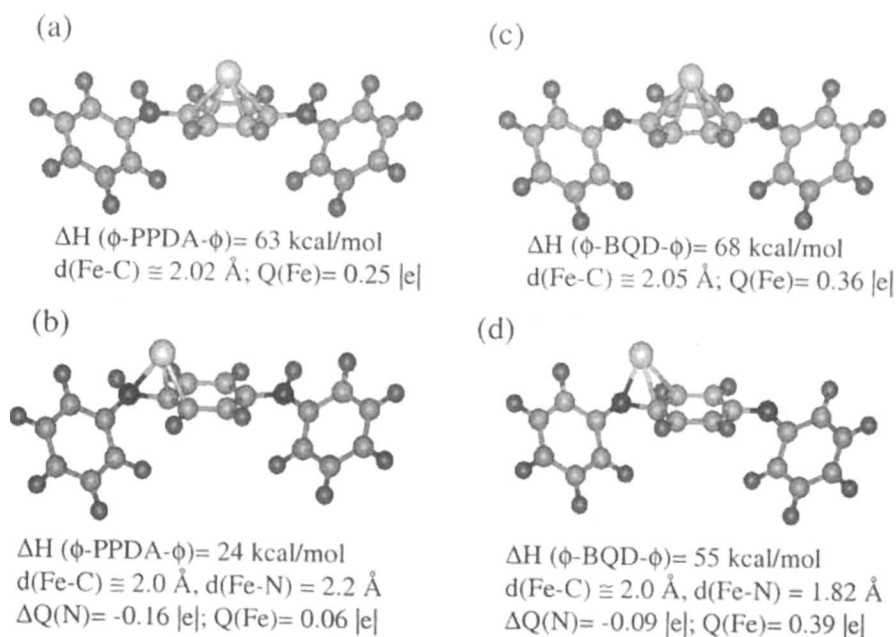


Figure 7. Sketches of the optimized structures of the complexes composed of an iron atom interacting with (a) the aromatic ring and (b) the amine nitrogen of PC-PPDA; and with (c) the quinoidic ring and (d) the nitrogen imine of PC-BQD.

Partial electron transfer from the iron atom to the aromatic ring of PC-PPDA or to the quinoid ring of PC-BQD occurs and is spread out over the whole conjugated

molecule. Consequently, the increase of the atomic charge over the carbon atom is small: $\Delta Q(C) = -1/10 \Delta Q(Fe)$. Because of this delocalization effect, the C(1s) peak of the emeraldine or the trimer is not expected to be significantly affected by the iron deposition, as was observed in the experiment. Note that both the iron-imine nitrogen and iron-amine nitrogen interactions lead to more negative charge on the nitrogen atoms. However, since the imine nitrogen is more reactive than the amine. Hence, at low iron coverage, the N(1s) peak of imine is expected to shift to lower binding energy and the imine shake-up peak to be reduced. From the theoretical results, the interpretation of the evolution of the N(1s) signal at high iron coverage is confirmed: (i) The 1 eV broadening of the N(1s) signal towards lower binding energies is due to the iron-imine nitrogen bond formation, since the imine nitrogen atom undergoes a small increase of charge ($\Delta Q(N) = -0.09 |e|$). (ii) The intensity decrease of the amine N(1s) contribution (399.7 eV), accompanied with an intensity increase at lower binding energy (overlapping the imine N(1s) feature of the pristine material), is due to the iron-amine nitrogen bond formation characterized by significant negative charge increase on the nitrogen ($\Delta Q(N) = -0.16 |e|$). The amine nitrogen bound to the iron appears at lower binding energy (under the peak contribution centered at 398.4 eV).

Summary

Based on the chemical shifts of the core level peaks: Fe(2p), N(1s) and C(1s), as well as the DFT calculations, iron was found to donate charge (e^-) into the trimer and EB films. Iron was determined to preferentially react with the imine nitrogen and (ring) carbon of EB and trimer at low coverage, and also with the amine nitrogen at higher coverage. The DFT quantum chemical calculations show that covalent bonding between iron and EB/trimer occurs. C(1s) core level shake up spectra suggest that for the reverse case of EB or trimer deposited onto iron substrates, charge transfer occur across the organic/metal interface. These results thus support the concept of an anodic-type corrosion protection of iron/steel.

Acknowledgments

Thanks are due to Dr. P. Spellane for extensive discussions. We acknowledge the financial support of Akzo Nobel Inc., and the AFOSR, Grant No. 732088. MF thanks the Swedish Research Council for Engineering Sciences (TFR), the Swedish Natural Science Research Council (NFR) and the Swedish Foundation for Strategic Research (SSF) financed Center for Advanced Molecular Materials (CAMP) for financial support.

References

- 1 Burroughes, J.H.; Bradley, D.D.C.; Brown, A.R.; Marks, R.N.; Mackay, K.; Friend, R.H.; Burn, P.L. Holmes, A.B. *Nature* **1990**, *347*, 539.
- 2 Gustavsson, G.; Cao, Y.; Treacy, G.M.; Klavetter, F.; Colaneri, N.; Heeger, A.J. *Nature* **1992**, *357*, 477.
- 3 Friend, R.; Burroughes, J.; Shimoda, T. *Phys. World* **1999**, *June*, 35.
- 4 Garnier, F.; Hajlaoui, R.; Yassar, A.; Srivastava, P. *Science*; **1994**, *265*, 684.
- 5 d. Leeuw, D. *Phys. World* **1999**, *March*, 31.
- 6 Siringhaus, H.; Kawase, T.; Friend, R. H.; Shimoda, T.; Inbasekaran, M.; Wu, W.; Woo, E.P.; *Science* **2000**, *290*, 2123.
- 7 Gelinck, G.H.; Geuns, T.C.T.; d. Leeuw, D.M. *Appl. Phys. Lett.* **2000**, *77*, 1487.
- 8 Sariciftci, N.S.; Smilowitz, L.; Heeger, A.J.; Wudl, F. *Science* **1992**, *258*, 1474.
- 9 Marks, R.N.; Halls, J.J.M.; Bradley, D.D.C.; Friend, R.H. *J. Phys. Cond. Matter* **1994**, *6*, 1379.
- 10 Halls, J.J.M.; Walsh, C.A.; Greenham, N.C.; Marseglia, E.A.; Friend, R.H.; Moratti, S.C.; Holmes, A.B. *Nature* **1995**, *376*, 498.
- 11 Bröms, P.; Birgersson, J.; Johnsson, N.; Lögdlund, M.; Salaneck, W.R. *Synth. Met.* **1995**, *74*, 179.
- 12 Hung, L.S.; Tang, C.W.; Mason, M.G. *Appl. Phys. Lett.* **1997**, *70*, 152.
- 13 Fahlman, M.; Beljonne, D.; Lögdlund, M.; Burn, P.L.; Holmes, A.B.; Friend, R.H.; Brédas, J.L.; Salaneck, W.R. *Chem. Phys. Lett.* **1993**, *214*, 327.
- 14 Fahlman, M.; Salaneck, W.R.; Moratti, S.C.; Holmes, A.B.; Brédas, J.L. *Chem. Eur. J.* **1997**, *3*, 286.
- 15 Lim, S.L.; Tan, K.L.; Kang, E.T. *Synth. Met.* **1998**, *92*, 213.
- 16 Greczynski, G.; Fahlman, M.; Salaneck, W.R. *J. Chem. Phys.* **2000**, *113*, 2407.
- 17 Greczynski, G.; Fahlman, M.; Salaneck, W.R. *J. Chem. Phys.* **2001**, *114*, 8628.
- 18 Salaneck, W.R.; Stafström, S.; Brédas, J.L. *Conjugated Polymer Surfaces and Interfaces* Cambridge University Press, Cambridge, 1996.
- 19 Ma, Z.H.; Lim, S.L.; Tan, K.L.; Li, S.; Kang, E.T. *J. Mat. Sci.*; **2000**, *11*, 311.
- 20 Ma, Z.H., Tan, K.L.; Kang, E.T. *Synth. Met.* **2000**, *114*, 17.
- 21 D. A. Jones, *Principles and prevention of corrosion* Prentice Hall, Englewood Cliffs, 1996.
- 22 Lu, W.-K.; Basak, S.; Elsenbaumer, R.L. in *Handbook of Conducting Polymers-II*, Skotheim, T. Reynolds, J.R.; Elsenbaumer, R.L., Eds. Marcel Dekker, New York, 1997, pp. 881.
- 23 DeBerry, D.W. *J. Electrochem. Soc.* **1985**, *132*, 1022.
- 24 Wroblewski, D.A.; Benicewicz, B.C.; Thompson, K.G.; Bryan, C.J. *ACS Polymer Preprints* **1994**, *35*, 265.
- 25 Wessling, B. *Adv. Mater.* **1994**, *6*, 226.
- 26 Jasty, S.; Epstein, A.J. *Pol. Mat. Sci. & Eng.* **1995**, *72*, 565.
- 27 Ahmad, N.; MacDiarmid, A.G. *Synth. Met.* **1996**, *78*, 103.
- 28 Wessling, B. *Mater. Corros.* **1996**, *47*, 439.
- 29 Kinlen, P.J.; Silverman, D.C.; Jeffreys, C.R. *Synth. Met.* **1997**, *85*, 1327.

- 30 Krstajic, N.V.; Grgur, B.N.; Jovanovic, S.M.; Vojnovic, M.V. *Electrochim. Acta* **1997**, *42*, 1685.
- 31 Fahlman, M.; Guan, H.; Smallfield, J.A.O.; Epstein, A.J. *Society of Plastics Engineers ANTEC, Vol. 2* Atlanta, Georgia, U.S.A., 1998, pp. 1238.
- 32 Santos, J.R.; Mattoso, L.H.C.; Motheo, A. *J. Electrochim. Acta* **1998**, *43*, 309.
- 33 MacDiarmid, A.G.; Chiang, J.C.; Richter, A.F.; Somasiri, N.L.D.; Epstein, A.J. *Conducting Polymers*, Alcear L. Ed., D. Reidel Publishing Co., Dodrecht, Netherlands, 1987, pp. 105.
- 34 Wei, Y.; Yang, C.C.; Wei, G.; Feng, G.Z. *Synth. Met.* **1997**, *84*, 289.
- 35 *Practical surface analysis by auger and x-ray photo-electron spectroscopy*, Briggs, D.; Seah, M.P.; Eds. Wiley, New York, 1983.
- 36 Calderone, A.; Lazzaroni, R.; Bredas, J.L. *Phys. Rev. B.* **1994**, *49*, 14418.
- 37 Parr, R.G.; Yang, W. *Density-Functional Theory of Atoms and Molecules* Oxford University Press, New York, 1989.
- 38 Sein, L.T.; Duong, T. Wei, Y.; Jansen, S.A. *Synth. Met.* **2000**, *113*, 145.
- 39 Lim, S.L.; Tan, K.L.; Kang, E.T.; Chin, W.S. **2000**, *112*, 10648.
- 40 Delley, B. *New. J. Chem.* **1992**, *16*, 1103.
- 41 Delley, B. *J. Chem. Phys.* **1990**, *92*, 508.
- 42 Vosko, H.; Wilk, L.; Nusair, M. *Can. J. Phys.* **1980**, *58*, 1200.
- 43 Delley, B.; Wrinn, M.; Lüthi, H.P. *J. Chem. Phys.* **1994**, *100*, 5785.
- 44 Hirshfeld, F.L.; *Theoret. Chim. Acta.* **1977**, *44*, 129.
- 45 Rabuck, A.D.; Scuseria, G.E. *J. Chem. Phys.* **1999**, *110*, 695.
- 46 Beguin, F.F.; Messaoudi, A. *J. Mater. Chem.* **1992**, *2*, 957.
- 47 Sjögren, B.; Salaneck, W.R.; Stafström, S. *J. Chem. Phys.* **1992**, *97*, 137.
- 48 Lazzaroni, R.; Grégoire, C.; Chtaib, M.; Pireaux, J.J. in *Polymer-Solid Interfaces* IOP Publishing Ltd, Bristol, 1992, pp. 213.

Chapter 5

Assessment of Electronic Factors Necessary for Corrosion Inhibition: An Analysis of Substituted Aniline Oligomers

Susan A. Jansen¹, Lawrence T. Sein, Jr. ¹, James M. Varnum³,
Thanh Duong¹, and Yen Wei²

¹Department of Chemistry, Temple University, Philadelphia, PA 19122

²Department of Chemistry, Drexel University, Philadelphia, PA 19104

³Kimmel Cancer Center, Thomas Jefferson University,
Philadelphia, PA 19107

Polyaniline, PANi, has demonstrated significant utility in anti-corrosive coatings and has been used in proto-type materials. Its utility appears to stem mainly from its remarkable electrochemical properties. However, because of the low solubility of the polymer, synthetic targets of PANi materials have included low molecular weight PANi and aniline oligomers. In this work, analyses of a series of “aniline oligomers” offer insight into the chemistry of PANi materials. Methods of analysis include *ab initio*-DFT calculations of structural and electronic phenomena coupled with spectrochemical techniques. The combination of these methods allows for an extensive characterization of the “electronic chromophore” and the requirements for anticorrosion behavior. The affect of solvent and substitution is also addressed. The methods employed are predictive and have guided substitution chemistries of the aniline oligomers.

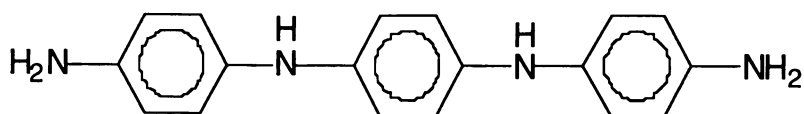
For the past 20-30 years, molecular electronic devices have been developed utilizing organic salts, conducting polymers and inorganic solids. Within the last ten years, conducting polymers have emerged in proto-typical anticorrosive coatings. These conducting polymers include polyaniline, polythiophene and polyphenylene. In many of these applications the conducting polymer is a component of a resinous matrix that may include other dopants. Strong electron

acceptors, such as the tetracyanoethylene, TCNE and tetracyanoquinodimethan, TCNQ were added to augment the band population of the conducting polymer by inducing positive carriers in the conduction band. Donors such as tetrathiafulvalene, TTF were used to provide negative carriers. It has been generally believed that the conductivity and redox character of the polymer were necessary requisites for the anticorrosive behavior. PANi showed greater diversity in its electrochemistry and could be prepared in highly conductive states and therefore appeared the most promising for electronic applications. In addition, the amphoteric nature of PANi allowed fairly easy preparation of acid or base PANi complexes, each showing different electronic characteristic. However, processing difficulties were encountered. The poor solubility of medium to high molecular weight PANi prohibited many applications (1-5). For many such PANi polymers, N-methyl-2-pyrrolidone, NMP, was one of the few solvents capable of dissolving utility polyaniline. (6) Concentrated acids were used in the dissolution but usually afforded the acid salt of the polymer. The acid salts have their own unique properties. Lower molecular weight polymers have slightly better solubility (6-9). Within the last five years, the question of chain length and conductivity has afforded some interesting ideas. "Aniline oligomers" have been prepared in which the number of intact aniline units has been monotonically increased from 3 to 8. The conductivity increases with intact aniline units such that the heptamer gives conductivity approaching that of polymeric PANi. These oligomers showed appreciable solubility in many common organic solvents. Studies such as these suggested that small oligomers of PANi might replace polyaniline in applications (10-14). In this work, the electronic features of the "trimeric" aniline oligomers are assessed to define requisites for corrosion protection.

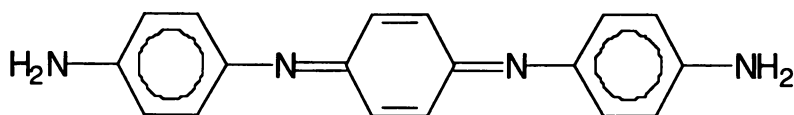
A number of methods have been reported for the preparation of oligomeric anilines. The "trimeric" aniline, N,N'-bis(4'-aminophenyl)-1,4-quinonediimine, used for these studies was synthesized by Wei et al. In this approach, phenylene diamine is combined under oxidation conditions with two equivalents of aniline. The resulting product can be described as an amino-capped aniline trimer. Like the parent polymer, the "trimer" can be prepared in multiple oxidation states with similarities to PANi. These are shown in Scheme 1 below.

The leucoemeraldine form represents the extreme of reduction; emeraldine is in an intermediate redox phase. The third form closely parallels that of pernigraniline. It is possible to interconvert between these forms using common oxidants and reductants. This simple synthetic strategy allows for substitution chemistries that can effect both the electronic nature and materials properties. Substituted anilines can be used directly in the synthesis. Halogenation is also easily accomplished. The former can affect the conformation of the "trimer" while augmenting the solubility. The latter may critically effect the electronic nature of the "trimer".

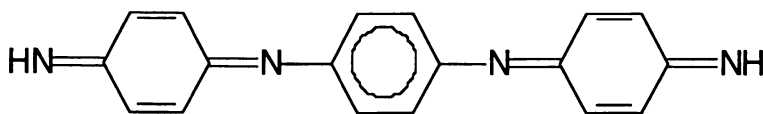
Scheme 1: Redox Forms of the Aniline Trimer



leucoemeraldine



emeraldine



Experimental Section

Synthesis: In the work, the aniline trimer, N,N'-bis(4'-aminophenyl)-1,4-quinonenediimine, was synthesized as described by Wei et al (15-17). ACS spectral grade acetonitrile was used without further purification. The reduced form of N,N'-bis(4'-aminophenyl)-1,4-quinonenediimine was prepared by reaction with excess NaBH₄ in acetonitrile. The resulting product, N,N'-bis(4'-aminophenyl)-1,4-diaminobenzene, the "leucoemeraldine" form of the trimer was yellow and air stable. The oxidized form of the compound was prepared by reaction with an excess of 3% hydrogen peroxide in dry acetonitrile. The reaction occurred within thirty minutes with mild heating at approximately 60° C. The product obtained was the protonated oxidized form of the trimer. It was blue and air stable. Reaction of this material with NaOH produced the "pernigraniline" form of the trimer, N,N'-bis(aminophenyl)-1,4-quinonenediimine, as a red air stable compound. Emeraldine salts of the "trimer" were produced by reaction with HCl in acetonitrile.

The 2,6-dialkylsubstituted emeraldine "trimers" were synthesized using the method of Wei et al. For each 2,6-dialkylemeraldine, the corresponding 2,6-dialkyl aniline was used. To increase the purity of the product, the crude material was dissolved in acetonitrile and reacted with an excess of sodium carbonate for approximately one hour. The solution was filtered and the product was collected and recrystallized.

Solution charge transfer complexes were formed in acetonitrile by mixing equimolar (10⁻⁴) solutions of the trimer material and the charge transfer agent. The charge transfer agents used were tetracyanoquinodimethane (TCNQ) and tetracyanoethylene (TCNE).

Electronic Spectra: Spectral measurements were made on all of the "trimers" using an HP8453A diode array spectrometer or a JASCO V-570, UV-Vis-NIR spectrometer. All measurements were performed at 1 nm resolution.

Electron Paramagnetic Resonance, EPR: EPR measurements were performed using a Bruker EMX Spectrometer. All materials were measured either in the solid state or as methylene chloride glasses prepared by rapid immersion in liquid nitrogen.

Computational Approach: Computational methods based upon density functional theory (DFT) provide a useful assessment of the trimers. In this method, there is a necessary compromise of accuracy versus cost of calculation. This is important to the theoretical applications to conducting polymers, which are large, and require consideration of electron correlation effects (which are critically important in conductors and semi-conductors). In the study of aniline

trimers, DFT calculations have been employed to predict molecular properties and to guide experimental investigation. The Gaussian 94 suite of programs was utilized for calculations of the optimized geometries, single point energies, ionization potentials, and electron affinities of all molecules, Becke's 3-parameter hybrid density functional B3LYP was used for all molecules. Single point energies and orbital eigenvalues were computed at the B3LYP/6-311G(2d,p) level. Configuration-Interaction Singles (CIS) calculations of electronic spectra employed the 6-311+G(d) basis set. Zero point energies, ZPE and enthalpic corrections to 298K used B3LYP/6-31G, unscaled (18-20).

Results and Discussion

The Trimer as the Electronic Chromophore for PANi. It is understood that the gross electronic properties of any complex system or polymer derive from some fundamental subunit. Therefore to understand the electronic nature of the polymeric form of PANi, we will assemble its electronic chromophore from its synthons, suggesting that propagation of the chromophore parallel polymer growth. In this work, we presume that it is possible to assemble the electronic chromophore of PANi by direct analysis of individual redox states of the smallest structure subunit. This subunit must include a "complete" phenylene diamine moiety such that two redox active nitrogen centers are included. With this unit, the primary redox forms of PANi can be represented. Furthermore, models and mechanisms for polymer growth clearly show that polymer formation is critically dependent on the oxidative chemistry of phenylenediamine, so phenylenediamine is a good place to start. The simplest PANi subunit is the amine-capped trimer, really aniline capped phenylene diamine.

Calculations on the trimer show that the trimer is neither linear nor planar. The terminal aniline rings of the trimer can exist either syn or anti forms. Table I shows the conformational preferences for representative trimer materials.

Table I. Conformational Assessment of Representative Trimers

From	To	Energy of Activation*
Syn-emeraldine	Anti-Emeraldine	18.92
Anti-emeraldine	Syn-Emeraldine	18.91
Syn-pernigraniline	Anti-pernigraniline	17.28
Anti-pernigraniline	Syn-pernigraniline	17.74

*All energies are in kcal/mole.

A comparison of UV-Vis spectral data with that obtained from the DFT calculations shows the accuracy and predictive nature of the calculations. These data are summarized for simple trimers in Table II. The Δ SCF method yields more accurate transition energies when compared with the CIS method. This is

likely because the CIS method is weighting certain excited states too heavily. The Δ SCF method computes the energy from specific coupling between two states. This suggests that there is little CI in the “trimer” and that attempts to include CI are simply erroneous.

Table II. UV-Vis Spectra of Syn-aniline Trimers Compared to Theoretical Prediction.

Trimeric Moiety	CIS/ 6-311++G(d)	Δ SCF method	Experiment
Leucoemeraldine	285 nm	309 nm	314 nm
Emeraldine	378 nm	274 nm	274 nm
		544 nm	544 nm
Emeraldine-HCl	N.A.	285 nm	300 nm
		637 nm	645 nm
Pernigraniline	357 nm	420 nm	412 nm

The data above clearly suggest that both the optical and electronic chromophore of PANi is the trimeric unit as shown in Scheme 1. These characteristics derive from the imbedded phenylene- diamine unit that is common to both the trimer and the polymeric form. In dye chemistry, phenylene diamines have been studied extensively. Aniline capping phenylene diamine produces a series of “trimeric” units in which the optical spectrum parallels that of the polymer and follows directly from the color chemistry of phenylene diamine. The electronic states are similar as well. The reduction potentials are within 0.3 V of the polymeric species with the conducting increasing once the oligomer length approaches three units. The corrosion protection offering by the trimer is equal to or better than PANi, depending on the application. Strengthening the assignment of the trimer, as the necessary chromophore is the observation that protonation of the trimer yields species with chemistries virtually identical to that of PANi. Reduction potentials of the three redox forms trimeric species closely resemble those of the related PANi species as well. This is summarized in Table III below.

Table III. Comparison of Trimers and Corresponding Form of PANi.

Trimer Form	Color Observed	PAni Form
Leucoemeraldine	Colorless	
Leucoemeraldine-HCl	Yellow	Leucoemeraldine-HCl
Emeraldine	Violet	Emeraldine
Emeraldine-HCl	Blue-green	
Emeraldine-2HCl	Green	Emeraldine-2HCl
Pernigraniline	Yellow	

Magnetic properties of the trimers have been assessed by the DFT approach. EPR analyses have been performed on solid materials and methylene chloride glasses. The trimeric materials in the “emeraldine” form are ground state singlets. EPR data show that the unsubstituted trimer in the emeraldine form is very weakly magnetic at room temperature. The hydrochloride salt gives a significant EPR signal that is representation of > 80% of the sample on a per weight basis relative to diphenylpicrylhydrazyl, DPPH. The EPR signal of all of the magnetic trimeric materials in the solid state is generally featureless with a line width of 2-4 G and g value of 2.0036. The magnetic nature of the hydrochloride prompted further analysis. Single point energy calculations give insight into the nature of the magnetism. The results are shown in Table IV.

Table IV. Enthalpies of Emeraldine Base and Salts (in hartrees).

Compound	Singlet	Triplet	$\Delta E_{ST}(eV.)$
Emeraldine	-914.440270	-914.416175	0.66
Emeraldine-HCl	-1375.284411	-1375.265902	0.50
Emeraldine-2HCl	-1835.477244	-1836.102323	-17.00

Complexes of the Aniline Trimer. In some applications, strong electron donors or acceptors were added to PANi to augment band populations. TCNE has been used in many applications. This chemistry suggests strong local interaction between the dopant and the PANi backbone. In an analogous manner, the complexation of the “trimers” with donors and acceptors has been assessed through both experimental and computational tools. To assess the ability of the “trimeric” anilines to form donor/acceptor complexes, we have computed the orbital energies, ionization potentials and electronic affinities of a series substituted “trimers”. DFT calculations of the frontier orbital levels of TTF (tetrathiafulvalene), TCNE (tetracyanoethylene), and TCNQ (tetracyanoquinodimethane), and emeraldine trimer explains why no reaction was found between TTF and emeraldine in experimental studies: emeraldine is predicted to be an even more effective electron donor than TTF. The calculation gives the donor state of TTF to be -4.89eV, whereas the donor state of emeraldine is computed at -4.74eV. The emeraldine trimer has its first acceptor state at -2.45eV, far too high for it to be an effective electron acceptor, even from a donor as such as TTF. On the other hand, with a donor state at -4.74eV, the emeraldine trimer is predicted to be an effective electron donor, especially since the acceptor states of TCNE and TCNQ are at -5.17eV and -5.02eV, respectively. A stable complex is predicted. This is shown schematically in Figure 1. This is in complete agreement with the experimental results.

UV-Vis spectra show that the TCNQ complex formed is stable in solution. This complex can be isolated and redissolved giving the same spectral features. The electronic spectrum for the emeraldine-TCNQ complex is shown in Figure 2. EPR studies on solid samples of the TCNQ “salt” give an expected doublet

resonance at $g = 2.0037$, characteristic of charge transfer complexes. The TTF complexes with emeraldine itself could not be prepared by the method described. Electrochemical methods have subsequently proved successful in the preparation of this TTF-emeraldine complex. Solid complexes have not yet been isolated for this complex and thus this salt is not fully characterized.

Substitution of the Terminal Aniline. The presence of electron donating groups (hydroxyl or alkyl) decreases the ionization potential as would be expected and effects the energy levels of frontier states. The electron-donating effect of these groups should have a profound effect on the trimer/polymer properties with regard to corrosion inhibition. The donation of electrons into the π -conjugated system is expected to increase the basicity of the imine nitrogens. With this increase in basicity, the equilibrium should be shifted further in the direction of the formation of the emeraldine salt (ES) in the presence of acids. It has long been known that the key to the inhibition of iron corrosion is the maintenance of the polymer/trimer as the ES. Therefore, better corrosion inhibition is to be expected for alkylsubstituted emeraldines as their increased basicity favors formation of and stability of the emeraldine salt. The ability to "tune" molecular properties such as the ionization potential or frontier state level is of critical importance in the design of charge transfer complexes. The DFT approach used has guided these substitutions. The energy of donor states of emeraldines can be computed using the DFT method. The results are given in Table V. Similarly the ionization potential and electron affinities can be assessed with this method. These data are shown in Table VI.

Table V. Frontier Energy/Donor Energy States for Substituted Aniline Trimers.

Emeraldine Derivative	HOMO Level/Donor State (eV)
Emeraldine	-4.74
2-hydroxyemeraldine	-5.00
2,6-dimethylemeraldine	-4.58
2,6-diethylemeraldine	-4.63

Table VI. Computed Ionization Potentials and Electron Affinities for Substituted Trimer Compounds (in kcal/mol)

Compound	Ionization Potential	Electron Affinity
Leucoemeraldine	121.8	N.A.
2,6-diethylemeraldine	127.1	N.A.
2-hydroxyemeraldine	130.8	N.A.
	133.9	-32.7
Emeraldine		
Emeraldine-HCl	148.9	-55.3
Emeraldine-2HCl	N.A.	-87.7

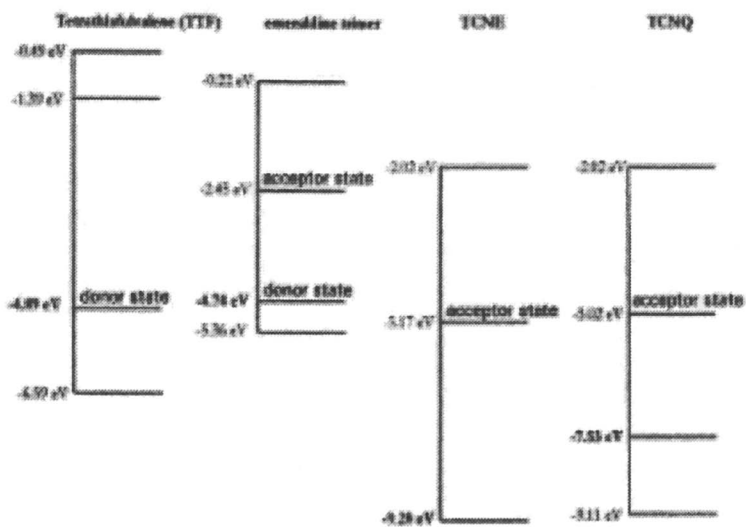


Figure 1. Frontier orbital levels of TTF, TCNE, TCNQ and the emeraldine trimer as calculated at B3LYP/6-311G(2d,p)

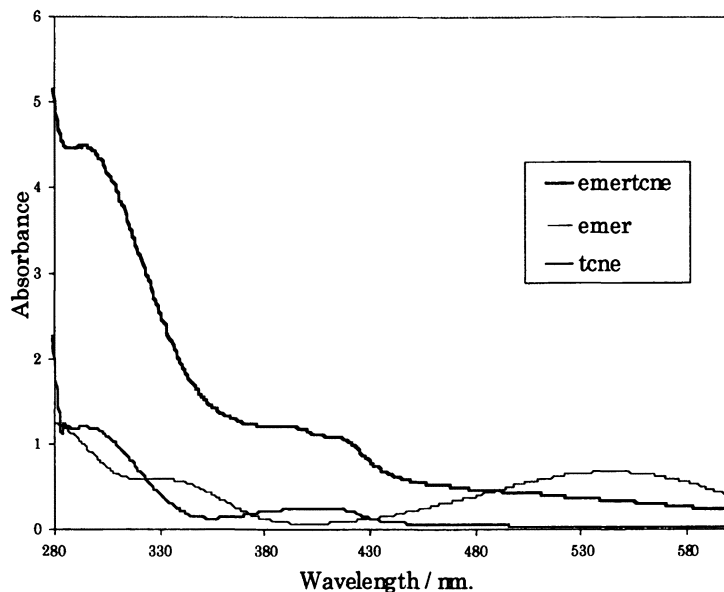


Figure 2 - UV-Vis spectra of trimeric emeraldine and its TCNE charge transfer complex.

Table VI. Computed Ionization Potentials and Electron Affinities for Substituted Trimer Compounds (in kcal/mol)

Compound	Ionization Potential	Electron Affinity
Leucoemeraldine	121.8	N.A.
2,6-diethylemeraldine	127.1	N.A.
2-hydroxyemeraldine	130.8	N.A.
	133.9	-32.7
Emeraldine		
Emeraldine-HCl	148.9	-55.3
Emeraldine-2HCl	N.A.	-87.7

To date, corrosion inhibition studies using the alkyl-substituted trimers has not been completed. However, the predictive nature of the calculations suggest that such materials in addition to showing a greater range of solubility in organic solvents should perform better as corrosion inhibitors.

Solvent and Conformational Effects for Substituted Trimeric Anilines. Aniline trimers can exist in several different isomeric forms depending on the steric and electronic requirements of the substituent. It is anticipated that isomers that possess very specific energetic requirements and they will display markedly different ionization potentials and electron affinities. Therefore, redox phenomena and the ability to form charge transfer complexes will be affected by the conformation of the trimer. Table VII shows the Boltzmann distribution of isomers for a series of substituted emeraldines.

Table VII. Energetics of Alkyl Substituted Emeraldine Trimers

Trimer	H*	Boltzmann Distribution**
Syn-emeraldine	-914.4402699	1.000
Anti-emeraldine	-914.4401319	0.862
Syn-2,6-dimethyl-emeraldine	-1071.635779	1.000
Anti-2,6-dimethyl-emeraldine	-1071.635563	0.793
Syn-2,6-diethyl-emeraldine	-1228.805866	1.000
Anti-2,6-diethyl-emeraldine	-1228.805263	0.522
Syn-2,6-diisopropyl-emeraldine	-1386.665746	1.000
Anti-2,6-diisopropyl-emeraldine	-1386.665226	0.571

*As computed by B3LYP/6-311G(2d,p)

** Most likely conformer scaled to a population of 1.00.

It has been suggested that alkyl substitution of the terminal anilines will decrease the conductivity by increasing the torsion angles within the oligomer or polymer, thus reducing π overlap. Conductivity is also decreased in alkyl substituted conducting polymers by decreased chain-to-chain interactions since the chains will be spaced farther apart. Gas phase calculations on all of the alkyl substituted trimers including the diisopropyl substituted trimer show no significant increase in the torsion angle. Electronic spectra obtained in acetonitrile show that the longest wavelength absorption undergoes a 41 nm red shift for the diisopropyl derivative thus suggesting that there is no disruption of the conjugation or electronic coupling between the terminal aniline groups.

Solvation appears to effect the frontier levels in solution, which may imply a matrix effect on the solid state band gap. Table VIII compares computed wavelengths of the primary electronic transitions with those obtained in hexane and acetonitrile.

Table VIII. Predicted UV-Vis Bands Compared with Experiment (nm)

Trimer	Δ SCF	Hexane	Acetonitrile
Syn-emeraldine	277, 544	N.A.	277, 544
Anti-emeraldine	277, 544	N.A.	277, 544
Syn-2,6-dimethyl-emeraldine	269, 549	N.A.	292, 556
Anti-2,6-dimethyl-emeraldine	271, 556	N.A.	292, 556
Syn-2,6-diethyl-emeraldine	270, 552	312, 530	305, 570
Anti-2,6-diethyl-emeraldine	268, 559	312, 530	305, 570
Syn-2,6-diisopropyl-emeraldine	273, 550	300, 554	300, 585
Anti-2,6-diisopropyl-emeraldine	274, 558	300, 554	300, 585

Much work has been performed comparing solid state band gaps and solution “band gaps”. A strong correlation is noted between the two. The computed band gaps for the syn 2,6-dialkyl substituted trimers show little variation from that of syn-emeraldine. Syn-emeraldine has a computed HOMO-LUMO gap of 2.29 eV. The syn 2,6 dialkyl substituted trimers all give a HOMO-LUMO gap of 2.25-2.24 eV. The data in Table VIII implies the solvent or matrix plays a critical role in ultimately determining the band properties or redox states. A few possibilities exist including a solvent induced change in the conformational distribution or formation of a solvation complex with unique electronic features.

Conclusion

In this work, we have demonstrated remarkable parallels between the electronic character of aniline trimers and PANi. In addition, computational modeling has shown to be predictive of important electronic properties such as ionization potential and electron affinity. These predictions have guided substitution chemistry and provide useful feedback to help with rationalizing the electronic nature afforded by the synthetic chemistry. This is an example where computational tools provided an understanding of PANi chemistries *and were predictive in determining synthetic targets and defining electronic characteristics. And perhaps most importantly, this series of calculations proposes that the emeraldine salt is the most important PANi form for corrosion inhibition.*

References

1. (a) Skotheim, T. A.; Eisenbaumer, R.L.; Reynolds, J.R., Eds. *Handbook of Conducting Polymers*, 2nd ed., Marcel Dekker: New York, 1997. (b) Skotheim, T.A., Ed. *Handbook of Conductive Polymers*, Vols. I and II, Marcel Dekker: New York, 1986.
2. (a) MacDiarmid, A.G.; Epstein, A.J., *Faraday Discussion, Chem Soc.* **1989**, *88*, 317. (b) Genies, E.M.; Boyle, A.; Lapkowski, M.; Tsintavis, C. *Synth. Met* **1990**, *36*, 139. (c) Roncali, J. *Chem. Rev.* **1992**, *92*, 711.

3. MacDiarmid, A.G.; Chang, J.C.; Richter, A.F.; Somasiri, N.L.D.; Epstein, A.J. In *Conducting Polymers*; Alcacer, L., Ed., Reidel Publishing Co.: Holland, 1987.
4. Sheikh-Ali, B.M.; Wnek, G.M. In *Chemistry in Advanced Materials*, Interante, L.V.; Hampden-Smith, M.J., Eds., Wiley-VCH: New York, 1998 pp.73-98
5. Roberts, S.; Ondrey, G., *Chem. Eng.* July 1996, p. 44.
6. Wei, Y.; Yang, C.; Ding, T., *Tetrahedron Lett* **1996**, 36, p 4535.
7. Ping, Z.; Nauer, G.E.; Neugebauer, H.; Thiener, J.; Neckel, A., *J. Chem. Soc. Faraday Trans.* **1997**, 92, p.121.
8. Frank, M.H.T.; Denault, G.J., *Electroanal. Chem.* **1994**, 379, p. 399.
9. Kogan, Y.L.; Shunina, I.G.; Gedrovich, G.V.; Yuzhanina, A.V., *Synth. Met.* **1991**, 43, p. 2911.
10. Lu, F.-L.; Wudl, F.; Nowak, M.; Heeger, A.J.; *J. Am. Chem. Soc.* **1986**, 108, p. 8311
11. (a) Honzl, J.; Ulbert, K.; Hadek, V.; Tlustakova, M. *Chem. Commun.*, **1965**, p. 440. (b) Honzl, J.; Tlustakova, M., *J. Polym. Sci.: Part C*, **1968**, 22, p. 451.
12. Shacklette, L.W.; Wolf, J.F.; Gould, S.; Baughman, R.H., *J. Chem. Phys.* **1988**, 88, p. 3955.
13. (a)Feng, J.; Zhang, W.J.; MacDiarmid, A.G.; Epstein, A.J., *Proc. SPE/ANTEC'97*, **1997**, 55(2), p. 1373. (b)Wienk, M.M.; Janssen, R.A.; *J. Am. Chem. Soc.*, **1996**, 118, p. 10626.
14. Bebert, P.H., Batich, C.D., Tanner, D.B., Herr, S.L., *Synth. Met.*, **1989**, p.34.
15. Yeh, J.M., Doctoral Dissertation, Drexel University, 1996.
16. Wei, Y.; Wang, W.; Yeh, J.M.; Wang B.; Yang, D.; Murray, J.K.; Jin, D.; Wei, G. *Am. Chem. Soc. Ser. No. 585*, **1995**, Chapter 11, p. 125.
17. Huang, H.; Orler, B.; Wilkers, G.L., *Macromol.*, **1987**, 20, p. 1322.
18. Frisch M.J.; Trucks, G.W.; Schlegel, H.B.; Gill, P.M.W.; Johnson, B.G.; Robb, M.A.; Cheeseman, J.R.; Keith, T.; Petersson, G.A., Montgomery, J.A.; Raghavachari, K.; Al-Laham, M.A.; Zakrewski, V.G.; Ortiz, J.V.; Foresman, J.B.; Cioslowski, J.; Stefanov, B.B.; Nanayakkara, A.; Challacombe, M.; Peng, C.Y.; Ayala, P.Y.; Chen, W.; Wong, M.W.; Andres, J.L.; Replogle, E.S.; Gomperts, R.; Martin, R.L.; Fox, D.J.; Binkley, J.S.; Defrees, D.J.; Baker, J.; Stewart, J.P.; Head-Gordon, M.; Gonzalez, C.; Pople, J.A., *Gaussian 94, Revision D-3*, Gaussian Inc., Pittsburgh PA, 1995
19. Foresman, J.B.; Frisch, A.E., *Exploring Chemistry with Electronic Structure Methods*, Gaussian Inc., Pittsburgh PA., 1996.
20. Foresman, J.B.; Head-Gordon, M.; Pople, J.A., Frisch, M.J.; *J. Phys. Chem.*, **1992**, 92, p. 135.

Chapter 6

Factors Influencing the Performance of Inherently Conducting Polymers as Corrosion Inhibitors: The Dopant

Gordon G. Wallace^{1,*}, Anton Dominis¹, Geoffrey M. Spinks¹,
and Dennis E. Tallman^{2,3}

¹Intelligent Polymer Research Institute, University of Wollongong,
Northfields Avenue, Wollongong, NSW 2522, Australia

²Department of Chemistry, North Dakota State University,
Fargo, ND 58105-5516

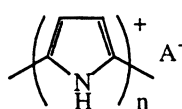
³Email: dennis_tallman@ndsu.nodak.edu

*Corresponding author: Email: gordon_wallace@uow.edu.au

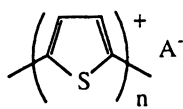
The dopant (A⁻) that is intimately associated with inherently conducting polymers (ICPs) such as polypyrroles and polyanilines plays a critical role in determining the performance of these materials as corrosion protection coatings. The dopant determines the processability of the ICP in that it can influence solution solubility and/or the potential at which the polymer is electrodeposited. The dopant also influences the redox and chemical properties of the resultant coating and so affecting its ability to provide corrosion protection.

INTRODUCTION

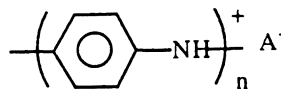
Inherently conducting polymers (ICPs) such as polypyrroles, polythiophenes and polyanilines (I-III) shown below are interesting structures in that they are electronic conductors, undergo redox reactions at moderate potentials and they are organic in nature, forming good-quality films and coatings.



(I)



(II)



(III)

Accompanying these redox changes are dramatic changes in the chemical, physical and electronic properties of the polymer (1). The multifaceted behaviour of these materials has provided numerous challenges in understanding their behaviour in complex environmental conditions. Perhaps none more so challenging than understanding the role they play when used as corrosion protection agents.

A number of studies into the use of conducting polymers for corrosion protection of either ferrous or non-ferrous substrates have been carried out and these areas have been reviewed recently (see references 2a and 2b respectively).

It appears the conducting polymer layer can provide protection in a number of ways

- as a barrier coating (3-5)
- by ennobling the underlying metal (6-8)
- by mediating the formation of corrosion products that form inert passive layers (9-11)

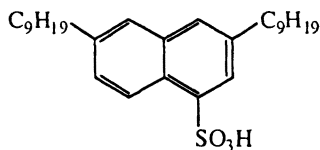
Given that the so called dopant (A^-) constitutes of the order of 50% of the weight of the polymer it obviously plays a critical role in determining the properties and performance of the overall material.

In the course of our recent studies we have been particularly interested in the effect of the dopant on the ability to provide corrosion protection using coatings based on inherently conducting polymers. How the dopant influences some of the key aspects of corrosion protection is discussed below using examples from our own laboratory and from recent literature reports.

EXPERIMENTAL

Reagents and Standard Solutions

The polyaniline used was that recently introduced by Kinlen and coworkers and described as a processable polyaniline. The polyaniline is in the emeraldine salt (PANi-ES) form and utilises dinonylnaphthalene sulfonic acid (DNNSA – IV shown below) as dopant.



IV \equiv DNNSA

The PANi-ES(DNNSA) was obtained from MONSANTO and was received as a liquid concentrate comprised of ~47(wt)% PANi(DNNSA) solids, ~30(wt)% butyl cellulose and ~20(wt)% xylene solvent. The 'as-received' concentrate was diluted with AR grade xylene to 5% (w/w) and casting carried out by "air-brush" spraying onto a heated glass microscope slide or cold rolled A06 grade plain carbon steel (PCS). A hand held "air-brush" spraying system operated at 400 kPa (60psi) nitrogen pressure was used. The PANi-ES(DNNSA) coating was then dried in an air oven at 80 °C for 24 hr.

De-protonation and re-protonation solutions were prepared using double distilled water and AR grade methanol (Univar). Sodium hydroxide (BDH) (1.0M dissolved in 50:50 water / methanol) was used to de-protonate the PANi.DNNSA films, while re-protonation was carried out using numerous inorganic and organic acids such as *p*-toluenesulfonic acid (Merck), tartaric (TA) acid (Univar), dodecylbenzenesulfonic acid (DDBSA) (Crown scientific), HCl (Ajax) and a water-soluble sulfonated polyaniline (PMAS, Nitto Chemical).

Full immersion testing of the corrosion protection behaviour of the various polyaniline coatings on plain carbon steel (PCS) was carried out in stagnant aerated solution containing 500 mg Cl⁻/L (NaCl, pH 5-6) or 3.5% NaCl at ambient temperature. Iron liberated into the saline solutions was determined using inductively-coupled plasma (ICP) analysis.

The galvanic cell set-up shown in Figure 1 was employed to determine the effect of the galvanic coupling on the steel corrosion rate. Polyaniline film electrical conductivities were measured using the four-point probe conductivity method.

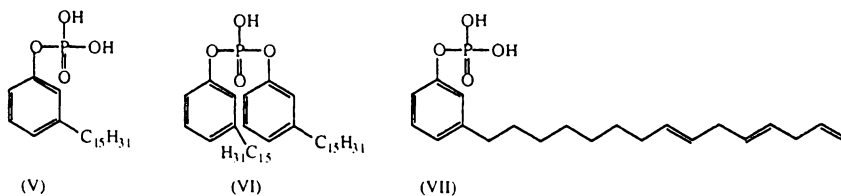
Electrocatalytic Deposition of Polypyrrole

Aluminium alloy 2024-T3 (Q-Panel) was prepared by polishing with 600-grit paper followed by degreasing with hexane. The electrodeposition solution contained 0.1 M pyrrole (freshly distilled) and 0.1 M tiron or p-toluenesulfonic acid sodium salt (Na-pTS). Electrodeposition was carried out in the galvanostatic mode at a current density of 1 mA/cm² using a stainless steel mesh counter electrode. Potentials were measured with respect to a saturated Ag/AgCl reference electrode.

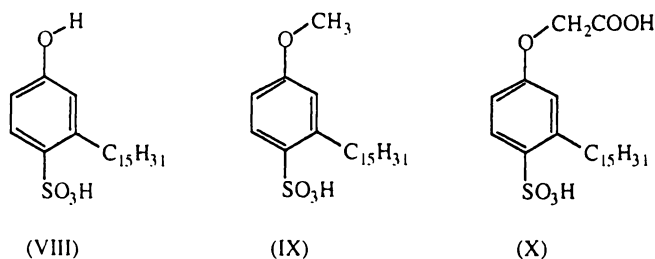
RESULTS AND DISCUSSION

Film Formation - Processability

The ability to form an impervious ICP layer using traditional coating technologies depends on the ability to form soluble polymers or stable dispersions. The dopant (A⁻) incorporated into polyaniline or polypyrrole plays a critical role in this regard. For example, it is well known that the solubility of conducting polyanilines is dopant dependent. Several sulfonated aromatics have been shown to render the material soluble in common organic solvents such as xylene, CH₂Cl₂ or CHCl₃ (12, 13). An interesting synergistic effect was observed recently (13a) with polyanilines doped with both chloride and camphorsulfonate having reasonably high conductivity (7.9 Scm⁻¹) and with solubility in common organic solvents. Others have carried out a detailed investigation into the effect of different sulfonic acid dopants on the structure and solubility (in m-cresol) of the resultant polyanilines (14). Besides the sulfonic acid dopants the other most interesting compounds used to induce processability in polyanilines are the phosphoric acid diesters (15) which render the conducting polymer both melt and solution processable (see structures below).



More recently (15a) the use of the sulfonic acid dopants (shown below) was shown to render polyanilines melt processable.



The dopant used will also influence the ability to form polymer blends (12) which may well be the processing route of choice for practically useful corrosion protection coatings.

Other workers (16, 17) have utilised alkylsulfonated dopants to produce polypyrroles soluble in chloroform and other common organic solvents. Interestingly there are no reports of dopant induced solubility in polythiophenes.

However, the role of the dopant in rendering the polymer soluble is only the initial requirement. The resultant polymer must also have good film forming capabilities, to do this it must "wet" the metal of interest. In addition, it should be compatible with top coats (such as epoxies, acrylics, polyurethanes and polyesters) and the curing procedures to be used for top coats (eg. baking or UV-curing) should not compromise the ICP layer.

The effect of the dopant on the contact angle (surface tension) of some polypyrroles has been investigated previously and shown to have a dramatic effect (18). Using dynamic contact angle analyses the effect of the dopant on polymer wettability was investigated (Table 1).

When NO_3^- was used as a dopant the relative polarity of the polypyrroles formed was the same as for the substrate employed. That is, the polymer grown on carbon foil is more hydrophobic than those deposited on platinum and glassy

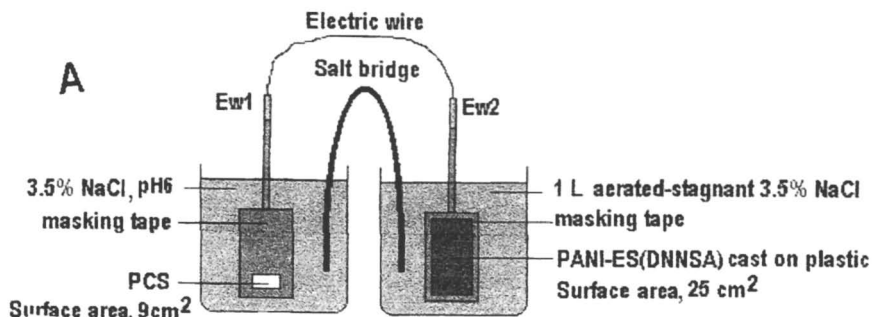


Figure 1. Schematic diagram showing galvanic coupling of PCS to polyaniline.

Table 1. Comparison of $\cos\theta$, θ and $\Delta\theta$ values for polypyrrole (NO_3^-) and polypyrrole (DS^-) on carbon foil (CF), glassy carbon (GC) and platinum (Pt) substrates (subscripts a and r refer to advancing and receding contact angles, respectively).

Sample	$\cos\theta_a$	$\cos\theta_r$	θ_a	θ_r	$\Delta\theta$
CF/PP(NO_3^-)	0.12	0.93	83°	21°	62°
CF/PP(DS^-)	0.74	0.84	42°	33°	9°
GC/PP(NO_3^-)	0.52	1.02	59°	<i>u</i>	59°
GC/PP(DS^-)	0.02	0.97	89°	14°	75°
Pt/PP(NO_3^-)	0.62	0.97	52°	5°	47°
Pt/PP(DS^-)	0.16	0.98	81°	12°	69°

Data extracted from reference 18.

CF: carbon foil

GC: glassy carbon

Pt: platinum

carbon. Therefore, the surface properties of the substrate material are influencing the surface properties of the polypyrrole. For the polymers prepared with DS⁻, which is a surfactant, we see the relative positions of the advancing contact angle values switched compared with those obtained for NO₃⁻. The coated carbon foil substrate now produces the lowest θ_a , and therefore the most polar surface, whereas the polymers deposited onto the glassy carbon and platinum substrates are much more non-polar. The DS⁻ has a charged, polar end and a hydrophobic end.

However, the result for the receding angle (θ_r) is quite high, in fact higher than occurs in any other polymer investigated here. A possible explanation for the high θ_r is that the DS⁻ groups undergo a reorientation upon wetting causing the hydrophobic ends to align at the interface, although the reasons for this occurrence are unknown. The very low hysteresis value (9°), much lower than has been observed for other conducting polymers, suggest that some additional types of interaction, such as reorientation, may be occurring.

These results indicate that the dopant used and the substrate onto which the polymer is deposited have a marked influence upon the surface properties of the resultant polymer coating.

Two studies from our laboratories are now discussed to highlight the important role in determining the corrosion protection capabilities of inherently conducting polymers.

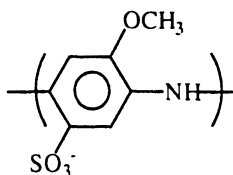
Polyanilines on Steel

In the case of polyaniline, the DNNSA (IV) dopant facilitates subsequent processing of the ICP into coatings for steel and other metals.

Introduced by Kinlen and coworkers (19) this dopant induces formation of stable polyaniline dispersions in xylene and butyl cellulosolve. In our laboratories we have shown that such dispersions can be sprayed onto hot metal surfaces to produce uniform, adherent films.

The use of the PANi.DNNSA coating system to protect plain carbon steel (PCS) has been investigated by us to determine the effect of dopant on corrosion protection. We have carried out a series of experiments (20) whereby the PANi-emeraldine salt (DNNSA) coatings are dedoped to remove the DNNSA and then redoped with a range of other anions: H₂PO₄⁻, tartrate, Cl⁻, dodecylbenzene

sulfonic acid or a sulfonated polyaniline (PMAS) XI shown below. Full immersion tests and monitoring of iron dissolution (Figure 2) showed that the effectiveness of corrosion protection was highly dopant dependent.



(XI)

This performance was confirmed by galvanic cell experiments carried out using the set up shown in Figure 1. Monitoring of the iron dissolution rate in the analyte showed that the steel corrosion rate was significantly influenced by the dopant used (Figure 3).

There are striking differences between galvanically coupled PANi-ES and PCS when tested as a coating of PANi-ES on steel or when they are physically separated (but electronically connected). In the latter case, as described above, the PANi-ES causes an acceleration of the PCS corrosion rate. However, when the PANi-ES is used as a primer between the steel and a polyurethane topcoat, the corrosion rate of the steel is decreased compared with PCS coated only with polyurethane. Presumably the difference in these two scenarios is the different nature of the chemical environment at the steel surface. When the polyaniline and the steel are physically separated the steel surface is exposed to the bulk electrolyte and only small changes in ion concentration, pH and dissolved oxygen are likely to occur. When the polyaniline is coated onto the steel (along with a polyurethane topcoat) the access of ions and oxygen to the steel surface is restricted. Furthermore, the release of counterions from the PANi-ES during reduction to leucoemeraldine will also change the chemical environment, as will cathodic reactions leading to an increase in local pH. Finally, the anode: cathode surface area ratio is likely to be different when the PANi-ES is applied as a coating compared to the case where the PANi-ES is physically separated from the steel. This surface area ratio will affect the extent of ennoblement and, therefore, the extent of galvanic reactions.

As with the galvanic coupling experiments, the nature of the dopant anion causes a significant effect on the rate of corrosion when the PANi-ES was used as a primer coating. PANi-ES doped with counterions such as PMAS and tartaric acid show corrosion rates considerably lower than the polyurethane coated steel (up to 90% lower after 15 days immersion). In contrast, PANi-ES doped with

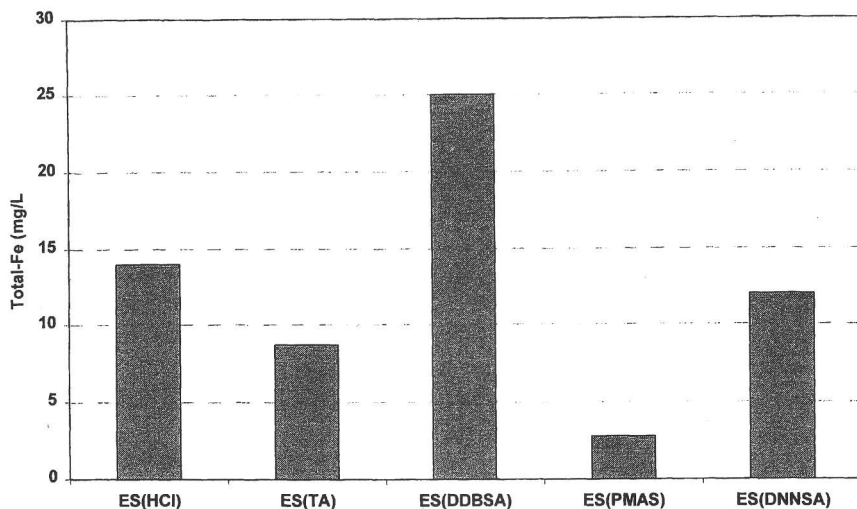


Figure 2. Concentration of soluble iron in test solution after 15 days immersion for polyaniline/polyurethane (PU) coated steels. Different dopants were incorporated into the polyaniline emeraldine salt (ES), as indicated.

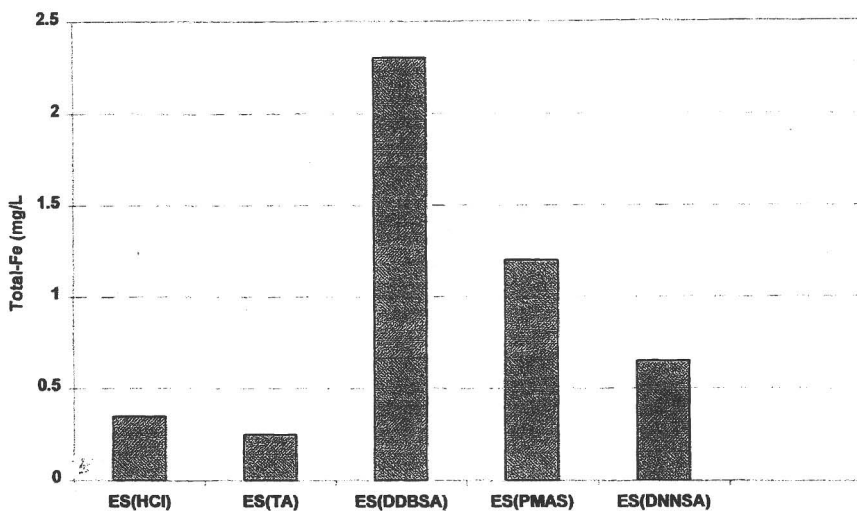
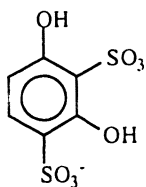


Figure 3. Concentration of soluble iron in test solutions after 60 hr immersion for PCS galvanically coupled to polyaniline emeraldine salt (ES) (various dopants), as indicated.

DDBSA showed only a slight decrease in corrosion rate compared with the polyurethane coated steel (approximately 20% reduction in corrosion rate after 15 days immersion). Interestingly, the DDBSA doped PANi-ES was shown to cause the greatest degree of corrosion acceleration in the galvanic coupling experiments. This trend was not generally observed, however, since the PMAS doped PANi-ES was also shown to be a strong corrosion accelerant when galvanically coupled, but this polymer showed the best corrosion protection when used as a primer coating.

Polypyrrole on Aluminium Alloy 2024-T3

This example highlights the role of the dopant (Tiron - XII shown below) in enabling effective electrodeposition of polypyrrole coatings on Al for corrosion protection.



(XII)

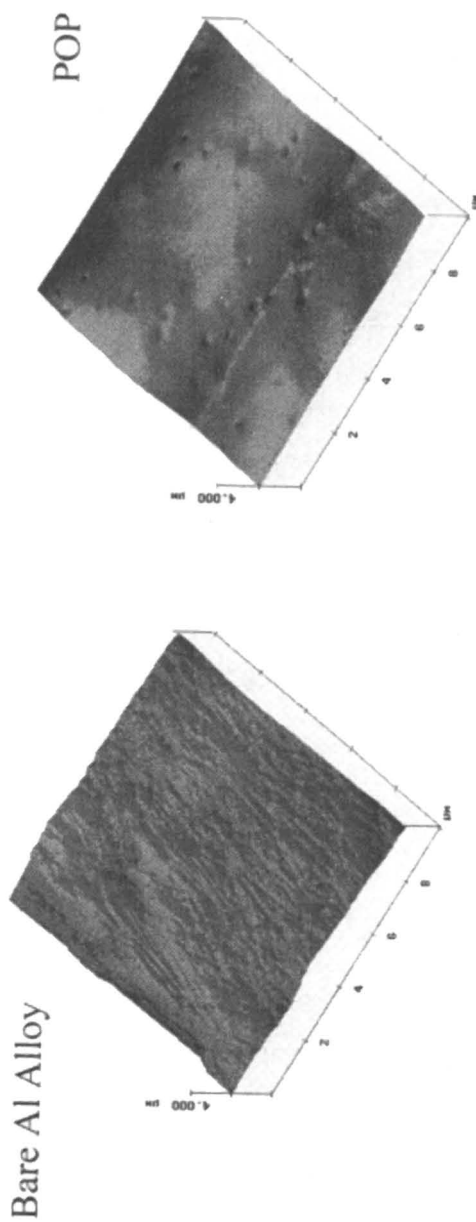
Adhesion and cohesion of the ECP film to the metal substrate is an important issue for many applications of ECPs, but particularly for corrosion control applications. Work in our laboratory with organic solvent soluble forms of polypyrrole indicates that modest adhesion can be achieved by a solvent casting approach. For example, a coating of poly(3-octyl pyrrole) having a mixture of perchlorate and *p*TS dopant anions on Al 2024-T3 (the POP film in Figure 4) exhibited an adhesion of 2.30 ± 1.43 MPa, with failure being primarily cohesive failure (21).

It is anticipated that the direct electrodeposition of ECPs onto active metals might lead to improved adhesion and cohesion. Improved adhesion might be achieved if a large number of nucleation sites on the oxide surface could be realized, providing a large number of attachment points for the polymer film. Improved cohesion might be anticipated due to the larger molecular weight achievable by direct electrodeposition compared to solvent casting, where typically only lower molecular weight fractions of the polymer are soluble. Larger molecular weight should lead to increased chain entanglement and

improved cohesion. However, since the electropolymerization of polypyrrole is an anodic process carried out at rather positive potentials, the anodic dissolution (or accelerated corrosion) of the active metals of the alloy during electropolymerization is an expected complication. In the case of aluminium and its alloys, the oxide layer that forms is an insulator that blocks electron transfer and impedes polymer formation and deposition. As a result, only patchy non-uniform polymer films are obtained.

Beck and coworkers described the electrodeposition of polypyrrole on iron (22-24) and on aluminium (25-27). Their electrodepositions on Al were carried out in non-aqueous (25) as well as in aqueous solutions (26, 27) using relatively pure aluminium metal (not an Al alloy). Electropolymerization of pyrrole on Al from aqueous solution was found to be strongly influenced by surface pretreatment of the Al, with diamond paste polishing or galvanostatic activation into the pitting region being required for acceptable coating formation (26). Even then, at low concentrations of pyrrole (0.1 M), film deposition was patchy and deposition potential increased during galvanostatic deposition, attributed to growth of an Al_2O_3 layer in parallel with the electropolymerization. Only at high (0.8 M) pyrrole concentration and in the presence of 0.1 M oxalic acid could smooth adherent films be produced. The polymerization was still accompanied by growth in the thickness of the Al_2O_3 layer (Al corrosion) and formation of some overoxidized polypyrrole was noted (26). Overoxidation increases the localization (i.e., hinders delocalization) of the charge carriers in the polymer, leading to reduced conductivity.

Electron transfer mediation is a well-known technique for overcoming kinetic limitations of electron transfer at metal electrodes and lowering the potential for such reactions. In work to be reported elsewhere, electron transfer mediation was used for the direct electrodeposition of polypyrrole onto aluminium and onto Al 2024-T3 alloy (28). Using Tiron[®] (4,5-dihydroxy-1,3-benzenedisulfonic acid disodium salt) as the mediator and also the dopant, electrodepositions were carried out under galvanostatic conditions at current densities of 1 mA/cm^2 . The mediator reduced the deposition potential by nearly 500 mV compared to deposition performed in the absence of mediator (where Tiron was replaced by *p*-toluene sulfonic acid sodium salt, *p*TS). Polypyrrole/Tiron electrodeposition occurred with nearly 100% current efficiency, leading to uniform, conducting (250 S/m) films. The adhesion of $6.11 \pm 0.78 \text{ MPa}$, was significantly higher than that of solvent cast polypyrrole films. Failure was characterized by cohesive failure only, with no observable adhesive failure at the metal/polymer interface. For comparison, electrodeposited polypyrrole/*p*TS films (i.e., without electron transfer mediation) exhibited an adhesion of only $0.37 \pm 0.03 \text{ MPa}$, with failure characterized by a mixture of cohesive and adhesive failure. Clearly,



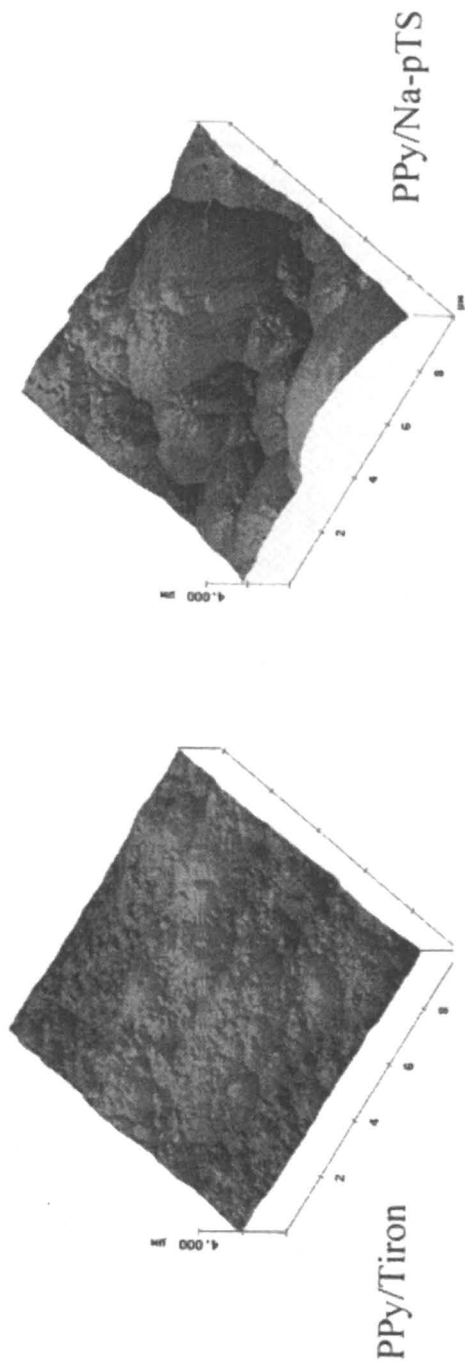


Figure 4. Atomic force micrographs of bare Al 2024-T3 alloy (top left) and various polypyrrole films deposited on the alloy: top right - a solvent cast poly(3-octyl pyrrole) film; bottom left - a polypyrrole film deposited galvanostatically in the presence of tiron (8-minute deposition); bottom right - a polypyrrole film deposited galvanostatically in the presence of Na-pTS (16-minute deposition).

Tiron mediated electrodeposition leads to a polypyrrole film with significantly improved cohesion and adhesion to the Al alloy. This improved adhesion appears to be due, at least in part, to an increase in the number of nucleation sites on the alloy surface promoted by the Tiron, as revealed by in-situ atomic force microscopy (28). The enhanced adhesion may also be due in part to the well-known metal complexing ability of the Tiron which might serve to stabilize the PPy/alloy interface. Thus, the Tiron appears to play several roles, serving as electron transfer mediator (29), as the dopant (counterion) and perhaps as adhesion promoter.

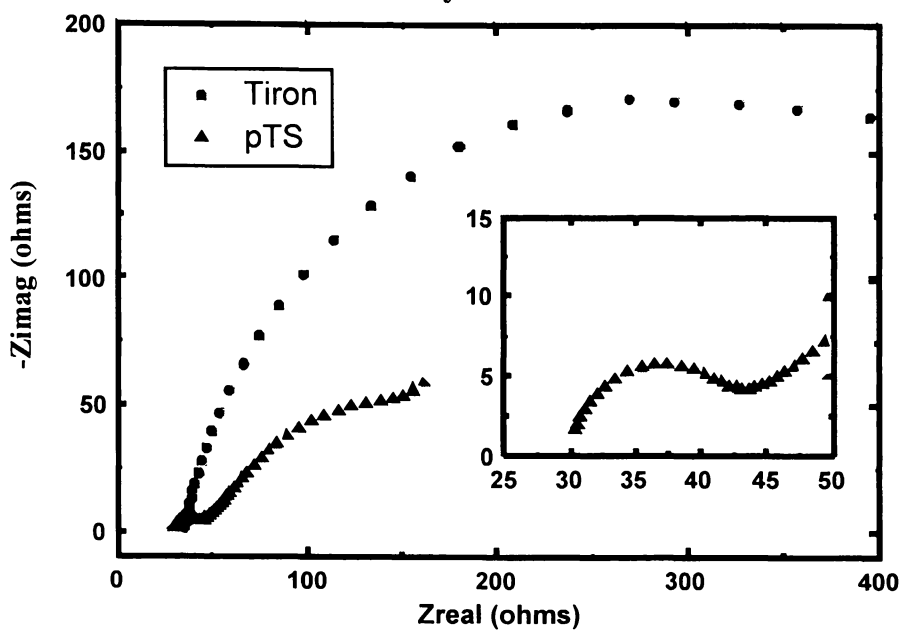
Long term corrosion experiments with PPy/Tiron films on Al 2024-T3 alloy are in progress, but some preliminary immersion data is available. The corrosion protection capabilities of the polypyrrole coatings electrodeposited on aluminium were investigated using traditional electrochemical methods. Electrochemical impedance spectroscopy was performed on the two electrodeposited films after ca. 30-min. immersion in dilute Harrison solution (0.35% $(\text{NH}_4)_2\text{SO}_4$, 0.05% NaCl in H_2O). This immersion solution is an aggressive electrolyte that simulates an industrial corrosive environment. Interestingly, the two spectra are quite different (Figure 5). The polypyrrole/pTS sample displayed a small arc at high frequencies followed by an apparent Warburg diffusion tail that bends back towards the real axis at low frequencies, indicative of finite diffusion of the pTS counterion within the thin polypyrrole film. The very low charge transfer resistance associated with the small arc (ca. 15 Ω) is likely due to the incomplete coverage of the alloy by the polymer film and/or to intimate contact between the polymer and Al metal exposed during the extensive alloy corrosion that accompanies electrodeposition of the polymer. A very similar result was obtained by Beck and coworkers for polypyrrole deposition in the presence of 0.1 M oxalic acid after anodic pretreatment of aluminium metal (26).

In contrast, the PPy/Tiron sample displayed much more capacitive behaviour with a much greater charge transfer resistance (larger diameter arc), suggestive of a much more continuous polymer film with much slower charge transfer kinetics. A continuous oxide layer formed and/or stabilized by the polymer at the metal interface would lead to such.

Some further thoughts on dopant effects

The proposed mechanism of corrosion protection for PANi on steel can be summarised by the scheme depicted in Figure 6.

Polypyrrole Electrodeposited on Al 2024-T3
EIS on Day 1 of Immersion



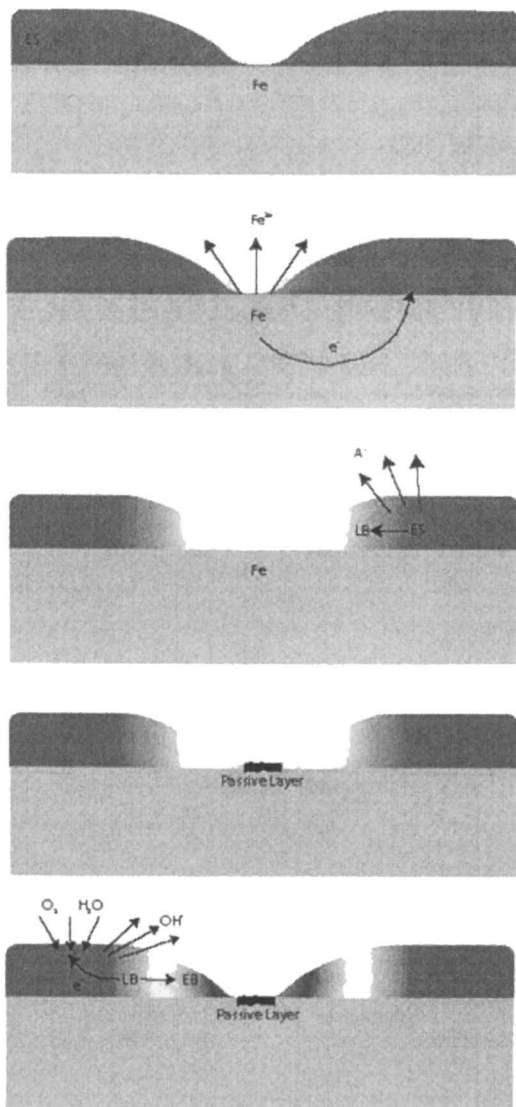
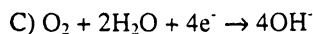
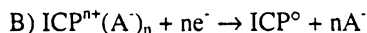
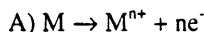


Figure 6. Proposed mechanism of corrosion protection by polyaniline coatings at pinholes (a). Oxidation of the metal (b). Causes electron flow to the emeraldine salt (ES) coating resulting in reduction of the ES to leucoemeraldine base (LB) and release of the A^- counterion into the corrosive environment (c). The local conditions are conducive to the formation of a stable oxide layer (d). That slows further corrosion at the pinhole. The LB is re-oxidised by atmospheric oxygen to the emeraldine base (EB) as shown in (e).

The dominant reactions will undoubtedly change depending on the state of the corrosion process with a series of reactions according to:



along with the formation of insoluble metal oxides and metal complexes. Obviously the extent and rate of these reactions determines the nature of the products formed especially the type of passivating film that may form. The kinetics of these reactions will be highly dependent upon many factors, including:

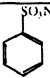
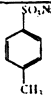
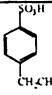
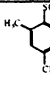
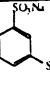
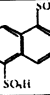
- (i) E° of polymer (dopant dependent).
- (ii) Rate of transport of ions and gaseous species to the points of redox reaction (depends on properties of ICP and topcoat).

Although not studied in detail in corrosion studies with ICPs the transport of simple ions (such as Na^{+}) as well as water and O_2 across ICP membranes and the effect of the oxidation state on these has been investigated in other work. For example, the effect of dopant on the transport characteristics of simple salts such as K^{+} and Na^{+} chlorides has been investigated (30, 31). Flux rates can vary over an order of magnitude with simple changes in dopant (see Table 2).

Others have investigated the permeation of oxygen across polypyrrole and polyaniline (32) membranes. The GPR (Gas Permeation Rate) values are quoted as low. Some are shown in Table 3. Others (33) have shown that the oxygen permeability of polyaniline varies (decreases) by a factor of almost 50 as the pH (and hence the degree of protonation of PANi) is varied from 1 to 5.

This effect of the degree of doping on oxygen permeability has also been reported by others (34, 35). The effect of the dopant on O_2 permeability has been studied with variation not so dramatic. eg. from 0.16 (Cl^{-} doped) to 0.10 (pTs doped) values reported (36). Martin and coworkers (37) reported that the O_2

Table 2. Effect of the counterion on the tensile strength, potassium ion flux rate and conductivity of the membranes.

Membranes ^a	PP/BSA	PP/PTS	PP/EBS	PP/MS	PP/BS	PP/NPS
Counterions						
Tensile strength (MPa)	17-23	70-80	60-70	36-47	40-55	40-50
Conductivity (S/cm)	19-20	90-110	90-110	50-70	47-70	50-70
Flux K ⁺ (mol·cm ⁻² ·sec ⁻¹)	2.8 x 10 ⁻¹⁰	1.9 x 10 ⁻⁹	1.3 x 10 ⁻⁹	1.6 x 10 ⁻⁹	1.4 x 10 ⁻⁹	2.2 x 10 ⁻⁹

^a Note this name in detail is used throughout the text to describe polypyrrole (PP) containing each of these counterions.

Table 3. Gas permeation rate for oxygen (9cm³ (STP) cm⁻² sec⁻¹ cm Hg⁻¹)

Polypyrrole	5 x 10 ⁻⁷
Polymethylpyrrole	1.5 x 10 ⁻⁶
Polyaniline	8.4 x 10 ⁻⁹

permeability of polypyrroles is also dependent on the oxidation state (level of doping) of the polymer.

The transport of water across polyaniline membranes has been investigated (38). It was found that the rates of permeation were oxidation state dependent (ES 4.1 g/m²h and EB 13.0 g/m²h). These rates of permeation are low when compared to other conventional polymers such as poly(dimethyl siloxane) 780 g/m²h and similar to polyvinylchloride 6.0 g/m²h. The effect of the dopant on all of these transport properties is significant and this will subsequently influence the corrosion processes occurring.

CONCLUSIONS

The role played by ICPs in providing corrosion protection is a somewhat complex one. The dopant employed also has a dramatic impact on this role. The nature of the dopant influences the nature of the redox process (eg. cation incorporation, induced anion release) by the onset of corrosion as well as the potential (and rate) at which these processes occur. There appears ample evidence to support the hypothesis that a barrier coating effect is also provided by the ICP coating. The dopant determines the physical attributes of the coating obtained on the metal surface either by solution casting or by electrodeposition. Other information from outside the field of corrosion protection can be used to show that this barrier coating characteristics in terms of ion, oxygen and water transport will change as a function of oxidation state and the dopant used.

ACKNOWLEDGEMENTS

DET acknowledges the financial support of the Air Force Office of Scientific Research, Grant Nos. F49620-96-1-0284 and F49620-99-1-0283, North Dakota State University.

REFERENCES

1. Wallace, G.G., Spinks, G.M., Teasdale, P.R., "Conductive, Electroactive Polymers: Intelligent Material Systems" *Technomic Publ. Co.*, Lancaster, 1997.

2. (2a) "Electroactive Conducting Polymers for Corrosion Control. Part 1. General Introduction and a Review of Non-Ferrous Metals" Tallman, D.E., Spinks, G., Dominis, A., Wallace, G.G., *Journal of Solid State Electrochemistry*, In Press. (2b) "Electroactive Conducting Polymers for Corrosion Control. Part 2. Ferrous Metals" Spinks, G.M., Dominis, A.J., Tallman, D.E., Wallace, G.G., *Journal of Solid State Electrochemistry*, In Press.
3. Beck, F, Haase, V., Schroetz, M., *AIP Conf. Proc.* 1996, 354, 115.
4. Wessling, B. *Advanced Materials*. 1994, 6, 226.
5. McAndrew, T.P, Miller, S.A., Gilicinski, A.G., Robeson, L.M. *Polym. Mater. Sci. Eng.* 1996, 74, 204.
6. Fahlman, M., Guan, H., Smallfield, J.A.O., Epstein, A.J. *Annu. Tech. Conf. – Soc. Plast. Eng.* 1998, 56th, 1238.
7. Santos, J.R., Mattoso, L.H.C., Motheo, A.J. *Electrochimica Acta*. 1998, 43, 309.
8. Attar, M.M., Scantlebury, J.D., Marsh, J. *Proc. – Electrochem. Soc.* 1998, 97-41, 1.
9. Li, P., Tan, T.C., Lee, J.Y. *Synth. Met.* 1997, 88, 237.
10. Talo, A., Passiniemi, P., Forsen, O., Ylasaari, S. *Synth. Met.* 1997, 85, 1333.
11. Fahlman, M., Jasty, S., Epstein, A.J. *Synth. Met.* 1997, 85, 1323.
12. Heeger, A.J. *Synth. Met.* 1993, 55, 3471.
13. Cao, Y., Smith, P., Heeger, A.J. *Synth. Met.* 1992, 48, 91; (a) Ruckenstein, E., Yin, W. *J. Appl. Polym. Sci.* 2001, 79, 80. (13a) Ruckenstein, E., Yin, W. *J. Appl. Polym. Sci.* 2001, 79, 80.
14. Huang, J., Wan, M. *J. Polym. Sci. Part A. Polym. Chem.* 1999, 37, 1277.
15. Paul, R.K., Pillali, C.K.S. *J. Appl. Polym. Sci.* 2001, 80, 1354. (15a) Paul, R.K., Pillai, C.K.S. *Polym. Int.* 2001, 50, 381.
16. Lee, J.Y., Kim, D.Y., Kim, C.Y. *Synth. Met.* 1995, 74, 103.
17. Lee, J.Y., Kim, D.Y., Song, K.T., Kim, S.Y., Kim, C.Y. *Mol. Cryst. Liq. Cryst.* 1996, 280, 135.
18. Teasdale, P.R., Wallace, G.G. *React. Polym.* 1995, 24, 157.
19. Kinlen, P.J., Liu, J., Ding, Y., Graham, C.R., Remsen, E.E. *Macromol.* 1998, 31, 1735.
20. Dominis, A., Spinks, G.M., Wallace, G.G. *Prog. Org. Coatings*. Submitted.
21. Gelling, V.J., Wiest, M.M., Tallman, D.E., Bierwagen, G.P. and Wallace, G.G. *Prog. Organic Coatings* (2001) In Press.
22. Shcirmesen, M., Beck, F. *J. Appl. Electrochem.* 1989, 19, 401.
23. Beck, F., Huelser, P., Michaelis, R. *Bull. Electrochem.* 1992, 8, 35.
24. Beck, F., Michaelis, R., Schloten, F., Zinger, B. *Electrochimica Acta*. 1994, 39, 229.
25. Beck, F., Huelser, P. *J. Electroanal. Chem.* 1990, 280, 159.
26. Huelser, P., Beck, F. *J. Appl. Electrochem.* 1990, 20, 596.
27. Huelser, P., Beck, F. *J. Electrochem. Soc.* 1990, 137, 2067.

28. "Direct Electrodeposition of Polypyrrole on Aluminum and Aluminum Alloy by Electron Transfer Mediation," Tallman, D.E., Vang, C., Wallace, G.G. and Bierwagen, G.P. *J. Electrochem. Soc.*, (2001) submitted.
29. Zinger, B. *J. Electroanal. Chem.* 1988, 244, 115.
30. Zhao, H., Price, W.E., Wallace, G.G. *J. Memb. Sci.* 1994, 87, 47.
31. Zhao, H., Price, W.E. Teasdale, P.R., Wallace, G.G. *React. Polym.* 1994, 23, 213.
32. Kamada, K., Kamo, J., Motonaga, A., Iwasaki, T., Hosodawa, H. *Polymer Journal.* 1994, 26, 141.
33. Jiping, Y., Quishi, S., Xiahuai, H., Meixiang, W. *Chin. J. Polym. Sci.* 1993, 11, 121.
34. Anderson, M.R., Mattes, B.J., Reiss, H., Kaner, R.B. *Science.* 1991, 252, 1412.
35. Anderson, M.R., Mattes, B.J., Reiss, H., Kaner, R.B. *Synth. Met.* 1991, 41, 1151.
36. Kawabata, S., Martin, C.R. *J. Memb. Sci.* 1994, 91, 1.
37. Parthasarathy, R.V., Menon, V.P., Martin, C.R. *Chem. Mater.* 1997, 9, 560.
38. Huang, S.C., Ball, I.J., Kaner, R.B. *Macromolecules.* 1998, 31, 5456.

Chapter 7

Synthesis and Characterization of Polymers with Oligoaniline Side Chains

Ru Chen and Brian C. Benicewicz

NYS Center for Polymer Synthesis, Department of Chemistry,
Rensselaer Polytechnic Institute, Troy, NY 12180

Polymers containing oligomeric aniline side chains were synthesized via free radical polymerization. All monomers with dimer aniline units and acrylates with trimer aniline unit were polymerized under standard conditions with AIBN as initiator. For acrylamides with trimer aniline unit, blocking of the diphenyl amine group was necessary for the successful polymerization. The UV-vis spectroscopy of the polymer with a trimer side chain was similar to that of polyaniline. Low electrical conductivity was observed for some of the polymers when doped with iodine.

Polyaniline (PANI) has been one of the most intensively studied conducting polymers in the last decade. It can be easily made by chemical or electrochemical oxidative polymerization. PANI has high electrical conductivity and good environmental stability. Many potential applications have been proposed and investigated, such as rechargeable batteries, electromagnetic shielding, antistatic fibers, separation membranes, sensors, and corrosion resistant coatings (*1*). In the past decade, PANI has been widely studied as a unique replacement for barrier coatings in corrosion protection of metal surfaces. Our early work showed that PANI was able to provide protection against corrosion to mild steel substrates, even when the coating was scratched and the bare metal exposed to aqueous salt and dilute HCl solutions. Subsequent outdoor testing verified the usefulness of these coatings in a severe

marine environment (2, 3). One of the challenges in the application of PANI is its processability. PANI is difficult to dissolve in common, environmentally benign solvents. In good solvents such as NMP, gelation occurs and is dependent on both the concentration of polymer and polymer molecular weight. Stabilization of these solutions can be achieved through additives (3). PANI is not melt processable, and crosslinks at elevated temperatures which leads to a decrease in the conductivity (4). Thus, it is necessary to develop new methods to improve the melt and solution processability of polyaniline.

Monodisperse π -conjugated oligomers have been the target of much research due to their well-defined structure, high solubility, and special properties (5). Oligomers serve initially as the model compounds to obtain information such as electronic, photonic and morphologic properties of corresponding intractable polymers. Additionally, research on conjugated oligomers has advanced because of their promising applications in molecular scale electronics and nanotechnology. Oligoanilines were one of the earliest studied π -conjugated oligomer systems. In the 1960s, Honzl and co-workers synthesized a series of aniline oligomers and found that high conductivity was obtained even in short chain oligomers upon doping with iodine (6). Wudl et al. showed that octaaniline has nearly identical spectroscopy and electrical conductivity as polyaniline (7). Other studies showed that the aniline oligomers can also protect metal from corrosion (8).

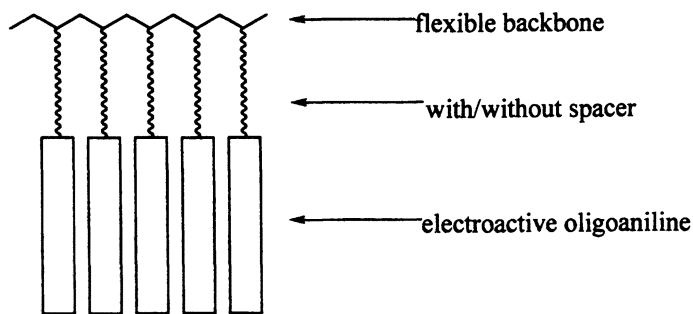


Figure 1 Schematic of polymer structure

In this paper, we report the synthesis of polymers with aniline side chains. The generalized structure is shown in Figure 1. The corresponding monomers are shown in Figure 2. Incorporation of aniline groups through covalent bonds prevents the loss of active species through migration. The polymer structure can be controlled precisely to obtain appropriate physical properties, such as glass transition temperature, and film forming properties through copolymerization with comonomers such as butyl acrylate and ethylhexyl acrylate, which are common in the coatings industry. The electroactivity of the coating can then be

readily controlled by the length of aniline oligomer and the content of oligomer in the final polymers. These monomers are anticipated to be incorporated in emulsion polymerization, which is widely used in water-based coatings.

The homopolymers of the oligomeric monomers were prepared by free radical polymerization in organic solvents. The thermal properties were characterized with TGA and DSC. Initial results of UV-vis spectroscopy and electrical conductivity are discussed for some of the polymers. The results were compared to that of polyaniline.

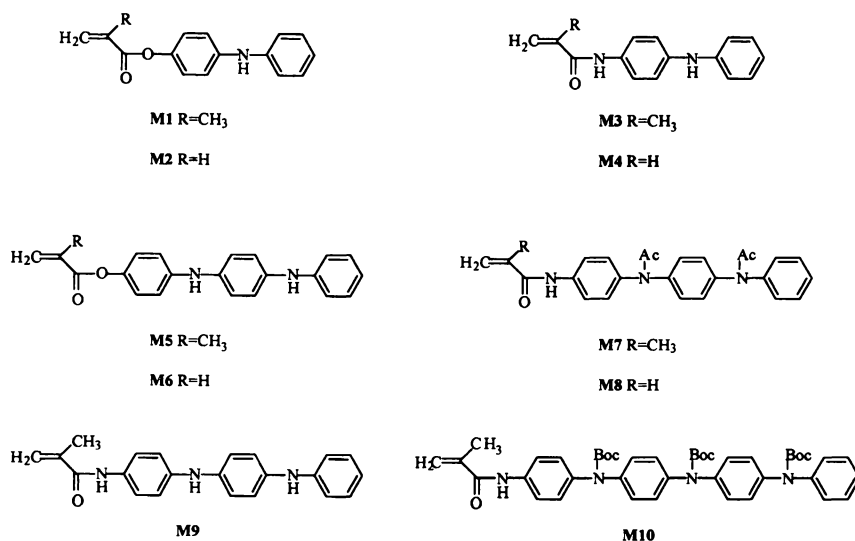


Figure 2 Chemical structures of monomers

Experimental

Materials and Instruments

All chemicals were purchased from ACROS. Bis[(2-diphenylphosphino)phenyl] ether (DPEphos) was prepared according to a literature method (9). Solvents were purified according to standard literature methods (10). ¹H NMR spectra were recorded on a Varian 500 spectrometer. Solvent residues were

used as reference. A Shimadzu GCMS-QP5000 spectrometer was used to confirm the chemical structures and determine monomer purity. UV-vis spectra were recorded on Perkin Elmer Lambda 4C UV/vis spectrophotometer. The electrical conductivity was measured on resistivity testing unit and hand applied four-point probe manufactured by Jandel Engineering Limited. Thermal analysis was carried out on differential scanning calorimetry (DSC) and thermal gravimetric analysis (TGA) Perkin Elmer 7 series instrument with Pyris™ software. Inherent viscosity was measured with an Ubbelohde viscometer at 30.00° on 5.0mg/mL DMF solutions. Molecular weights of the polymers were measured on a Waters GPC system equipped with refractive index detector Waters 2410 and 3 Styragel® columns (HR 1, HR 3, and HR 4) using THF as the eluent at a flow rate of 0.3mL/min. The instrument was calibrated with polystyrene standards.

Oligoaniline Synthesis

4-(4'-Aminophenylamino) diphenylamine (3) was synthesized according to a method in the literature, Scheme 1 (11,12).

4-[[4-(phenylamino)phenyl]amino]-phenol (4) was prepared according to Scheme 2. N-phenyl 1,4-phenylenediamine (5.00 g, 27.2 mmol), hydroquinone (5.68 g, 51.6 mmol) and zinc chloride (0.72 g, 5.3 mmol) were charged into a three-necked flask. The mixture was heated to 180°C with stirring in nitrogen atmosphere. The reaction was continued for 4h. The reaction mixture was cooled to room temperature and 0.1M HCl aq. solution (50mL) was added. The mixture was heated to 100 °C with stirring for 1h and filtered. The product was recrystallized from toluene in the presence of small amount of phenylhydrazine. Slightly pink crystals, 3.92 g, 52% yield: mp 140-141°C. ¹H NMR (500MHz, DMSO-*d*₆) δ 8.87(s,1H), 7.70 (s,1H), 7.44 (s, 1H), 7.13 (t, J= 7.3 Hz, 2H), 6.98-6.93 (m, 2H), 6.90-6.82 (m, 6H), 6.69-6.62 (m, 3H). MS (EI) m/z 276 (M⁺). Anal. Calcd. for C₁₈H₁₆N₂O: C,78.24; H,5.84; N, 10.14. Found C, 78.10; H, 5.89; N, 9.90.

Compound 6: p-Aminodiphenylamine (22.32g, 121.3mmol) and benzophenone (20.00g, 109.9mmol) were added to toluene (125mL). 5A molecular sieves (30.0g) were added to the solution under nitrogen atmosphere. The mixture was refluxed for 48h. The solution was decanted, and the molecular sieves were washed with ethyl ether until the filtrate was colorless. The organic solutions were combined and solvent was removed. The solid residue was taken up in ethyl acetate and washed with NaOH solution and brine. The organic solution was dried with anhydrous sodium sulfate and concentrated. The yellow solid was dried in vacuo at 50°C for 24h. Product 5: 37.80g. Compound 5 (25.00g, 71.84mmol) was dissolved in THF (180mL). Di-tert-butyl dicarbonate (18.79g, 86.19mmol) and 4-(dimethylamino)pyridine (1.31g, 10.74mmol) were added. The solution was refluxed for 6h. The solvent was removed by rotary evaporation. The solid was recrystallized in ethyl

acetate/hexane and dried in vacuo at 50°C for 24h. Pale yellow needles, 25.73g, 80% yield: mp 154-155°C. ¹H NMR (500MHz, CDCl₃) δ 7.74(d, J=8.3Hz, 2H), 7.49-7.44(m, 1H), 7.43-7.33 (m, 2H), 7.32-7.20 (m, 5H), 7.18-7.06(m, 5H), 6.97(d, J=8.5Hz, 2H), 6.67(d, J=8.3Hz, 2H), 1.40(s, 9H). Anal. Calcd. for C₃₀H₂₈N₂O₂: C, 80.33; H, 6.29; N, 6.25. Found C, 79.78; H, 6.31; N, 6.32.

Compound 7: Compound 5 (8.53g, 24.5mmol) was dissolved in dichloromethane (50 mL) and tetra-n-butylammonium tribromide (13.03g, 27.03mmol) was added in one portion. The solution was stirred at room temperature for 1h, then saturated sodium sulfite solution (50mL) was added with stirring for 30min. followed by sodium hydroxide solution(2.0M, 25mL). The layers were separated, and the organic phase was washed with distilled water, dried over anhydrous sodium sulfate, and concentrated. The residue was dissolved in THF (60mL), then di-tert-butyl bicarbonate (6.41g, 29.40mmol) and 4-(dimethylamino)pyridine (0.45g, 3.7mmol) were added. The solution was refluxed for 6h. and concentrated. The residue was recrystallized in methanol and dried in vacuo at 50 °C for 24h. Slightly pink crystals, 8.86g, 69% yield: mp 163-165°C. ¹H NMR (500MHz, CDCl₃) δ 7.74(d, J=7.3Hz, 2H), 7.50-7.33(m, 5H), 7.31-7.20(m, 3H), 7.11(dd, J= 7.9, 1.3Hz, 2H), 7.02(d, J=8.8Hz, 2H), 6.94(d, J=8.5Hz, 2H), 6.68(d, J= 8.5Hz, 2H), 1.39(s, 9H). Anal. Calcd. for C₃₀H₂₇BrN₂O₂: C, 68.31; H, 5.16; N, 5.31. Found C, 68.27; H, 5.20; N, 5.30.

Compound 9: Compound 6 (24.00g, 53.57mmol), ammonium formate (40.61g, 644.6mmol) and palladium on carbon (5%, 2.83g, 1.33mmol Pd) were charged into a round-bottomed flask, and purged with argon. THF (100mL) and methanol (250mL) were added. The reaction mixture was heated to 55°C for 12h. The solution was concentrated and taken up with dichloromethane, filtered through Celite and concentrated. The solid was triturated with hexanes, and filtered. The white powder was dried in vacuo at 50 °C for 24h. Product 8: 14.92g. Compound 8 (0.50g, 1.76mol), palladium acetate (6.6mg, 2.9×10⁻²mmol) and DPEphos (21.0mg, 3.9×10⁻²mmol) were charged into a flask and purged with argon. Compound 7 (0.77g, 1.46mmol) was added, followed by toluene(6mL). The solution was warmed to 50°C to help the dissolution. Sodium tert-butoxide (0.21g, 2.19mmol) was added in one portion. Additional toluene (4mL) was added to wash the flask wall. The reaction mixture was heated to 100°C with stirring for 24h. The solvent was removed by rotary evaporation. The residue was dissolved in dichloromethane, washed with distilled water and dried over anhydrous sodium sulfate, and concentrated. The residue was dissolved in THF (10mL) and di-tert-butyl bicarbonate (0.47g, 2.2mmol) and 4-(dimethylamino)pyridine (43.3mg, 0.355mmol) were added. The reaction mixture was heated to 60°C for 12h. The solvent was removed, and the solid was recrystallized in methanol. Pink powder, 0.59g, 49% yield: mp 184-185°C. ¹H NMR (500MHz, CDCl₃) δ 7.74(d, J= 8.3Hz, 2H), 7.50-7.44(m, 1H), 7.43-7.38(m, 2H), 7.33-7.22 (m, 5H), 7.21-7.06(m, 13H), 6.95(d, J=8.5Hz, 2H), 6.67(d, J= 8.4Hz, 2H), 1.44(s, 9H); 1.43(s, 9H); 1.39(s, 9H). Anal. Calcd. for C₅₂H₅₄N₄O₆: C, 75.16; H, 6.55; N, 6.74. Found C, 74.94; H, 6.63; N, 6.75.

Compound 10: Similar procedure to the synthesis of compound 8. Product: white powder, 96% yield. $^1\text{H NMR}$ (500MHz, CDCl_3) δ 7.34-7.25(m, 2H); 7.22-7.07(m, 11H); 6.96(dd, $J=8.5, 1.2\text{Hz}$, 2H); 6.61(dd, $J=8.7, 1.3\text{Hz}$, 2H); 3.65(broad, 2H), 1.46-1.42(m, 27H).

Monomer Synthesis

Aniline oligomer was dissolved in THF with nitrogen protection. Triethylamine was added. The reaction mixture was cooled in an ice bath. Methacryloyl chloride (or acryloyl chloride) solution in THF was added slowly into the solution. After completion, the reaction mixture was stirred at room temperature for 24h. The precipitate was filtered off and washed with THF. The solutions were combined and the solvent was removed with rotary evaporation. The residue was taken up with dichloromethane, washed with HCl aqueous solution, Na_2CO_3 solution and distilled water. The solution was dried with anhydrous sodium sulfate. The solvent was removed and the residue was crystallized from ethyl acetate/hexanes. The product was dried in vacuo at 50°C for 24h.

4-Anilinophenyl methacrylate (M1): white needle crystals from heptanes in 60% yield: mp $72-73^\circ\text{C}$. $^1\text{H NMR}$ (500MHz, $\text{DMSO}-d_6$) δ 8.19 (s, 1H), 7.23 (t, $J=7.9\text{Hz}$, 2H), 7.14-6.96 (m, 6H), 6.82 (t, $J=7.3\text{Hz}$, 1H), 6.25 (s, 1H), 5.86 (s, 1H), 2.06-1.94 (m, 3H). GC/MS (EI) m/z 253 (M^+). Anal. Calcd for $\text{C}_{16}\text{H}_{15}\text{NO}_2$: C, 75.87; H, 5.97; N, 5.53. Found: C, 76.65; H, 6.00; N, 5.55.

4-Anilinophenyl acrylate (M2): pale yellow crystals from heptanes in 40% yield: mp $47-49^\circ\text{C}$. $^1\text{H NMR}$ (500MHz, $\text{DMSO}-d_6$) δ 8.20 (s, 1H), 7.23 (t, $J=7.0\text{Hz}$, 2H), 7.14-6.96 (m, 6H), 6.82 (t, $J=7.3\text{Hz}$, 1H), 6.51 (dd, $J=17.3, 1.2\text{Hz}$, 1H), 6.39 (dd, $J=17.3, 10.2\text{Hz}$, 1H), 6.12 (dd, $J=10.3, 1.2\text{Hz}$, 1H). GC/MS(EI) m/z 239(M^+). Anal. Calcd for $\text{C}_{15}\text{H}_{13}\text{NO}_2$: C, 75.30; H, 5.48; N, 5.85. Found: C, 74.91; H, 5.49; N, 5.82.

N-(4-Anilinophenyl)-methacrylamide (M3): was prepared according to a literature method (13). Pale blue crystals, 80% yield: mp $109 - 110^\circ\text{C}$. $^1\text{H NMR}$ (500 MHz, CDCl_3) δ 7.49 (s, 1H), 7.44 (d, $J=8.8\text{Hz}$, 2H), 7.28-7.20 (m, 2), 7.09-6.96 (m, 4H), 6.90(tt, $J=7.3, 1.2\text{Hz}$, 1H), 5.78 (s, 1H), 5.70 (s, 1H), 5.46-5.40 (m, 1H), 2.07-2.04 (m, 3H). GC/MS (EI) m/z 252(M^+). Anal. Calcd for $\text{C}_{16}\text{H}_{16}\text{N}_2\text{O}$: C, 76.16; H, 6.39; N, 11.10. Found: C, 76.11; H, 6.44; N, 11.04.

N-(4-Anilinophenyl)-acrylamide (M4): pale yellow solid, 50% yield: mp $150-152^\circ\text{C}$. $^1\text{H NMR}$ (500MHz, CDCl_3) δ 7.54 (s, 1H), 7.46 (d, $J=8.5\text{Hz}$, 2H), 7.32-7.12 (m, 2H), 7.10-6.94 (m, 4H), 6.90 (t, $J=7.3\text{Hz}$, 1H), 6.41 (d, $J=16.8\text{Hz}$, 1H), 6.25 (dd, $J=16.8, 10.3\text{Hz}$, 1H), 5.80-5.60 (dd+broad peak, $J=10.1, 1.3\text{Hz}$, 2H). GC/MS (EI) m/z 238 (M^+). Anal. Calcd for $\text{C}_{15}\text{H}_{14}\text{N}_2\text{O}$: C, 75.61; H, 5.92; N11.76. Found: C, 75.11; H, 5.97; N, 11.20.

Monomer 5: pale blue solid, 82% yield: mp $99-100^\circ\text{C}$. $^1\text{H NMR}$ (500MHz, $\text{DMSO}-d_6$) δ 7.93(s, 1H), 7.89(s, 1H), 7.20-7.15(m, 2H), 7.06-6.88(m, 10H), 6.72(t, $J=7.3\text{Hz}$, 1H), 6.24(s, 1H), 5.85(s, 1H), 1.99(s, 3H). GC/MS (EI) m/z

344(M⁺). Anal. Calcd for C₂₂H₂₀N₂O₂: C, 76.70; H, 5.85; N, 8.13. Found: C, 76.19; H, 5.70; N, 8.03.

Monomer 6: separated with liquid chromatography, pale blue solid, 26% yield: mp 107-110°C. ¹H NMR (500MHz, DMSO-*d*₆) δ 7.94(s, 1H), 7.89(s, 1H), 7.20-7.15(m, 2H), 7.07-6.90(m, 10H), 6.72(t, J= 7.3Hz, 1H), 6.50(dd, J=17.3Hz, 1.5Hz, 1H), 6.38(dd, J= 10.4, 1.5Hz, 1H), 6.10(dd, J=10.3Hz, 1.5Hz, 1H). GC/MS (EI) m/z 330 (M⁺). Anal. Calcd for C₂₁H₁₈N₂O₂: C, 76.34; H, 5.49; N, 8.48. Found: C 76.13; H, 5.61; N, 8.36.

Monomer 7: white powder from acetone, 51% yield: mp 194-195°C. ¹H NMR (500MHz, CDCl₃) δ 7.88(s, 1H), 7.70-6.92(m, 13H), 5.78(s, 1H), 5.46(s, 1H), 2.04(s, 9H). GC/MS (EI) m/z 427 (M⁺). Anal. Calcd for C₂₆H₂₅N₃O₃: C, 73.05; H, 5.89; N, 9.83. Found: C, 72.64; H, 5.97; N, 9.38.

Monomer 8: pale yellow powder from ethyl acetate, 72% yield: mp 203-204°C. ¹H NMR (500MHz, CDCl₃) δ 8.30(s, 1H), 7.75-6.90(m, 13H), 6.40(d, J=16.8Hz, 1H), 6.23(dd, J=16.8Hz, 10.3Hz, 1H), 5.69(d, J=10.3Hz, 1H), 2.06(d, 6H). Anal. Calcd for C₂₅H₂₃N₃O₃: C, 72.62; H, 5.61; N, 10.16. Found: C, 71.24; H, 5.60; N, 9.64.

Monomer 9: pink powder from ethanol, 80% yield: mp 163-164°C. ¹H NMR (500MHz, CDCl₃) δ 7.39-7.30(m, 3H), 7.20-7.13(m, 2H), 7.01-6.86(m, 8H), 6.78(t, J=7.3Hz, 1H), 5.70(s, 1H), 5.49(s, 2H), 5.36(s, 1H), 1.99(s, 3H). GC/MS (EI) m/z 343(M⁺). Anal. Calcd for C₂₂H₂₁N₃O: C, 76.94; H, 6.16; N, 12.24. Found: C, 74.38; H, 6.30; N, 11.58.

Monomer 10: separated by liquid chromatography, white powder, 93% yield. ¹H NMR (500MHz, DMSO-*d*₆) δ 9.84(s, 1H), 7.68(d, J=8.8Hz, 2H), 7.37-7.31(m, 2H), 7.23-7.14(m, 13H), 5.81(s, 1H), 5.51(s, 1H), 1.95(s, 3H), 1.38(s, 27H). Anal. Calcd for C₄₃H₅₀N₄O₇: C, 70.28; H, 6.86; N, 7.62. Found: C, 69.58; H, 6.83; N, 7.38.

Polymer Synthesis

Monomer (0.50g) and AIBN (5mg) were dissolved in DMF (5mL). The reaction mixture was degassed by three freeze-pump-thaw cycles, sealed under nitrogen and heated to 70°C for 24 h with stirring. The polymer was precipitated into methanol, filtered and dried in a vacuum oven at 60°C for 24 h.

Results and Discussion

Oligomer Synthesis

Several methods have been used for the preparation of oligoanilines. Ullmann condensation is the traditional method for the preparation of arylamines. However, vigorous conditions such as strong base, high

temperature, and elongated reaction times are required (14). Honzl prepared aniline oligomers by the reaction of diethyl succinoylsuccinate and aromatic amines, followed by hydrolysis, decarboxylation and aromatization (6). This procedure was modified by Wudl et al. for the preparation of octaaniline (7). Condensation between aryl amines and phenol using a condensing reagent was applied in the oligomer synthesis by Furusho et al (15). Monkman et al. prepared aniline trimer and tetramer compounds by a modified Ullmann reaction (12). In the last five years, palladium catalyzed amination has emerged as a powerful method for the synthesis of arylamines. The versatility of the methodology has been demonstrated by the synthesis of aniline oligomers with different functional endgroups (16).

In this paper, the aniline trimer was synthesized by Ullmann condensation using copper as catalyst and reagent (Scheme 1). The excess amount of copper eliminates the need for the inorganic base and reduces side reactions. In the first step, the commercially available dimer was protected by acyl groups, which serves two functions in the reaction. The NH is blocked, preventing the further arylation of diphenylamine and activates the amide group toward condensation. When the iodonitrobenzene is used in excess, the dimer derivative was converted completely to the desired intermediate. The nitro group can be reduced to an amine group with sodium borohydride. The acyl protective groups were removed by hydrolysis in a potassium hydroxide-methanol solution.

Anilinophenol was reported to be prepared by coupling of aniline with hydroquinone at 180°C in the presence of zinc chloride as catalyst (17). In this work, we attempted to prepare hydroxyl trimer 4 from aniline dimer in a similar way (Scheme 2). GC/MS analysis showed that the dimer was converted quantitatively after 4h. A small amount of N,N'-diphenyl-1,4-phenylenediamine was present in the reaction mixture. The product was washed with a 0.1M hydrochloride solution. The product (silver in color) was recrystallized in toluene to afford pale pink crystals. (An unknown residue was left in the flask which was insoluble in toluene, but soluble in polar solvent such as acetone, THF, and DMF.) The pale pink crystals turned blue when exposed to air for several weeks.

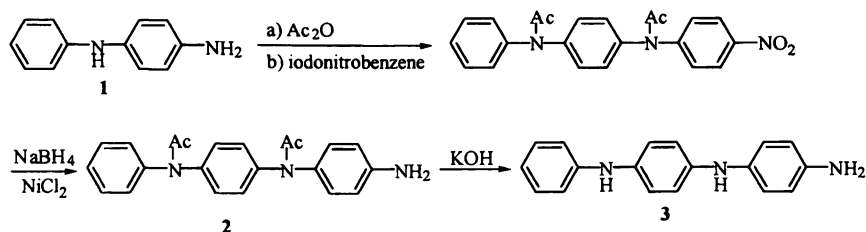
Aniline tetramer was synthesized by palladium-catalyzed amination. This method has been widely used in the formation of aromatic C-N bonds. Different catalyst/ligand systems have been studied for this reaction. The most common system is Pd₂(dba)₃ and BINAP. Here, palladium acetate was used in the coupling reaction. Compared with other catalysts, palladium acetate is more stable in the air and lower in price. The ligand, DPEphos, was made by a two step, one pot reaction. It is easy to prepare, and stable in air. The catalyst system showed high efficiency in the coupling reaction of primary anilines and aryl bromides (18). Its application in the synthesis of higher aniline oligomers has not been reported. In our experiments, we found that the catalyst system is effective for the preparation of aniline trimer and tetramer. In this reaction, the NH group was protected as a tert-butyl carbamate, which is a widely used protecting group and can be readily removed by pyrolysis or chemical methods.

The introduction of *t*-Boc groups prevents oxidation of phenylenediamine units and the formation of triarylamines. The *t*-Boc group also improves the solubility of intermediates and products. The deprotection of the amine groups was carried out in the presence of palladium on carbon, which proved to be highly efficient. Compound **10** was heated to 190°C in an argon atmosphere for 10h and the proton NMR showed that the removal of protecting group was complete to afford tetraaniline. Aniline tetramer was reported to be synthesized by oxidation reaction of dimer with ferric chloride (19). The NMR spectra and DSC thermograms of tetramer made by these two methods were identical.

Monomer Synthesis

Monomers were synthesized by the reaction between (meth)acryloyl chloride and the appropriate oligoaniline. Since there is more than one amine functionality in the oligomers, it is possible that multiple substitutions can occur. In our experiments, it was found that only the endgroup functionality underwent nucleophilic substitution when (meth)acryloyl chloride was used in slight excess. This may be due to the higher nucleophilicity and lower steric hindrance of the amine endgroup.

Scheme 1

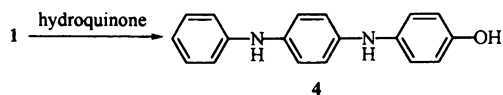


Polymer Synthesis

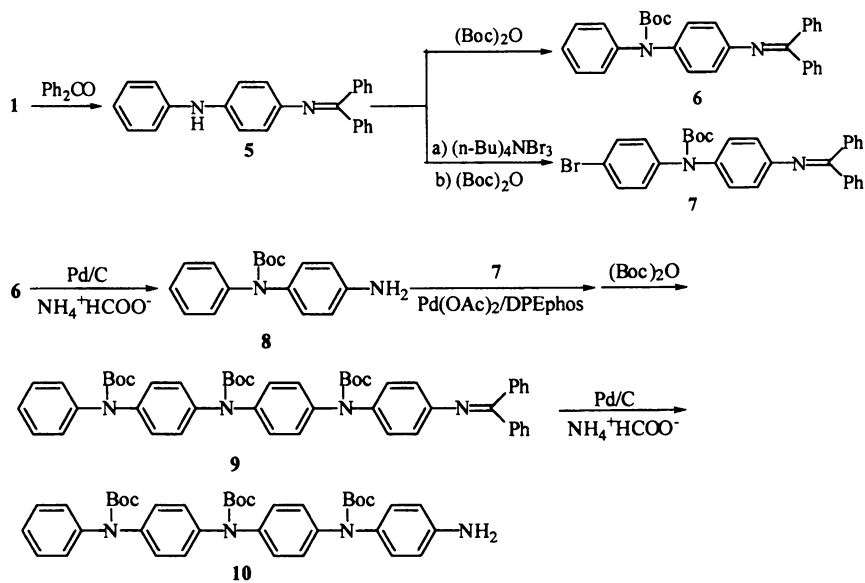
Diphenylamine has long been known as a radical inhibitor. When the diphenylamine reacts with radical species, the hydrogen is abstracted by the radical. The resulting aminyl radical may couple to other radicals, thus eliminating the radical species. Aminyl radicals can undergo self-coupling to form a neutral compound (20).

Previous research regarding the polymerization of monomers **M1** and **M2** showed that only azo-initiators were able to initiate the polymerization. Other radical initiators such as dibenzoyl peroxide and cumene hydroperoxide failed (21). In this work, AIBN was used in all polymerization reactions. Monomers

Scheme 2



Scheme 3



of the aniline dimer (**M1-M4**), (meth)acrylamides and (meth)acrylates, could be polymerized under standard conditions. For those monomers made from the aniline trimer, the polymerization reactivities were different. Monomer **M5** polymerized under standard conditions, however, **M6** only gave polymer of lower molecular weight and lower yield. Polymerization of **M9** is completely inhibited. When the NH groups on trianiline were blocked by acyl groups (**M7,M8**), the polymerization occurred readily. This indicates that the diaryl amine NH does inhibit the polymerization and it is necessary to block the NH groups in the longer oligoaniline-based monomers. Research on protected **M1** and **M2** showed that the introduction of acyl groups lowered the solubility of the resulting polymers. However, to obtain electroactive polymers, protective groups need to be removed after the polymerization. Hydrolysis of the amide groups requires vigorous reaction conditions, which can also break the amide bonds connecting the backbone and side chains.

The structure of the polymers was confirmed by proton NMR. The characteristic proton peaks of the carbon-carbon double bond in the monomer disappeared after the polymerization reaction. All other peaks attributed to the side chains remained unchanged indicating that polymerization occurred through the addition of carbon-carbon double bonds. The properties of the polymers are summarized in Table I.

The polymers (**M1-M6**) are soluble in polar solvents, such as THF, DMSO, DMF and NMP. Polymers **M7** and **M8** did not dissolve in THF, but were soluble in the other solvents. Thin polymer films were cast from solvents, but the films were brittle. This may be due to the low molecular weights and rigidity of the oligomer side chains. The incorporation of aniline oligomers directly onto the backbone as side chains led to polymers with Tg's in the range of 73-208° C.

t-Boc protected compounds showed good solubility. Monomer **M10** was soluble in dichloromethane, ethyl acetate, chloroform, DMSO and THF. The thermal stability was studied by TGA. A two-step weight loss was observed. In the first step, t-Boc group was removed. The calculation from the TGA weight loss showed that the removal was quantitative. This was further confirmed by proton NMR. Unprotected compound was stable and no weight loss was observed until the sample decomposed at higher temperatures. The t-Boc protected monomer **M10** was polymerized under the similar reaction conditions as the other monomers.

Polymer Characterization

Thermal properties of polymers were measured by TGA and DSC in nitrogen at heating rates of 20 and 10 °C/min, respectively. All polymers began to lose weight at temperatures higher than 250°C as measured by the temperature at which the polymers lost 5% of their original weight. It is clear from the data in Table I that the polyacrylates have lower Tg's than

polyacrylamides. Also, polyacrylamides and polyacrylates showed lower Tg's than the corresponding polymethacrylamides and polymethacrylates.

The polymers were prepared under the same, non-optimized polymerizations conditions (70°C, 24h, N₂). Moderate number average molecular weights were obtained in the range of 11,000-58,000 daltons.

The UV-Vis spectra were recorded for polymer M5 in DMF (Figure 3). The reduced colorless polymer exhibited a single strong absorption at 311nm ($\epsilon_{\text{max}} = 2.3 \times 10^4$). After oxidation in the air, the blue polymer solution showed a sharp peak at 300nm (2.2×10^4) and a broad band at 578nm (6.3×10^3). The higher energy band is believed due to the $\pi \rightarrow \pi^*$ transition of benzenoid ring, and the lower energy is due to the charge transfer from benzenoid ring to quinoid ring (22, 23). The solution turned green when doped with sulfuric acid. There were three peaks in the spectrum, 292nm, 396nm and 830nm. Thus, the characteristic absorptions of polymer M5 are similar to that of polyaniline as reported in literature.

Polymer M5 powder was doped with iodine for a week, and pressed into pellet. The conductivity was measured by the four-point probe method. The conductivity was low, 5.6×10^{-7} S/cm. Further work on the doping and conductivity of these new polymers is planned.

Conclusions

New meth(acrylate) and meth(acrylamide) monomers containing oligoaniline side chains were designed and synthesized. The polymerization of these monomers was studied using standard free radical polymerization techniques. Monomers containing dimer aniline units were readily polymerized. For longer aniline oligomers, protection of diphenylamine moiety was necessary to prevent the polymerization inhibition. Polyacrylates displayed lower Tg's than polyacrylamides. Polyacrylates and polyacrylamides displayed lower Tg's than corresponding polymethacrylates and polymethacrylamides. The polymers were soluble in polar solvents and possessed good thermal stabilities with decomposition temperatures above 250°C. UV-vis spectra of polymer M5 were similar to that of polyaniline. This polymer showed low electrical conductivity when doped with iodine. Further doping experiments will be conducted to fully explore the redox properties and conductivity of these new polymers.

Polymer properties will be further tailored by copolymerization with commercially available monomers. These copolymers will be spray-coated onto metal coupons such as mild steel and aluminum for laboratory testing. Promising candidates will be scaled up and subjected to outdoor corrosion testing.

Acknowledgements. We are grateful to the China Lake Naval Air Warfare Center, SERDP program for the financial support of this research.

Table I. Properties of polymers

<i>Monomer</i>	<i>IV</i> (dL/g)	<i>M_n</i> (10 ³)	<i>M_w</i> (10 ³)	<i>PDI</i>	<i>T_{5%}</i> (°C)	<i>T_g</i> (°C)
M1	0.26	30.1	80.3	2.67	250	116
M2	0.12	13.3	24.4	1.83	269	73
M3	0.27	58.4	134.9	2.31	263	184
M4	0.25	28.4	---	broad	280	155
M5	0.14	14.7	31.3	2.16	290	110
M6		11.0	16.0	1.50		
M7	0.29	---	---	---	324	208
M8	0.10	---	---	---	291	184

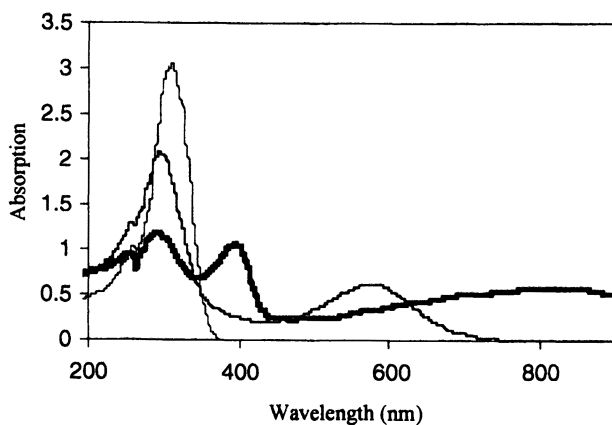


Figure 3 UV-vis spectra of polymer M5: a) reduced state (—); b) oxidized state (- - -); c) oxidized state doped with sulfuric acid (———).

References

1. Trivedi, D. C. in *Handbook of Organic Conductive Molecules and Polymers: vol. 2. Synthesis and Electrical Properties*; Nalwa, H. S., Ed.; John Wiley & Sons Ltd: New York, NY, 1997; pp 505-784.
2. Wroblewski, D. A.; Benicewicz, B. C.; Thompson, K. G.; Bryan, C. *Polym. Prepr.* **1994**, *35*, 265-266.
3. Wroblewski, D.A. and Benicewicz, B.C. *Polym. Prepr.* **1994**, *35*, 267-268.
4. Chandrakanthi, N.; Careem, M. A. *Polym. Bull.* **2000**, *44*, 101-108.
5. Martin, R.E.; Diederich, F. *Angew. Chem. Int. Ed.* **1999**, *38*, 1350-1377.
6. Honzl, J.; Tlustáková, M. *J. Polymer. Sci.* **1968**, *C22*, 451-462.
7. Lu, F.-L.; Wudl, F.; Novak, M. Heeger, A. J. *J. Am. Chem. Soc.* **1986**, *108*, 8311-8313.
8. Wei, Y.; Yang, Y.; Ding, T.; Yeh, J.-M.; Wei, G. *Polym. Mater. Sci. Eng.* **1996**, *74*, 209.
9. Kranenburg, M.; van der Burgt, Y.E.M.; Kamer, P. C. J.; van Leeuwen, P. W. N. M.; Goubitz, K.; Fraanje, J. *Organometallics* **1995**, *14*, 3081-3089.
10. Armarego, W. L. F.; Perrin, D. D. *Purification of Laboratory Chemicals, 4th ed.*; Butlerworth-Heinemann: Oxford, 1997.
11. Benicewicz, B.C.; Chen, R. *Polym. Prepr.* **2000**, *41*, 1733-1734.
12. Rebourt, E.; Joule, J. A.; Monkman, A. P. *Synth. Met.* **1997**, *84*, 65-66.
13. Parker, D. K.; Schulz, G. O. *Rubber Chem. Technol.* **1989**, *62*, 733-749.
14. Lindley, J. *Tetrahedron* **1984**, *40*, 1433-1456.
15. Ochi, M.; Furusho, H.; Tanaka, J. *Bull. Chem. Soc. Jpn.* **1994**, *67*, 1749-1752.
16. Sadighi, J. P.; Singer, R. A.; Buchwald, S. L. *J. Am. Chem. Soc.* **1998**, *120*, 4960-4976.
17. Terdic, M. H. *Rev. Roumaine Chim.* **1984**, *29*, 489-495.
18. Sadighi, J. P.; Harris, M. C.; Buchwald, S. L. *Tetrahedron Lett.* **1998**, *39*, 5327-5330.
19. Zhang, W. J.; Feng, J.; MacDiarmid, A. G.; Epstein, A. J. *Synth. Met.* **1997**, *84*, 119-120.
20. Lucarini, M.; Pedrielli, P.; Pedulli, G. F.; Valgimigli, L.; Gignes, D.; Tordo, P. *J. Am. Chem. Soc.* **1999**, *121*, 11546-11553.
21. Tanaka, Y.; Noguchi, K.; Shibata, T; Okada, A. *Macromolecules* **1978**, *11*, 1017-1021.
22. Cao, Y.; Smith, P.; Heeger, A. J. *Synth. Met.* **1989**, *32*, 263-281.
23. McCall, R. P.; Ginder, J. M.; Leng, J. M.; Ye, H. J.; Manohar, S. R.; Masters, J. G.; Asturias, G. E.; MacDiarmid, A. G.; Epstein, A. J. *Phys. Rev. B* **1990**, *41*, 5202-5213.

Chapter 8

Improved Synthesis and Corrosion Properties of Poly(bis-(dialkylamino)phenylene vinylene)s (BAMPPV)

Nicole Anderson, David J. Irvin, Jennifer A. Irvin,
John D. Stenger-Smith, Andrew Guenther, Cindy Webber,
and Peter Zarras

Naval Air Warfare Center Weapons Division, Department of the Navy,
Code 4T4220D, 1 Administration Circle, China Lake, CA 93555

Abstract: An alternative material for corrosion protection on 2024 T3 aluminum alloy in aqueous alkaline environments has been synthesized and tested. The alternative material is a poly(phenylene vinylene) derivative called poly(bis-(N-methyl-N-hexylamino)phenylene vinylene) (BAMPPV). The synthesis of this material is discussed including improvements in overall yield of polymer and reduction in the side products. The BAMPPV was coated onto 2024 T3 Al alloy plates using a draw down method and an atomization and flame deposition process. The material has performed well in both neutral and alkaline (pH=8) environments and has shown excellent adhesion to the 2024 T3 aluminum alloy. A comparison of panels coated with BAMPPV to panels coated with chromate conversion coatings using B117 salt-fog tests (pH=7) showed similar performance results.

Introduction

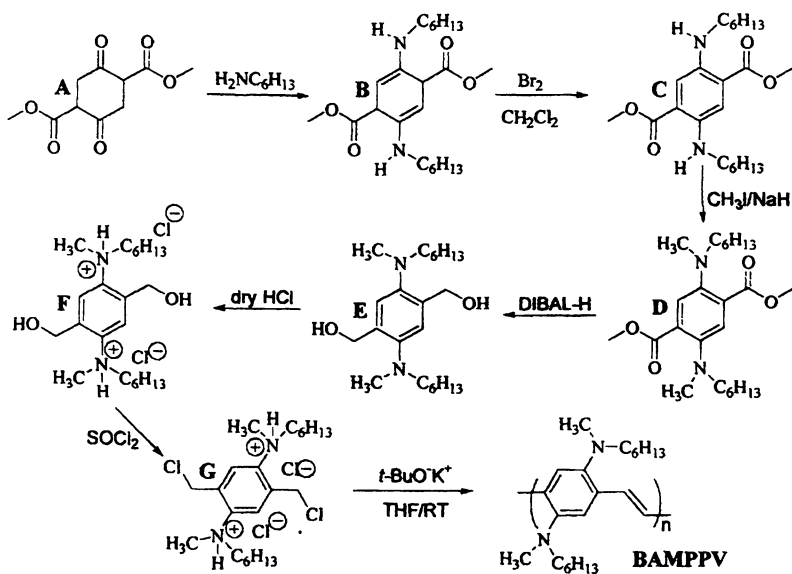
Current methods of corrosion protection, including marine coatings that contain hexavalent chromium, volatile organic compounds (VOCs) and other heavy metal conversion coatings, are coming under increasing scrutiny from the EPA (1). New coatings and coating methods are needed to replace existing coating systems that are not environmentally friendly. Estimates from the United States DoD indicate that corrosion costs billions of dollars annually for the military (2). Initial studies based on conductive polymers have demonstrated their corrosion-inhibiting properties (3,4). Polyaniline (PANI), one of the most widely studied conductive polymers, has been demonstrated as a corrosion-protective coating in acidic environments (5). There is a need for a more versatile coating that will protect in neutral and basic environments as well as acidic environments. Environmentally benign applications of coatings for marine environments are under development using conductive polymers. Our efforts have focused on using conductive polymers based on poly(phenylene vinylene)s.

Synthetic strategies for the synthesis of poly(bis-(N,N,-dialkylamino)phenylene vinylene)s, developed by NAWCWD, have been previously reported (6). One of these materials, poly(bis-(N-methyl-N-hexylamino)phenylenevinylene) (BAMPPV), has shown promise as a corrosion inhibiting coating on 2024 Al T3 aluminum alloy in simulated seawater (7-11). Quantitative evidence was obtained from these initial studies using potentiostatic and galvanostatic techniques (12-14). The polymers were prepared via a seven-step synthesis with overall yields between 10-20% (Scheme I). The current paper will examine current attempts to reduce the number of synthetic steps and increase the overall yield. In addition to the time and cost of materials for the 7-step synthesis of BAMPPV, there is also the issue of the quantity and type of waste produced from each of the respective steps. The reduction of waste materials generated from the synthesis of BAMPPV was accomplished by modifying the 7-step synthesis (Scheme II) and developing two alternative methods for the production of poly(bis-(N-methyl-N-hexylamino)-phenylenevinylene). Each of these methods can reduce cost and waste generation. Additionally, this paper will present new data regarding the physical and corrosion properties of BAMPPV. Immersion tests using simulated seawater and neutral (pH = 7.0) salt-fog experiments are presented.

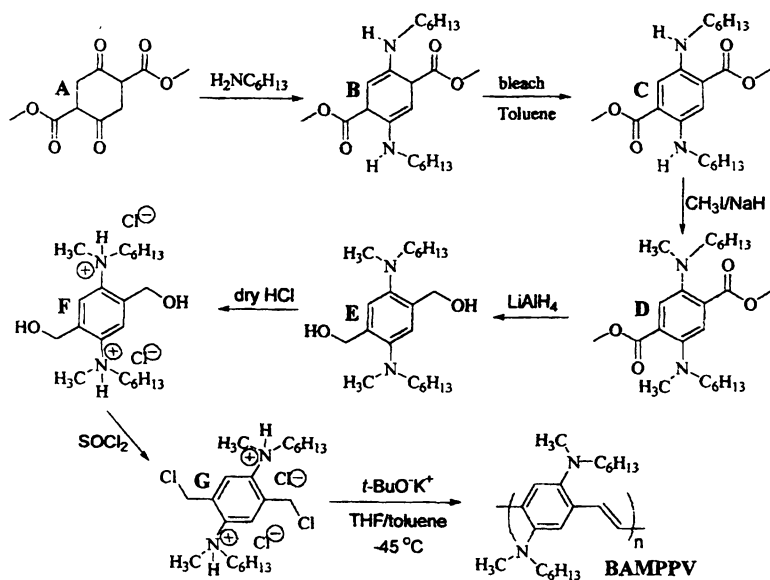
Experimental

Materials and Methods

Dimethyl 1,4-cyclohexanedione-2,5-dicarboxylate was purchased from Acros Chemical and used as received. All other chemicals were purchased from Aldrich Chemical and used as received. Bruker Instruments 200 MHz NMR (for monomers and intermediates) and 400 MHz NMR (for polymers)



Scheme I. Original 7-step synthesis for BAMPPV



Scheme II. Improved 7-step synthesis for BAMPPV

spectrometers were used. Infrared analyses were performed using a Nicolet 870 FTIR Spectrophotometer. Differential scanning calorimetry (DSC) was performed using a TA Instruments 2910 Differential Scanning Calorimeter at a heating rate of 10°C/min. under nitrogen. Thermogravimetric analysis (TGA) was performed using a TA Instruments 2950 TGA scanning at 5°C/min (under nitrogen). Elemental analysis was performed by Galbraith Laboratories. Size-Exclusion Chromatography (SEC) was done at 1.5mL/min using a Jordy mixed-bed column at 20°C in THF using polystyrene standards. The density of the polymer was determined by measuring the immersed volume of pre-weighed samples in water at 20°C.

Adhesion Testing

All adhesion tests were performed according to ASTM D3359-97.

Immersion Testing

The initial investigation done at NAWCWD to determine if the BAMPPV polymers showed signs of corrosion inhibition involved an immersion test in simulated seawater. BAMPPV was incorporated as a 3-weight percent additive in an epoxy formulation and coated onto 2" x 2" 2024-T3 anodized aluminum panels via the draw-down method using a Gardner Blade. The same method was used to coat additional panels with the pure epoxy as control samples. The panels were then cured for 24 hours at 95°C. A seawater solution was made by addition of 4-weight percent sea salt into deionized water. The panels were immersed in seawater, then removed and dried after 2 weeks of immersion, exposed to air for 1-2 days and then re-immersed into the seawater solution. This pattern was repeated for a total exposure time of 6900 hours.

Neutral Salt Fog Test

Coated Al coupons were exposed to 1164 hours of neutral pH salt fog (ASTM B-117). This controlled salt fog test consisted of six aluminum 2024-T3 panels coated with BAMPPV (3 scribed and 3 unscribed) and six aluminum panels coated with a chromate conversion coating (3 scribed and 3 unscribed).

The polymer coated Al panels were coated by MicroCoating Technologies, Inc., (Chamblee, GA). The application was done using a proprietary atomization and flame deposition process in which no degradation was seen (according to FTIR analysis) after flame deposition of the BAMPPV.

Improved Synthesis of BAMPPV (15)

Synthesis of methyl 2,5-bis(N-hexylamino)-4-(methoxycarbonyl)cyclohexa-1,4-diene carboxylate (B). Dimethyl 1,4-cyclohexane dione-2,5-dicarboxylate

(Compound A) (1.89kg, 7.92mol) and methanol (12L) were combined in a 22L reactor. To this suspension, n-hexylamine (2.3L, 1.75kg, 17.3mol) was added drop-wise via a dropping funnel. The mixture was heated at reflux overnight. An orange-yellow precipitate was observed. The contents were cooled to room temperature and filtered, and the residue was washed with methanol. The product was then dried overnight under vacuum to yield an orange solid (2.42kg, 74%). mp: 120-122°C. ¹H NMR (CDCl₃): 8.8, m, 4H; 3.65, s, 6H; 3.21, t, 4H; 1.5, m, 4H; 1.35, m(br) 12H; 0.9 t, 6H.

Synthesis of methyl 2,5-bis(N-hexylamino)-4-(methoxycarbonyl)benzoate (C). In an open-topped 20L reactor, Compound B (1.5kg 3.8mol) was dissolved in dichloromethane (4L). To this solution, sodium hypochlorite (10% in water, 5.7L) was added with rapid stirring. The reaction was exothermic, and over the next 16h most of the dichloromethane had evaporated to yield reddish-brown crystals. The crude product was slurried in acetone and was collected via suction filtration to yield red crystals (1.0kg, 71%). mp: 104-105°C. ¹H NMR (CD₂Cl₂): 7.28, s, 2H; 3.86, s, 6H; 3.14, t, 4H; 1.62, m, 4H; 1.36, m(br) 12H; 0.91 t, 6H.

Synthesis of methyl 2,5-bis(N-hexyl-N-methylamino)-4-(methoxycarbonyl)benzoate (D). Into a 22L round bottom flask were placed Compound C (1.5kg, 3.9mol), sodium hydride (~455g, 19mol), and dry THF (8L). The mixture was stirred for 15 min and iodomethane (500mL, 8mol) was added drop-wise to the suspension. After all of the iodomethane was added, the mixture was heated at 60°C for 16h. The mixture turned from red to yellow and was then cooled to room temperature. Hexanes (4L) were added to the reaction vessel, and the mixture was filtered through celite. The filtrate was washed with water and separated, and solvent was removed under reduced pressure. The residue was dried under vacuum to yield an orange-brown oil (1.2kg, 75%). ¹H NMR (CD₂Cl₂): 7.18, s, 2H; 3.58, s, 6H; 2.92, t, 4H; 2.70, s, 6H, 1.49, m, 4H; 1.26, m, 12H; 0.87, t, 6H.

Synthesis of (2,5-bis(hexylmethylamino)-4-(hydroxymethyl)phenyl)-methanol (E). Lithium aluminum hydride (126g 3.3mol) was slurried in THF (11L) in a 22L reactor and then cooled to 7°C. To this cooled mixture, Compound D (1.4kg 3.3mol) was added drop-wise. After the addition was complete, the reaction mixture was heated overnight at 50°C. The solution was cooled to room temperature, and ethyl acetate (4L) was added to consume excess LiAlH₄. The reaction was quenched with water, a very thick precipitate formed. The mixture was filtered and the residue was washed with ethyl acetate. The filtrate was evaporated to dryness to yield an orange oil (0.78kg, 64%), which was used immediately for the next step.

Synthesis of (2,5-bis(N-hexyl-N-methylamino)-4-(hydroxymethyl)-phenyl)-methanol Dihydrochloride (F). Compound E (0.5kg, 1.37mol) was dissolved in methanol (2L). Dry HCl was bubbled through the solution for approximately

1.5h (the solution turned a pale yellow color after sufficient HCl was added).⁶ The methanol was removed using the rotary evaporator, leaving a brown oil. The oil was stirred for 20 min in cold, dry acetone (1L) and filtered and the residue was rinsed 3 times with dry acetone. The residue was dried overnight under vacuum to yield a white solid (170g, 30%) mp: 146°C (dec). ¹H NMR (CD₃OD): 7.98, s, 2H; 5.07, s, 4H; 3.66, t, 4H; 3.34, s, 6H; 1.55, m, 4H; 1.30, m, 12H; 0.88, t, 6H.

Synthesis of (2,5-bis(chloromethyl-4-(hexylmethylamino)-phenyl)-Hexylmethyl-amine Dihydrochloride (G). In a 4L reactor, thionyl chloride (400mL) was cooled with an ice bath to ~0°C. Compound F (150g, 0.35mol) was added slowly as a solid while maintaining the reaction temperature below 5°C. After the addition was complete, the reaction was allowed to warm to room temperature over 3h. The thionyl chloride was removed under reduced pressure to yield a brown oil. The oil was stirred in acetone, and a white solid was isolated via vacuum filtration. The solid was dried under vacuum overnight to yield an off-white solid (79g, 50%). mp: 156-161°C (dec). ¹H NMR (CD₃OD): 8.13, s, 2H; 5.07, s, 4H; 3.68, t, 4H; 3.33, s, 6H; 1.54, m(br), 4H; 1.29, m(br), 12H; 0.87, t, 6H.

Polymerization. Polymerization was accomplished in a 5L reactor with a mechanical stirrer. The reactor was placed inside a large stainless steel secondary container, and toluene (2L) and THF (2L) were added to the reactor. Dry ice was added to the secondary container with acetonitrile to cool the reactor to -45°C. While the solvent was cooling, monomer G was added (100-150g, varied per batch). When the temperature reached -45°C, potassium tertbutoxide was added (1 mol monomer/8 mol K-*t*-OBu). The temperature was kept between -45°C and -55°C for 2h. The solution was then allowed to warm to room temperature overnight. After 18h the reaction mixture had become a very viscous orange, almost gelatinous material. This material was then precipitated into methanol, filtered through a fine glass frit, and dried under vacuum at 100°C overnight. When the polymer was dry, it was placed in a soxhlet thimble and methanol was used to extract the oligomers and some remaining salts, giving an orange-yellow powder in 93% yield. Further purification of the polymer was achieved by liquid-liquid extraction using water to extract the salts from a polymer solution in tetrachloroethane for 7-10 days. The extraction was followed by precipitation into methanol, filtering and drying. The NMR spectrum of this material is identical to the spectrum reported previously (6).

Results and Discussion

Optimization of Literature Method

In general, the scale-up follows the published procedure with only two exceptions (6-15). The original reaction path is shown in Scheme I. The

bromine oxidation of Compound B has been replaced with a sodium hypochlorite (10%, i.e. pool bleach) oxidation (16). The use of bleach is a step towards reducing hazards, cost, and waste generation during the synthesis. Another change in the synthesis is the replacement of DIBAL-H (Step 4) with the more economical and lower cost reagent LiAlH_4 (see Scheme II).

These changes result in less waste generation during purification and reduction of hydrogen gas generation during the reaction of Compound D. The above improvements resulted in increased overall yield and fewer side products. The yield of the reduction step (step 3) is currently being optimized, which would further increase the overall yield. Our estimations indicate that an overall yield of 35% is possible assuming typical yields for compounds E, F and G.

The Gilch polymerization is not known for its high yields but rather for the often high molecular weights achieved (17). Our first attempts at polymerizations afforded high molecular weight polymers (M_n , 130kg/mol vs. PS), however, the yields were low (~30%) for the purified polymer. Using the results of Johansson et al. (18), we were able to optimize the polymerization of G to produce >65% yield of the polymer. For our system an operating temperature of -45°C was found to be optimal.

Analysis of the residual salt content in the polymers reveals that the amount of salt remaining depends greatly upon the method of purification. Residual salt content was not a problem during small-scale polymerization (elemental analysis reveals the polymer to be 99.9% pure); however, the large scale polymerization had residual salt ranging from 3.5% (soxhlet extraction) to 0.15 % residual chloride (liquid-liquid extraction using tetrachloroethane/water). Studies are underway to determine whether the residual chlorine is from potassium chloride or from chloromethyl end group. The removal of residual salt is critical for further optimization of adhesion (particularly steel) and corrosion protection.

Alternate Synthetic Routes

The reduction in the number of synthetic steps is of the utmost importance for the commercialization of BAMPPV. A number of alternate synthetic routes are currently being investigated in our labs (19). The two most promising routes involve monomers based on the Gilch and Heck polymerizations. The Gilch polymerization is currently employed and results in good yields and allows control of the molecular weight. Alternative methods such as the Heck reaction (20) would allow the use of ethylene as a comonomer thus reducing solvent costs. Although none of our new routes are both reliable and high yielding enough to perform on a large scale, we are currently optimizing and investigating these alternative techniques.

Characterization of BAMPPV Polymers

Thermal and Physical Analysis

Figure 1 shows the weight loss of BAM-PPV produced via Scheme I as a function of temperature measured with the TGA. The 5% weight loss temperature is about 260°C in nitrogen. This weight loss is associated with a strong exotherm in DSC traces, which begins at 200-250°C. For this reason, thermal analysis of BAMPPV is confined to temperatures of 225°C or less in order to ensure the stability of the samples.

In Figure 2, three different DSC heating curves of BAMPPV produced by our previously published route are compared (11,15). The uppermost curve is from a sample that was mixed at 1.5 wt% in xylene and then rapidly dried at 120°C, with no additional thermal treatment. A small exotherm (1.1 J/g) with a peak at 140°C is followed by a somewhat larger endotherm (1.7 J/g) with a peak at 168°C. This pattern is typically seen in semicrystalline polymers. In this case, the rapidly dried sample was able to reach only a small degree of crystallinity, as indicated by the ratio of exotherm to endotherm area and by the small amounts of heat involved in the crystallization and melting events.

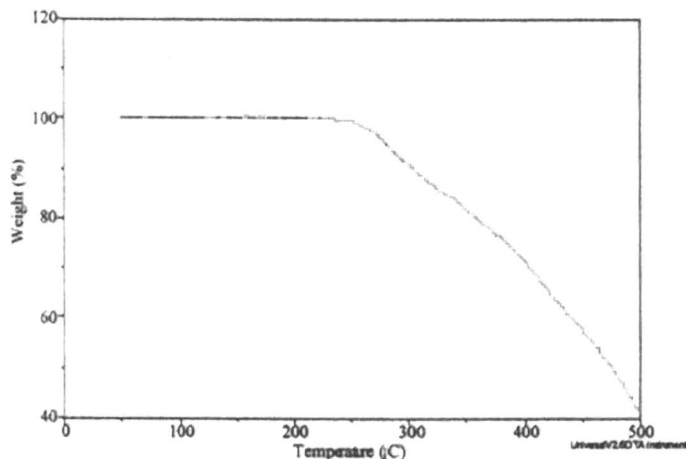


Figure 1. Weight loss versus temperature curve of BAMPPV synthesized via Scheme I, obtained from thermogravimetric analysis (TGA) with a heating rate of 5°C/min under nitrogen atmosphere

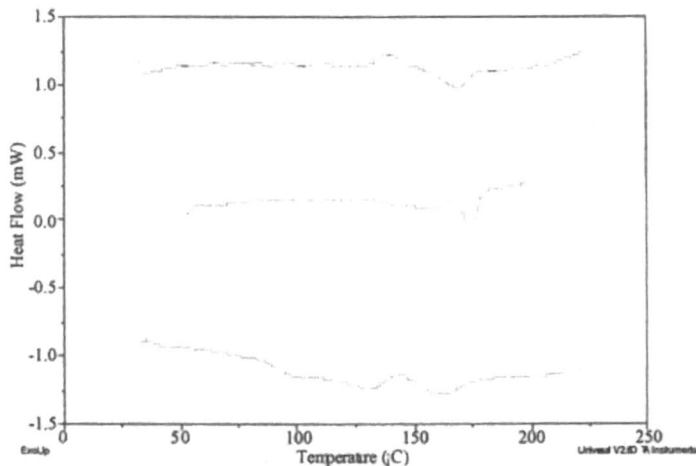


Figure 2. DSC heating curves of BAMPPV produced via Scheme I with three different thermal histories. The solid curve (uppermost) is the first heating from a sample rapidly dried from a 1.5% mixture in xylenes at 120°C. The dot-dashed curve (lowermost) is the first heating from a sample as-received after polymerization. The dashed curve (middle) is the fourth heating from the same sample. The thermal cycle involved heating at 10°C/min to 225°C, followed by cooling to room temperature at 5°C/min.

The lowermost curve, on the other hand, represents the first heating of a sample consisting of the powder obtained at the end of the BAMPPV polymerization procedure, i.e., slow drying after precipitation into methanol. It shows two endotherms, one with a peak at 130°C (possibly due to residual xylenes), and the other (6.6 J/g) at 161°C. The lower temperature of the melting event suggests that the crystals present are more disordered (most likely due to the lower temperature at which they were formed), while the larger amount of heat absorbed and the lack of a significant exotherm suggests that the degree of crystallinity in this sample is higher, although still small.

Finally, the middle curve is from the same sample after three cycles of heating to 225°C and cooling at around 5°C/min. back to room temperature. This sample shows two endotherms, a broad one peaking at 158°C (about 3 J/g) overlapping with a much sharper one (about 4.5 J/g) peaking at 175°C. The most reasonable explanation for this occurrence is that the heating cycles have acted as annealing events, transforming part of the crystal population into a more ordered state. To date, no melting events in any BAMPPV samples have been seen at temperatures higher than about 175°C, suggesting that this is the melting point of the most crystalline regions of BAMPPV polymers.

In total, the semicrystalline nature of BAMPPV (seen in the uppermost curve) along with the dependence of crystal melting point on thermal history (seen in the lowermost curve) and the structural rearrangement to form higher melting crystals on annealing (as evidenced by the middle curve), are all typical behaviors for slowly crystallizing rigid polymer materials, such as polyetherimides (PEI) blended with poly(ether ether ketone)s (PEEK) (21).

Additional evidence for the slightly crystalline nature of BAMPPV has been obtained through density measurements. According to topological correlation methods developed by Bicerano (22), the density of amorphous BAMPPV polymer should be 1.13 ± 0.02 g/cc. The density of small pellets of compression molded BAMPPV has been measured at 1.15 ± 0.01 g/cc. Using the rule of thumb that the density of crystalline material is generally about 15% greater than that of amorphous material, the most likely degree of crystallinity based on density measurements would be about 12% by volume. Although the uncertainty in this estimate is quite large, it nonetheless suggests that a majority of BAMPPV exists as amorphous material, with a few scattered crystallites acting to bind separate polymer chains together. Such an arrangement should result in a coating with enhanced toughness and better environmental resistance than coatings made from purely amorphous materials (such as MEH-PPV) of the same molecular weight.

Environmental Testing of Substrates Coated with BAMPPV films.

Adhesion Testing

Initial test results indicate good adhesion to the substrate. In pull tests up to 1000psi, all of the coatings remained bonded to the substrates.

Immersion Test

The following photographs (Plates 1-6) were taken of coated 2"x 2" 2024-T3 anodized aluminum panels samples after an exposure time of 6900 hours.

Plates 1 and 2 are panels coated only with epoxy. On panel 1, (Plate 1), there is clearly corrosion along the scribe. There is also an area along the scribe where the coating has a defect that allowed for localized blistering. The corrosion products are more visible under 40x magnification of the center of the scribe lines on panel 1 (Plate 6). Panel 2 (Plate 2) also an epoxy-coated sample, shows no signs of corrosion along the scribe line. From visual inspection using 200x magnification, it was determined that the scribe did not go through the epoxy coating to the base metal. It was clear under 200x magnification that the base metal was exposed on all other panels.

Plates 3 and 4 are coated with the 3% BAMPPV/epoxy coating. There are some obvious areas on both panels where coating defects have allowed localized blistering possibly due to small amounts of residual potassium chloride. Other than these localized areas, there is no corrosion within the scribe lines in either BAMPPV/epoxy panel.

Plate 5 is a 40x magnification photograph of the center of the scribe lines in the BAMPPV/epoxy coating on panel 3. Plate 6 is a photograph of the scribe lines on panel 1, coated with epoxy, under the same magnification (both substrates are anodized aluminum). The comparison of Plates 5 and 6 shows that the BAMPPV/epoxy mixture provides greater corrosion protection within the scribes of the panels than the pure epoxy.

In addition to offering some degree of corrosion protection, the BAMPPV also appears to act as an adhesion promoter. A 40x magnification analysis of a representative unscribed area of the BAMPPV/epoxy coating shows no signs of blistering within the coating on either panel that contained the BAMPPV. A 40x magnification analysis of a representative unscribed area within the epoxy coating containing no BAMPPV shows blistering throughout the pure epoxy coatings on both panels 1 and 2.

Neutral Salt Fog Test (23)

Plates 7 and 8 are photographs of coated Al panels (BAMPPV and chromate conversion respectively) after exposure to salt-fog (616 hours). Overall, the performance of the polymer coatings was similar to the performance of the chromium conversion coatings after 616 hours of exposure in neutral salt fog. Under 6x magnification, evidence of corrosion can be seen within the scribe lines of both the chromate conversion coated panels and the polymer coated panels. Under high magnification (60x) there is slightly more evidence of corrosion within the scribes of the polymer coated panels than the chromium conversion coated panels. However, the intact portion of the polymer coating is unaffected by the exposure to salt spray.

The panels were later removed from the salt fog chamber for evaluation after an exposure time of 1146 hours. It can be seen in Plates 9 and 10 that the polymer coated and chromium conversion panels still had a similar appearance overall. Both panels had evidence of corrosion within the scribed areas, but the overall coating was largely unaffected. Both panels also exhibited more corrosion along the edges than through the bulk of the coatings.

The panels were returned to the salt fog chamber and removed again after an exposure time of 3000 hours. Plate 11 is the polymer coated panel and Plate 12 is the chromated panel.

A comparison of the BAMPPV coated panel and the conversion coated panel after an exposure time of 3000 hours indicates that the polymer coating performs similarly to the hexavalent chrome conversion coating.

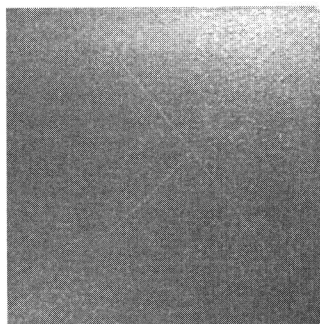
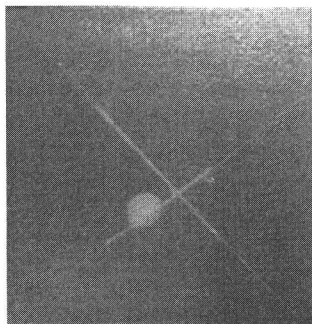


Plate 1. Panel 1. Pure epoxy coating on aluminum substrate.

Plate 2. Panel 2. Pure epoxy coating on aluminum substrate.

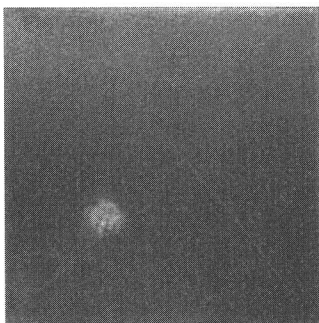


Plate 3. Panel 3. 3% BAMPPV/epoxy coating on aluminum substrate.

Plate 4. Panel 4. 3% BAMPPV/epoxy coating on aluminum substrate.

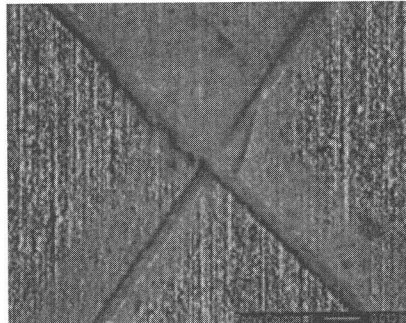
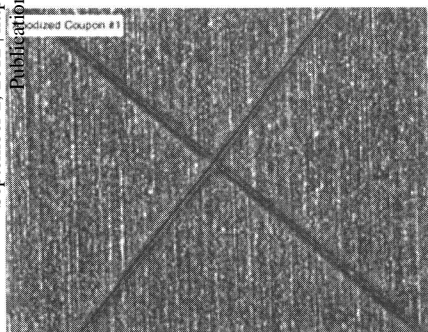


Plate 5. Panel 3. 40X magnification of the scribe lines in the 3% BAMPPV/epoxy coating. (Reproduced from reference 12.)

Plate 6. Panel 1. 40X magnification of the scribe lines in the 3% pure epoxy coating. (Reproduced from reference 12.)

These figures can also be found in the color insert.

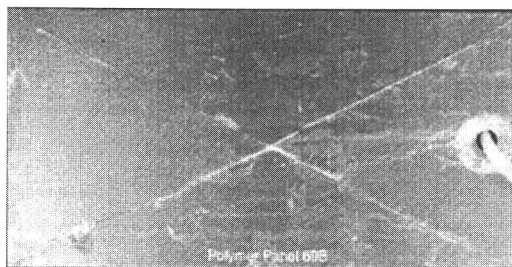


Plate 7. Scribed polymer coated Al panel after 616 hours of exposure. (Reproduced from reference 12.)

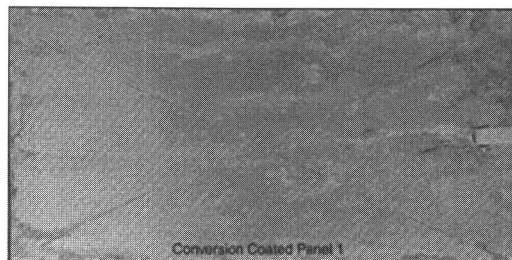


Plate 8. Scribed conversion coated Al panel after 616 hours of exposure. (Reproduced from reference 12.)

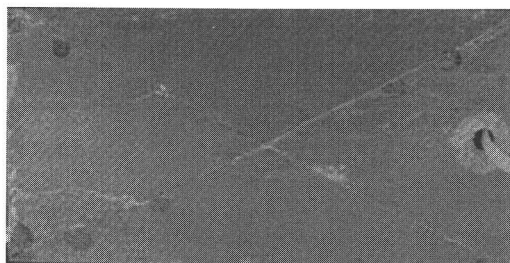


Plate 9. Scribed polymer coated Al panel (1146 hours of exposure). (Reproduced from reference 12.)

These figures can also be found in the color insert.

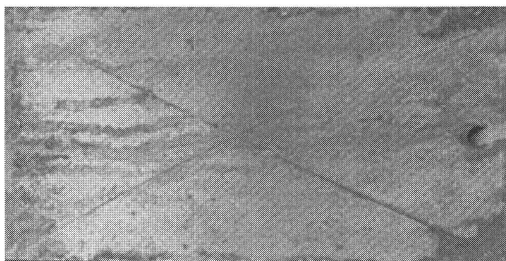


Plate 10. Scribed conversion coated Al panel (1146 hours of exposure). (Reproduced from reference 12.)

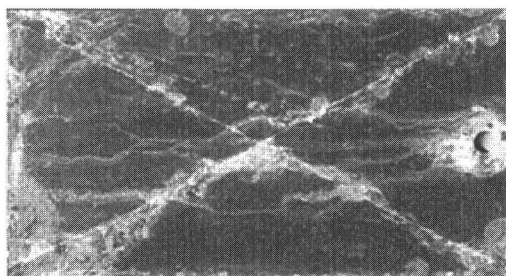


Plate 11. Scribed polymer coated Al panel (3000 hours of exposure). (Reproduced from reference 12.)



Plate 12. Scribed conversion coated Al panel (3000 hours of exposure). (Reproduced from reference 12.)

These figures can also be found in the color insert.

Conclusions

The synthesis and scale-up of BAMPPV has been successfully accomplished. Improved synthetic procedures have resulted in increased yields of polymer with lower amounts of hazardous waste generation and lower cost. New polymer purification procedures allow for quantitative removal of residual salt. Initial corrosion tests of the BAMPPV coatings on Al alloy indicate that the polymer may function as both a corrosion inhibitor and an adhesion promoter. Future tests need to be done not only to determine the amount of corrosion protection possible with these polymers, but also to optimize coating systems (epoxy and urethane) and their applications on different substrates.

Acknowledgments

The authors would like to acknowledge the continuing support of the Office of Naval Research, particularly Dr. A. J. Sedriks and Dr. K. J. Wynne (currently at Virginia Commonwealth University), the Strategic Environmental Research and Development Program (SERDP), particularly Mr. C. Pellerin, and Dr. J. W. Fischer and Dr. G. A. Lindsay of NAVAIR.

References

1. National Emissions Standards for Chromium Emissions from Hard and Decorative Chromium Electroplating and Chromium Anodizing Tanks. Environmental Protection Agency. *Federal Register*. RIN 2060-AC14, January 25, 1995.
2. 4th International Aircraft Corrosion Workshop, Solomons Island, Maryland, August 22-25, 2000.
3. DeBerry, D. W., *J. Electrochem. Soc.*, **1985**, 132, 1022.
4. McDiarmid, A. G., Short Course on Conductive Polymers, SUNY, New Platz, New York, 1985.
5. Wroblewski, D. A., Benicewicz, B. C., Thompson K. G., and Bryan, C.J., *Polym. Prepr.*, **1994**, 35, 265.
6. Zarras, P.; Stenger-Smith, J. D.; Ostrom, G. S.; Merwin, L. H.; Cameron, D. A.; Reynolds, J. R. *Polym. Prepr.*, **1998**, 39(1), 67.
7. Stenger-Smith, J. D.; Miles, M. H.; Norris, W. P.; Nelson, J.; Zarras, P.; Fischer, J. W.; Chafin, A. P. US Patent 5,904,990 May 18, 1999.
8. Stenger-Smith, J. D.; Norris, W. P.; Chafin, A. P. US Patent 5,585,522 Dec 17, 1996.
9. Stenger-Smith, J. D.; Norris, W. P.; Chafin, A. P. US Patent 5,587,488 Dec 24, 1996.

10. Stenger-Smith, J. D.; Norris, W. P.; Chafin, A. P.; Sackinger, S. T. US Patent 5,604,292 Feb 18,1997.
11. Stenger-Smith, J.D., Zarras, P., Merwin, L.H., Shaheen, S.E., Kippelen, B., and Peyghambarian, N., *Macromolecules*, **1998**, 31(21), 7566.
12. Anderson, N.M.; Stenger-Smith, J. D.; Irvin, D. J.; Guenther, A. J.; Zarras, P. In *A Review of Conductive Polymers as Environmentally Benign Corrosion Control Coatings*, Proceedings of the Navy Corrosion Information and Technology Exchange, Louisville, KY, July 16-20, 2001.
13. Stenger-Smith, J.D., Zarras, P., Ostrom, G., Miles M.H., *Review of Poly(bis-dialkylamino-p-phenylene vinylene)s as Corrosion Inhibiting Materials. ACS Symposium Series 735*, (1999), 18, p. 180-293 Hsieh, Wei, Ed. ACS Washington, DC Chapter 18.
14. Zarras, P., Stenger-Smith, J.D., Miles, M.H., *Polym. Mat. : Sci. Eng.*, **1997**, 76, 589.
15. Anderson, N., Irvin, D. J., Webber, C., Stenger-Smith, J. D., and Zarras, P., *Polym. Mater.: Sci. Eng.*, **2002**, 86, 6.
16. Stenger-Smith, J. D., Anderson, N., and Webber C., private communication with Spectra Group Ltd. (Maumee, OH), December 2001-June 2002, Phase II ONR SBIR Program.
17. Gilch, H. G. and Wheelwright, W. L., *J. Polym. Sci., Part A: Polym. Chem.*, **1966**, 4, 1337.
18. Johansson, D. M., Theander, M., Srdannov, G., Yu. G., Inganas, O. and Andersson, M.R., *Macromolecules*, **2001**, 34, 3716.
19. Irvin, D. J., Anderson, N., Webber, C., Fallis, S., and Zarras, P., *Polym. Prepr.*, **2002**, 43(1) .
20. Chang, C. C., Chen, K. J., and Yu, L. J., *J. Org. Chem.*, **1999**, 64, 5603.
21. Bicakci, S., and Cakmak, M., *Polymer*, **2002**, 43, 149.
22. Bicerano, J., *Prediction of Polymer Properties*, p. 65, 2nd Ed. Marcel Dekker, New York, **1996**.
23. ASTM B117, *Annual Book of ASTM Standards*, ASTM, West Conshohocken, PA 2001, vol. **03.02**, p. 1.

Chapter 9

Synthesis and Study of Phenyl-Capped Tetraaniline as an Anticorrosion Additive

Wanjin Zhang^{1,*}, Youhai Yu¹, Liang Chen¹, Huaping Mao¹,
Ce Wang¹, and Yen Wei²

¹Department of Chemistry, Jilin University, Changchun 130023,
Peoples Republic of China

²Department of Chemistry, Drexel University, Philadelphia, PA 19104

Abstract: Phenyl-capped tetraaniline was synthesized via a pseudo-high-dilution technique. The mechanism most likely involves the formation of an intermediate trianiline salt and the subsequent coupling reaction of the trianiline salt with diphenylamine. Preliminary tests on the performance of phenyl-capped tetraaniline as an anticorrosion additive to a bicomponent polyurethane lacquer on cold rolled mild steel were performed. The results show that phenyl-capped tetraaniline is not only able to retard the formation of rust, but also exhibits throwing power and the ability of removing rust.

Introduction

Polyaniline is one of the most studied conjugated polymers because of its convenience of synthesis and air stability. In order to elucidate its conducting mechanism, oligomers were synthesized by researchers in the past. The first oligoaniline, tetramer called zuirin, was reported without a comprehensive analysis in 1907¹⁾. In 1968, Honzl²⁾ reported a synthetic method which involved the condensation of small oligoanilines (i.e., dimer and trimer) with diethyl

succinoylsuccinate, followed by hydrolysis, decarboxylation, and aromatization. Phenyl-capped tetraaniline (PCAT) and hexaaniline can be synthesized by this method. In 1986, based on a modified Honzl's approach, Wudl and his co-workers³⁾ synthesized a phenyl-capped octamer, which had essentially the same electrical and spectroscopic properties as polyaniline.

More recently, other methods for the synthesis of oligoanilines have been emerged. Wei et al. has shown a one-step method for synthesizing amine-capped trianiline⁴⁾. An Ullmann coupling reaction between acetanilide and 4-iodonitrobenzene was used in an iterative coupling/reduction sequence followed by deacetylation to afford parent trianiline and tetraaniline⁵⁾. In 1998, Buchwald and co-workers reported a palladium-catalyzed synthetic approach for the synthesis of oligoanilines and their derivatives⁶⁻⁷⁾. Wudl's phenyl-capped octamer in the doped form was re-synthesized with a little difference in UV/Vis spectrum by this method.

A literature report of a blue solid deposited onto platinum metal in the electrochemical oxidation of aniline indicated that the aniline polymer could be prepared as a coating on metal, though unrecognized as such, in a laboratory 134 years ago⁸⁾. In the past 15 years, specific observations on the anticorrosion effect of polyaniline have come from Mengoli et al.,⁹⁾ DeBerry,¹⁰⁾ Ahmad, and MacDiarmid.¹¹⁾ The use of conducting polymers as coatings for protecting mild steel from corrosion was discussed by Troch-Nagels et al.¹²⁾ Recent reports from Wessling¹³⁾ and from Epstein and Jasty¹⁴⁾ give a support to the claim that polyaniline electrically effects on the passivation of steel or iron.

In our previous work, we reported a general method to synthesize parent oligoanilines, such as tetramer, octamer and hexadecamer¹⁵⁾. In this work, we present a pseudo-high-dilution technique to synthesize PCAT and the results of its anticorrosion performance.

Experimental

Materials.

The following chemicals were used as received: diphenylamine (98%, Aldrich), p-phenylenediamine (98%, Aldrich), ammonium persulfate (98%, Shengyang Chemical Factory, China), ammonium hydroxide (30%, Changchun Chemical Factory, China), hydrochloric acid (37%, Changchun Chemical Factory, China) dimethylformamide (99%, DMF, Beijing Chemical Factory, China), acetaldehyde (40%, Tianjin Nankai Chemical Factory, China),

bicomponent polyurethane lacquer (BP-lacquer, Xingtian Wancai Coating Ltd., Sunde, China).

Instrumentation.

IR Spectra of KBr powder-pressed pellets were recorded on a Nicolet Impact 410 Spectrometer. $^1\text{H-NMR}$ was run on a Varian Unity-400 spectrometer, referenced to internal tetramethylsilane, d^6 -DMSO as solvent. Mass spectra were performed on an LDI-1700 laser desorption ionization flying time spectrometer (Biomolecular Co., USA). Elemental analysis results were obtained on a Perkin Elmer 2400 CHN elemental analysis instrument.

Synthesis. PCAT was synthesized by a two-step method:

a. Preparation of Schiff-base *a*.

9.7g of *p*-phenylenediamine was dissolved in a mixture solvent of 250mL ethanol and 20mL acetaldehyde in a 500ml beaker. 10ml of concentrated H_2SO_4 was added into the solution slowly under a magnetic stirring. After 0.5 h, the reaction mixture was filtered through a Buchner-funnel. The precipitate was washed with ethanol three times. The obtained Schiff-base *a* without further purification was used for the following reaction. The experiment was carried out at room temperature in air.

b. Preparation of PCAT.

3.2g of Schiff-base *a* and 10.4g of diphenylamine were dissolved in 200ml DMF containing 20ml distilled water and 15ml concentrated HCl. The reaction system was cooled to 0 °. Then, a solution of $(\text{NH}_4)_2\text{S}_2\text{O}_8$ (10.2g in 1M HCl of 40ml) was added into the reaction system at about 60 drops/min under a strong stirring. The resulting solution was stirred for another 1 hour at the same temperature. It was then transferred into a 2000mL-beaker containing 1000ml distilled water to get a precipitate. The precipitate was collected by vacuum filtration through a Buchner-funnel and washed by 1000mL HCl (0.1M) three times and dedoped by 0.1M ammonium hydroxide. Upon drying at 40 ° under vacuum, the crude product was obtained as a blue-black powder. This was reduced by phenyl-hydrazine in DMF and recrystallized from 1,4-dioxane. A

typical elemental analysis for $C_{30}H_{26}N_4$: Cal.: C, 81.42; H, 5.92; N, 12.66; Found: C, 80.58; H, 5.75; N, 12.95.

Test of anticorrosion performance.

1g of PCAT was suspended in 9.5g of component **b** of the BP-lacquer under a magnetic stirring. After standing for ten minutes, the suspension was ground with a colloidal mill for 30 minutes to get a 5%-PCAT-lacquer..

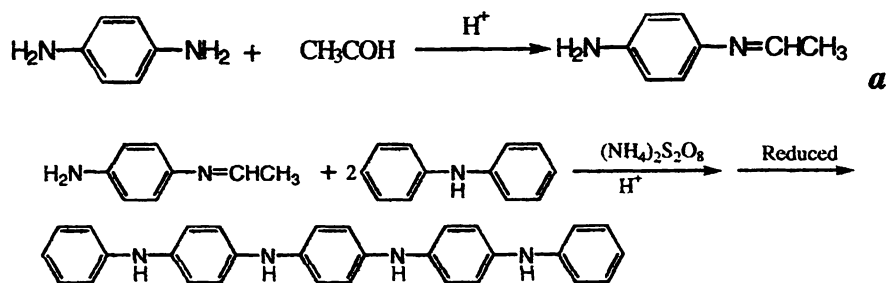
Several pieces of cold rolled steel plates with a size of $5 \times 10 \text{cm}^2$ were cleaned to get rid of grease with a sandblast and then washed with acetone, and dried. For comparison, one of the steel plates was coated with the 5%-PCAT-lacquer, the other was coated with the pure BP-lacquer. The coatings on the plates were dried under ambient condition for several days. For the examination of anticorrosion ability, the experiments were divided into three groups: 1). A nick of $0.5 \times 2 \text{cm}^2$ was scraped in the coating sheets of the samples with and without PCAT before immersion in 0.1M HCl, respectively. A fresh HCl solution was used instead each week. Four weeks later, the coating was removed from the sheets with dimethylformamide. 2). The 5%-PCAT-lacquer was coated on a plate in a form of circle with a diameter of $> 0.1 \text{cm}$. 3). The 5%-PCAT-lacquer was coated on the upper and lower sides of the plates. After drying, it was immersed in a 0.1 M HCl solution for one week and then put in air for one month.

Results and discussion

1. Formation of PCAT

At the beginning of the experiments, we attempted to use *p*-phenylenediamine and diphenylamine to directly synthesize PCAT. However, we found that a series of higher oligomers as byproducts emerged according to mass spectrometry (Figure 1), although the reaction temperature was decreased to -15°C . Purifying the compounds appears to be very difficult. So, we designed a pseudo-high-dilution technique to synthesize the desired PCAT

Similarly, an oxidation coupling reaction was used in the technique and went in two stages. First *p*-phenylenediamine and aldehyde were condensed under an acidic conditions to produce an intermediate – Schiff-base *a*. Then, the Schiff-base *a* was reacted with an excess amount of phenylenediamine to get end product (Schiff-base *a*:phenylenediamine = 1:2, mol), in view of phenylenediamine being able to self-condense to dimer, which leads to the reaction stopping. The reaction equations are shown in Scheme 1.



Scheme 1. Synthesis of PCAT

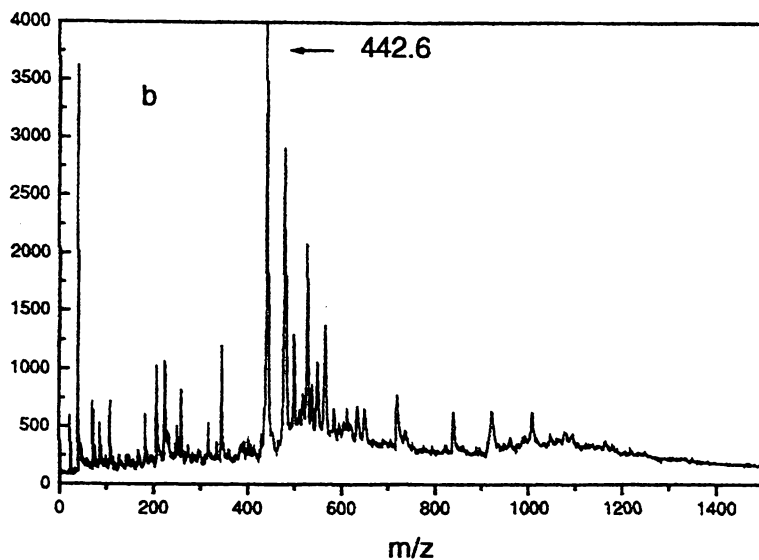
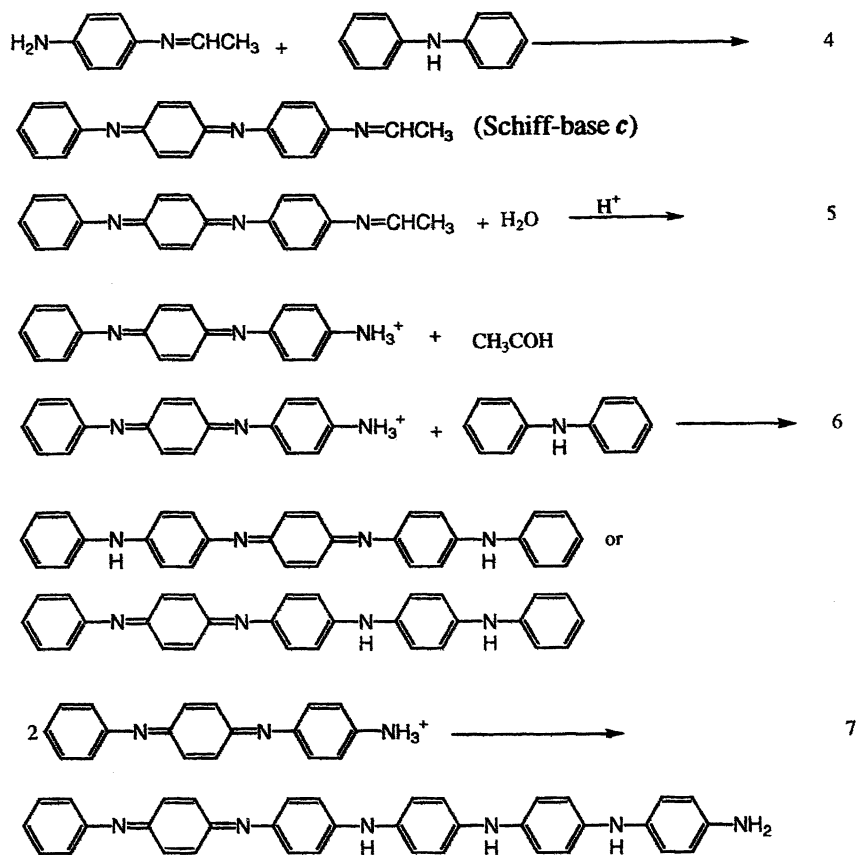


Figure 1. Mass spectrum of PCAT synthesized directly from p-phenylenediamine and diphenylamine



Scheme 2. A Possible Formation Mechanism of PCAT

Based on the results, a reaction mechanism was suggested as shown in Scheme 2. It can be known that a rapid coupling reaction leads to the formation of Schiff-base *c* (eq. 4) upon the addition of the oxidizing agent $(\text{NH}_4)_2\text{S}_2\text{O}_8$ to the mixture solution of Schiff-base *a* and diphenylamine. The presence of a small amount of water brought by HCl solution was likely to cause the hydrolysis of Schiff-base *c* to a trianiline salt (eq. 5), which reacted with diphenylamine at once. It means that the trianiline salt could be rapidly consumed by reacting with diphenylamine. The trianiline salt concentration was much lower than that of diphenylamine in the reaction system. The preparation technique is therefore called pseudo-high-dilute technique. The self-coupling reaction of the trianiline salt (eq. 7) can not take place by using this technique and PCAT is the main product. This has been proved by mass spectrum shown in Figure 2.

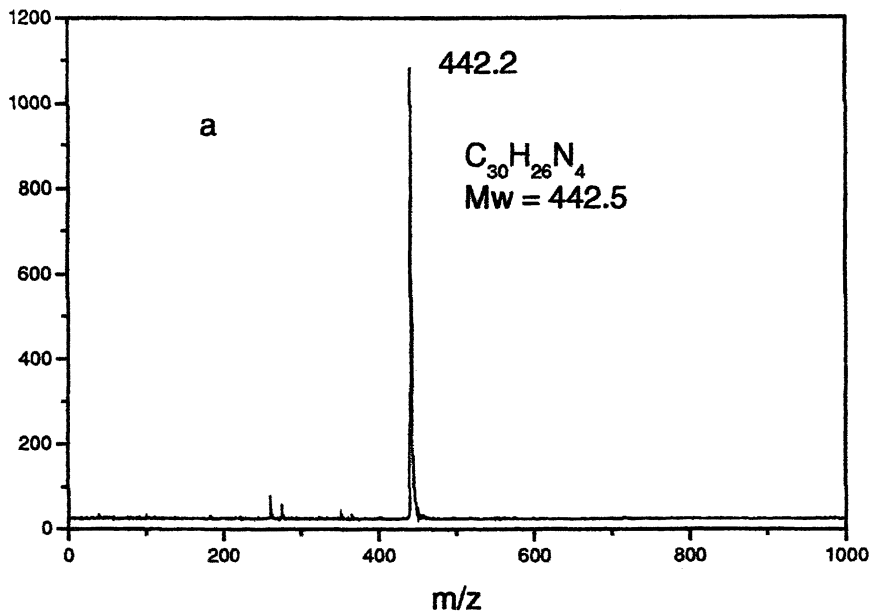


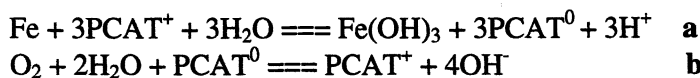
Figure 2. Mass spectrum of PCAT synthesized by a pseudo-high-dilute technique.

2. The anticorrosive performance of the coating containing PCAT

During the examination of anticorrosion ability of PCAT, we surprisingly found that it not only has some features that the other anticorrosion additives do have, but also shows some peculiar department that the others do not show.

First, it shows a good retardation effect on the formation of rust, as shown in Plate 1. The right picture shows the appearance of the steel surface with the pure BP-lacquer and the left side with the 5%-PCAT-lacquer. It is not difficult to observe that many rusty spots appear on the right plate and at the nick, whereas on the left photo a smooth surface is given in contrast.

The anticorrosion mechanism is related to the intrinsic property of PCAT having three types of oxidation state (oxidation state, median state, and reduction state). In the presence of water, iron is oxidized to a layer of $\text{Fe}(\text{OH})_3$ converting to Fe_3O_4 afterwards and PCAT was reduced (eq. A). After that, PCAT is oxidized to the primary state in air (eq. B). The Fe_3O_4 layer formed ensures that the steel plates are not corroded.



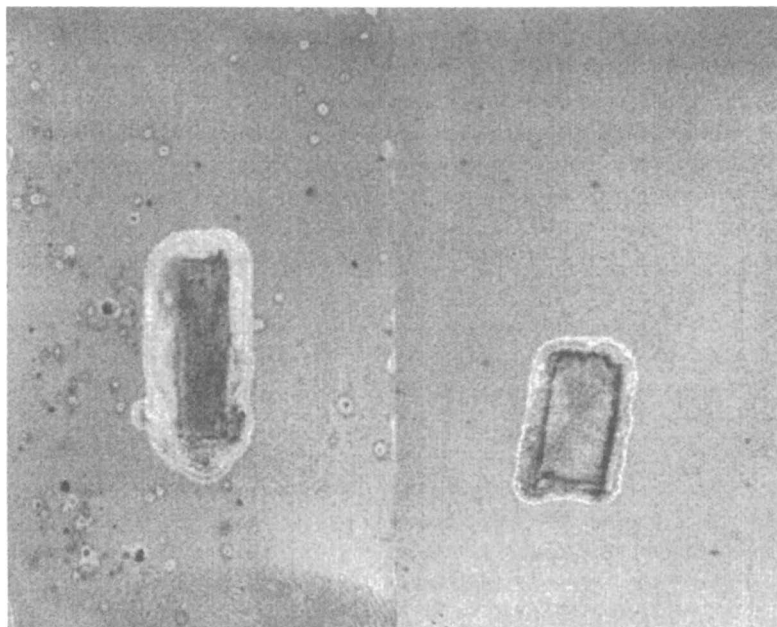


Plate 1. The retardation phenomenon of PCAT. The surface of steel plates were coated with the pure BP lacquer (right) and with the 5%-PCAT-lacquer (left).

This figure can also be found in the color insert.

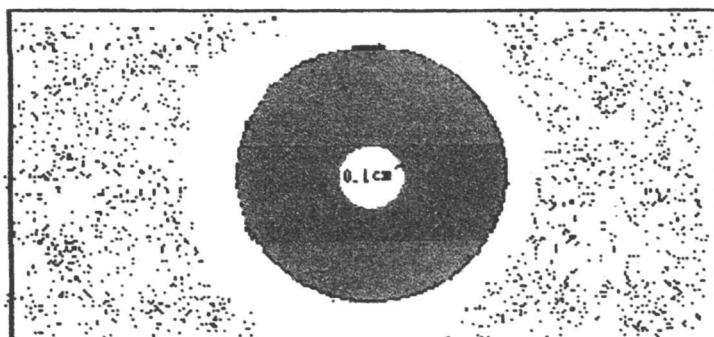


Figure 3. The phenomenon of throwing power of PCAT

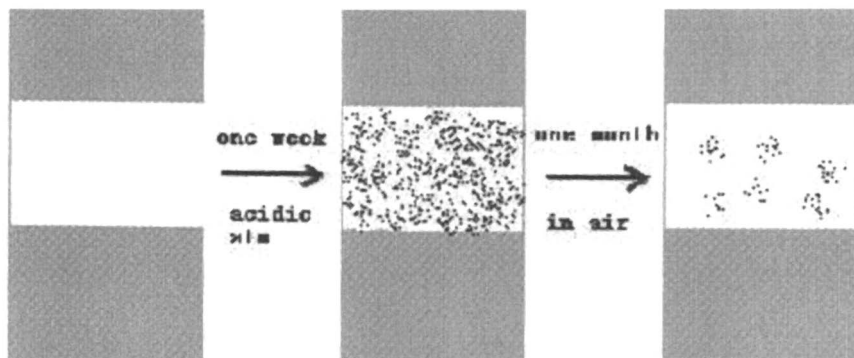


Figure 4. The phenomenon of “removing rust” of PCAT

Additionally, it is noticeable that the oxide layer can extend from the bottom of the coating to the place near the coating sheet, as shown in Figure 3. Namely, as we coated the 5%-PCAT-lacquer on the plate in a circle form, no rust emerged not only in the center but also around the outside of the coating circle. The phenomenon demonstrates that there is an electron transfer among Fe atoms on the surface, which is called throwing power phenomenon.

Furthermore, another interesting phenomenon is ability of PCAT “removing rust” (Figure 4). We found that rust can be rapidly formed on the bare surface, as coating a steel plate on its upper and lower sides with the 5%-PCAT-lacquer, followed by putting it in a dilute HCl solution for one week. However, one month after it stands in air, a part of the rust disappeared again. For this phenomenon, We assume that acid might be a driving force. As a large amount of acid is present, iron is corroded through the acid and a small amount of the doped PCAT is insufficient to prevent the steel from corrosion. In air, the excessive acid is evaporated, the doped PCAT is able to reduce the rust to Fe. However, its reduction mechanism is not clear yet, assuming that humidity was low enough that the plates were “dry”.

Conclusion

We have developed a pseudo-high-dilution technique to synthesize phenyl-capped tetraaniline. The mechanism probably involves the formation of an intermediate trianiline salt and the subsequent coupling reaction of it with diphenylamine. The technique is characteristic of easy operation and high yield.

The obtained phenyl-capped tetraaniline has a very good ability of anticorrosion. It is able to not only retard the formation of rust, but also has the function of throwing power and removing rust.

References

- 1) Willstatter, R. and Moore, C.W. *Ber.*, **1907**,40, 2665.
- 2) Honzl, J. and Tlustakova, M. *J. Polym. Sci. Pt. C*, **1968**,22 , 451.
- 3) Liu, F.L.; Wudl, F.; Novak, M. and Heeger, A.J. *J. Am. Chem. Soc.*, **1986**, 108, 8311.
- 4) Wei, Y.; Yang, C. and Ding, T. *Tetrahedron Lett.* **1996**,37, 731.
- 5) Rebourt, E.; Joule, J.A. and Monkman, A.P. *Syn. Met.* **1997**,84, 65.
- 6) Singer, Rovert A.; Sadighi, Joseph P. and Buchwald, Stephen L. *J. Am.Chem. Soc.*, **1998**,120, 213.
- 7) Sadighi, Joseph P.; Singer, Rovert A. and Buchwald, Stephen L. *J. Am.Chem. Soc.*, **1998**,120, 4960.
- 8) Lethedy, H. *J. Chem. Soc.* **1862**, 15, 161.
- 9) Mengoli, G; Munari, M. T.; Bianco, P.; Musiani, M. M. *J. Appl. Polym. Sci.* **1981**, 26, 4247.
- 10) DeBerry, D. W. *J. Electrochem. Soc.* **1985**, 132, 1022.
- 11) Ahmad, N.; MacDiarmid, A. G. *Bull. Am. Phys. Soc.* **1987**, 32, 548.
- 12) Troch-Nagels, G; Winand, R.; Weymeersch, A.; Renard, L.J. *Appl. Electrochem.* **1992**, 22, 756.
- 13) Wessling, B. *Adv. Mater.* 1994, 6, 226; Lu, Wei-Kang; Elsenbaumer, R. L.; Wessling, B. *Synth. Met.* **1995**, 71, 2163.
- 14) Jasty, S.; Epstein, A.J., *Polym. Mater. Sci. Eng.*, **1995**,Vol. 72, pp. 565-566.
- 15) Zhang, W.J.; Feng, J.; MacDiarmid, A.G. and Epstein, A.J. *Syn. Met.*, **1997**,84, 119 ; Feng, J.; Zhang, W.J.; MacDiarmid, A.G. and Epstein, A.J. *Pro. Soc. of Plastics Engineers Annual Conference*, **1997**, 1352.

Chapter 10

Sulfur–Quinone Polyurethanes and the Protection of Iron against Corrosion

Yongqi Hu^{1,3}, A. Brent Helms^{1,3}, David E. Nikles^{1,3,*},
Rahul Sharma^{2,3}, Shane C. Street^{1,3}, Garry W. Warren^{2,3},
and Dehua Yang³

Departments of ¹Chemistry and ²Metallurgical and Materials Engineering
and ³Center for Materials for Information Technology, The University of
Alabama, Tuscaloosa, AL 35487–0209

*Corresponding author: Email: dnikles@mint.ua.edu

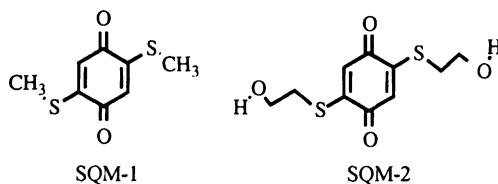
A sulfur-quinone diol monomer, 2,5-bis-(2-hydroxyethylthio)-1,4-benzoquinone (SQM-2), was prepared by the reaction of 2-mercaptoethanol with 1,4-benzoquinone. SQM-2 and polycaprolactone diol ($M_n = 1250$) were condensed with toluene diisocyanate to give a sulfur-quinone polyurethanes, SQPU-1, containing 7 mole percent SQM-2. SQPU-1 was coated onto an iron square and exposed to either 0.1 M sodium chloride electrolyte or substitute ocean water. Electrochemical impedance spectroscopy monitored any degradation of the coatings and showed that the sulfur-quinone polyurethane protected the iron against corrosion. Reflectance absorption infrared spectroscopy showed that the chemisorbed sulfur-quinone functional group lies parallel to the iron surface.

For more than a decade polymers containing the 2,5-diamino-1,4-benzoquinone functional group have been of interest, since Erhan's observation that this class polymers have a strong affinity for the surface of iron.¹ They found that the amine-quinone polymers could displace moisture from the surface of iron, making it hydrophobic. If the amine-quinone polymers would prevent moisture from adsorbing onto the iron surface, then they would inhibit corrosion. Indeed, they reported salt-spray testing data showing that amine-quinone polymers prevent corrosion.²

We have synthesized amine-quinone polyurethanes by condensing the amine-quinone monomer, 2,5-bis(N-2-hydroxyethyl-N-methylamino)-1,4-benzoquinone, and an oligomeric diol monomer (e.g., polycaprolactone diol,

polytetrahydrofuran diol) with a diisocyanate (TDI, MDI or IPDI).³ These polyurethanes were shown to inhibit the corrosion of the commercial iron particles used in state-of-the-art metal particle tape.⁴ They also promoted the adhesion of epoxy to steel.⁵

Curiosity led us to explore the possibility of replacing the amine group with a thioether group. We have developed the synthesis of a sulfur-quinone diol monomer and the preparation of polyurethanes containing this sulfur-quinone monomer.⁶ We also demonstrated that the sulfur-quinone polyurethanes protect commercial iron particles against corrosion by pH 2 aqueous buffer. Here we report further investigations of the corrosion protection of iron by sulfur-quinone polymers. We also report evidence for bonding interactions between the sulfur-quinone functional group and an iron surface.



Experimental

Materials. Cyclohexanone (HPLC grade), was purchased from Fisher and used as received. Iron squares (99.5+%, 1.5 mm thick, 25 mm x 25 mm or 50 mm x 50 mm) were purchased from Goodfellow. The synthesis of SQM-1, SQM-2 and sulfur-quinone polyurethane (SQPU) were described in previously.⁶ SQPU-1 was made by a random copolymerization of 4 mmol polycaprolactone diol (PCL with molecular weight of 1250), 0.7 mmol SQM-2 and 4.7 mmol toluene diisocyanate.

Electrochemical Impedance Spectroscopy. The polished iron squares (50 mm x 50 mm) were spin coated with SQPU-1 polymer solution (10 weight percent in cyclohexanone). A thickness of 10 μm was obtained by coating iron square twice in order to minimize the number of defects or D-type areas. The coating was dried in air for 24 hr then in a vacuum oven at 40°C for another 24 hr. The coating thickness was determined with a Sloan Dektak II surface profilometer from the average of at least five measurements in different locations. Electrochemical impedance spectroscopy (EIS) measurements on the coated metal square were carried out using an electrochemical cell consisted of a Plexiglass cylinder (25 mm inner diameter) placed on top of the coated substrate in order to create a vessel to hold the aqueous electrolyte, either 0.1M NaCl or substitute ocean water.⁷ The experimental details have been reported elsewhere.⁸

Surface Spectroscopy. Iron squares (25 mm x 25mm) were polished with 240, 400, 600 silicon carbide grit papers, then with 1 and 3 μm Al_2O_3 slurries, followed by degreasing with CH_2Cl_2 vapor. Films of SQM-1 were deposited by spin coating from a 0.005 weight percent solution in cyclohexanone) at 1500 rpm. The films were dried in vacuum oven at 40°C for 24 hr. XPS spectra were collected with an AXIS 165 X-ray Photoelectron/Auger Scanning Surface Analysis system using Al monochromatic K_{α} X-rays as the excitation source. The samples were pumped down to 5×10^{-7} torr before being put into sample transfer chamber and analytical testing chamber, where the measurements were

taken at 4×10^{-9} torr. The spectrometer work function was adjusted so that the 4f peak of a pure Au sample was at 84.0 eV. High resolution scans were made with the analyzer set at a 80 eV constant pass energy and an average irradiation time of 1 min. was used to scan. Charge compensation was made for the testing of SQM-1 powder pellet.

Reflectance IR spectra were obtained using a Digilab FTS-40 spectrometer with room temperature DTGS detector and single reflection accessory at 70° angle of incidence. The number of scans was 4000 with 16 cm^{-1} resolution. Background spectra were measured on a polished bare iron surface.

Results and Discussion

EIS was used to investigate the ability of SQPU-1 to inhibit the corrosion of iron during exposure to 0.1 M aqueous NaCl. In figures 1 and 2 are plots of impedance and phase angle as a function of frequency. The initial spectrum showed the coatings were behaving like a dielectric over a wide range of frequencies. The resistance of the coating exceeded 10^6 ohms. After 95 days of exposure, the EIS spectrum for the commercial polyurethane, fig. 1, showed a new peak in the phase angle curve, indicative of an electrochemical double layer. The electrolyte had diffused through the coating and broken the adhesive bond between the polymer and the iron. Pitting corrosion was observed soon after this feature appeared. After 95 days exposure SQPU-1, fig. 2, showed very little change, indicating the coating was acting as a barrier, preventing moisture from penetrating to the iron surface and breaking the adhesive bond between the polymer and the iron. SQPU-1 also resisted attack by substitute ocean water, fig. 3.

The sulfur-quinone polyurethane contained many different function groups that confound the interpretation of the x-ray photoelectron spectra. We tried obtaining data on the sulfur, but the photoelectron yield was so low, that beam damage occurred before we could obtain a reasonable signal to noise. Therefore we adsorbed the simple model compound, SQM-1 onto iron and obtained spectra, figure 4. The oxygen 1s peak for the bulk sample had a binding energy of 530 eV. When adsorbed to iron there were two oxygen peaks, one at 530 eV and a new feature with a 1 eV higher binding energy. This higher binding energy suggested that the oxygen atoms in SQM-1 were donating electron density to iron surface, forming a coordination bond. This coordinate bond could be main source for strong interfacial reaction between SQPU polymers and metal surface. In other words this coordination bond is a key factor for the control of metal corrosion rate by sulfur-quinone polymers. We attempted to obtain sulfur XPS data for SQM-1 on iron. Unfortunately XPS data for sulfur were very noisy due to a small cross section of sulfur requiring more collecting time imposed which led to the decomposition of SQM-1, especially in the case of spin coated thin layer on iron surface.

A grazing incidence reflectance infrared spectrum, fig. 5, for SQM-1 on iron showed the absence of the quinone C-H stretching mode at 3045 cm^{-1} . The quinone carbonyl stretching mode at 1640 cm^{-1} was also missing, fig. 6. This suggests that the quinone lies parallel to the iron surface.

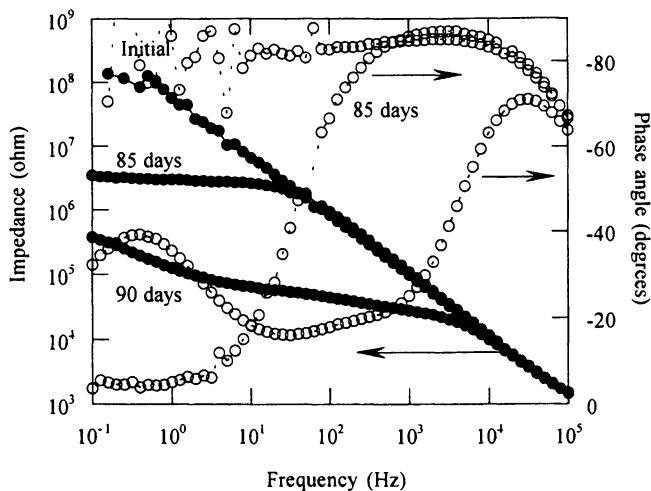


Figure 1. Bode plot for a commercial polyurethane binder exposed to 0.1M NaCl electrolyte. Open circles - phase angle curves, closed circles - impedance curves.

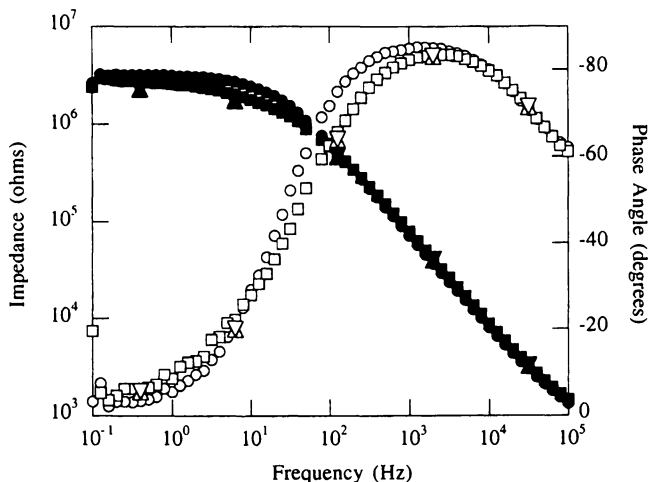


Figure 2. Bode plots for data obtained for an iron sample coated with SQPU-1 and exposed to 0.1M NaCl electrolyte. The closed symbols are the impedance curves. The open symbols are the phase angle curves. Circles - initial curve, squares - 70 days exposure, triangles - 85 days exposure, upside down triangles - 95 days exposure.

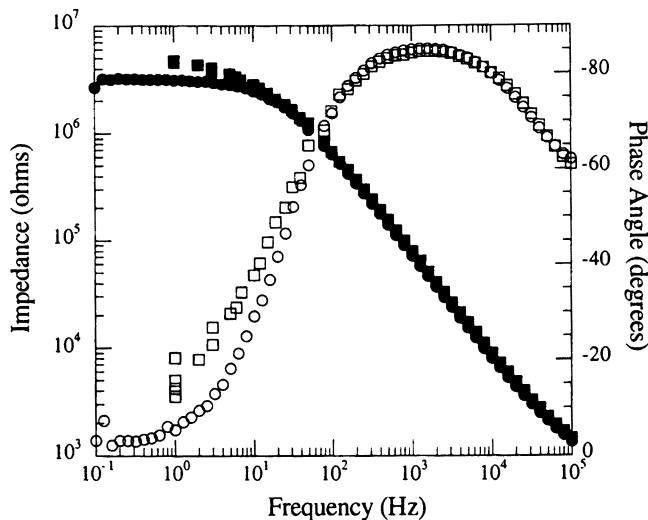


Figure 3. Bode plots for data obtained for an iron sample coated with SQPU-1 and exposed to substitute ocean water. The closed symbols are the impedance curves. The open symbols are the phase angle curves. Circles - initial curve, squares - 40 days exposure.

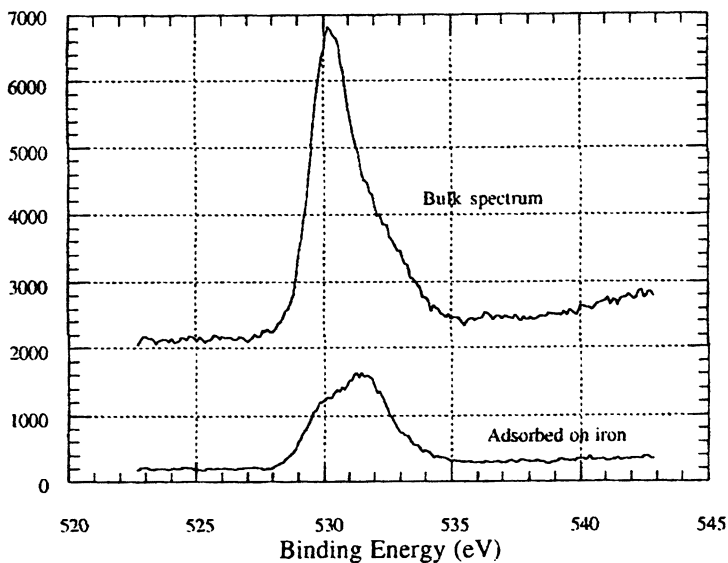


Figure 4. Oxygen 1s XPS for SQM-1.

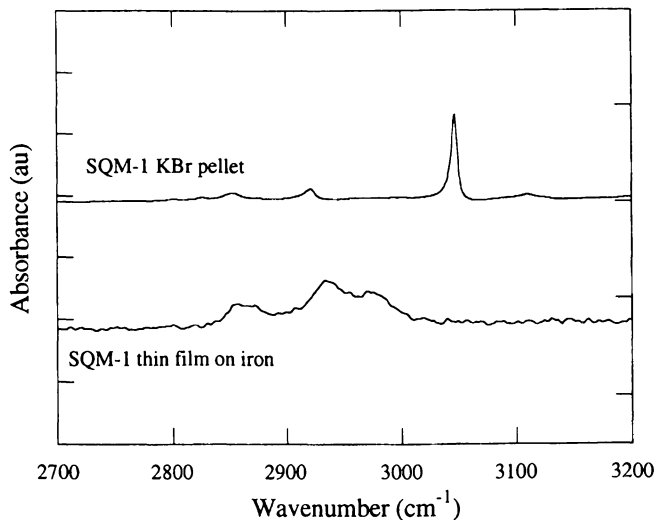


Figure 5. Reflectance infrared spectrum for SQM-1. Spectra recorded in the C-H stretching region.

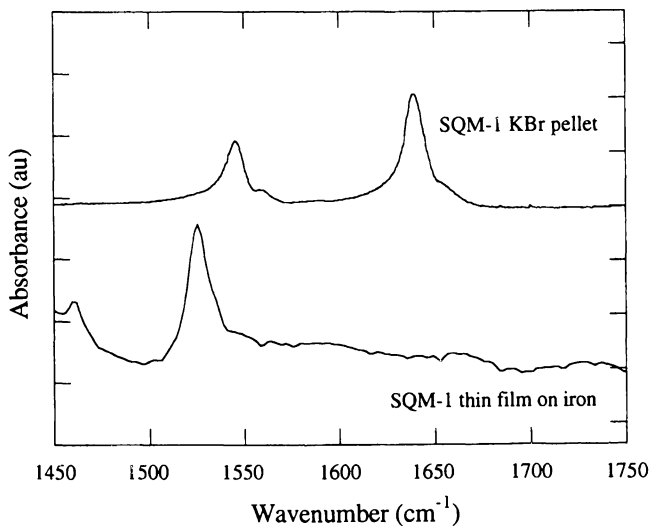


Figure 6. Reflectance infrared spectra for SQM-1. Spectra recorded in the C=O stretching region.

Conclusions

SQPU polymers were good candidates for the protection of metal corrosion. Sulfur-quinone functional groups in SQPU polymers provided a high affinity for the iron surface by forming coordinate bonds. The adhesive bond was so strong that it can not be broken by water. This interfered with the ability of water to adsorb to the iron surface and form an electrolyte, effectively inhibiting down corrosion.

Acknowledgments

This work was supported by the sponsors of the Center for Materials for Information Technology. Y. Hu was supported by the School of Graduate Studies by a Graduate Council Fellowship. D. Yang was supported by the NSF Materials Research Science and Engineering Center award DMR-9809423. The MRSEC also provided shared user instrumentation. The x-ray photoelectron spectrometer was purchased under the NSF Academic Research Infrastructure award DMR-9512264.

References

- (1) Kaleem, K.; Chertok, F.; Erhan, S. *Prog. Organ. Coatings* **1987**, *15*, 63-71, Nithianandam, V. S.; Erhan, S. *J. Appl. Polym. Sci.* **1991**, *42*, 2387-2389, Nithianandam, V. S.; Erhan, S. *Polymer* **1991**, *32*, 114, Kaleem, K.; Chertok, F.; Erhan, S. *J. Polym. Sci, Pt A, Polym. Chem.* **1989**, *27*, 865-871, Nithianandam, V. S.; Chertok, F.; Erhan, S. *J. Appl. Polym. Sci.* **1991**, *42*, 2899-2901, Nithianandam, V. S.; Kaleem, K.; Chertok, F.; Erhan, S. *J. Appl. Polym. Chem.* **1991**, *42*, 2893-2897, Reddy, T. A.; Erhan, S. *J. Polym. Sci, Pt A, Polym. Chem.* **1994**, *32*, 557-565.
- (2) Nithianandam, V. S.; Chertok, F.; Erhan, S. *J. Coating Technol.* **1991**, *63*, 47-49.
- (3) Nikles, D. E.; Liang, J.-L.; Cain, J. L.; Chacko, A. P.; Webb, R. I.; Belmore, K. *J. Polym. Sci., Pt. A.: Polym. Chem.* **1995**, *33*, 2881-2886.
- (4) Liang, J.-L.; Nikles, D. E. *IEEE Trans. Magnetics* **1993**, *29*(6), 3649-3651, Nikles, D. E.; Cain, J. L.; Chacko, A. P.; Webb, R. I. *IEEE Trans. Magnetics* **1994**, *30*(6), 4068-4070.
- (5) Vaideeswaran, K.; Bell, J. P.; Nikles, D. E. *J. Adhes. Sci. Technol.* **1999**, *13*(4), 477-499.
- (6) Hu, Y.; Nikles, D. E. *J. Polym. Sci., Pt A, Polym. Chem.* **2000**, *38*(18), 3278-3283.
- (7) ASTM Standard D1141-86, Substitute Ocean Water (1986).
- (8) Warren, G. W.; Sharma, R.; Nikles, D. E.; Hu, Y.; Street, S. Materials Research Society Proceedings, Volume 517, 439-444, 1998., Warren, G. W.; Sharma, R.; Hu, Y.; Nikles, D. E.; Street, S. *J. Magn. Magn. .Mat.* **1999**, *193*, 276-278.

Chapter 11

Amine–Quinone Polyimides for Protecting Iron against Corrosion

Mijeong Han^{1,3}, Huimin Bie^{2,3}, David E. Nikles^{1,3,*},
and G. W. Warren^{1,3,*}

Departments of ¹Chemistry and ²Metallurgical Materials Engineering and
³Center for Materials for Information Technology, The University of
Alabama, Tuscaloosa, AL 35487–0209

*Corresponding author: Email: dnikles@mint.ua.edu

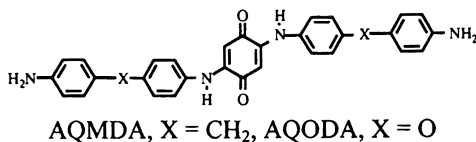
Two dianiline monomers, 2,5-bis (4,4'-methylenedianiline)-1,4-benzoquinone (AQMDA) and 2,5-bis (4,4'-oxydianiline)-1,4-benzoquinone (AQODA), were prepared by condensing 1,4-benzoquinone and 4,4'-methylenedianiline and by 1,4-benzoquinone and 4,4'-oxydianiline, respectively, via Michael addition. The monomers were condensed with 3,3',4,4'-benzophenone tetracarboxylic dianhydride (BTDA) or 3,3',4,4'-hexafluoroisopropylidene tetracarboxylic dianhydride (6FDA) to give polyamic acids. The polyamic acids were soluble in NMP and films were cast onto glass or iron squares. The films were thermally imidized at 290°C to give the corresponding polyimides. The amine-quinone polyimides had thermal decomposition temperatures greater than 440°C and glass transitions in the range 279 to 310°C. The tensile strength for the amine-quinone polyimides was in the range 92 to 166 MPa and the modulus was in the range 0.9 to 1.5 GPa. The amine-quinone polyimide made from AQMDA and BTDA protected iron against corrosion by aqueous sodium chloride electrolyte.

Introduction

Polymers containing the 2,5-diamino-1,4-benzoquinone functional group have been of interest, since this class polymers has a strong affinity for the surface of iron and can protect iron against corrosion.^{1,2}

Nikles' group has synthesized amine-quinone polyurethanes by condensing an amine-quinone diol monomer and an oligomeric diol monomer (e.g., polytetrahydrofuran diol) with a diisocyanate (e.g., TDI).³⁻⁵ These polyurethanes were shown to inhibit corrosion of the commercial iron particles used in state-of-the-art metal particle tape.^{6,7} Electrochemical impedance spectroscopy showed that amine-quinone polyurethanes protect iron against corrosion by providing a strong adhesive bond that could not be broken by water.⁸⁻¹¹ Amine-quinone polyurethanes also promote the adhesion of epoxy to steel.¹²

In this study, we report the synthesis of new aromatic diamine monomers and the preparation of amine-quinone polyimides containing these monomers. Our objective was to demonstrate whether we could combine the high temperature properties inherent with polyimides with the corrosion protection of metal afforded by the amine-quinone functional group.



Monomer and Polymer Synthesis

2,5-Bis (4,4'-methylenedianiline)-1,4-benzoquinone (AQMDA) and 2,5-bis (4,4'-oxydianiline)-1,4-benzoquinone (AQODA) were prepared by condensing 1,4-benzoquinone and 4,4'-methylenedianiline (MDA) and by 1,4-benzoquinone and 4,4'-oxydianiline (ODA), respectively, via Michael addition. Oxygen was bubbled into the reaction mixture during the reaction as an oxidizing agent and ethanol was the solvent. In the case of AQODA, ODA was not very soluble in ethanol at room temperature and the solution was warmed up to 40-50°C to complete dissolution. Both compounds precipitated from the reaction mixture and brown solids were collected by filtering. The compounds were purified by washing with fresh methanol several times, recrystallized from ethanol and dried at 50°C under vacuum. The structures of the monomers were confirmed by means of ¹H-NMR, ¹³C-NMR and high-resolution mass spectroscopy.

Amine-quinone polyimides were prepared by a two-step polymerization of amine-quinone monomers (AQMDA or AQODA) and aromatic dianhydrides, either 3,3',4,4'-benzophenone tetracarboxylic dianhydride (BTDA) or 3,3',4,4'-hexafluoroisopropylidene tetracarboxylic dianhydride (6FDA) in N-methyl-2-pyrrolidinone (NMP), **Table I**. The solid contents (weight % of monomers) were varied from 5 to 12 weight percent depending on the solubility of the

polyamic acids. The polyamic acid from AQODA and 6FDA could not be obtained because it always made a gel. When AQODA was used as a monomer, the amount of solvent was increased to avoid making a gel. We do not know why AQODA needed more solvent.

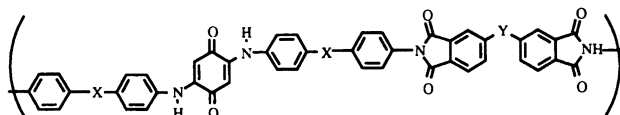


Figure 1. Amine-quinone polyimides, where X is CH_2 or O and Y is $\text{C}=\text{O}$ or $\text{C}(\text{CF}_3)_2$.

Table I. Composition of the polyimides

Polymer	Monomers	Molar Ratio	Solids (wt%)
PI	MDA, BTDA	1 : 1	10
AQPI-2	AQMDA, BTDA	1 : 1	10
AQPI-3	AQMDA, 6FDA	1 : 1	10
AQPI-4	AQODA, BTDA	1 : 1	8
AQPI-5	AQODA, 6FDA	1 : 1	—*
AQPI-6	AQMDA, MDA, BTDA	0.5 : 0.5 : 1	10
AQPI-7	AQMDA, MDA, 6FDA	0.5 : 0.5 : 1	10
AQPI-8	AQODA, ODA, BTDA	0.5 : 0.5 : 1	10
AQPI-9	AQODA, ODA, 6FDA	0.5 : 0.5 : 1	5

*AQPI-5 could not be prepared because polyamic acid from AQODA and 6FDA was always obtained as a gel.

For the coatings on iron squares, the amine-quinone polyamic acids were prepared with higher solid contents (12 wt%) to obtain thicker coatings on the iron squares. The double-coated films had a thickness of 12 μm .

For the comparison studies on corrosion protection, a conventional polyimide was made from MDA and BTDA. The polyamic acid was double-coated coated on iron squares. The coatings were dried and imidized by exactly the same method as AQPI. The thickness of the coating was 12 μm .

The coatings were thermally imidized under nitrogen by successive heating at 50 $^\circ\text{C}$ for one hour, then at 150 $^\circ\text{C}$ for one hour, then at 250 $^\circ\text{C}$ for one hour, and finally at 290 $^\circ\text{C}$ for one hour. All polyimides gave tough, flexible free-standing films. The IR spectrum of AQPI-2 showed

Table II. Thermal Properties

<i>Polymer</i>	$T_{5\%}$ ($^{\circ}\text{C}$) ^a	$T_{10\%}$ ($^{\circ}\text{C}$) ^a	<i>Char yield (%)</i> ^b	T_g ($^{\circ}\text{C}$)
PI	525	554	61.8	282
AQPI-2	472	551	69.0	292
AQPI-3	448	536	62.5	286
AQPI-4	455	530	67.6	280
AQPI-6	440	538	64.2	289
AQPI-7	453	538	59.8	279
AQPI-8	479	557	62.8	296
AQPI-9	474	514	58.0	310

^a Temperature at which 5 or 10 % weight loss was recorded by means of thermogravimetric analysis at a heating rate of 10°C/min in nitrogen.

^b Residual weight % at 800°C in nitrogen.

Table III. Tensile Properties

<i>Polymer</i>	<i>Modulus</i> (<i>GPa</i>)	<i>Strength</i> (<i>MPa</i>)	<i>Elongation at break (%)</i>
PI	1.5	169	19.3
AQPI-2	1.1	140	24.4
AQPI-3	1.1	146	24.6
AQPI-4	0.9	92	16.4
AQPI-6	1.0	131	21.6
AQPI-7	1.3	133	13.5
AQPI-8	1.5	166	16.5
AQPI-9	1.2	138	18.3

characteristic imide absorption bands at 1778 and 1722 cm^{-1} (C=O), 1374 cm^{-1} (C-N), and 725 cm^{-1} (imide ring).

Thermal and Mechanical Properties

The relative thermal stability of amine-quinone polyimides were compared by the temperature of 5 and 10 % weight loss ($T_{5\%}$ and $T_{10\%}$) and percent char yield at 800°C. Table II lists the TGA data for the polyimides. All amine-quinone polyimides showed the excellent thermal stability one would expect for polyimides. The polymers exhibited $T_{5\%}$ ranging from 440 to 479°C and $T_{10\%}$ ranging between 514 and 557°C in nitrogen, and the char yields at 800°C ranged between 60 and 69 %. There was no dependence of thermal stability on the monomers used and all amine-quinone polyimides showed excellent thermal stability in high temperature.

Most of these polyimides gave transparent, flexible and tough films suitable for the measurements of tensile properties and they are summarized in **table III**. Only AQPI-5 could not make free standing film because the polyamic acid was obtained as a gel. In the case of

AQPI-4, the film was not very uniform and gave poor mechanical properties. Tensile modulus was between 0.9 and 1.5 GPa and tensile strengths were ranged from 92 to 166 MPa. All polymer films behaved as ductile materials with good modulus and high strength with moderate elongation at break.

Corrosion Studies

The coated iron squares were exposed to 0.1 M NaCl electrolyte. The degradation of the polymer coating was monitored by EIS. The results are shown in Fig. 2 and 3. These are Bode plots consisting of impedance and phase angle as a function of frequency. The initial plot was taken after five minutes exposure to 0.1 M NaCl aqueous solution.

In Fig. 2, the initial Bode plots for the PI film (12 μm thick) on iron showed an impedance of $3.9 \times 10^5 \Omega$ at low frequency. Values of phase angle were less than the -90° and implied that the polymer film was behaving as a dielectric. After two days exposure, the impedance decreased to $2 \times 10^3 \Omega$. A second time constant was appeared at low frequency in the phase angle curve, which has been attributed to a double layer capacitance. The electrolyte had diffused through the polymer and broke the adhesive bond between the polymer and iron. The appearance of the second time constant in phase angle was regarded as the beginning of the failure of the coating, and pitting corrosion was observed soon thereafter.

The iron samples coated with amine-quinone polyimides showed a different behavior after exposure to NaCl electrolyte. Fig. 3 shows Bode plots of an iron sample with double coating of AQPI-2, 12 μm thickness. The initial impedance was $6.02 \times 10^8 \Omega$ and the phase angle was -90° over a wide range of frequencies. After 2 days and 34 days exposure, there was very little change in the impedance spectra. The impedance remained in the range of $10^8 \Omega$ and the phase angle was almost identical to that of initial curve. The adhesion bond between the amine-quinone polyimide and iron surface was strong enough to resist attack by NaCl electrolyte. These experiments will be continued until we observe failure in the coatings.

Conclusions

Amine-quinone polyimides have the excellent thermal stability and tensile properties, one expects from polyimides. They are insoluble, suggesting good chemical resistance. These polymers also show an ability to protect iron against corrosion by NaCl electrolyte, similar to that we have reported for amine-quinone polyimides.

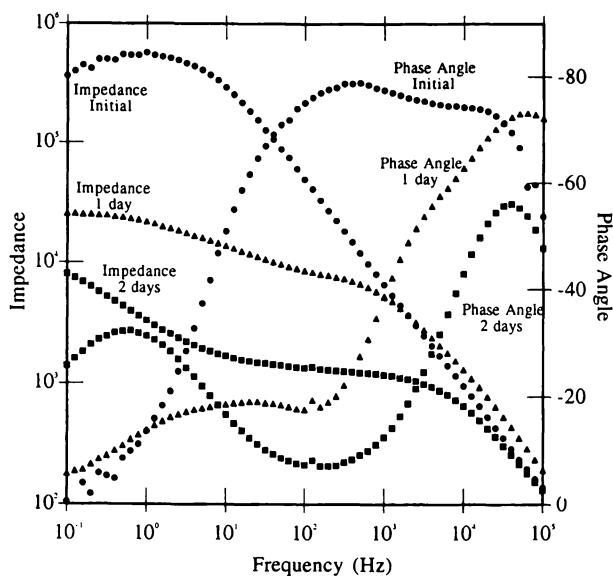


Figure 2. Bode plots for the conventional polyimide (PI) coated on a iron square. The circles are the initial impedance and phase angle curves. The triangles are after 1 day exposure to 0.1 M NaCl. The squares are after 2 days exposure.

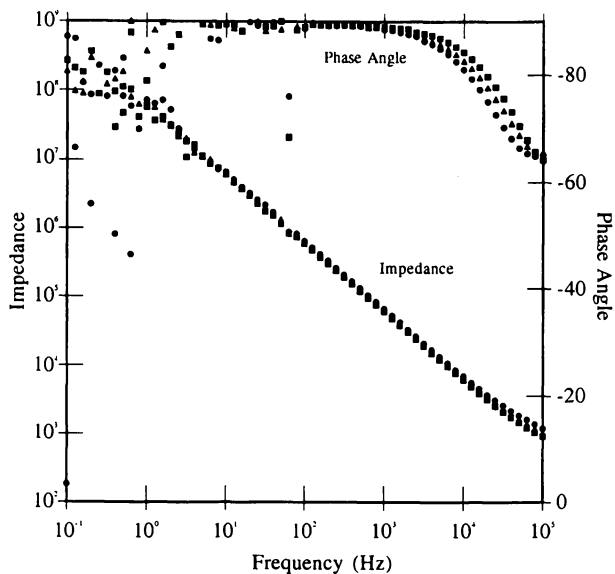


Figure 3. Bode plots for the amine-quinone polyimide (AQPI-2) coated on a iron square. The circles are the initial impedance and phase angle curves. The triangles are after 2 days exposure to 0.1 M NaCl. The squares are after 34 days exposure.

Acknowledgments

M. Han was supported by the School of Graduate Studies by a Graduate Council Fellowship.

References

1. Kaleem, K.; Chertok, F.; Erhan, S., *Prog. Organ. Coatings*, **1987**, 15, 63-71.
2. Nithianandam, V.S.; Chertok, F.; Erhan, S., *J. Coating Technol.*, **1991**, 63, 47-49.
3. Nikles, D.E.; Liang, J.-L.; Cain, J.L.; Chacko, A.P.; Webb, R.I.; Belmore, K., *J. Polym. Sci., Pt A, Polym. Chem.*, **1995**, 33, 2881-2886.
4. Nikles, D. E.; Warren, G. W. *Polymer News* **1998**, 23, 223-231.
5. Nikles, D. E.; Chacko, A. P.; Liang, J.-L.; Webb, R. I. *J. Polym. Sci., Pt. A: Polym. Chem.* **1999**, 37, 2339-2345.
6. Liang, J.-L.; Nikles, D. E. *IEEE Trans. Magnetics* **1993**, 29(6), 3649-3651.
7. Chacko, A. P.; Nikles, D. E. *J. Appl. Phys.* **1996**, 79(8), 4863-4865.
8. Arroyo, J.C.; Warren, G.W.; Nikles, D.E., *NIST-IR. 5960, Proceedings 6th Int'l Workshop on Moisture in Microelectronics*, Gaithersburg, MD **1996**
9. Sharma, R.; Warren, G.W.; Nikles, D.E.; Hu, Y.; Street, S.C., *Mat. Res. Soc. Symp. Proc.* **1998**, 517, 439-444.
10. Warren, G. W.; Sharma, R.; Hu, Y.; Nikles, D. E.; Street, S. *J. Magn. Magn. Mat.* **1999**, 193, 276-278.
11. Han, M.; Helms, A. B.; Hu, Y.; Nikles, D. E.; Nikles, J. A.; Sharma, R.; Street, S. C.; Warren, G. W. *IEEE Trans. Magnetics* **1999**, 35(5), 2763-2765.
12. Vaideeswaran, K.; Bell, J. P.; Nikles, D. E. *J. Adhes. Sci. Technol.* **1999**, 13(4), 477-499.

Chapter 12

Lignosulfonic Acid-Doped Polyaniline (LIGNO-PANI™) for the Corrosion Prevention of Cold-Rolled Steel

B. C. Berry, A. U. Shaikh, and T. Viswanathan

**Department of Chemistry, University of Arkansas at Little Rock,
2801 South University Avenue, Little Rock, AR 72204**

Lignosulfonic acid-doped polyaniline (LIGNO-PANI™) was shown to significantly reduce corrosion on cold rolled steel samples. Steel coupons coated with LIGNO-PANI™ mixed with a water-reducible resin were exposed to a 3.55% NaCl solution over a period of time. Results from electrochemical corrosion tests in the form of linear polarization, Tafel plots, as well as Electrochemical Impedance Spectroscopy (EIS) were performed. These tests indicate a 10-20 fold improvement in corrosion protection for the samples containing as little as 1-2% LIGNO-PANI™. Experiments were also performed on coatings containing 5 & 10 % LIGNO-PANI™. These experiments showed an increased rate of corrosion that is likely due to inadequate cross-linking of the coating caused by the addition of the larger percentages of LIGNO-PANI™. Samples containing LIGNO-PANI™ and an active metal such as aluminum were studied and found to further inhibit the corrosion process on the steel coupons.

Introduction

Polyaniline is an intrinsically conductive polymer (ICP) that has the potential to be used in a number of applications (1) including corrosion prevention. Corrosion costs the U.S. economy 4% of the gross national product (GNP) or approximately 220 billion dollars each year (2). It has been found that ICPs, such as polyaniline, can inhibit corrosion when applied to a metal surface. Conventional polyaniline, however, is limited by its processibility (3). Emeraldine base, the non-protonated, non-conducting form of polyaniline has only limited solubility in organic solvents such as NMP, N,N-dimethylacetamide, and dimethyl formamide. The doped conducting form, emeraldine salt, is insoluble in all common organic solvents. This inhibits the ability to blend the conducting polymer easily with resins which in turn limits the possibility of using polyaniline to prevent corrosion.

The emeraldine base form of polyaniline has also received considerable amount of attention as an alternative to the emeraldine salt form as a corrosion inhibitor of iron and steel (4). Research has also been conducted which indicates that the base form also protects aluminum from corrosion (5). The base form, however, still requires the use of organic solvents for dispersion. This limits the use of the base form in real life application to organic coating systems which are steadily being spotlighted by the EPA as environmentally detrimental materials and has lead to increasing restriction on VOC content.

Several methods for improving the processibility of conducting polyanilines have been developed (6). The most common of these is the use of acids which generate soluble counter-ions upon doping the non-conducting or base form of the polymer. A variety of sulfonic acids have been used as dopants due to the increased solubility of the sulfonate counter-ion. LIGNO-PANITM is one such polyaniline that is dispersible in water and soluble in polar aprotic solvents such as DMSO and NMP in its conducting state due to the high solubility of the lignosulfonic acid incorporated as a dopant (7).

Lignin is the major non-cellulosic constituent of wood. It is a polyphenolic compound with superficial resemblance to phenol formaldehyde resins. Lignosulfonate is a waste product from the paper pulping process. Essentially, all of the lignosulfonates commercially available are isolated as byproducts from the paper industry from either the sulfite or the Kraft process. The estimated annual production of lignins by these two methods alone is 21.5 million tons in the U.S. annually (8). The use of this renewable resource provides not only increased processibility but reduced cost as well.

Lignosulfonates are obtained either as spent sulfite liquor (SSL) or by sulfonation of lignin in the Kraft process. SSL obtained from the sulfite process consists of lignosulfonates (~55%), sugars (30%, monosaccharides) and other ingredients in smaller amounts. Figure 1 shows a typical monomeric unit of Kraft

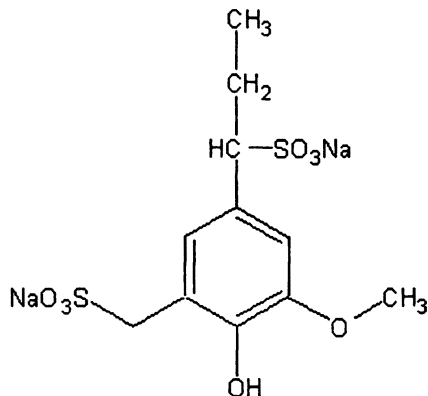


Figure 1: Lignin monomer unit after sulfomethylation via the Kraft process.

lignin that has been sulfomethylated at the aromatic ring and sulfonated on the aliphatic side chain. The aliphatic sulfonation occurs preferentially in the alpha position of the side chain of the phenylpropane units.

The functionality of the lignosulfonate provides an advantage over conventional dopants in that spectroscopic evidence has shown the dopant to be very tightly bound or possibly grafted to the polyaniline chains (9). LIGNO-PANI™ has been shown to retain its redox activity above pH 8 (10) due to the continual presence of the dopant, where as HCl-PANI has been shown to lose its redox capability above pH 5-7. Additionally, the lignosulfonic acid can be permanently cross-linked into the resin with which LIGNO-PANI™ is blended. This prevents the dopant from being leached away from the polymer even in basic environments such as seawater.

There has been much research into corrosion inhibition using polyaniline. The most probable mechanism proposed is the transfer of electrons from the metal surface to the conductive polymer (11). This redox process forms a passive oxide layer on the surface of the metal that inhibits further corrosion. This oxide layer is unlike natural rust that flakes off exposing more metal to oxidation. This oxide has been shown to be a layer of Fe₃O₄ coated with a very compact layer of Fe₂O₃ that remains intact (12). The ICP can continue to prevent corrosion and repair defects in the metal surface as long as it remains redox active. Although corrosion protection by an ICP is believed to be anodic (i.e.

passivation of the anode which inhibits the corrosion process), combining a more active metal with the ICP and coating it on the metal surface may also produce cathodic protection which is more commonly referred to as sacrificial protection (13). With increasing restrictions by the EPA on volatile organic compounds (VOCs), chromates, and other heavy metal conversion coatings, alternative additives for corrosion inhibition which can be dispersed in water based coatings are of increasing importance (14).

Experimental

Preparation of LIGNO-PANITM

LIGNO-PANITM was prepared by dissolving 1.00 g of sulfonated lignin, REAX 825E obtained from Westvaco, in a minimal amount of distilled water. This solution was then passed through a column packed with Dowex 50WX8-40 strongly acidic cation exchange resin. The solution was then diluted to a volume of 34 mL with distilled water. A 1.00 mL aliquot of aniline was then added to the solution. The temperature was reduced to 0° C while stirring. To the solution, 1.92 g of sodium persulfate was added. The solution was stirred at 0° C for 4 hrs. The solution was removed and centrifuged twice with washing by distilled water to remove all excess lignosulfonate and salts. The wet cake was then stored at 0° C until use. A new method of synthesis has also been developed independently that allows the polymer to be filtered easily and eliminates the need for the cation exchange resin. The conductivity of this polymer was found to be between 1 and 5 S/cm with significant dispersibility in water. Conductivity values were obtained for compressed pellets using an Alessi four-point conductivity probe.

Coating Preparation

For this study, a series of coatings consisting of a water-based acrylic resin containing different concentrations of LIGNO-PANITM were prepared. These coatings were prepared by mixing an acrylic resin obtained from McWhorter (Acrylamac WR 232-3312) with a melamine formaldehyde resin obtained from Monsanto [Resimene (HMM 747)] and diethylethanolamine to produce a water reducible system. LIGNO-PANITM was dispersed into this resin without the need for a high shear dispersing mechanism. The final compositions contained 1, 2, 5,

and 10 percent LIGNO-PANITM. The panels were thermally cured in an oven for recommended time and temperature. A wet cake of inhibited aluminum was obtained from Silberline (Aquasil BP SN inhibited aluminum pigment) and dispersed into the above resin containing 1% LIGNO-PANITM with the following Al compositions: 0, 0.5%, 10%, and 20 %. The coatings were applied to cold rolled steel (CRS) coupons purchased from Q-panel (SAE 1010 type QD). These coupons were washed with acetone, methanol, and water prior to coating. An airbrush was used to obtain a coating of uniform composition and thickness. The dry film thickness of the coatings was measured using a screw caliper to be approximately 1-2 mils.

Electrochemical studies

Cyclic voltammograms were obtained using a PAR 283 potentiostat with Power CV software. The experiments were performed in a 50 ml cell after purging with nitrogen, at varying scan rates in aqueous solutions of differing pHs. Electrochemical corrosion measurements were also performed using a PAR 283 potentiostat. SoftCorrIII corrosion measurement software was used to generate Tafel plots, linear polarization curves, and cyclic polarization curves. A PAR 5210 lock-in amplifier was used in conjunction with the potentiostat to perform electrochemical impedance spectroscopy (EIS) measurements. Electrochemistry Powersuite software was used to generate plots and manipulate the data. Coupons were tested in a conventional flat cell with a platinum counter electrode and a saturated calomel reference electrode. The electrolyte which also served as the corrosive media was 3.55% NaCl. The exposure area was 1 cm². Coupons were exposed on one side in a container filled with 3.55% NaCl. The plates were removed periodically and placed in the flat cell for testing.

Salt Fog Studies

Salt fog studies were performed on plates containing a proprietary amount of CatizeTM dispersed in a water-based acrylic resin (Rustoleum 5281). Coating preparation as well as salt fog testing was performed by GeoTech Chemical Company, Tallmadge, Ohio. Coating thickness was determined to be approximately 2-3 mils. The panels were scribed and exposed for varying amounts of time to a continuous salt spray according to ASTM B-117 in a salt fog chamber (Singleton Corp. Model # 20-22).

Results and Discussion

Even though dispersions of doped polyaniline are available, none are inexpensive and easily dispersed additives which limits the applicability. LIGNO-PANITM, however, can be dispersed in both organic and water-based systems. Although dispersibility is an important issue, it is also important that the polymer be redox active at a value more positive than that of steel. Figure 2 is a cyclic voltammogram indicating that LIGNO-PANITM has a redox

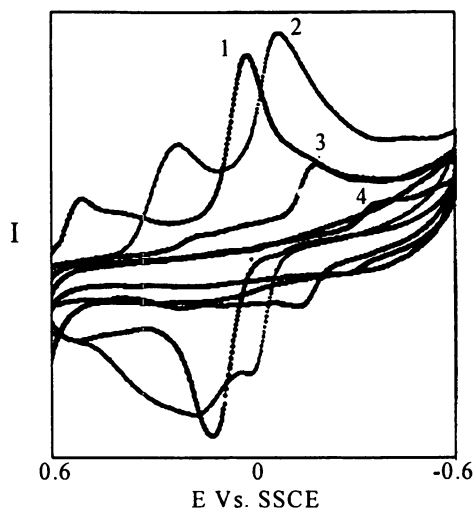


Figure 2. Cyclic Voltammogram of LIGNO-PANITM in water at pH values of 1) 2.00, 2) 4.00, 3) 6.00, and 4) 8.00. (Reproduced with permission from reference 15. Copyright 2002 Kluwer Publishers.)

potential more positive than that of iron indicating that the oxidation of the metal surface by the ICP will occur spontaneously. The voltammogram also indicates that LIGNO-PANITM can remain redox active well into the basic region. This increased pH range at which the polymer is redox active is believed to be due to the sulfonic acids which are tightly bound or grafted to the polymer.

The steel coupons were tested before exposure and at intervals over a period of 20 days or more during exposure. This allowed sufficient time for the corrosion rate to reach equilibrium. From the initial results, it appears that LIGNO-PANITM inhibits corrosion by passivating the metal surface. The plates

containing 1% LIGNO-PANITM show a more noble, i.e. more positive, open circuit potential (OCP) than the water-based coatings alone. Figure 3 shows the

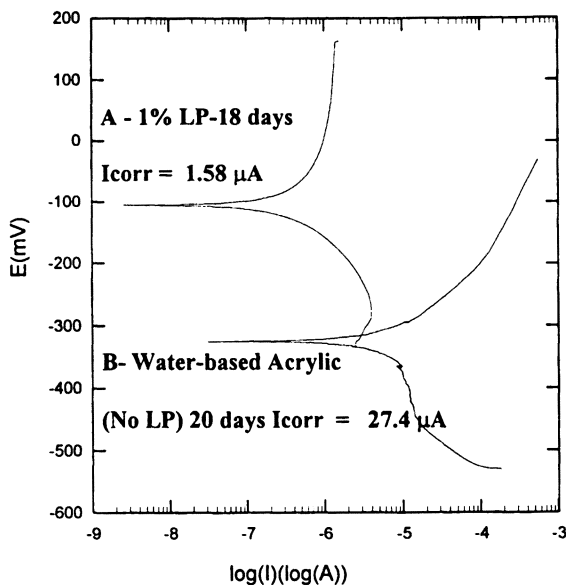


Figure 3. Tafel plots of a water based-acrylic coating containing 1% LIGNO-PANITM and of a water-based acrylic containing no LIGNO-PANITM. The Tafel plot of the coating containing 1% LIGNO-PANITM shows a more noble potential and a lower corrosion current (Reproduced with permission from reference 15. Copyright 2002 Kluwer Publishers.)

Tafel plots of the steel coupons coated with the acrylic resin containing LIGNO-PANITM (A) as well as steel coated with only the water-based acrylic resin (B). As seen, the LIGNO-PANITM containing coating exhibits not only a significant shift to a higher OCP, but to a lower corrosion current which translates into a lower corrosion rate. The corrosion currents for A and B were 1.58 μA and 27.4 μA respectively. This lower corrosion rate as well as the increased OCP indicates that the passive oxide layer is probably inhibiting the electron transfer between the electrolyte and the metal. The branches of the anodic branches of the Tafel plots in figure 3 seem to also indicate a passivation mechanism. When the slope of the anodic branch is less than that of the cathodic branch, it can be said that the corrosion process is anodically controlled indicating that the oxidation process is occurring readily (9). This can be seen for the Tafel plot of the steel plate coated only with the water-based acrylic resin. If, however, the slope of the cathodic branch is less than that of the anodic branch, as in figure 3,

it can be said that the corrosion process is cathodically controlled. This indicates that the anodic process is no longer the determining factor in the corrosion rate. This difference can possibly be attributed to the formation of an oxide layer which impedes further oxidation processes.

EIS results also confirm that LIGNO-PANITM significantly reduces the corrosion rate. EIS results show an increase in impedance indicating a less active double layer and therefore a lower corrosion rate. Figure 4 is a Nyquist plot for

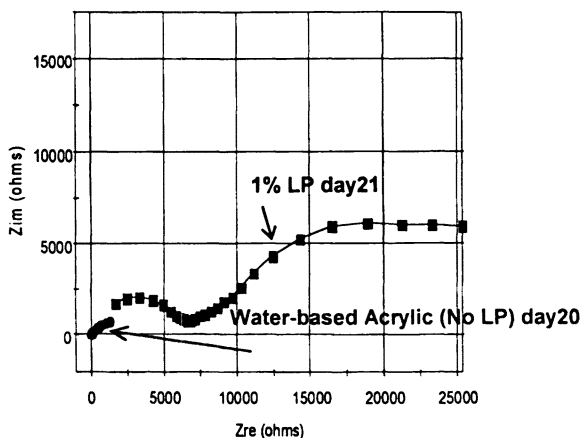


Figure 4. Nyquist plots generated using EIS for the coatings containing 1% LIGNO-PANITM and 0% LIGNO-PANITM (Reproduced with permission from reference 15. Copyright 2002 KluwerPublishers.)

the water-based acrylic coating containing LIGNO-PANITM and the water-based acrylic coating containing no LIGNO-PANITM. As the figure indicates, the impedance for the control is significantly lower which results in a lower corrosion rate. Indications of a third time constant can also be seen in Bode plots (not shown) for the LIGNO-PANITM containing plate. A third time constant was occasionally observed at very low frequencies. This time constant was difficult to study due to the low frequencies and the extended time needed to perform these tests. Low frequency testing resulted in long test times during which the electrode inevitably changed leading to inconsistencies in the data. It is believed, however, that this third time constant is actually the time constant for the double layer. The second time constant would therefore most likely be due to an oxide layer that is formed by the LIGNO-PANITM. This lends further evidence to the theory of a passive oxide layer formation.

Coupons coated with higher concentrations of LIGNO-PANITM were also evaluated. The 2% LIGNO-PANITM coating performed almost as well as the 1% coating showing a reduction of 10-20 fold in the corrosion current. Another interesting phenomenon was observed with coatings containing 2% LIGNO-PANITM. Overlaid Nyquist plots in Figure 5 indicate a “correction” behavior for

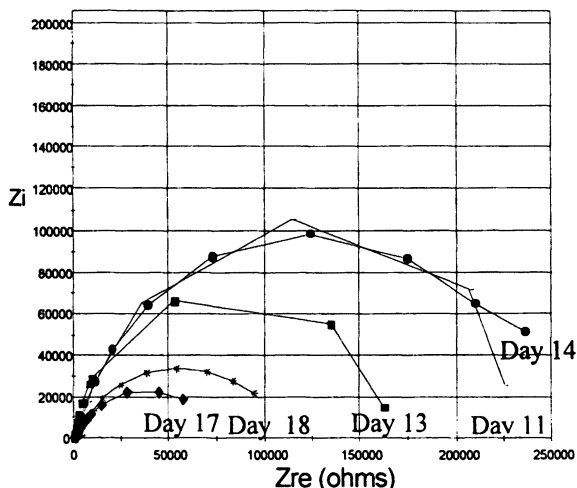


Figure 5. Nyquist plot for 1% LIGNO-PANITM in a water-reducible acrylic coating over a period of time indicating a repassivation mechanism. (Reproduced with permission from reference 15. Copyright 2002 KluwerPublishers.)

LIGNO-PANITM. As exposure time increased, a decrease is observed in the impedance for all coatings. LIGNO-PANITM, however, shows a decrease in impedance followed by an increase a few days later. This occurs consistently possibly indicating that the oxide layer is being destroyed due to infiltration of the bulk solution and is then repassivated by LIGNO-PANITM. The extent of this repassivation, however, decreases with time indicating that with increasing failure of the coating, the dissolution of the oxide layer and eventually the metal surface becomes so rapid that the repassivating power of LIGNO-PANITM is no longer sufficient.

The results from the 5 and 10 percent coatings indicate that coating failure is accelerated by the incorporation of such a high percentage of LIGNO-PANITM. After 10 days both coatings showed significant signs of failure as well as increased corrosion currents. Leaching of the LIGNO-PANITM by the electrolyte was also observed. On both of the plates, a significant amount of green color was

observed on the backside of the plate as well as in the electrolyte solution. This indicates that the LIGNO-PANI™ was possibly not cross-linked sufficiently into the resin. When the LIGNO-PANI™ was leached out, open pores probably formed in the resin allowing corrosion to occur freely on the metal surface. Figure 6 contains the Tafel plots of the coatings containing 2, 5 and 10 percent

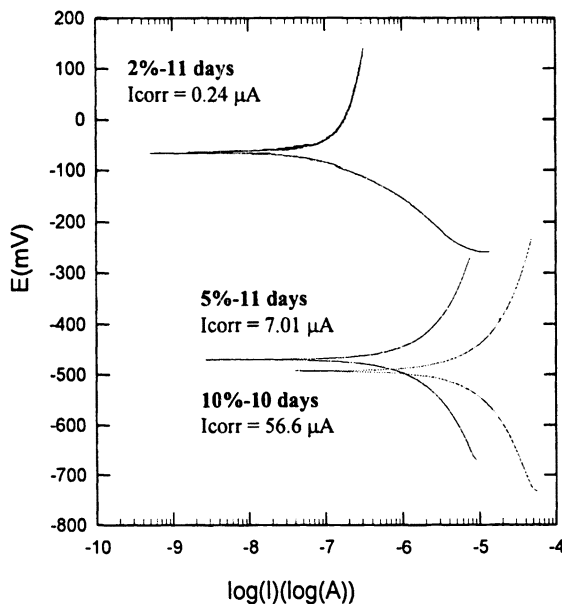


Figure 6. Tafel plots for coatings containing 2, 5, and 10% LIGNO-PANI™. (Reproduced with permission from reference 15. Copyright 2002 Kluwer Publishers.)

LIGNO-PANI™ approximately 10 days. The coatings with 5 and 10 percent LIGNO-PANI™ show a lower OCP as well as an increased corrosion current versus the one containing 2 percent LIGNO-PANI™. It is unclear as to whether the higher concentrations of LIGNO-PANI™ would be beneficial if it were fully cross-linked into the resin.

Experiments on coatings containing both LIGNO-PANI™ in combination with an inhibited form of aluminum have also been performed. These early experiments seem to indicate that the addition of aluminum into the coating has a beneficial result. Figure 7 contains Tafel plots of only the acrylic resin (A), the resin containing 1% LIGNO-PANI™ and 0.5% Al (B), resin containing 1% LIGNO-PANI™ and 10% Al (C), and resin containing 1% LIGNO-PANI™ and

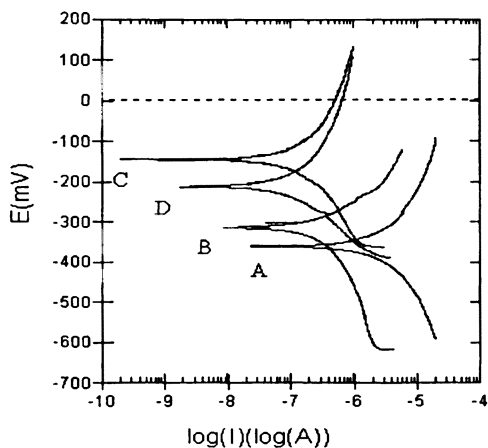


Figure 7. Tafel plots of only the acrylic resin (A), the resin containing 1% LIGNO-PANITM and 0.5% Al (B), resin containing 1% LIGNO-PANITM and 10% Al (C), and resin containing 1% LIGNO-PANITM and 20% Al (D). Corrosion protection is improved with increasing concentration of Aluminum. (Reproduced with permission from reference 15. Copyright 2002 KluwerPublishers.)

20% Al (D). The Tafel plots indicate a positive shift in the open circuit potential as well as a decrease in the corrosion current resulting in corrosion values of 4.45, 0.28, 0.18, 0.076 mpy respectively. Interestingly, values obtained early in the testing cycle indicated high corrosion rates for the aluminum containing samples. It may be possible that the instrument was actually reading the current from the oxidation of the aluminum on the surface of the coating. This is possible due to the bulk conductivity of the entire coating. After two days, however, the corrosion rate decreased to below that of the LIGNO-PANITM alone. To fully understand both the true corrosion rate as well as the mechanism, the scanning vibrating electrode technique (SVET) may be needed. This would provide information about the sacrificial nature of the coating.

Figure 8 is the result from salt fog data collected at 280 hours. The panel on the left is coated with only a water-based acrylic resin while the plate on the right is coated with a water-based coating containing CatizeTM which is a patented formulation containing a water-dispersible ICP (in this case LIGNO-PANITM) and a water-based inhibited aluminum (12). As shown, protection of the scribed area is evident for the CatizeTM coating. The exact method of protection is not yet fully understood. However, it would appear that there is some amount of cathodic protection based on the performance in the salt fog tests. Surface

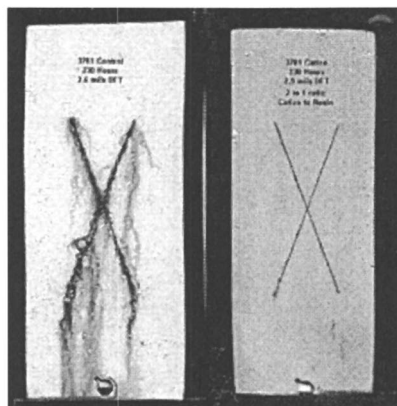


Figure 8. Salt fog of a scribed panel coated with only a water-based acrylic resin containing no Catize™ (left) and one containing a proprietary amount of Catize™ (right) after 230 hours exposure.

analysis may provide additional information about the identity of corrosion products at the scribe. If the process is truly sacrificial, the majority of the corrosion products at the scribe should be oxidized aluminum species. It is also possible that additional corrosion protection is afforded only by the added barrier properties of the aluminum oxide being formed by the oxidation of the inhibited aluminum by the conducting polymer.

Conclusions

The use of conducting polymers for the prevention of corrosion represents a substantial advancement in the corrosion field as well as in the area of conducting polymer field. The use of LIGNO-PANI™ as a corrosion preventing agent is of major industrial importance in that it is the first commercially mass produced water-borne conducting polymer in the United States. As with any industrial application, cost, processibility, applicability and performance are of substantial concern. LIGNO-PANI™ allays all these concerns. The processibility of LIGNO-PANI™ is enhanced due to the water dispersibility provided by the lignosulfonic acid dopant. The use of this renewable resource is economically and environmentally advantageous. Its applicability is augmented by the fact that it can be sold as an additive for organic as well as water-based systems and does not require any special means of blending. The efficacy of corrosion protection provided by LIGNO-PANI™ has also been demonstrated to

be significant. A decrease of 10-20 fold in the corrosion rate was observed. Additional corrosion protection, although the mechanism may be significantly different from that of ICPs, has been demonstrated with the addition of a more active metal such as aluminum. This development may be an improvement upon existing sacrificial coatings in that formulation is much easier due to the presence of an ICP which renders the matrix conductive.

Acknowledgements. We would like to thank NASA/KSC and NASA/EPSCoR for funding and GeoTech Chemical Inc., Tallmadge, OH for the salt fog data.

References

1. Kuhn, H. H., Child, A.D. *Chapter 35: Electrically Conducting Textiles in Handbook of Conducting Polymers*, Eds. Skotheim, Terje A.; Elsenbaumer, Ronald L.; Reynolds, J. R.; Marcel Dekker Inc.: New York, NY, 1998; p. 993.
2. Verink, E.D. *Chapter 2: Economics of Corrosion in Uhlig's Corrosion Handbook, 2nd Edition*, Ed. Revie, R.W. John Wiley & Sons Inc.: New York, NY, 2000; p. 11
3. Gregory, R.V. *Chapter 18: Solution Processing of Conductive Polymers: Fibers and Gels from Emeraldine Base Polyaniline in Handbook of Conducting Polymers*, Eds. Skotheim, Terje A.; Elsenbaumer, Ronald L.; Reynolds, J.R.; Marcel Dekker Inc.: New York: NY, 1998; p. 437.
4. Wei, Y; Wang, J; Jia, X.R.; Yeh, J.M.; Spellane, P. *Polymer*. **1995**, 36(23), 4535
5. Epstein, A.J.; Smallfield, J.A.O.; Guan, H; Fahlman, M. *Synthetic Metals*. **1999**, 102, 1374-1376
6. Sudhakar, M.; Stoecker, P.W.; Viswanathan, T. *Recent Res. Devel. In Polymer Science*. **1998**, 2, 173
7. Viswanathan, T., US Patent 6,059,999, 2000
8. Sudhakar, M.; Toland, A.D.; Viswanathan, T. *Chapter 6. Conducting Waterborne Lignosulfonic Acid-Doped Polyaniline in Semiconducting Polymers*. Eds. Hsieh, Bing R.; Wei, Yen; American Chemical Society: Washington: D.C., 1999; p. 76.
9. Berry, B.C.; Shaikh, A.U.; Viswanathan, T. *ACS Polymer Preprints*. **2000**, 41, 327.
10. Lu, Wei-Kang; Basak, S., Elsenbaumer, R.L.; *Chapter 31: Corrosion Inhibition of Metals by Conductive Polymers in Handbook of Conducting Polymers*, Eds. Skotheim, T.A.; Elsenbaumer, R.L.; Reynolds, J.R.; Marcel Dekker Inc.: New York: NY, 1998; p. 881.

11. Wessling, B.; Schröder, S.; Gleeson, S.; Merkle, S., Baron, F. *Materials and Corrosion*. **1996**. 439-445
12. Lu, W.K.; Elsenbaumer, R.; Wessling, B. *Synth. Met.* **1995**. 71. 2163-2166
13. Hawkins, T.R.; Geer, S.R., US Patent 5,976,419, 1999
14. "National Emissions Standards for Chromium Emissions from Hard and Decorative Chromium Electroplating and Chromium Anodizing Tanks. Environmental Protection Agency", *Federal Register*. January 25, 1995
15. Berry, B.C.; Viswanathan, T. *Chapter 2: Lignosulfonic Acid-doped Polyaniline (LIGNO-PANITM) – A Versatile Conducting Polymer in Chemical Modification, Properties and Uses of Lignin*; Ed. Hu, T.; Kluwer Academic Publishers; New York, NY; pp. 21-40

Chapter 13

Electroactive Polymer for Corrosion Inhibition of Aluminum Alloys

S. C. Yang¹, R. Brown², R. Racicot³, Y. Lin¹, and F. McClarnon¹

Departments of ¹Chemistry and ²Chemical Engineering,
University of Rhode Island, Kingston, RI 02881

³Department of Chemistry, United States Air Force Academy,
USAFA, CO 80840

Introduction

Corrosion is a significant problem for lightweight high-strength aluminum alloys that contain significant amount of copper. For example the AL2024-T3 alloy contains about 4.6% of copper in aluminum. The corrosion rate is high due to the inherent galvanic coupling between the copper-rich micro-domain in the alloy and the aluminum matrix. Although the current technology of chromate based primer and chromate surface conversion is effective for corrosion inhibition of aluminum alloys, the toxic hexavalent chromate species is a health hazard and an environmental problem.

DeBerry¹ first reported the use of a conducting polymer in corrosion inhibition of stainless steel in acidic environment. Other researchers reported the observation of corrosion inhibition of steel by polyaniline², corrosion inhibition of aluminum by polyaniline³, the corrosion inhibition of aluminum by the chemical derivatives of poly(phenylene vinylene)⁴.

A serious problem with the conventional polyaniline is its limited thermal and chemical stability. Dedoping by heat, water or solvent will convert polyaniline from the conductive state to the insulating state. We have

previously found that the insulating state is far less effective comparing to the conductive form for corrosion inhibition. It is desirable to develop an improved polyaniline that is not easily dedoped when exposed to ambient environment.

Another problem with the conventional conducting polymer is that it is difficult to disperse conducting polymers in a paint system. A typical molecular ion doped polyaniline is insoluble in water or solvents. High-energy mechanical dispersion method is presently used to disperse polyaniline in highly acidic primer paint. This dispersion method is not easily incorporated in ordinary paint formulation process. Although solvent dispersible polyaniline has been developed, the surfactant dopants (e.g. camphor sulfonic acid and nonyl-naphthalene sulfonic acid) used for this type of polyaniline still carries the liability of dedoping and the problem with thermal stability. It is desirable to design a modified polyaniline that is dispersed in water and has stable dedopants.

In this paper, we first describe the synthesis of a polymeric complex of polyaniline and a polymeric dopant. The resulting product is a water-borne polyaniline that is easy to be used in water-borne paint formulation. Having a stable polymeric dopant, this water-borne polyaniline has sufficient chemical and thermal stability for coatings applications.

In this paper we demonstrate that an observable improvement in corrosion inhibition is obtained when the water-borne polyaniline is used as an additive at a 1% concentration in conventional water-borne epoxy primer.

The inter-polymer complex of polyaniline

The inter-polymer complex of polyaniline and a poly acid is illustrated in figure 1. The polyaniline and the poly acid are non-covalently bonded in a side-by-side fashion and can be considered as a double-strand polymer. Examples of the poly anions are poly(acrylic acid), poly(styrenesulfonic acid), poly(methylvinylether-alt-maleic acid), etc.

The inter-polymer complexes were synthesized by a template-guided synthetic method⁵. Here, we use the synthesis of the polyaniline:poly(acrylic acid), or PAN:PAA, complex as an example to illustrate the synthetic strategy. When an aqueous solution of aniline and the poly(acrylic acid) is mixed, the aniline monomers bind to the poly(acrylic acid) backbone due to various intermolecular forces including hydrogen bonding and electrostatic attractions. After the solution of precursor adducts is acidified, the aniline is polymerized by

an oxidant such as sodium persulfate or hydrogen peroxide. The resulting product is a green colored solution.

Previous studies^{6, 7} established that the reaction product is a molecular complex between polyaniline and the polyacid. The polyaniline chain and the poly(acrylic acid) chain are bonded non-covalently in a side-by-side configuration.

A similar synthesis procedure was used to synthesize the inter-polymer complex of polyaniline and poly(vinylmethyether-alt-maleic acid), PAN:PVME-MLA. The resulting polymer is a stable dispersion of the conducting polymer in aqueous solution. The second strand, PAA, provided enough number of solvatable functional groups to maintain the complex as water dispersion. This property is highly useful for the application of polyaniline as a coating material.

The conductive state of the complex is stable in marine environment

Polyaniline doped with HCl undergoes deprotonation in aqueous solution with pH 4. Polyaniline doped with other non-polymeric, molecular anions (e.g. p-toluenesulfonic acid, camphor sulfonic acid) show the same tendency for deprotonation at pH 4. Accompanying the deprotonation process is the conductor-to-insulator transition. The electrically conductive emeraldine salt is converted to the non-conductive emeraldine base form.

The seawater has a pH value of 8.2. The molecular ion doped polyaniline will undergo the emeraldine salt to emeraldine base transition and lose its electrical conductivity. The instability of the conductive form in seawater will restrict the application of the conventional polyaniline as a corrosion inhibitor under marine environment.

Although there have been reports that the emeraldine base form exhibit corrosion inhibition behavior, our laboratory tests show that the conductive form is more effective than the insulator form for protecting aluminum alloys from corrosion⁸. Electrochemical Impedance Spectroscopy study shows that the impedance value of a coating on aluminum alloy drops by 3 orders of magnitude when the conductive form is transformed into the insulator form. Salt-fog spray tests also show that a coating in the green conductive form resists corrosion much better than the blue emeraldine base form.

The polymeric complexes PAN:PAA, PAN:PVME-MLA are different from the polyaniline doped with small molecular dopants. The conductive state of these "double-strand" polyaniline is stable in seawater. This is advantageous for its application as coating material in the marine environment.

Figure 2 shows the pH titration curves for the single-strand polyaniline PAN:HCl, and the double-strand polyaniline, PAN:PAA, and polyaniline:poly(styrene sulfonic acid) complex. This figure shows that the conductor-to-insulator transition takes place at pH= 4 for PAN:HCl, but at pH=9 for the polymeric complexes of polyaniline with poly(acrylic acid), PAN:PAA, the complex of polyaniline with poly(styrenesulfonic acid), PAN:PSSA. In this experiment, the single- strand PAN:HCl was synthesized by electrochemical polymerization of aniline to form a thin film on a transparent tin oxide electrode, and then it was immersed in a pH buffer solution. The same set of pH buffers was used to dilute the PAN:PAA complex. After the solutions are equilibrated for 30 minutes, the UV-visible absorption spectra were measured and the absorbance at 800 nm is used as a measure of the amount of the conductive form of polyaniline.

When a film of chloride-doped polyaniline is immersed in water, the color of the PAN:HCl film changes from green to blue and eventually changes to purple color. The electrical conductivity of the dried film also decreases by 6 orders of magnitude. In contrast, PAN:PAA and PAN:PVME-MLA complexes can be suspended in seawater at pH 8 and remain as a green-colored solution. These facts are consistent with the titration curves.

The substantial shift in pKa can be understood from the polyelectrolyte effect.⁹ The polyanion carries a high linear density of negatively charged anionic pendent groups. Because of the long-range nature of the coulombic force, there is a cylindrical volume of unscreened electrostatic field surrounding the polyanion backbone. The diameter of this cylinder is on the order of the electrostatic Debye length (about 5 to 10 nm). Since the polyaniline chain is located almost entirely within the Debye length, the strong negative electrostatic field stabilizes its positively charged polarons. Because the positive charge of the polyaniline is stabilized, the pKa is shifted by 5 units in favor of the conductive form of polyaniline.

Water-borne electroactive primer

The inter-polymer complexes PAN:PAA or PAN:PVME-MLA are used as additives in commercial water-borne epoxy. Coating formulation were prepared by adding 1% to 5% water dispersible polyaniline in commercial water-borne epoxy paints. The aluminum alloys AA2024-T3, AA7075-T6 and AA6061 (supplied by Metal Samples, Munford, AL) were polished by 600 grid sand papers. No surface pre-treatment was applied to aluminum metal before coating.

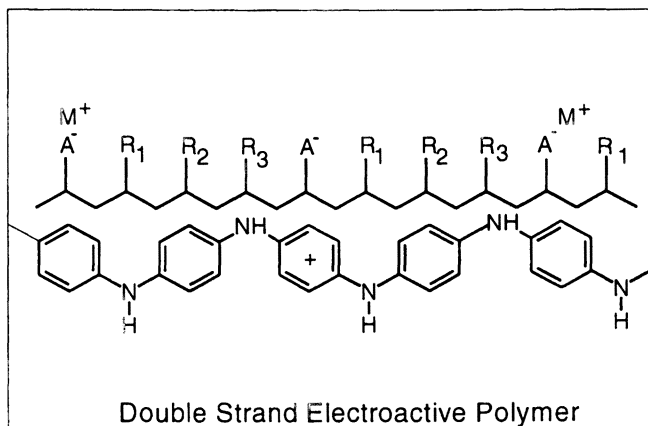


Figure 1 Structure of an inter-polymer complex of polyaniline and a polyanion. "A" is an anionic functional group, e.g. a carboxylate or sulfonate. "R" is an organic functional group.

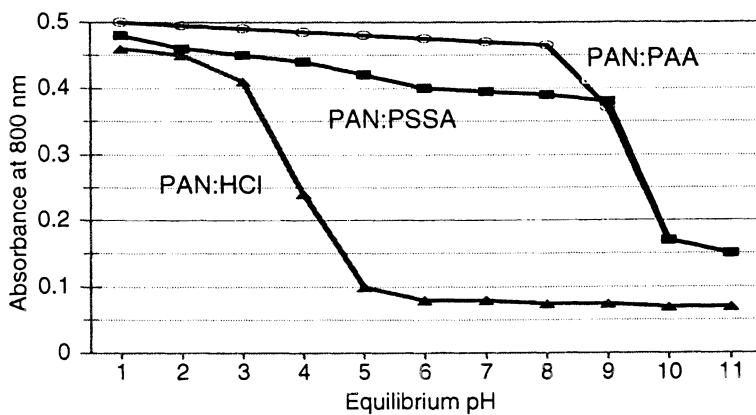


Figure 2 Titration curves of the single-strand PAN:HCl, and the polymeric complexes PAN:PAA and PAN:PSSA. The conductor-to-insulator transition occurs at pH 4 for PAN:HCl, at pH 9.5 for PAN:PAA and PAN:PSSA.

One of the methods for coating the water-borne epoxy is to use cathodic electrophoretic deposition. The aluminum alloy was connected to a DC power supply as a cathode in the electrophoretic bath. The electrophoretic deposition was carried out at 90 V for 90 seconds. The coating was cured at 160 °C for 20 minutes. For a non-pigmented epoxy, the cured sample has a green colored coating indicating that the polyaniline is in its conductive emeraldine salt form. The control samples were coated with the same epoxy primer (PPG Powercron 640) but without the polyaniline additive. The thickness of both the control coatings (without polyaniline) and the sample coatings (with polyaniline) were about 0.8 mil.

Corrosion Tests

The electroactive epoxy with 1% double-strand polyaniline was electrophoretically coated on the AL2024, AL6061, and AL7075 alloys with out surface pretreatment. Control samples were prepared from the same commercial e-coat formulation. Controls and samples were scratched to expose the underlying (with no surface pretreatment) aluminum alloy surface. Samples and controls were tested by salt-fog spray, acid-dip filiform corrosion test, and immersion in seawater.

Salt-fog spray test

The 1000-hour salt-fog spray tests (ASTM B-117) show that the polyaniline additive is effective for preventing blister formation near the scratch line that exposes the untreated aluminum surface. Figure 3 shows that after 1000-hour ASTM B-117 test, a control samples (epoxy on bare AA7075) shows blistering of the primer near the cut which is not surprising for epoxy coatings on aluminum surfaces without surface pretreatment or surface conversion. The same AL7075 aluminum alloy without surface pretreatment, when coated with epoxy primer with 1% double-strand polyaniline, shows no undercut, no blister except for the accumulation of white aluminum oxide at the scratched lines. The corrosion test results show that the conducting polymers are effective in inhibiting corrosion with small amount of conducting polymer as additive to the epoxy primers.

Immersion in sea water

Scratched test samples were immersed in air-saturated seawater for 40 days with weekly refreshing of the seawater. The pH of the seawater measures from 8.0 to 8.2. Figure 4 shows blister formation in the control samples show blistering of the primer coating, while the samples that contain polyaniline additive show substantial resistance to corrosion.

Filiform corrosion test

Scratched test samples were tested by acid dip cycles. The samples were dipped in HCl solution for 2 minutes followed with air-drying for a day. The samples were then placed in 85% humidity chamber for 6 days. The cycles were repeated for 8 weeks. Figures 5, 6 and 7 show controls and samples of AL 2024 and AL7075 tested. The samples with 1% of double-strand polyaniline show substantially less filiform corrosion.

Conclusions

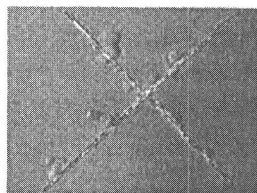
A template-guided synthetic method was used to synthesize inter-polymer complexes of polyaniline. The complexes of polyaniline and the polymeric dopant are advantageous comparing to the single-strand polyaniline. The “double-strand” polyaniline are more stable in the conductive state and they are easier to be processed as additives to paints.

A water-borne double-strand polyaniline was used as additive to commercial water-borne epoxy primers. The electroactive, water-borne primer was coated on aluminum alloys by electrophoretic coating process. Uniform coatings (0.8 mil thickness) on AA7075, AA2024 and AA6061 alloys were obtained and were used for salt-spray, seawater immersion and filiform corrosion tests.

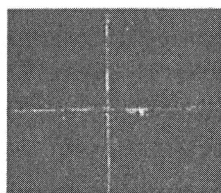
The corrosion test results show that the conducting polymers are effective in inhibiting corrosion with small amount of conducting polymer as additive to the epoxy primers.

Comparing with the small ion doped single strand polyaniline, the double-strand polyaniline used in this study has the advantage of the ease in integration in epoxy resin, and the resistance to dedoping in pH 8 seawater.

Salt Fog Spray (ASTM B117) 1000 hr
AL7075, no surface pre-treatment



Control: Epoxy primer
0.8 mil coating



Sample: 1% PAN in
Epoxy, 0.8 mil coating

Figure 3 Salt-fog spray test (ASTM B-117) after 1000 hours. Coatings: 0.8 mil thick primer on aluminum ally AL 7075-T6 with no metal surface pretreatment. Left: Control sample, epoxy primer without polyaniline. Right: Epoxy primer with 1% PAN:PAA inter-polymer complex.

Sea water immersion 40 days
A7075

- Control sample
 - 0.8 mil commercial epoxy
 - blistering
- With 1% PAN additive
 - 0.8 mil on bare aluminum
 - no blistering

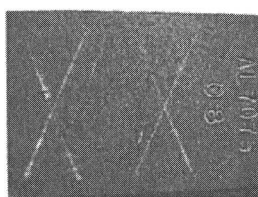
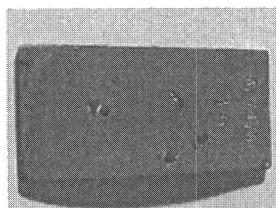


Figure 4 Samples immersed in seawater for 40 days. Left: control sample, epoxy primer (0.8 mil thick) on AL 7075-T6 alloy with no surface pretreatment. Right epoxy with 1% PAN:PAA (0.8 mil thick) on AL 7075-T6 with no surface pretreatment.

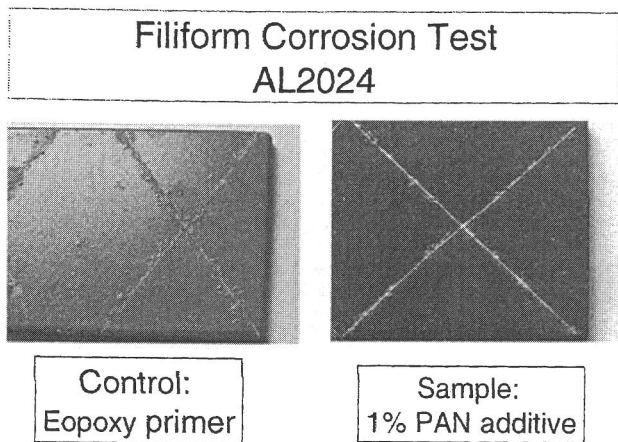


Figure 5 Filiform corrosion test of coatings on AL2024. Left: control sample, epoxy primer (0.8 mil thick) on AL 2024-T3 alloy with no surface pretreatment. Right epoxy with 1% PAN:PAA (0.8 mil thick) on AL 2024-T3 alloy with no surface pretreatment.

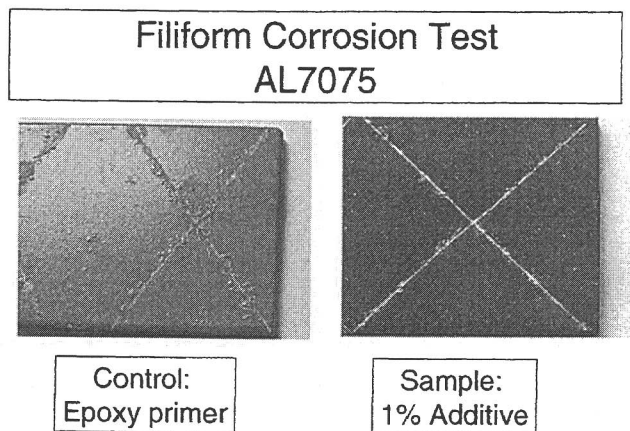


Figure 6 filiform corrosion tests of coatings on AL7075. Left: control sample, epoxy primer (0.8 mil thick) on AL 7075-T6 alloy with no surface pretreatment. Right epoxy with 1% PAN:PAA (0.8 mil thick) on AL 7075-T6 with no surface pretreatment.

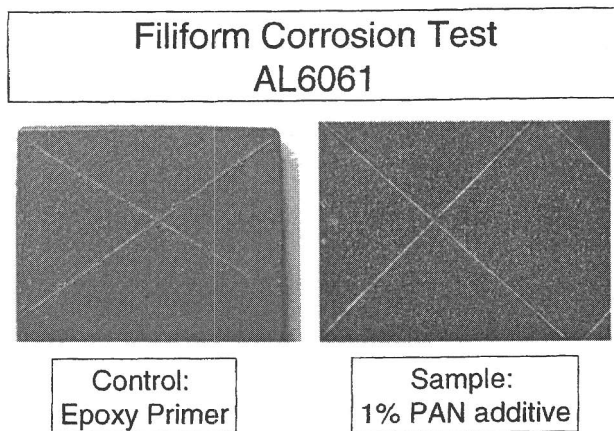


Figure 7 filiform corrosion tests of coatings on AL6061. Left: control sample, epoxy primer (0.8 mil thick) on AL 6061 alloy with no surface pretreatment. Right epoxy with 1% PAN:PAA (0.8 mil thick) on AL 6061 with no surface pretreatment.

Acknowledgement

This research was partially supported by an Alcoa Foundation Grant, a URI Foundation Grant, a URI SST Partnership fund, and a URI DOT grant.

References

- ¹ D. W. DeBerry, *J. Electrochem. Soc.*, **132**, 1022 (1985). D. W. DeBerry and A. Viehback, *Electrochemical Society Softbound Proceedings Series*, 308-323, Pennington, NJ, 1984.
- ² a) N.H. Ahmad and A..G. MacDiarmid, *Bulletin of American Physical Society* , 32, No. 3, 548 (1987) b) Ren and D. Barkey, *J. Electrochem. Soc.*, **139**, 1021 (1992). c) B. Wessling, *Adv. Materials*, **6**, 226 (1994). d) D. B. Wroblewski, B. C. Benicewicz, K. G. Thompson and C. J. Bryan, *ACS Polymer Preprints*, **35**, 265 (1994). e) S. Jasty and A. J. Epstein, *ACS Poly. Preprints*, **72**, 565 (1995). f) Y. Wei, J. Wang, X. Jia, J. M. Yeh and P. Spellane, *ACS Polymer Preprints*, **72**, 563 (1995). g) W-K Lu, R. L. Elsenbaumer and B. Wessling, *Syn. Met.* **71**, 2163 (1995).

- ³ a) R. Racicot, R. L. Clark, H.-B. Liu, S.C. Yang, M.N. Alias and R. Brown, SPIE Proceedings, **2528**, 251 (1995). b) R. Racicot, M.N. Alias, R. Brown, R. L. Clark, H.-B. Liu and S.C. Yang, Proc. Materials Res. Soc., **413**, 529-534 (1996). c) B. Wessling, Syn. Metals, **93**, 143-154 (1998). d) A. J. Epstein, J. A. O. Smallfield, H. Guan and M. Fahlman, Synth. Metals, **102**, 1374 (1999), e) R. J. Racicot, S. C. Yang, R. Brown, *Mat. Res. Soc. Symp. Proc.* **488**, 733-740 (1998), f) H. Liu, R. Clark, S. C. Yang, *Mat. Res. Soc. Symp. Proc.* **488**, 747-752 (1998),.
- ⁴ P. Zarras, J. D. Stenger-Smith, M. H. Miles, Polymeric Materials Science and Engineering, Proceedings of the ACS Division of Polymeric Materials Science and Engineering, Proceedings of the 1997 Spring ACS Meeting, p 589-590
- ⁵ L. Sun, H. Liu, R. Clark, S. C. Yang, *Syn Met* **85**, 67 (1997). J.-M. Liu, L. Sun, J.-H. Hwang and S. C. Yang, *Materials Research Society Symposium Proceedings*, **247**, 601 (1992).
- ⁶ Linfeng Sun and Sze C. Yang, *Mat. Res. Soc. Symp. Proc.*, **328**, 167 (1994).
- ⁷ L. Sun, H. Liu, R. Clark, S. C. Yang, *Syn Met* **85**, 67 (1997)
- ⁸ R. J. Racicot, S. C. Yang, R. Brown, *Mat. Res. Soc. Symp. Proc.* **488**, 733(1998).
- ⁹ G. S. Manning, *J. Chem. Phys.*, **89**, 3772 (1988), *J. Chem. Phys.* **51**, 924 (1969)

Chapter 14

Corrosion Protection Properties of Coatings of the Epoxy-Cured Aniline Oligomers Based on Salt Spray and UV-Salt Fog Cyclic Tests

Yen Wei^{1,3}, Homayoun Jamasbi¹, Shuxi Li¹, Shan Cheng¹,
Susan A. Jansen², Lawrence T. Sein, Jr.², Wanjin Zhang³,
and Ce Wang³

¹Department of Chemistry, Drexel University, Philadelphia, PA 19104

²Department of Chemistry, Temple University, Philadelphia, PA 19122

³Department of Chemistry and The Alan G. MacDiarmid Laboratory,
Jilin University, Changchun 130023, Peoples Republic of China

Anticorrosion performance of various amino-terminated aniline oligomers cured with epoxy resin as coatings on cold-rolled steel has been investigated systematically using two industrial standard tests, i.e., salt spray (ASTM B117–97) and cyclic UV-salt fog exposures (ASTM D5894–96). Data are evaluated based on the standard method ASTM D1654–92. In the salt spray tests up to 2500 hours, the amino-terminated aniline oligomers, particularly the trimer, crosslinked with epoxy resin at 1:3 molar ratio at relatively low dry film thickness of 3–4 mils have outstanding anticorrosion properties. Their performance is far superior over the commercial acrylic and epoxy coatings with or without pigments such as zinc molybdenum phosphate, calcium ion exchanged amorphous silica, and chromium oxide and over the epoxy-cured non-conjugated 1,4-xylenediamine system at the same film thickness. Besides barrier properties, the electroactivity of the aniline oligomer systems could be the main contributing factor to the observed anticorrosion properties. The cyclic test results up to 2016 hours are similar to the salt spray for all the epoxy-based coatings. Because of the good UV resistance, the acrylic coatings show excellent performance that is comparable to the epoxy-cured trimer system. In all the tests, the amino-terminated aniline trimer system has the best overall corrosion protection performance.

Conventional polyanilines with high molecular weights have been studied by many researchers and demonstrated as a potential replacement for the chromium-containing coatings due to its good anticorrosion properties.¹⁻⁶ In 1995, polyanilines in their nonconductive but electroactive base form (e.g., emeraldine base) were also found to possess excellent anticorrosion properties,^{4,5} which is of great importance because the elimination of the need for strong acids as dopants in formulating the coatings. However, conventional polyanilines of high molecular weight are generally hard to process, poorly soluble, and in many cases possess poor adhesion properties. Wei and co-workers⁷ have shown that a small amount of aromatic additives, such as 1,4-phenylenediamine, could significantly increase the rate of oxidative polymerization of aniline monomers. These additives function essentially as chain initiators in such a reactivation chain polymerization and, therefore, the molecular weight of polyanilines can be reduced by increasing the molar ratio of the additives to aniline in the system.^{8,9} At high additive-to-aniline ratios, more soluble and processible oligomers with designed end groups could be obtained. These electroactive oligomers can be employed as monomers and further polymerized with other traditional monomers to afford a variety of new electroactive polymers, such as polyamides, polyimides, polyurethanes, polyureas, polyimines, epoxy and vinyl polymers.¹⁰

Electrochemical and theoretical studies demonstrated that the aniline oligomers have excellent anticorrosion properties, much better than conventional polyanilines.¹¹⁻¹³ Such good performance might be attributed to the possibility that the oligomers have better "adhesion" to (or more intimate contact and electroactive interactions with) the surface of metal substrate. The cold rolled steel coated with oligomer-cured epoxy resin showed very high (sometimes, positive) corrosion potential E_{corr} values and high polarization resistance ($R_p > 10^7 \Omega/\text{cm}^2$). The corrosion current (i_{corr}) values were too low to be measured reproducibly, suggesting very slow rates of electrochemical corrosion of the cold rolled steel.¹¹ The similar results were obtained for the amino-terminated aniline trimer-cured epoxy coatings.¹²

Despite extensive electrochemical investigations, however, never before was a systematic and comprehensive comparative exposure study of anticorrosion properties performed on the coatings containing various aniline oligomers. Such standardized exposure studies with detailed documentation would yield practical assessments of the coating performance with industrial significance. In this study, amino-terminated aniline oligomers were employed as crosslinking agents to cure epoxy resins at various compositions. Coatings were formulated and applied on the cold rolled steel panels. The anticorrosion performance of the coatings was evaluated systematically against the commercially available industrial systems using two widely accepted industrial standard tests per

American Society for Testing and Materials (ASTM): ASTM B117–97 Standard Practice for Operating Salt Spray (Fog) Apparatus¹⁵ and ASTM D5894–96 Cyclic Salt Fog/UV Exposure of Painted Metal (Alternating Exposures in a Fog/Dry Cabinet and a UV/Condensation Cabinet).¹⁶ In order for the data to have universal acceptance, we performed grading and interpretation based on ASTM D1654–92 Standard Test Method for Evaluation of Painted or Coated Specimens Subjected to Corrosive Environments.¹⁷

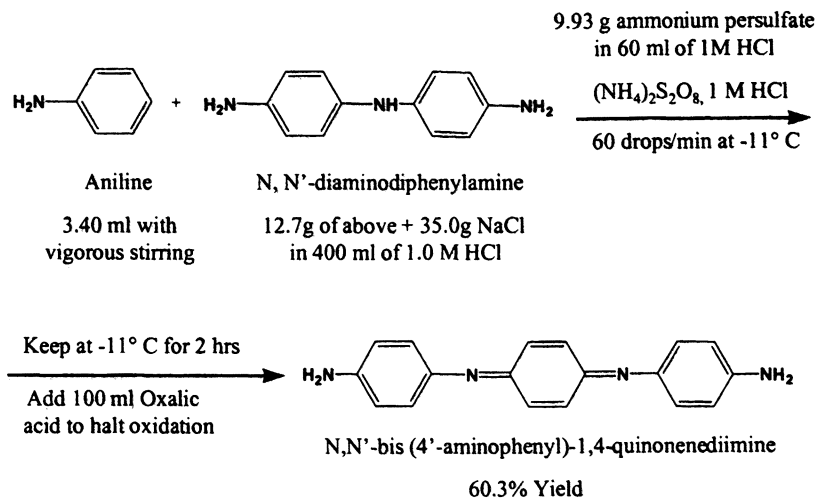
Experimental Section

Synthesis of Aniline Oligomers.

Most recently, a new general scheme of polymerization is proposed—namely, reactivation chain polymerization or nonclassical chain polymerization.¹⁸ We have successfully applied this new theory in the synthesis of aniline oligomers of well-defined structures with controllable end-groups and molecular weights. A convenient, one step method has been developed by Wei and coworkers^{8–10} for the synthesis of an amino-terminated aniline trimer, i.e., *N,N'*-bis(4-aminophenyl)-1,4-quinonediimine, and its derivatives from the oxidation of *p*-phenylenediamine in the presence of aniline or substituted aniline in an acidic aqueous medium. These diimine compounds can be readily reduced to afford their corresponding diamine derivatives.

In this study the amino-terminated aniline trimer was prepared by the following modified procedure (Scheme I). 12.70 g (0.0363 mol) of *N,N*-diaminodiphenylamine sulfate, 35.0 g of sodium chloride, and 400 mL of 1.0 M hydrochloric acid were placed into a 1000-mL 3-neck round bottom flask, equipped with an efficient mechanical stirrer, a thermometer, and a dropping funnel. 3.40 mL (0.0363 mol) of aniline was added with very vigorous stirring. After the formation of homogeneous solution, the flask was then moved to a refrigerated bath cooled down to $-11\text{ }^{\circ}\text{C}$. A solution of 9.93 g (0.0512 mol) of ammonium persulfate in 60 mL of 1.0 M hydrochloric acid was prepared and added into reaction at a rate of 60 drops per minute. The internal reaction temperature during addition was about $-8\text{ }^{\circ}\text{C}$. After addition of ammonium persulfate solution, the reaction was stirred at $-11\text{ }^{\circ}\text{C}$ for 2 hours. 100 mL of saturated oxalic acid solution was added to quench the reaction and the flask was held in the refrigerated bath for another 15 minutes. The dark blue reaction mixture was filtered through a Buchner funnel with P8 filter paper. Upon washing with 200 mL of 1.0 M HCl the solid was transferred to a 800-ml beaker and neutralized by 200 mL of 15% ammonium hydroxide. The blue solid was filtered and dried to yield 7.0 g product in 67% yield based on the amount of *N*,

Scheme I. Synthesis of the amino-terminated aniline trimer.



N-diaminodiphenylamine sulfate. After extracting with acetone, 6.3 g of the trimer was obtained in an overall yield of 60%.

Preparation of Coating Systems.

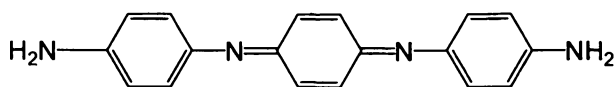
Three industrial coating systems were selected as references in this study as follows:

1. A commercially available two pack solvent based epoxy resin system.
2. A commercially available water based acrylic resin used as DTM (Direct To Metal).
3. A commercially available water based acrylic resin used as primer containing zinc molybdenum phosphate, calcium ion exchanged amorphous silica, and chromium oxide pigments.

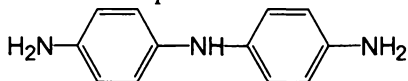
It is important to note that, the two pack epoxy was used as neat resin with no pigment. However, the other two resins were formulated into finished coatings based on the most up to date formulation information available. The details of the two industrial formulations are discussed later in this section. The primer system was formulated using a combination of inhibitive pigments that in a separate study proved to be the best for corrosion protection properties. As a fourth reference a polyaniline in emeraldine base form was used. However, several attempts in preparing polyaniline at 1:3 and 1:6 molar ratios failed. This

was due to the presence of fewer functional amino sites in polyaniline in comparison with the aniline trimer at any given sample weight. At 1:3 molar ratio this resulted in coatings that were too dry to flow properly and at 1:6 molar ratio the coating remained tacky even after 48 hours at 120 °C. Finally, a sample of polyaniline with epoxy resin at 1:2 by weight ratio was prepared. However, even at this ratio the processibility was so poor that after several attempts the final coating film still had high porosity. On the other hand, when polyaniline was directly applied as coatings, delamination often occurred soon after the commence of the tests because of the poor adhesion to the substrate. Hence the polyaniline system was not further discussed in this work.

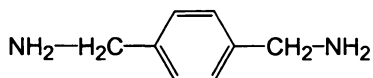
In addition to the industrial references, the following compounds were selected for this study: amino-terminated aniline trimer, *N,N'*-bis(4'-aminophenyl)-1,4-quinonenediimine was prepared using the one step method as described above. 4,4'- Diaminodiphenylamine (aniline dimer), 1,4-xylenediamine (a non-conjugated diamine as a control), 1,4-phenylenediamine, and polyaniline were purchased from Aldrich Chemical Company.



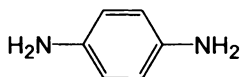
Amino functional aniline trimer, *N,N'*-bis(4'-aminophenyl)-1,4-quinonenediimine



4,4'-Diaminodiphenylamine



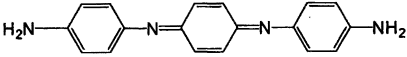
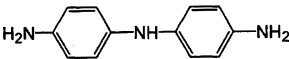
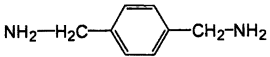
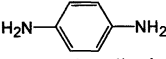
P-Xylenediamine



1,4-Phenylene diamine

All samples were crosslinked with epoxy resin (Araldite GY 2600 from Ciba-Geigy) at 1:3 molar ratio. Thus, these reactive α,ω -diamino compounds were employed to cure epoxy resin¹¹ instead of conventional hardners in commercial two-pack epoxy system (e.g., HY 265 in Ciba-Geigy product). In addition to 1:3 molar ratio aniline trimer was also crosslinked at 1:6 molar ratio. Table 1 shows the designation assigned to each sample.

Table 1. Sample matrix and identification.

<p>Aqueous Emulsion Acrylic Resin (White Direct to Metal formulation)</p> <p>1</p>	 <p>N,N'-bis (4'-aminophenyl)-1,4-quinonedimine</p> <p>2A = 1:3 molar ratio</p> <p>2B = 1:6 molar ratio</p>
<p>Aqueous Emulsion Acrylic Resin (Green Primer / Inhibitive Pigments)</p> <p>4</p>	 <p>4,4'-Diaminodiphenylamine</p> <p>7 = 1:3 molar ratio</p>
<p>A commercially available epoxy from Ciba-Geigy (Araldite GY 2600/hardner HY-265)</p> <p>6</p>	 <p>P-Xylenediamine</p> <p>8 = 1:3 molar ratio</p>
<p>Polyaniline crosslinked / epoxy (Araldite GY 2600) at 1:2 wt</p> <p>5</p>	 <p>1,4-phenylene diamine</p> <p>3 = 1:3 molar ratio</p>

As industrial references, two formulations were prepared using two different state of the art commercial aqueous emulsion acrylic resins. Formulation I was a mid-gloss white direct to metal coating and Formulation IV was a metal primer containing a synergistic blend of pigments (zinc molybdenum phosphate, calcium ion exchanged amorphous silica, and chromium oxide). The detailed ingredients in Formulations I and IV are listed in Table 2 and 3, respectively.

Preparation of Substrate and Coatings.

Cold rolled steel panels (CRS) from ACT laboratories were used as substrate. Panels were polished with sand paper (grid #600) to remove oxidation layer. The surface was then washed with distilled water, ethanol, and acetone. Finally, panels were dried using the pressured air. Solution of various coatings were applied over the CRS panels using a 8-path wet film applicator with an overall width of 4 inches and a path width of 3 inches using a path depth of 10 mils wet from Paul N. Gardner Company. At least 4 sample panels of each coating were prepared, two for salt spray and two for cyclic exposure. All polyaniline and aniline oligomer samples as well as the two pack epoxy resin

Table 2. List of ingredients for Formulation I: (White DTM)

Ingredients	By weight	By volume
<u>GRIND</u>		
(Solvent) Dipropylene glycol methyl ether	18.00	2.28
Water	35.00	4.20
(Dispersant) Hydrophobic acrylic copolymer	9.50	1.08
28% Aqueous Ammonia	1.00	0.13
(Surfactant)	1.50	0.17
(Defoamer)	1.50	0.18
(Pigment) Titanium dioxide	195.00	5.85
<i>Grind the above at high speed until a 7+ Hegman, at low speed add:</i>		
Water	5.00	0.60
<u>LETDOWN</u>		
Aqueous acrylic resin (DTM binder)	523.00	61.71
28% Aqueous ammonia	4.00	0.52
(Solvent) Dipropylene glycol n-propyl ether	55.00	7.22
Water	85.00	10.20
(Plasticizer) Dibutyl phthalate	14.00	1.60
(Defoamer)	1.50	0.18
(Flash rust additive) 15% aqueous sodium nitrite	9.00	1.08
(Rheology modifier) Hydrophobically modified ethylene oxide urethane	3.00	0.35
Total:	961.00	97.35

Table 3. List of ingredients for Formulation IV: (Green primer)

Ingredients	By weight	By volume
<u>GRIND</u>		
Water	170.00	20.40
<i>(Dispersant)</i> Hydrophobic acrylic copolymer	11.00	1.25
<i>(Solvent)</i> Butyl cellosolve	35.90	4.77
<i>(Plasticizer)</i> Dibutyl phthalate	7.20	0.82
28% Ammonium hydroxide	2.00	0.26
<i>(Extender pigment)</i> Talc	100.00	4.45
<i>(Pigment)</i> Chromium oxide	50.00	1.17
<i>(Inhibitive pigment)</i> Calcium ion exchanged amorphous silica	25.00	1.67
<i>(Inhibitive pigment)</i> Zinc molybdenum phosphate	50.00	1.62
Water	5.00	0.60

Grind the above at high speed until a 7+ Hegman, at low speed add:

LETDOWN

Aqueous acrylic resin (Primer binder)	471.80	54.21
Water	4.00	0.48
Grind (from above)	482.10	40.10
<i>(Solvent)</i> Ethanol	19.90	2.95
<i>(Flash rust additive)</i> 15% aqueous sodium nitrate	9.00	1.08
<i>(Rheology modifier)</i> Hydrophobically modified ethylene oxide urethane	6.60	0.73
Water	4.93	0.59
Total	997.33	100.00

were cured at 80 °C for 24 hours. The two water based industrial coatings were cured at room temperature. These coatings were kept at room temperature for two weeks prior to testing. The edges and the back of all panels were taped and sealed prior to exposure testing. The dry film thickness of all panels were measured, before the testing, at five random places using an electronic nondestructive coatings-film thickness meter model 6000 from DeFelsko Corporation. The film thickness was reported in mils (1 mil = 25 μ). All samples had an average film thickness of about 3 to 4 mils (75 to 100 μ). A 3 inch scribe was made over the coating on every panel deep enough to dig all the way to the CRS substrate.

Finally, all panels were marked and placed in salt spray cabinet (Model SASS/1000 from Sheen Instruments Ltd., England) per ASTM B117-97 and UV/Salt Fog cabinets (QUV Model UVA-340 and Q-FOG from Q-Panel Lab Products, Ohio) for the cyclic exposure per ASTM D 5894-96. All panels were graded based on ASTM D1654-92. Photographic documentation and grading took place at intervals of every 250 hours for the salt spray and every 336 hours for the cyclic test. The 336 hours (2 weeks) constitute a full cycle of alternative exposure in the UV cabinet (1 week) and prohesion, i.e., salt fog, cabinet (1 week). Each sample tested and evaluated was at least in duplicates. The results between the duplicated specimen were very close and reproducible.

Results and Discussion

Salt Spray

Plates 1 and 2 show the conditions of all panels after salt spray testing for 1500 and 2500 hours, respectively. Tables 4 and 5 summarize the salt spray results after 1500 and 2500 hours, respectively. The detailed observations at intervals of 250 hours for each sample are given below.

Sample 1. Acrylic emulsion direct to metal coating (Formulation I) showed sign of failure after the first 250 hours. This was the first sample that failed.

Sample 2A. Amino-terminated aniline trimer crosslinked with epoxy resin at 1:3 molar ratio was by far the best performing sample. There was no sign of corrosion on the unscribed portion of the panel after 2500 hours of exposure. The rust creepage in the scribed area was less than 0.5 millimeter (1/64").

Sample 2B. Amino-terminated aniline trimer crosslinked with epoxy at 1:6 molar ratio also had excellent corrosion protection properties. There was no sign of corrosion on the unscribed portion of the panel even after 2500 hours of exposure. The rust creepage in the scribed area was about 1.0 mm (1/32").

Sample 3. 1,4-Phenylenediamine crosslinked with epoxy resin at 1:3 molar ratio, although demonstrated a comparable corrosion protection performance to aniline trimer at 1500 hours, it showed lower performance at 2500 hours. There was no sign of corrosion on the unscribed part of the panel. However, in the scribe the rust creepage was about 2.5 mm (about 1/12").

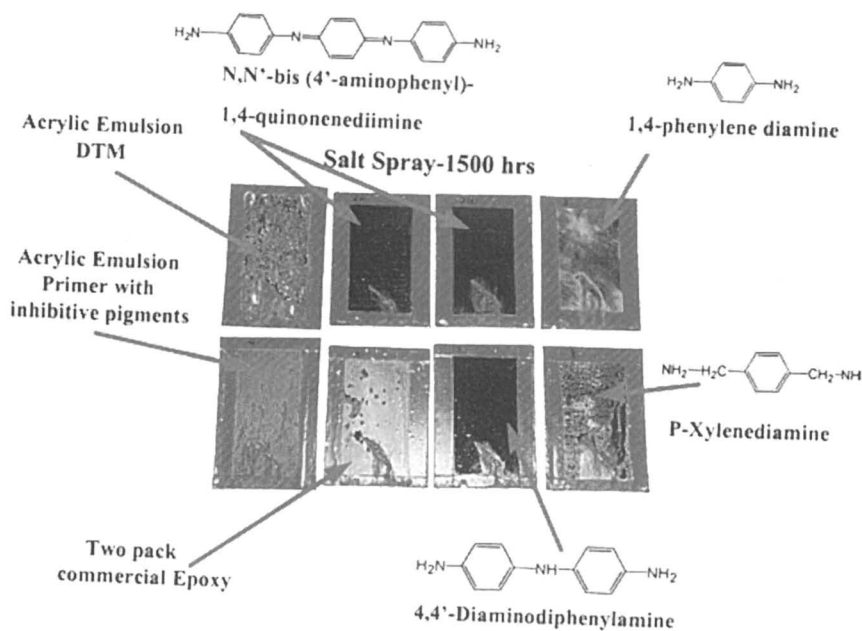


Plate 1. Condition of panels after 1500 hours of salt spray
(This figure is also in the color insert.)

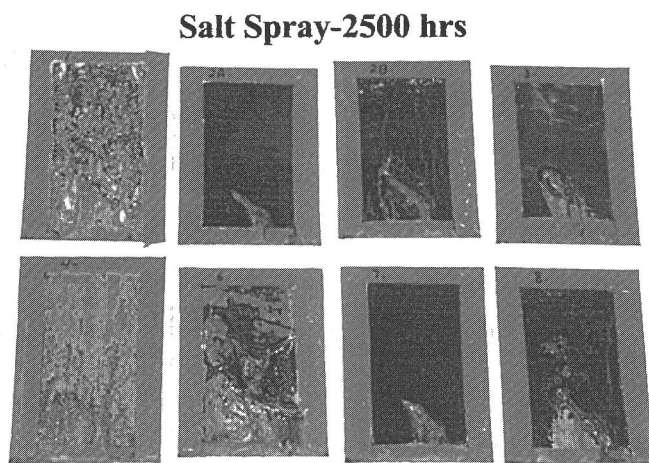


Plate 2. Condition of panels after 2500 hours of salt spray
(This figure is also in the color insert.)

Table 4. Results of salt spray (ASTM B117-97) after exposure for 1500 hours, graded based on ASTM D1654-92. All samples were in duplicates.

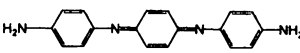
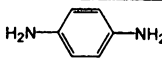
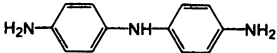


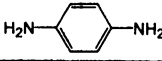
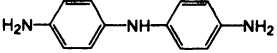

<i>Sample</i>	<i>No.</i>	<i>Unscribed</i>	<i>Scribed</i>
Acrylic Emulsion DTM	1	0	0
	2A 2B	10 10	10 10
	3	10	10
Acrylic Emulsion Primer with inhibitive pigments	4	3	7
Two pack commercial Epoxy	6	3	7
	7	10	10
	8	3	6

Table 5. Results of salt spray (ASTM B117-97) after exposure for 2500 hours, graded based on ASTM D1654-92. All samples were in duplicates.

<i>Sample</i>	<i>No.</i>	<i>Unscribed</i>	<i>Scribed</i>
Acrylic Emulsion DTM	1	0	0
	2A 2B	10 10	10 8
	3	10	6
Acrylic Emulsion Primer with inhibitive pigments	4	0	0
Two pack commercial Epoxy	6	0	0
	7	10	9
	8	0	0

Sample 4. Water based acrylic emulsion formulated into a primer with inhibitive pigments (Formulation IV), although considered to be a high-performance industrial system, failed in comparison with the crosslinked aniline oligomers. After 1500 hours about 30% of the surface of the panel was covered with rust. This level elevated to over 75% after 2500 hours of salt spray exposure. In the scribed area the rust creepage was about 2 mm (about 1/16") at 1500 hours, which increased to about 16 mm (about 5/8") after 2500 hours.

Sample 6. The two pack epoxy system performed comparable to the water based acrylic emulsion that contained inhibitive pigments. Basically, after 1500 hours about 30% of the surface of the panel was covered with black rust. The rust coverage elevated to well over 75% with severe delamination of the coating from the substrate surface after 2500 hours. In the scribed area the rust creepage was about 2 mm (about 1/16") at 1500 hours, which increased to more than 16 mm (about 5/8") after 2500 hours.

Sample 7. 4,4'- Diaminodiphenylamine (aniline dimer) crosslinked with epoxy at 1:3 molar ratio had an excellent corrosion protection performance. After 1500 hours there was no sign of corrosion on the unscribed part of the panel and there was no rust creepage in the scribed area. After 2500 hours the unscribed area remained rust free and the rust creepage was only about 0.5 mm (about 1/64"). This system was the second best in comparison to the crosslinked aniline trimer.

Sample 8. 1,4-Xylenediamine (the non-conjugated sample) crosslinked with epoxy at 1:3 molar ratio had about 30% and over 75% of the surface of the panel was covered with rust after 1500 and 2500 hours, respectively. In the scribed area after 1500 hours the rust creepage was about 2 mm (about 1/16"), which increased to about 16 mm (about 5/8") after 2500 hours.

Figure 1 shows the comparative performance of all the systems investigated in this series of tests. The comparison is based on the cumulative time of the 250-hour intervals when apparent failure of the coating system occurred on each panel, i.e., when the rust appeared on the unscribed surface of the panel and/or there was rust creepage on the scribed portion of the panels.

All the results from the salt spray testing indicate that the amino-terminated aniline oligomers, particularly the trimer, have outstanding corrosion protection properties. At the same dry film thickness (3-4 mils or 75-100 μm), the electroactive aniline oligomer systems outperformed the typical barrier coatings such as two-pack epoxy and DTM acrylic systems, but also, more significantly, the acrylic system containing inorganic corrosion inhibitors. This is a strong indication that other mechanisms are involved in addition to barrier properties. The most important factor could be the electroactivity of the coating system. In these aniline oligomers the amino groups are conjugated with benzenoid and/or quinoid rings and, hence, highly electroactive.^{10,13,14} Especially in the amino-terminated aniline trimer, there are four amine nitrogen atoms and three benzenoid and quinoid rings, which represents the minimum structure unit for all the key redox reactions of polyaniline.^{10,13,14} Indeed, the trimer system was found to be the best in anticorrosion performance. The importance of the

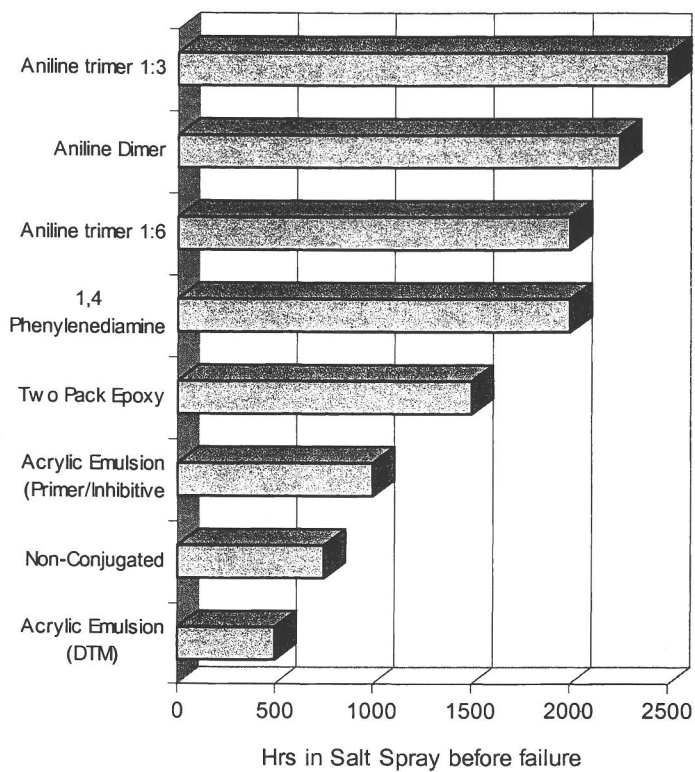


Figure 1. Comparison of coating systems based on the cumulative time of the 250-hour intervals when apparent failure of the coating system occurred up to 2500 hours.

conjugation and electroactivity is further supported by the fact that the system with non-conjugated 1,4-xylenediamine, in which the conjugation between the amino groups with phenyl ring is interrupted by methylene groups, (Sample 8) has much lower corrosion protection effect than those with conjugated aniline oligomers (Samples 2, 3 and 7). Besides the electroactivity, other factors might also contribute to the anticorrosion properties of the oligomer systems to various extents, such as film adhesion, intimacy of the contact and interactions between the electroactive oligomers and the metal substrates, and doping, etc.¹¹⁻¹⁴

It is noteworthy that industrial testing of a coating system by salt spray often considers a good performance after 500 hours of exposure to be acceptable for many conventional applications. The outstanding performance of our electroactive oligomer systems even after 2500 hours of exposure at relatively low coating thickness of 3-4 mils is of great industrial value and commercial potential.

Cyclic Test

Plate 3 shows the condition of all panels after 2016 hours (6 complete 336-hour cycles of alternative exposure to UV and to dry salt fog) and the results are summarized in Table 6. The detailed observations for each sample are given below.

Sample 1. Acrylic emulsion direct to metal coating (Formulation I) had a good performance in the cyclic test. There was no sign of corrosion on the unscribed portion of the panel. The rust creepage in the scribed area was less than 0.5 mm (1/64").

Sample 2A. The performance of amino-terminated aniline trimer crosslinked with epoxy at 1:3 molar ratio was similar to that of the acrylic emulsion. There was no sign of corrosion on the unscribed portion of the panel. The rust creepage in the scribed area was between 0.5 mm (1/64") and 1.0 mm (1/32").

Sample 2B. Amino-terminated aniline trimer crosslinked with epoxy at 1:6 molar ratio did well. However, it did not do as good as the aniline trimer at 1:3 molar ratio. The higher content of epoxy employed made the sample harder. Although, there was no sign of corrosion on the unscribed portion of the panel, the rust creepage in the scribed area was between 2.0 to 3.0 mm (1/16 to 1/8").

Sample 3. 1,4-Phenylenediamine crosslinked with epoxy resin at 1:3 molar ratio did very poorly. More than 75% of the surface of the panel was covered with rust. The rust creepage in the scribed area was between 13.0 to 16.0 mm (1/2 to 5/8 of inch).

Sample 4. Water based acrylic emulsion formulated into a primer with inhibitive pigments (Formulation IV), had an excellent performance in the cyclic test. There was no sign of corrosion on the unscribed portion of the panel. The rust creepage in the scribed area was less than 0.5 mm (1/64").

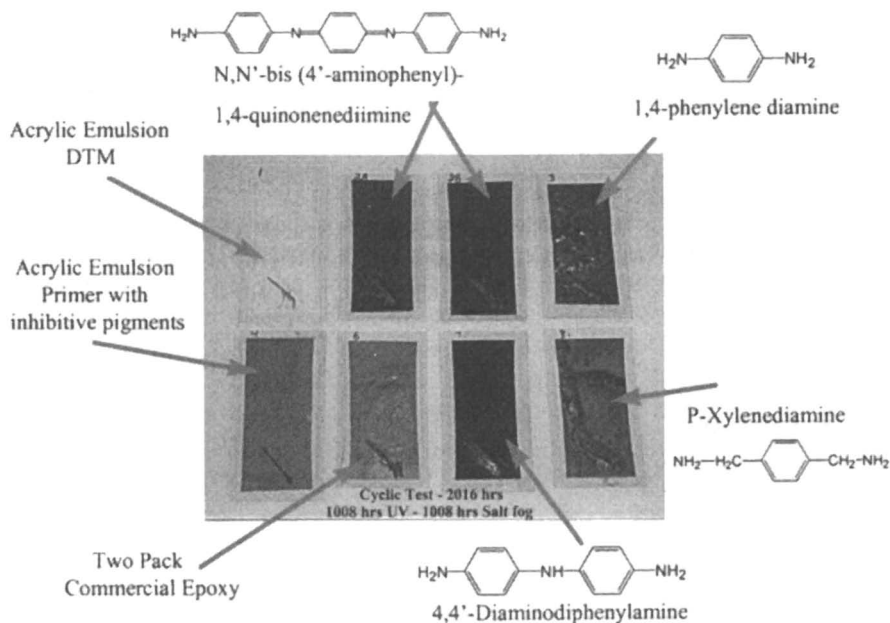
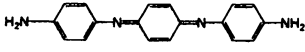
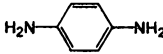
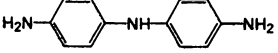
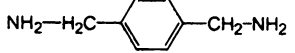


Plate 3 . Condition of panels after 2016 hours of cyclic test
(This figure is also in the color insert.)

Table 6. Results of cyclic test (ASTM 5894-96) after exposure for 2016 hours, graded according to ASTM D1654-92. All samples were in duplicates.

<i>Sample</i>	<i>No.</i>	<i>Unscribed</i>	<i>Scribed</i>
Acrylic Emulsion DTM	1	10	9
	2A 2B	10 10	8 6
	3	0	1
Acrylic Emulsion Primer with inhibitive pigments	4	10	9
Two pack commercial Epoxy	6	0	0
	7	10	6
	8	1	1

Sample 6. The two pack epoxy had the poorest performance. This can be attributed to the very poor UV resistance of the epoxy resin. The UV caused the coating to crack and as a result accelerated the migration of salt and moisture to the substrate leading to severe corrosion. More than 75% of the surface of the panel was covered with rust. The rust creepage in the scribed area was about 16.0 mm (5/8").

Sample 7. 4,4'-Diaminodiphenylamine (aniline dimer) crosslinked with epoxy at 1:3 molar ratio had a very good performance. However, it was not as good as the aniline trimer crosslinked at 1:3 molar ratio (sample 2A). But, was very similar to the aniline trimer crosslinked at 1:6 molar ratio (sample 2B). There was no sign of corrosion on the unscribed portion of the panel. The rust creepage at the scribed area was between 2.0 to 3.0 mm (1/16 to 1/8").

Sample 8. 1,4-Xylenediamine (the non-conjugated sample) crosslinked with epoxy at 1:3 molar ratio showed poor performance. About 55% of the surface of the panel was covered with rust. The rust creepage in the scribed area was 13 mm (1/2").

Figure 2 shows the comparative performance of all the systems investigated in this series of UV-salt fog tests. The comparison is based on the cumulative time of the 336-hour intervals when the apparent failure of the coating system occurred on each panel.

The cyclic testing results indicate, again, that the amino-terminated aniline oligomers, particularly the trimer, have excellent corrosion protection properties. The general trends in the performance of the coatings are similar to those observed in the salt spray tests, except for the acrylic systems that also show an outstanding performance as the aniline trimer system. This is understandable because acrylic polymers are known to be more resistant to UV degradation than epoxy resins. Nonetheless, despite the poor UV resistance of epoxy polymers, the epoxy-cured aniline trimer coatings at the trimer to epoxy molar ratio of 1:3 still exhibit outstanding corrosion protection effect. Currently we are investigating the anticorrosion performance of other polymer systems, such as polyacrylics, polyurethanes, polyamides, polyimides, polyureas, etc., that contain the electroactive aniline oligomers as building units.⁹⁻¹¹

Summary and Concluding Remarks

We have presented the first systematic investigation of the anticorrosion performance of amino-terminated aniline oligomers cured with epoxy resin as coatings on cold-rolled steel using two widely accepted industrial standard tests, i.e., salt spray (ASTM B117-97) and cyclic UV-salt fog exposures (ASTM D5894-96). The data are evaluated also based on the industrial standard method (ASTM D1654-92). The corrosion protection effects of these conjugated

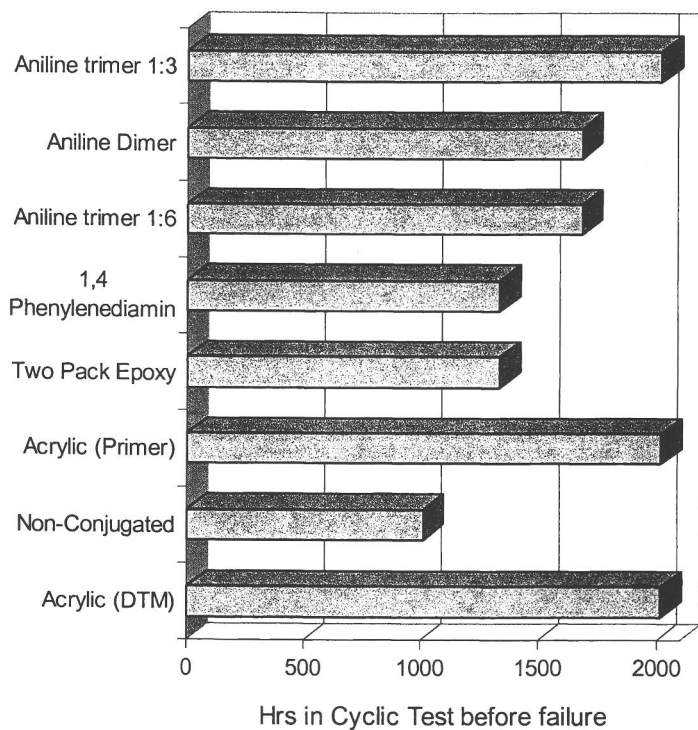


Figure 2. Comparison of coating systems based on the cumulative time of the 336-hour intervals when apparent failure of the coating system occurred up to 2016 hours.

oligomer systems are compared directly with those of the commercially available industrial coatings including the two-pack epoxy system, the water-borne DTM acrylic emulsion and the acrylic emulsion that contains inorganic corrosion-inhibitive (zinc molybdenum phosphate, calcium ion exchanged amorphous silica, and chromium oxide) pigments. In the salt spray tests up to 2500 hours, the amino-terminated aniline oligomers and in particular the amino-terminated aniline trimer crosslinked with epoxy resin at 1:3 molar ratio at relatively low dry film thickness of 3-4 mils (75-100 μm) have outstanding corrosion protection properties. The performance of the oligomer systems are far superior over the commercial coatings with or without inorganic corrosion inhibitors and over the epoxy-cured non-conjugated aromatic diamine (i.e., 1,4-xylenediamine) system at the same film thickness. This strongly indicates that other mechanisms are involved in addition to barrier properties. The electroactivity of the aniline oligomer coating system could be the main contributing factor to the observed outstanding anticorrosion properties. The results from the cyclic tests up to 2016 hours are similar to those from the salt spray for all the epoxy-based coatings. Because of the good UV resistance, the acrylic coatings show excellent performance that is comparable to the epoxy-cured trimer system. In all the tests, the amino-terminated aniline trimer system has the best overall corrosion protection performance.

Recently we have also been investigating the electroactive aniline oligomers as additives in conventional coatings, room-temperature curable epoxy-oligomer coatings and water-borne oligomer-based systems. The results are very promising and will be reported elsewhere in due course. The electroactive oligomer systems, we believe, are of great industrial and commercial value.

Acknowledgments. This work was supported in part by the US Army Research Office (ARO No. 41495-II). We wish to dedicate this paper to the establishment of the Jilin University Alan G. MacDiarmid Laboratory in China in November 2001.

References

- (1) (a) Genies, E.M.; Boyle, A.; Lapkowski, M.; Tsintavis, C. *Synth. Met.* **1990**, *36*, 139; (b) MacDiarmid, A. G.; Epstein, A. J. *Faraday Discussion, Chem. Soc.* **1989**, *88*, 317; (c) Diaz, A. Z.; Logan, J.A. *J. Electroanal. Chem.* **1980**, *111*, 111; (d) Wei, Y.; Focke, W. W.; Wnek, G. E.; Ray, A.; MacDiarmid, A. G. *J. Phys. Chem.* **1989**, *93*, 495; (e) Hsieh, B. R.; Wei, Y., Eds., *Semiconducting Polymers: Applications, Properties and Synthesis*, (Am. Chem. Soc. Symp. Ser. No. 735); American Chemical Society: Washington DC, **1999**; (f) Bierwagen, G. P., Ed. *Organic Coatings for Corrosion Control*, (ACS Symp. Ser. No. 689); American Chemical Society: Washington DC, **1998**.

- (2) (a) For a recent collection of papers on corrosion protection, see: *Polym. Prepr. (Am. Chem. Soc., Div. Polym. Chem.)* Vol. 41(2), 2000; (b) Sathiyarayanan, S.; Dhawan, S.K.; Trivedi, D.C.; Balakrishnan, K. *Corrosion Sci.* **1992**, *33*, 1831; (c) MacDiarmid, A.G., personal communication, 1986; (d) Wroblewski, D.A.; Benicewicz, B.C.; Thompson, K.G.; Bryan, C.J. *Polym. Prepr. (Am. Chem. Soc., Div. Polym. Chem.)* **1994**, *35(1)*, 265; (e) Deng, Z.; Smyrl, W.H.; White, H.S. *J. Electrochem. Soc.* **1989**, *136*, 2152; (f) Yeh, J.-M.; Liou, S.-J.; Lai, C.-Y.; Wu, P.-C.; Tsai, T.-Y. *Chem. Mater.* **2001**, *13*, 1131; (g) DeBerry, D.W. *J. Electrochem. Soc.* **1985**, *132*, 1027.
- (3) (a) Lu, W.; Elsenbaumer, R.; Wessling, B. *Synthetic Metals* **1995**, *71*, 2163. (b) Wessling, B. *Adv. Mater.* **1994**, *6*, 226.
- (4) Wei, Y.; Wang, J.; Jia, X.; Yeh, J.-M.; Spellane, P. *Polym. Mater. Sci. Eng.* **1995**, *72*, 563.
- (5) Jasty, S.; Epstein, A.J. *Polym. Mater. Sci. Eng.* **1995**, *72*, 565.
- (6) Wei, Y.; Wang, J.; Jia, X.; Yeh, J.-M.; Spellane, P. *Polymer* **1996**, *36*, 4535.
- (7) (a) Wei, Y.; Jang, J.-W.; Hsueh, K.F.; Hariharan, R.; Patel, S.; Chan, C.-C.; Whitecar, C.K. *Polym. Mater. Sci. Eng.* **1989**, *61*, 905; (b) Wei, Y.; Sun, Y.; Jang, G.-W.; Tang, X. *J. Polym. Sci., Part C* **1990**, *28*, 81; (c) Wei, Y.; Jang, J.-W.; Hsueh, K.F.; Hariharan, R.; Patel, S.A.; Chan, C.-C.; Whitecar, C.K., *J. Phys. Chem.* **1990**, *94*, 7716.
- (8) (a) Wei, Y.; Yang, C.; Ding, T. *Tetrahedron Lett.* **1996**, *37*, 731. (b) Wei, Y.; Yang, C.; Wei, G.; Ding, T.; Feng, G. *Synth. Metals* **1997**, *84*, 289.
- (9) (a) Wei, Y.; Yang, C.; Chen, M.H.; Li, W. *ANTEC, Soc. Plast. Eng.* **1997**, *55(II)*, 1369; (b) Wang, Z.Y.; Yang, C.; Gao, J.P.; Lin, J.; Wei, Y.; Li, S. *Macromolecules* **1998**, *31*, 2702.
- (10) Wei, Y.; Li, S.; Jia, X.; Chen, M.H.; Mathai, M.W.; Yeh, J.-M.; Li, W.; Wang, Z.Y.; Yang, C.; Gao, J. P.; Jansen, S.A.; Narkis, M.; Siegmann, A.; Hsieh, B. R. in *Semiconducting Polymers: Applications, Properties and Synthesis (ACS Symp. Ser. No. 735)*, Hsieh, B.; Wei, Y., Eds.; American Chemical Society: Washington DC, **1999**, pp. 384-398.
- (11) Wei, Y.; Yeh, M.; Wang, J.; Jia, X.; Yang, C.; Jin, D. *Polym. Mater. Sci. Eng.* **1996**, *74*, 202-203.
- (12) Wei, Y.; Yang, C.; Yeh, M.; Ding, T.; Wei, G.; Jin, D.; Wang, J.; Jia, X.; Jansen, S.A. In *Organic Coatings for Corrosion Control*, (ACS Symp. Ser. 689), Bierwagen, G. P., Ed.; American Chemical Society: Washington DC, **1998**; pp. 382-395.
- (13) (a) Sein, Jr., L.T.; Wei, Y.; Jansen, S.A. *Comp. Theor. Polym. Sci.* **2000**, *11*, 83; (b) Vallerio, R.; Keyer, R.; Jansen, S.A.; Wei, Y. *Mater. Res. Soc. Symp. Proc.* **1996**, *413*, 523; (c) Sein, Jr., L.T.; Levarity, L.; Keyer, R.; Wei, Y.; Jansen, S.A. *Plast. Eng.* **1998**, *45*, 1.
- (14) (a) Sein, Jr., L.T.; Duong, T.; Major, A.; Kolla, S.; Wei, Y.; Jansen, S.A. *J. Mol. Struct.: (THEOCHEM)* **2000**, *498*, 37; (b) Sein, Jr., L.T.; Wei, Y.; Jansen, S.A. *Synth. Metals* **2000**, *108*, 101; (c) Sein, Jr., L.T.; Wei, Y.; Jansen, S.A. *J. Phys. Chem. A* **2000**, *104*, 11371.

- (15) ASTM B117-97 *Standard Practice for Operating Salt Spray (Fog) Apparatus*; American Society for testing and Materials: 100 Barr Harbor Drive, West Conshohocken, PA 19428-2959, United States, **1997**; Section 6, Vol. 06.01.
- (16) ASTM D5894-96 *Standard Practice for Cyclic Salt Fog/UV Exposure of Painted Metal, (Alternating Exposures in a Fog/Dry Cabinet and a UV/Condensation Cabinet)*; American Society for Testing and Materials: West Conshohocken, PA, **1996**; Section 6, Vol. 06.01.
- (17) ASTM D1654-92 *Evaluation of Painted or Coated Specimens Subjected to Corrosive Environment*. American Society for Testing and Materials: West Conshohocken, PA., **1997**; 6.01, pp. 305-308.
- (18) Wei, Y. *J. Chem. Educ.* **2001**, 78(4), 551.

Chapter 15

Scanning Vibrating Electrode Studies of Electroactive Conducting Polymers on Active Metals

Dennis E. Tallman¹, Jie He¹, Victoria Johnston Gelling¹,
Gordon P. Bierwagen², and Gordon G. Wallace³

Departments of ¹Chemistry and ²Polymers and Coatings, North Dakota
State University, Fargo, ND 58105

³Intelligent Polymer Research Institute, University of Wollongong,
Wollongong, NSW 2522, Australia

Various electrochemical techniques such as linear sweep voltammetry and electrochemical impedance spectroscopy have proven very useful for the study of electroactive conducting polymers (ECPs). However, such techniques are global in the sense that the measured response is surface-averaged and they are not capable of providing detailed spatial information. Local electrochemical methods, such as local electrochemical impedance spectroscopy (LEIS) and mapping (LEIM) and the scanning vibrating electrode technique (SVET) (also known as the scanning vibrating probe, SVP) have proven very valuable in corrosion research. Such techniques are capable of providing more detailed insight into the mechanism by which ECPs alter the corrosion behavior of active metals. This chapter provides a brief review of local electrochemical techniques, emphasizing the SVET, and presents recent results from our laboratory of SVET studies of various ECPs on active metals.

Introduction

There is increasing interest in the use of electroactive conducting polymers (ECPs) as components of corrosion resistant coating systems, either directly as a primer coating or surface treatment, or as a component blended with more conventional coatings. In part, this interest in ECPs is motivated by the desire to find suitable replacements for currently used chromate-based coatings, particularly for aluminum alloys (1). ECPs, in addition to being conductive, are redox active materials, typically with equilibrium potentials that are positive of iron and aluminum. Thus, as with chromate, interesting and potentially beneficial interactions of ECPs with active metal alloys such as steel and aluminum are anticipated, with concomitant alteration of their corrosion behavior. A recent two-part review surveys the applications of ECPs to the corrosion control of non-ferrous (2) and ferrous (3) metals.

Various electrochemical methods have been used to study the corrosion of metals, including linear sweep (polarization) techniques, electrochemical impedance spectroscopy (EIS) and electrochemical noise methods (ENM). These methods, while very useful, are global techniques that provide surface-averaged responses for the substrate under test (i.e., no spatial information is available). Corrosion, on the other hand, typically consists of local events occurring at discrete sites on the metal surface. Measurement of the temporal and spatial behavior of such local corrosion events requires use of techniques that are capable of detecting, resolving (temporally and spatially) and mapping such processes across a substrate surface. Such techniques are referred to as local techniques and include scanning electrochemical microscopy (SECM) (4), local electrochemical impedance mapping (LEIM) and spectroscopy (LEIS)(5,6), the scanning reference electrode technique (SRET) (7), and the scanning vibrating electrode technique (SVET) (8,9). The SVET is also known as the scanning vibrating probe (SVP) or the current density probe (CDP). These local techniques have only recently become commercially available and are capable of providing unique information about the interactions between ECPs and active metals. For a more in-depth discussion of these techniques the reader is referred to a recent review (10).

In this chapter we provide a brief review of local electrochemical techniques, emphasizing the SVET. We then present recent results from our laboratory of SVET studies of various ECPs on active metals, with emphasis on polypyrrole on aluminum alloy. In particular, the SVET has been used to map current flow in and around defects introduced into the ECP coatings on aluminum 2024-T3 alloy. Results from similar experiments conducted on topcoated samples are also presented.

Local Electrochemical Techniques

Consider a metal substrate immersed in an electrolyte. The metal substrate may be coated in some way or it may be bare. It is convenient to refer to this metal substrate as the sample and we will do so throughout this discussion. Any electrochemical processes occurring on the surface of the sample while it is immersed in the electrolyte necessarily result in current flow (i.e., an ion flux) through the electrolyte, a consequence of the requirement for charge balance throughout the system. The electrochemical processes (and thus the current) may be spontaneous, as for a freely corroding metal (at its open circuit potential) with distinct anode and cathode sites on the same metal surface, in which case the current flow through the electrolyte will be between anode(s) and cathode(s) on the sample surface. Alternatively, the electrochemical processes may be forced, as is the case with EIS where a current or voltage perturbation is applied to the sample, in which case the current flow is between the sample and an auxiliary electrode. In either case, there is current flow through the electrolyte. Global techniques such as EIS measure the total current flowing at the sample (and thus through the electrolyte). Local techniques such as LEIS and SVET measure the local electrolyte current very close to the sample surface. These local electrolyte currents reflect the local processes occurring at the sample surface. Keep in mind, however, that the terms “global” and “local” are relative and are used here to reflect the manner in which current measurements are made. A global EIS measurement may be dominated by one or more local events (e.g., a coating defect), whereas a local SVET measurement with a resolution of tens of microns might be considered global for processes occurring at the micron or sub-micron scale.

Measurements of local current (actually local current density, i.e., current flowing through unit area) are based on the fact that electrolytes have a finite conductivity and, thus, exhibit resistance to current flow. Indeed, the electrolyte behaves like a three-dimensional resistor and the local current density at a given point in the electrolyte can be represented by a vector having length (magnitude) and direction. The local current density results in a corresponding voltage gradient (i.e., an ohmic or IR drop) given by the expression

$$\nabla \bar{E}(x, y, z) = \frac{\rho}{A} \bar{I}(x, y, z)$$

where $\nabla \bar{E}(x, y, z)$ is the potential gradient vector at location (x, y, z) , $\bar{I}(x, y, z)/A$ is the current density vector at location (x, y, z) and ρ is the resistivity of the electrolyte (which may be determined in a calibration experiment). Thus, measurement of the local potential gradient permits determination of the local current density.

There are two approaches to measuring the local potential gradient, $\nabla E(x,y,z)$. In one approach, a twin-electrode assembly is used consisting of two micro-reference electrodes (e.g., Ag/AgCl) separated from one another by ca. 1 mm along the direction normal to the sample surface (the z direction) (11,12). The difference in potential between the two electrodes provides a measure of the local potential gradient along the z direction and, thus, the current density normal to the sample surface. In the second approach, a single microelectrode is vibrated, either in one direction (the z direction) or in two directions (the x and z directions, each at different vibration frequencies) (9,13). Vibration in two directions provides more complete mapping of the direction of current flow. Phase sensitive detection is used to obtain the potential gradient (and, hence, the current density) along the z (and perhaps x) directions, with a signal-to-noise advantage inherent to such an approach. The vibrating electrode approach also appears to have somewhat better spatial resolution than the twin-electrode approach (14). However, the electrode vibration may introduce some solution convection. The probes (either twin-electrode or vibrating electrode) are positioned a few tens of micrometers above the sample surface. Unlike SECM, there is no feedback to maintain a constant distance from the sample surface, i.e., to compensate for variations in sample surface topography. Rather, the probe is scanned in a fixed plane that is nominally parallel to the sample surface.

LEIS and LEIM

The global technique of EIS typically employs a three-electrode arrangement to control the dc potential and to apply a small amplitude ac potential to the sample under test. The total ac current flow through the sample in response to the ac excitation is then measured and used to compute the global impedance of the sample. For LEIS and LEIM, a similar three-electrode arrangement is used to apply the ac perturbation to the sample. Local current flow through the electrolyte just above the sample surface is then measured, typically using the twin-electrode approach described above (15). The LEIS experiment involves varying the frequency of the ac perturbation at a fixed position of the twin-electrode (or perhaps at several different fixed positions) above the sample surface, whereas the LEIM experiment involves scanning the twin-electrode probe in the x-y plane above the sample surface while holding the ac perturbation frequency constant. Employing higher frequencies of the ac perturbation applied to the sample lowers the impedance of dielectric-type samples, such as coated metals. Thus, LEIS and LEIM can be used for both bare and coated metals under immersion. Recently this approach has been used to probe intrinsic and extrinsic defects in organic coatings applied to metals (6).

Recent variations of the SVET permit local ac current measurement using a single vibrating electrode (14,16,17). In this case two phase sensitive detectors

are used, one detecting the “instantaneous” z-direction current density, the other detecting the time dependence of the z-direction current density at the frequency of the applied ac perturbation. The electrode vibration frequency places an upper limit on the frequency of ac perturbation that can be used.

SVET

The most common use of the SVET in corrosion research is to measure the direct (dc) current flow through an electrolyte due to development of local anode(s) and cathode(s) on the sample surface. Typically, dc current flow through in-tact barrier coatings on metals is minuscule, which restricts the technique to the study of bare metal substrates or coated-metals having coating defects (18,19). The local potential gradient (and, thus, the dc current flow) is measured by vibrating a single electrode either in one direction (normal to the substrate surface) or in two directions (one normal and one parallel to the substrate surface) as described above. The latter approach has the advantage of providing additional information about current flow parallel to the substrate surface. The SVET exhibits a much-improved signal-to-noise ratio compared to SRET, a result of the superior noise rejection inherent in the phase-sensitive detection of the SVET signal.

Experimental Conditions

Sample Preparation

The poly(3-octyl pyrrole) (POP) and poly(3-octadecyl pyrrole) (PODP) were synthesized electrochemically by the Intelligent Polymer Research Institute (Wollongong, Australia). Three POP polymers were prepared differing only in the anion incorporated as counterion: POP with perchlorate (POP-PC), POP with paratoluene sulfonate (POP-PTS) and POP with a mixture of perchlorate and paratoluene sulfonate (POP-PCPTS). Only one PODP polymer was prepared, incorporating a mixture of the counterions perchlorate and paratoluene sulfonate (PODP-PCPTS). The polymers were generated galvanostatically at a platinum electrode at a current density of 1 mA/cm² from a solvent mixture of CCl₄ (80%) and CH₂Cl₂ (20%) containing 0.1 M monomer (3-octyl pyrrole or 3-octadecyl pyrrole) and either 0.1 M counterion (POP) or a mixture of 0.1 M tetrabutylammonium perchlorate and 0.025 M tetrabutylammonium *p*-toluenesulfonate (POP, PODP). The soluble fraction of the electrosynthesized polymer was recovered from the liquor and excess electrolyte removed. Molecular weights were estimated from gel permeation chromatography to be

8,500 to 10,500 (depending on counterion) for POP and 9,300 for PODP-PCPTS. The polymers prepared in this way were both electroactive and conductive (20). Further synthetic details and polymer characterization are provided elsewhere (20).

The aluminum alloy 2024-T3 (Q-Panel) was polished using 600 grit silicon carbide, washed with hexane and air-dried. POP and PODP coatings were then applied by solution casting from a 1% solution in a solvent consisting of carbon tetrachloride/dichloromethane/acetonitrile in a ratio of 48/48/4. The coatings were allowed to dry overnight. The average coating thickness was $2.3 \pm 1.6 \mu\text{m}$. For some POP-coated samples, a high gloss 2K polyurethane topcoat (Mil-PRF-85385C from Deft Chemical Coatings, Irvine CA) was applied by spray coating. The thickness of the topcoat was 25-30 μm .

Samples (coated metal panels) were prepared for SVET measurement by cutting into 1-cm x 1-cm squares and masking with a Polyester 5 adhesive tape (3M Company) such that only a 2-mm x 2-mm square opening of the sample was exposed to electrolyte. For all samples an artificial defect was made through the coating into the metal surface using a scribing tool. The area of the defect ranged from 0.1 to 0.3 mm^2 . The sample was mounted in a Teflon sample cell and ca. 5 mL of immersion electrolyte was added. The immersion electrolyte used in the work reported here was dilute Harrison solution, an aqueous solution containing 0.35% $(\text{NH}_4)_2\text{SO}_4$ and 0.05% NaCl.

SVET Measurements

The instrument used in our laboratory was from Applicable Electronics (Forestdale, MA). The vibrating probe was an electrochemically etched Pt/Ir (80%/20%) wire coated with parylene and arced at the tip to expose the metal. To lower the impedance of the tip, a small ball of platinum black was deposited, approximately 20 μm in diameter. This probe was vibrated in two dimensions, in the z direction (perpendicular to the sample surface) at ca. 260 Hz and in the x-direction (parallel to the sample surface) at ca. 380 Hz. The vibration amplitude was approximately one tip diameter in each direction. The probe was incrementally scanned in the x-y plane at a height of 100-200 μm above the sample surface. At each increment in the scan, 2-channel phase sensitive detection at the two probe vibration frequencies permitted calculation of a current density vector representing both the magnitude and direction of current flow at that x-y position. Calibration involved generation of a known current density from a point source calibration electrode.

Typically scans were initiated within 1-2 minutes of immersion and a scan was collected every 30 minutes for the duration of the experiment. Experiment durations varied from one day to a week. Each scan was of the 2-mm x 2-mm exposed sample area and consisted of 400 data points obtained on a 20 x 20 grid.

An integration time of 1-second per point was used. Thus, a complete scan required ca. 10 minutes and was followed by a 10-minute rest period prior to the next scan. The measurements were taken at the open-circuit potential and 3-4 specimens of each sample type were prepared and scanned to assess reproducibility. The background noise in our SVET instrumentation was estimated to be $2 \mu\text{A}/\text{cm}^2$, determined from the standard deviation of the variations in current density at sufficiently large distance (ca. 1 mm) from the point source calibration electrode passing 60 nA of current.

In this report, two methods are used to display the measured current density. One method displays the current density as a 3-dimensional surface, with the z-component of the measured current density plotted as a function of the x,y position in the probe scan plane. In this format, positive and negative current densities represent anodic and cathodic regions, respectively. The other method displays current density vectors (representing current density magnitude and direction) superimposed onto an optical micrograph of the immersed sample. In all cases, the bottom edge of the optical micrograph corresponds to the x-axis of the 3-dimensional plot. This latter display permits correlation of anodic and cathodic current processes with visual features on the substrate surface.

Results and Discussion

Previous SVET Studies of ECPs

Although there have been numerous reports on the use of SVET, SRET, LEIS and related techniques for probing corrosion processes (for example, see (10) and references therein), there have been only three previous reports on the use of these techniques for probing corrosion control by ECPs (21-23). Kinlen and coworkers used the SRET to investigate the mechanism of corrosion protection by polyaniline coatings on carbon steel immersed in aerated municipal tap water (21). Pinholes were introduced into the ca. 25 μm -thick coatings down to the bare steel. Without a topcoat, sulfonic acid-doped and phosphonic acid-doped polyaniline-coated carbon steel exhibited anodic activity in the pinholes and cathodic activity on the ECP surface. With time, the pinholes were observed to passivate. With an epoxy topcoat applied over the polyaniline coating, both anodic and cathodic pinholes were observed, with behaviors that depended on the nature of the dopant. For the sulfonic acid dopants examined, the pinholes alternated between anodic and cathodic behavior while the overall current flow remained relatively constant. For the phosphonic acid dopants, there was a general decrease in current with time, indicating pinhole passivation. This difference in behavior was attributed to instability of an iron/sulfonate passive layer compared to that of an iron/phosphonate passive

layer. In control experiments, carbon steel coated with only epoxy having a single 1-mm diameter pinhole drilled through the coating to the metal surface exhibited both anodic and cathodic reactions occurring within the single defect. With five pinholes, three were cathodic and two anodic immediately after immersion and 8 hours later. The onset of corrosion was immediate and the corrosion rate did not appear to diminish over the 8-hour duration of the experiment.

In related work, Gašparac and Martin used the SRET to examine a 1-mm diameter pinhole in a 2- μm thick polyaniline coating on stainless steel (23). The coating was solvent cast in the emeraldine base form from N-methylpyrrolidone and then doped protonically by immersion in H_2SO_4 solution. Shortly after immersion in 0.01 M H_2SO_4 , anodic current (corrosion) in the pinhole was observed with reduction apparently occurring on the conducting polymer surface. After ca. 4-hours, the pinhole passivated as evidenced by the current decreasing to the noise level. This result for polyaniline-coated stainless steel is similar to that observed by Kinlen and coworkers (described above) for polyaniline-coated carbon steel (21), though different dopant ions and immersion solutions were employed in the two studies.

Our laboratory previously reported results of SVET studies of poly(3-octyl pyrrole) coatings on cold-rolled steel (immersed in 3% NaCl) and on aluminum 2024-T3 alloy (immersed in dilute Harrison solution) (22). The POP dopant was a mixture of perchlorate and paratoluene sulfonate (POP-PCPTS). For each of these metal substrates, the POP-PCPTS displayed the ability to delay the onset of corrosion within a defect for several hours. In a related study, chromated-epoxy coatings were also found to produce delays before the onset of current flow in and around the defect, though typically the delays were of shorter duration (24). In control experiments with epoxy coatings (no POP-PCPTS) on aluminum alloy and steel, the onset of corrosion within the defect was within the time required to obtain the first scan (a couple of minutes). It was suggested that the defect was protected by a mechanism involving formation and/or stabilization of a passive layer within the defect, a consequence of the ability of these coatings to render the surface potential within the defect more positive (noble). For both aluminum and steel, oxidation and reduction currents eventually ensued, and at that point the behaviors of steel and of aluminum alloy diverged.

On cold-rolled steel, an oxidation current was observed within the defect and a reduction current was spread rather uniformly across the POP-PCPTS polymer surface. This observation was similar to that described by Kinlen and co-workers for polyaniline on steel (21). It was also noted that once oxidation commenced within the defect, it was sustained for a significantly longer period of time than observed with the inert (plain epoxy) control coating. Furthermore, a more adherent corrosion product was formed in the presence of the POP coating. These observations for POP-PCPTS coated steel were similar to those

reported for chromated-epoxy coated steel (24) and indicate that active ECP coatings such as POP-PCPTS clearly alter the corrosion mechanism relative to the inert epoxy control coating.

In contrast to the behavior for steel, on POP-PCPTS coated Al 2024-T3 a significant oxidation current was never observed within the defect. Rather, only reduction current was observed in the defect and only then after a significant delay (typically ca. 1 day) from the time of initial immersion. Oxidation current was observed only at coated regions of the sample away from the defect, and from scanning electron microscopy coupled with x-ray analysis, it was determined that the oxidation process involved removal of metal from copper-rich regions of the alloy surface beneath the POP-PCPTS coating. It was suggested that the POP-PCPTS polymer provided a thermodynamic assist to the process through metal ion complexation.

In the sections that follow, we provide new SVET data on PODP-PCPTS coated Al 2024-T3, demonstrating a behavior very similar to that described above for POP-PCPTS. Next, we show that the dopant ion plays a role in the corrosion behavior of the alloy, illustrated by the differing behavior of POP-PC and POP-PTS coatings. We then report initial SVET results on Al 2024-T3 having a POP-PCPTS primer coat and a polyurethane topcoat. We conclude by providing some comments on possible mechanisms by which ECPs alter corrosion behavior.

PODP-PCPTS

The poly(3-octadecyl pyrrole) with mixed counterions of perchlorate and paratoluene sulfonate was applied to Al 2024-T3, a defect was introduced into the coating to expose bare metal and the sample was immersed in dilute Harrison solution. Figure 1 shows an optical micrograph of this sample with the defect clearly visible. The SVET detected no current flow in the defect until after 12-hours of immersion. At that point a very small oxidation process appeared at one end of the defect as shown in Figure 1 (note that the defect runs parallel to the x-axis). This oxidation current rapidly disappeared as the surface passivated and by 13.5 hours immersion there was no longer a detectable oxidation occurring in the defect (Figure 2). By way of contrast, control experiments (in which the PODP-PCPTS coating was replaced by an epoxy coating) revealed anodic and cathodic current flow in the defect within minutes of immersion and continuing for several hours, resulting in buildup of corrosion products within the defect area (24). With the PODP-PCPTS coating the defect area visible in Figure 1 remains shiny throughout the immersion period.

While the oxidation process in the defect was small and short-lived, a second oxidation process developed outside the defect after 13.5 hours immersion. As revealed in Figure 2, this oxidation was at a coated region of the

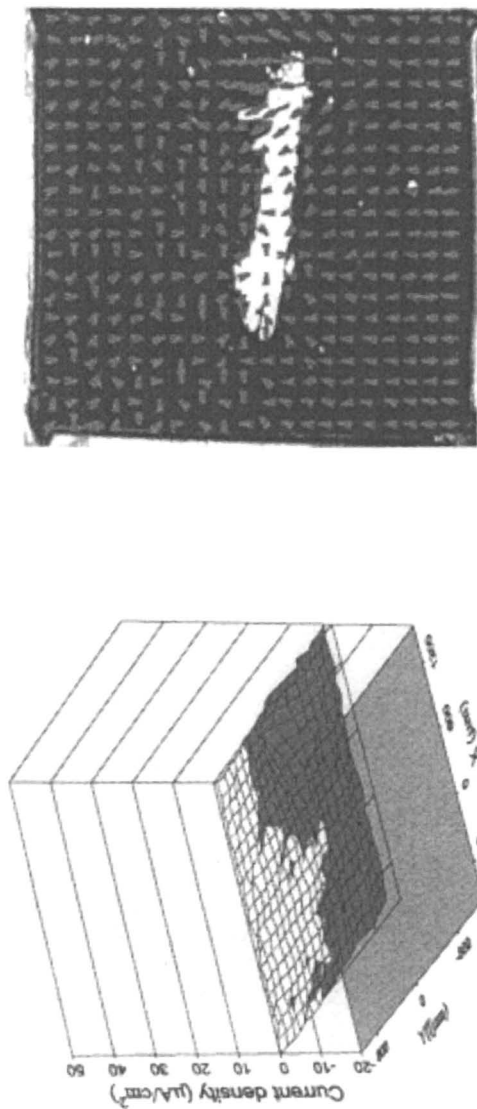


Figure 1. Current density map and optical micrograph for PODP-PCPTS on Al 2024-T3 at 12-hours immersion in dilute Harrison solution. Left: 3-dimensional representation of the z-component of the current density. Right: optical micrograph of sample with current vectors superimposed.

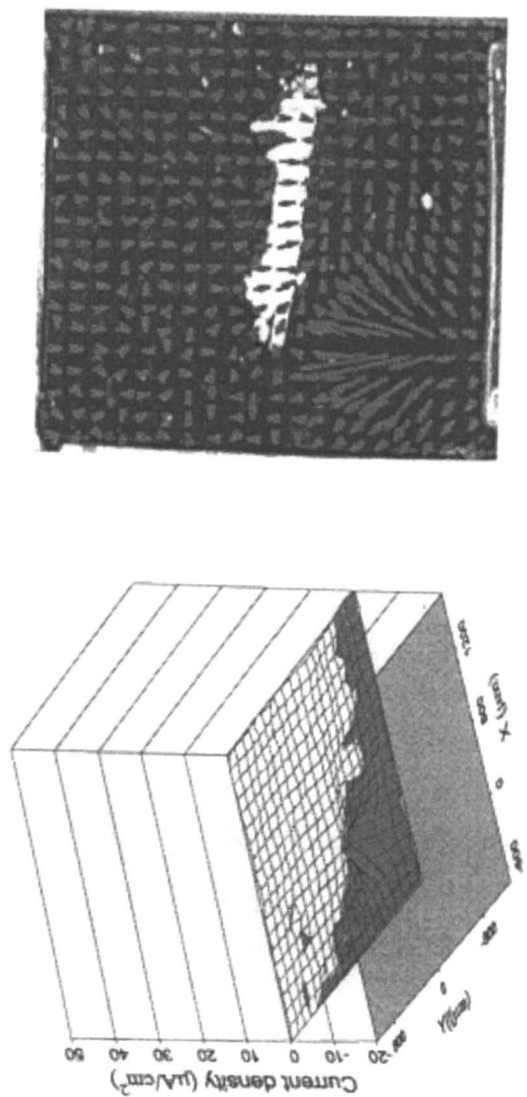


Figure 2. Current density map (left) and optical micrograph (right) for PODP-PCPTS on Al 2024-T3 at 13.5-hours immersion in dilute Harrison solution.

sample with reduction occurring primarily in the defect. The current density associated with this oxidation process increased with time, reaching several tens of $\mu\text{A}/\text{cm}^2$ at 50-hours immersion (Figure 3), at which point the reduction occurring in the defect was more evident.

As discussed in the previous section, very similar SVET results were obtained for POP-PCPTS coated Al 2024-T3 (22), where it was confirmed that the oxidation process was due to metal oxidation at Cu-rich regions of the alloy surface. The interesting question remains as to why metal oxidation occurs at coated regions and not in the exposed and more accessible defect region. One possibility is that the polymer might provide a thermodynamic assist to the process through complexation of Al^{3+} and/or Cu^{2+} . The incorporation of metal ions into polypyrrole by complexation has been reported previously (25,26). A similar argument has been suggested for polyaniline on Al 2024-T3, where X-ray photoelectron spectroscopy verified depletion of Cu from the alloy surface by the conducting polymer (27).

In any event, the consistency of these observations for several replicates of each of the two different (albeit similar) conducting polymer coatings provides strong evidence that these ECP coatings significantly alter the corrosion process of Al 2024-T3 alloy by preventing corrosion in exposed defect areas. The addition of a topcoat is expected to significantly influence the observed behavior and is the topic of a subsequent section of this chapter.

POP-PC and POP-PTS

The previously reported SVET studies of the corrosion behavior of POP-coated Al 2024-T3 utilized conducting polymer containing a mixture of dopant anions, perchlorate and p-toluene sulfonate (22). The work on PODP described in the previous section of this chapter also utilized this mixture of counterions. This particular mixture of counterions was found to give an optimum combination of film properties in earlier studies (20) and was, therefore, used in our initial corrosion studies. In this section we report results of SVET experiments on POP coatings in which these counterions have been separated, one polymer containing only perchlorate (POP-PC) and one only p-toluene sulfonate (POP-PTS). It was anticipated that the counterion might have an influence on corrosion behavior. Indeed, counterion effects have been observed in polyaniline-coated steel corrosion studies (21,28).

Indeed, interesting differences in the behavior of POP-PC and POP-PTS have been observed in our experiments. Figure 4 shows the result for POP-PTS shortly after immersion. As with the POP-PCPTS coated alloy (22), a small (few $\mu\text{A}/\text{cm}^2$) uniform oxidation current is noted in the defect immediately after immersion, perhaps reflecting the development of a protective oxide coating within the defect, as suggested in our earlier work (22). This current diminishes

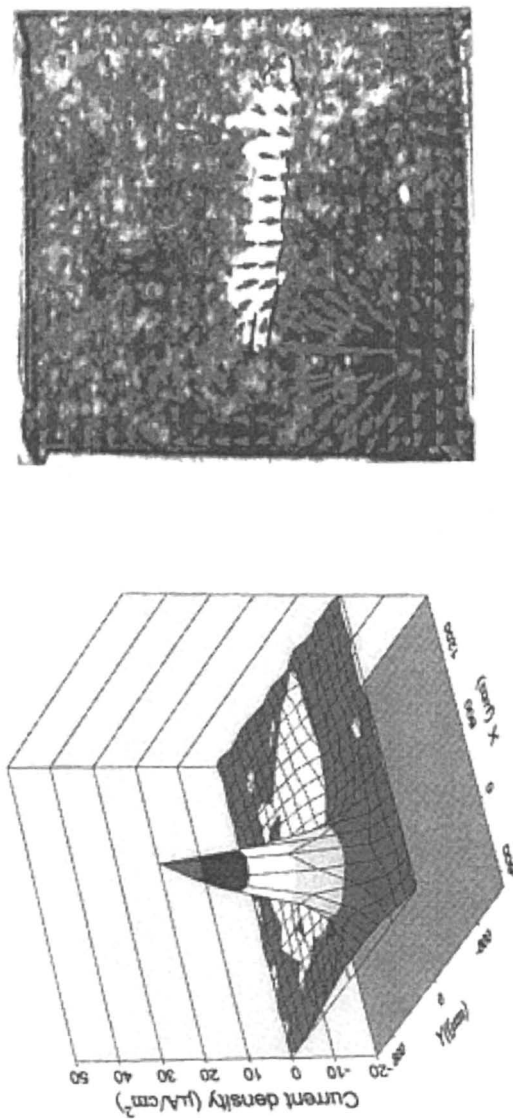


Figure 3. Current density map (left) and optical micrograph (right) for PODP-PCPTS on Al 2024-T3 at 50-hours immersion in dilute Harrison solution.

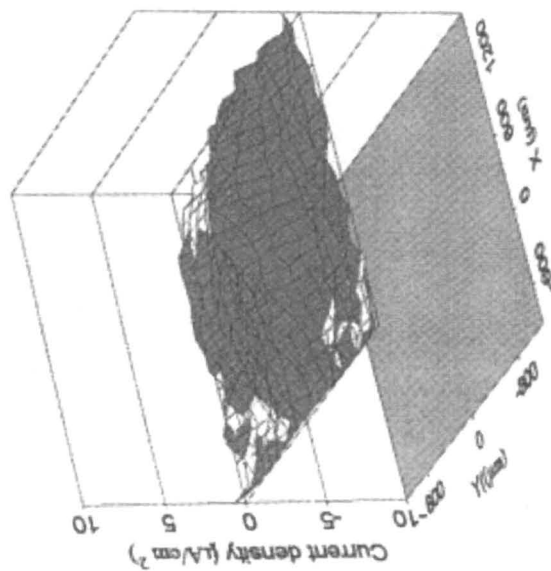


Figure 4. Current density map (left) and optical micrograph (right) for POP-PTS on Al 2024-T3 at 5-minutes immersion in dilute Harrison solution.

to below background levels within several minutes and then no further activity is observed in the defect for several hours. Eventually, after 3-days of continuous immersion (the typical delay observed with this polymer); a significant oxidation is observed at a coated region of the sample, with reduction spread rather uniformly across the remaining surface (Figure 5). Again, this behavior is similar to that observed with the POP-PCPTS coated alloy (e.g., see Figure 7 of reference (22)), and the oxidation is attributed to alloy oxidation at the metal-coating interface. The defect remains shiny and free of corrosion product through the immersion period (Figure 5).

In contrast to the above behavior for POP-PTS, the POP-PC coated alloy exhibited a considerably shorter delay before the onset of current flow, typically ca. 8-hours compared to ca. 76-hours for POP-PTS. We note, however, that the film forming properties of the POP-PC were somewhat poorer than that of POP-PTS and uniform coatings were difficult to achieve. Figure 6 displays the current density maps for two different samples (one at 6-hours and one at 10.5 hours immersion). In each case, the oxidation and reduction currents were confined primarily to the defect (which runs through the center of each sample parallel to the x-axis), although some reduction also appears on the polymer surface of one of the samples (see the left map of Figure 6).

At this stage, we can only speculate about the reasons for the differences in behavior of these two polymers. Two possibilities are 1) differences in polymer equilibrium redox potentials and 2) specific counterion effects. It is well established that the redox behavior of an ECP is coupled to motions of ions required to maintain electroneutrality within the polymer, and variation of the electrochemical behavior of an ECP with counterion is expected (29-32). The cyclic voltammograms of the various polymers deposited on a platinum electrode are displayed in Figure 7, where it is observed that the half-peak potentials for reduction follow the order POP-PC > POP-PCPTS > POP-PTS. The open circuit potentials of the coated alloy follow this same order, ranging from 100 mV to 200 mV more noble (positive) than the uncoated alloy. We have previously reported an ennobling of active metals by ECPs (33). It is interesting that POP-PC has the most positive potential but the shortest delay (ca. 6 hr.) to onset of current flow. POP-PTS has the least positive potential and the longest delay (76 hr.). POP-PCPTS exhibits an intermediate potential and also an intermediate delay (ca. 24 hr.) (22). The equilibrium potential of the ECP should certainly be an important factor governing the interaction between the ECP and the active metal. However, the order observed here seems counterintuitive, since one might expect that the ECP with the more positive potential (thus, greater ennobling ability) would be the most effective at delaying the onset of corrosion. Work is underway in our laboratory to better understand the role of ECP equilibrium potential in corrosion control.

Specific counterion effects in corrosion control by ECPs have been reported previously (21,28,34) and may be responsible for the differences in behavior observed among the ECPs used in this work. For example, p-toluenesulfonate is expected to complex more strongly with Al ions than the weakly coordinating

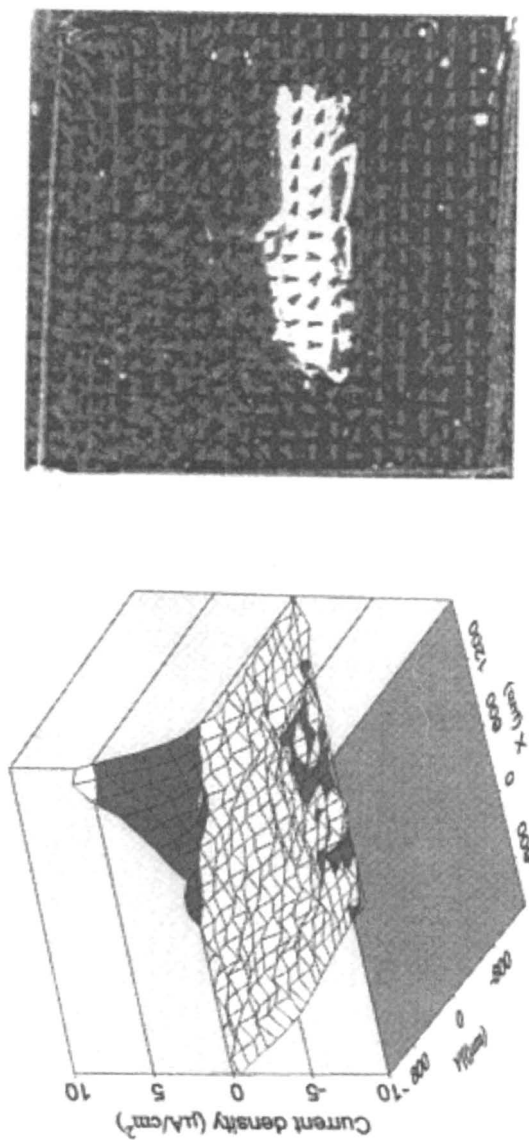


Figure 5. Current density map (left) and optical micrograph (right) for POP-PTS on Al 2024-T3 at 76-hours immersion in dilute Harrison solution.

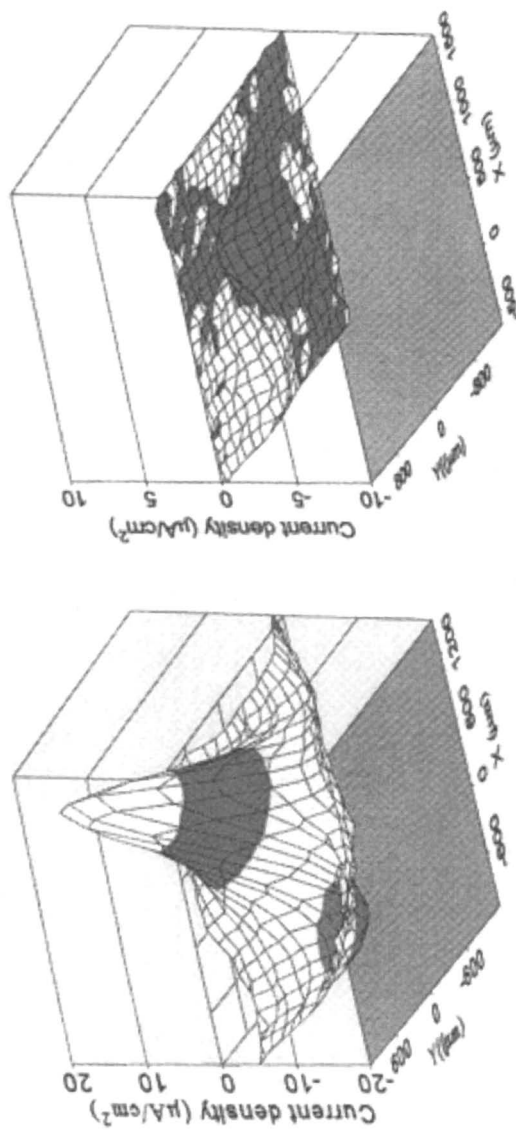


Figure 6. Current density maps for two samples of POP-PC on Al 2024-T3 at 6-hours (left) and 10.5-hours (right) immersion.

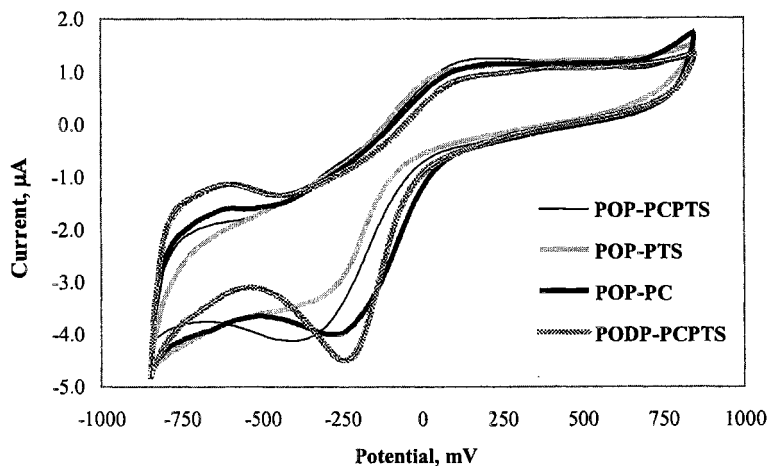


Figure 7. Cyclic voltammograms of four electroactive conducting polymers deposited on a 1.6 mm diameter Pt electrode. Scan rate: 50 mV/sec. Reference electrode: saturated Ag/AgCl.

perchlorate ion, possibly leading to increased passivation of exposed metal in the defect. The observation that no oxidation current occurred in defects protected by p-toluenesulfonate containing polymers (POP-PCPTS, POP-PTS and PODP-PCPTS) is consistent with this hypothesis. X-ray photoelectron spectroscopy experiments are being initiated to further explore this conjecture. Finally, we note that the film formation characteristics of ECP coatings will most certainly depend on the nature of the counterion, which accounts for up to 30% (or more) of the mass of the coating (29). Such variations in film properties (which, in turn, can influence such things as film conductivity, adhesion/cohesion, and redox behavior) may also contribute to the differences observed among the ECPs of this work.

POP-PCPTS with Polyurethane Topcoat

All of the experiments described in the previous sections of this chapter were conducted on ECP-coated alloy without a topcoat. Such samples under constant immersion typically fail within a few weeks, but then so do most primers without a protective topcoat. With a polyurethane topcoat, six out of six POP-PCPTS coated Al 2024-T3 samples have sustained nearly three years of constant immersion without coating failure (35). In this section we describe preliminary results of SVET experiments on such samples.

First we describe a control experiment where a defect was scribed into a polyurethane coating applied directly on Al 2024-T3 alloy. After immersion in dilute Harrison solution, the sample was scanned every 20-minutes by the SVET until corrosion activity was detected in the defect area. The polyurethane coating is an excellent barrier coating, especially during the early stages of immersion, and no current flow above the coating was expected or observed. After a time delay that ranged from a few hours to ca. a day for triplicate control samples, redox activity was observed in the defect of each control sample. Figure 8 shows one of these control samples at 6-hours immersion, at which time substantial current was flowing. For this sample, the current was first detected after four hours immersion, significantly longer than observed for epoxy-coated control samples (24) where current in the defect was observed within minutes. This longer delay to initial current is attributed to the corrosion inhibitors that the manufacturer formulates into this polyurethane aircraft coating, including Sicorin RZ (a corrosion inhibitor based on an organic nitro compound) and zinc phosphate pigments. Further experiments are under way using epoxy topcoats containing no corrosion inhibitors.

Three replicate samples of a POP-PCPTS coated alloy with a polyurethane topcoat were examined by SVET. Recall that without a topcoat, no significant oxidation was ever observed in the defect. Instead, after a significant delay, oxidation was observed under the POP-PCPTS coating, manifested by a current flow through and above the coating. With the addition of a good barrier topcoat, this under coating oxidation should be prevented, since direct current flow to the electrolyte would then have to pass through the highly resistive topcoat, and it was expected that current flow would then be forced to occur only within the defect area. The samples were scanned by the SVET every 30-minutes during the first day of immersion and every hour during subsequent days for a period of one week. No oxidation current was detected in the defect of these samples. The scan shown in Figure 9 was at 6.5-days immersion. The defects remained shiny throughout the immersion period. As an aside, we note here that a shiny defect does not necessarily mean no corrosion is occurring. Indeed, we have observed defects that remained shiny for many hours of immersion while the SVET indicated intense oxidation current flowing at the defect (22).

Although there was considerable variability in the time at which current was first observed for the control samples, current flow was typically observed within a day. For topcoated POP-PCPTS samples, no significant current flow was observed within the duration of the observation period (ca. 7 days). These results are preliminary and additional replicate measurements will be made to further ensure that we are observing representative behavior. As noted above, we also intend to eliminate the complication of corrosion inhibitors in the topcoat. Nevertheless, the results suggest that the POP-PCPTS coating is able to delay the onset of corrosion in a defect and are consistent with the observation that this coating arrested blister development in long-term immersion studies (35).

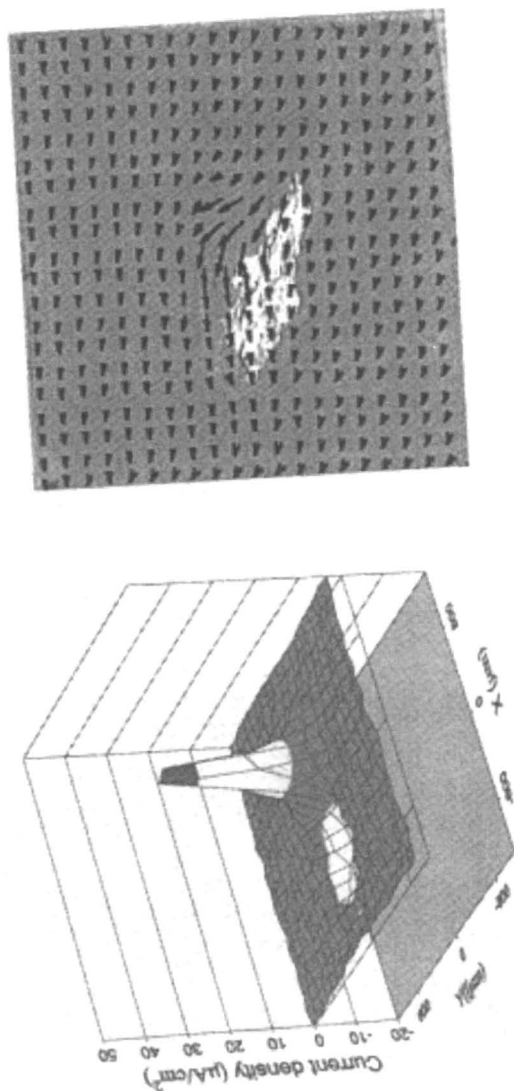


Figure 8. Current density map (left) and optical micrograph (right) for a polyurethane coating on Al 2024-T3 at 6-hours immersion in dilute Harrison solution.

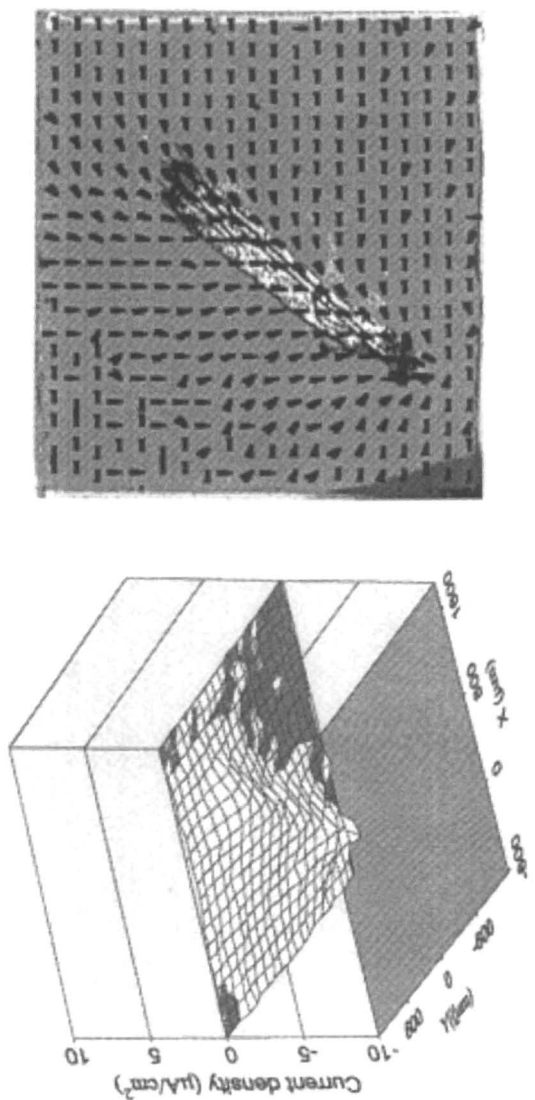


Figure 9. Current density map (left) and optical micrograph (right) for a POP-PCPTS coating with a polyurethane topcoat on Al 2024-T3 at 6.5-days immersion in dilute Harrison solution.

Comments on Corrosion Protection by ECPs

We conclude this chapter with some brief comments on possible mechanisms by which ECPs alter the corrosion behavior of active metals. This discussion will pertain primarily to coatings consisting of undiluted conducting polymer, that is, the ECP is not blended with any other component such as a binder. However, such blended systems have shown promising corrosion control properties (2,3), and some of the concepts discussed here might also apply to certain of these coatings.

First we note that ECPs are not good barrier coatings. Indeed, these polymers have high ionic content that facilitates ingress of water and electrolyte ions. Without a topcoat, these coatings do not survive long, but then neither do most primer coatings. The topcoat plays a critical role in sustaining the protective properties of the ECP coating and may alter the interactions between ECP and active metal, as demonstrated in the previous section.

The ECP coating, like the active metal to which it is applied, is electronically conductive. This has important implications, since the two electronic conductors couple when brought into contact with each other. The result is a modification of the average energy of available electrons, the Fermi level, in each conductor. The Fermi energy of electrons in a phase α is the same as the electrochemical potential of electrons in the phase and is given by

$$E_F^\alpha = \bar{\mu}_e^\alpha = \mu_e^{\circ\alpha} - F\phi^\alpha$$

where

E_F^α is the Fermi energy of electrons in phase α

$\bar{\mu}_e^\alpha$ is the electrochemical potential of electrons in phase α

$\mu_e^{\circ\alpha}$ is the standard chemical potential of electrons in phase α

ϕ^α is the electrical potential of phase α

F is the Faraday constant.

Thus, the more negative the potential of a phase, the more positive the Fermi energy and the more easily electrons may be extracted from the phase. Active metals such as Al and Fe have potentials that are considerably negative of those of p-doped (i.e., partially oxidized) ECPs. When a metal such as aluminum and an ECP such as polypyrrole are brought into contact, electrons flow from metal to the ECP, lowering the Fermi level of the metal and raising that of the ECP until the Fermi levels of the two materials are equal (36). The extent of change

in Fermi energy in each material depends on a number of factors, including the number of charge carriers available in each of the materials. From this point of view, a thick ECP coating is expected to lower the Fermi level of an active metal more than a thin coating. In any case, the Fermi level of the metal is lowered (i.e., its potential raised, as observed experimentally) so that extraction of electrons from the metal becomes more difficult. The metal becomes more noble-like, and reduction reactions on exposed metal surfaces are impeded.

Related to the above purely electronic effect is the fact that ECPs are oxidants towards active metals. This means that even greater flow of electrons from metal to polymer is possible beyond that attributed to the electronic effect discussed above. Thus, ECPs are capable of forming and/or stabilizing oxidized (passive) layers at the ECP/metal interface. There is very likely an optimum range of ECP potentials for stabilizing (passivating) any given active metal alloy. If the ECP is too strong an oxidant, runaway oxidation (corrosion) of the metal may occur. Too weak an oxidant may lead to insufficient passivation. The metal complexation properties of the polymer may also play an important role in interface chemistry, as discussed earlier. Work in progress in our laboratory is examining a series of polythiophene coatings having a range of equilibrium potentials spanning nearly a volt. It is anticipated that this work will provide insight into the role of polymer equilibrium potential on corrosion behavior.

Because the ECP coating is electronically conductive, the reduction reaction, which normally is confined to the metal surface, may occur at the ECP coating surface instead. This has been verified by SVET measurement, first by Kinlin and coworkers for polyaniline on steel (21) and subsequently by He and coworkers for POP-PCPTS on steel (22). The implications of these observations are two-fold. First, the oxidized state of the ECP can be maintained as a result of its ability to reduce oxygen and/or shuttle electrons from the metal to oxygen (22). Second, cathodic delamination of a coating is generally associated with a high local hydroxide concentration generated by the reduction reaction occurring at the coating-metal interface (37). Thus, removal of the reduction reaction from the metal interface may be an important aspect of the mechanism by which ECP coatings extend the lifetime of the complete coating system (38).

Finally, the ECP can act as a reservoir for corrosion inhibiting ions, releasing them as a result of redox reaction between the ECP and metal or perhaps through ion exchange processes. By incorporating appropriate counterions during polymer synthesis (or, in the case of polyaniline, by dedoping the polymer followed by redoping with the desired counterion-containing acid), a variety of corrosion inhibiting ions can be explored. To date, there have been only a couple of systematic studies of this type (21,28). As

noted in an earlier section of this chapter, the counterion can influence other properties of the polymer such as its equilibrium (redox) potential and film-forming properties. Separation of these coupled effects will be challenging.

In summary, it is clear that coatings based on electroactive conducting polymers alter the corrosion behavior of active metals, a consequence of the electronic, redox and perhaps complexing properties of such polymers. The trick is to design or tune these properties of the conducting polymer so that they alter the corrosion mechanism of a particular active metal or alloy in the most desirable way. Each active metal or alloy will likely require a tailored ECP coating system for optimum corrosion protection. Much work remains to be done to better understand how to design such ECP coatings.

Conclusions

Local electrochemical methods such as the scanning vibrating electrode technique are valuable tools in corrosion research. These methods are capable of providing details and insights into the mechanism(s) by which electroactive conducting polymers alter the corrosion behavior of active metals, details that are not obtainable from traditional global techniques. To date these local techniques have found limited application in conducting polymer research. However, the availability of commercial instrumentation for performing local electrochemical measurements combined with the increasing number of reports illustrating the power of these techniques in conducting polymer research will almost certainly lead to a substantial increase in their use in the future.

Acknowledgments

This work was supported by the Air Force Office of Scientific Research, Grant Nos. F49620-96-1-0284, F49620-99-1-0283 and F49620-97-1-0376 (AASERT), North Dakota State University. GGW acknowledges the continued support of the Australian Research Council in the form of a Senior Research Fellowship.

References

1. Cohen, S. M. *Corrosion* **1995**, *51*, 71-78.
2. Tallman, D. E.; Spinks, G.; Dominis, A.; Wallace, G. G. *J. Solid State Electrochem.* **2002**, *6*, 73-84.
3. Spinks, G. M.; Dominis, A. J.; Wallace, G. G.; Tallman, D. E. *J. Solid State Electrochem.* **2002**, *6*, 85-100.

4. Bard, A. J.; Fan, F. R. F.; Kwak, J.; Lev, O. *Anal. Chem.* **1989**, *61*, 132-138.
5. Isaacs, H. S.; Kendig, M. W. *Corrosion* **1980**, *36*, 269-274.
6. Wittmann, M. W.; Leggat, R. B.; Taylor, S. R. *J. Electrochem. Soc.* **1999**, *146*, 4071-4075.
7. Voruganti, V. S.; Luft, H. B.; Degeer, D.; Bradford, S. A. *Corrosion* **1991**, *47*, 343-351.
8. Jaffe, L. F.; Nuccitelli, R. *J. Cell. Biol.* **1974**, *64*, 614-628.
9. Isaacs, H. S. *Corr. Sci.* **1988**, *28*, 547-558.
10. Taylor, S. R.; Hillier, A. C.; Seo, M. In *Localized In-Situ Methods for Investigating Electrochemical Interfaces*; Taylor, S. R., Hillier, A. C., Seo, M., Eds.; The Electrochemical Society, Pennington, NJ, 2000; Vol. ECS Proceedings PV99-28.
11. Isaacs, H. S.; Vyas, B. In *Electrochemical Corrosion Testing*; Mansfield, F., Bertocci, U., Eds.; American Society for Testing and Materials: Philadelphia, PA, 1981; Vol. ASTM STP-727, pp 3-31.
12. Lillard, R.; Krugar, J.; Tait, W. S.; Moran, P. J. *Corrosion* **1995**, *51*, 251-259.
13. Sargeant, D. A. *Corrosion Prevention and Control* **1997**, *44*, 91-105.
14. Bayet, E.; Garrigues, L.; Huet, F.; Keddami, M.; Ogle, K.; Stein, N.; Takenouti, H. In *Localized In-Situ Methods for Investigating Electrochemical Interfaces*; Taylor, S. R., Hillier, A. C., Seo, M., Eds.; The Electrochemical Society, 2000; Vol. ECS Proceedings PV99-28, pp 200-211.
15. Lillard, R. S.; Moran, P. J.; Isaacs, H. S. *J. Electrochem. Soc.* **1992**, *139*, 1007-1012.
16. Bayet, E.; Huet, F.; Keddami, M.; Ogle, K.; Takenouti, H. *J. Electrochem. Soc.* **1997**, *144*, L87-90.
17. Bayet, E.; Huet, F.; Keddami, M.; Ogle, K.; Takenouti, H. *Electrochimica Acta* **1999**, *44*, 4117-4127.
18. Sekine, I.; Yuasa, M.; Tanaka, K.; Tsutsumi, T.; Koizumi, F.; Oda, N.; Tanabe, H.; Nagai, M. *Shikizai Kyokaishi* **1994**, *67*, 424-430.
19. Sekine, I. *Prog. Org. Coatings* **1997**, *31*, 73-80.
20. Ashraf, S. A.; Chen, F.; Too, C. O.; Wallace, G. G. *Polymer* **1996**, *37*, 2811-2819.
21. Kinlen, P. J.; Menon, V.; Ding, Y. *J. Electrochem. Soc.* **1999**, *146*, 3690-3695.
22. He, J.; Johnston-Gelling, V.; Tallman, D. E.; Bierwagen, G. P.; Wallace, G. G. *J. Electrochem. Soc.* **2000**, *147*, 3667-3672.
23. Gašparac, R.; Martin, C. R. *J. Electrochem. Soc.* **2001**, *148*, B138-B145.
24. He, J.; Johnston-Gelling, V.; Tallman, D. E.; Bierwagen, G. P. *J. Electrochem. Soc.* **2000**, *147*, 3661-3666.
25. Inoue, M. B.; Nebesny, K. W.; Fernando, Q.; Castillo-Ortega, M. M.; Inoue, M. *Synthetic Metals* **1990**, *38*, 205-212.

26. Deronzier, A.; Moutet, J.-C. *Coordination Chemistry Reviews* **1996**, *147*, 339-371.
27. Epstein, A. J.; Smallfield, J. A. O.; Guan, H.; Fahlman, M. *Synthetic Metals* **1999**, *102*, 1374-1376.
28. Dominis, A.; Spinks, G. M.; Kane-Maguire, L. A. P.; Wallace, G. G. *Polymer Preprints* **2000**, *41*, 1748-1749.
29. Wallace, G. G.; Spinks, G. M.; Teasdale, P. R. *Conductive Electroactive Polymers*; Technomic Publishing Company, Inc.: Lancaster, PA, 1997.
30. Zhou, Q. X.; Kolaskie, C. J.; Miller, L. L. *J. Electroanal. Chem. Interfacial Electrochem.* **1987**, *223*, 283-286.
31. Kaufman, J. H.; Kanazawa, K. K.; Street, G. B. *Phys. Rev. Lett.* **1984**, *53*, 2461-2464.
32. Curtin, L. S.; Komplin, G. C.; Pietro, W. J. *J. Phys. Chem.* **1988**, *92*, 12-13.
33. Tallman, D. E.; Pae, Y.; Bierwagen, G. P. *Corrosion* **2000**, *56*, 401-410.
34. Uehara, K.; Ichikawa, T.; Serikawa, T.; Yoshikawa, S.; Ehara, S.; Tsunooka, M. *Thin Solid Films* **1998**, *322*, 198-205.
35. Johnston Gelling, V.; Wiest, M. M.; Tallman, D. E.; Bierwagen, G. P.; Wallace, G. G. *Prog. Org. Coatings* **2001**, *43*, 149-157.
36. Leising, G.; Tasch, S.; Graupner, W. In *Handbook of Conducting Polymers*; 2nd ed.; Skotheim, T. A., Elsenbaumer, R. L., Reynolds, J. R., Eds.; Marcel Dekker, Inc.: New York, 1998; pp 847-880.
37. Wicks, Z. W., Jr.; Jones, F. N.; Pappas, S. P. In *Organic Coatings: Science and Technology*; 2nd ed.; Wiley-Interscience: New York, 1999; pp 131-133.
38. Kinlen, P. J.; Silverman, D. C.; Jeffreys, C. R. *Synthetic Metals* **1997**, *85*, 1327-1332.

Chapter 16

Solvent-Free Polyaniline Coating for Corrosion Prevention of Metal

Xianhong Wang, Jinlong Lu, Ji Li, Xiabin Jing, and Fosong Wang

Polymer Material Engineering Laboratory and Open Laboratory of Polymer Chemistry, Changchun Institute of Applied Chemistry, Chinese Academy of Sciences, Changchun 130022, Peoples Republic of China

Solvent free emeraldine base/epoxy resin coating was prepared employing liquid aliphatic polyamine as the “solvent” for emeraldine base(EB) as well as the “hardener” for epoxy resin(EPR). EB/EPR Coatings with EB loading of 1-2wt% showed good corrosion prevention on mild steel either in 0.1M HCl solution or in 3.5wt% NaCl solution. Electrochemical impedance spectra analysis found new elements in the equivalent circuits due to the introduction of EB into the coating. Quasi-periodic change in the oxidation degree of EB was found when EB reacted with iron powder. This was a sound evidence that EB acted as the “catalyst” for the iron to form a dense iron oxide layer. Therefore, it was reasonable that even the EB/EPR coating with very low EB loading exhibited long term corrosion prevention effect on mild steel.

Introduction

Recently, intrinsically conducting polymers like polyaniline have been demonstrated to be promising corrosion prevention materials for mild steel(1,2,3). Both EB and emeraldine salt(ES) exhibit corrosion prevention properties in lab studies, but they are difficult to process in the solvents widely acceptable in the coating industry. This is more serious with EB. Since only very strong oxidative acid like concentrated sulfuric acid, or very strong polar solvent like N-methylpyrrolidone(NMP) or dimethylacetamide, could be used to dissolve or disperse EB(4). These solvents are difficult to remove since they have high boiling point, and therefore, they are not welcome to the coating industry. Even though sometimes aniline oligomer was used for the same purpose in place of EB, the solvent was still NMP(5). Recently, Wei *et al.* successfully employed amine capped aniline oligomer as anti-corrosion agent where the oligomer itself was the hardener of epoxy resin, however, this idea was only suitable for aniline oligomer(6).

Recently, a solvent free method was developed in this lab, where liquid aliphatic polyamine-tetraethylene pentaamine was used as the "solvent" for EB as well as the hardener for epoxy resin(EPR). Corrosion prevention coating free of organic solvent was therefore prepared(7,8). In the context, electrochemical impedance spectra technique, UV-vis spectra and surface morphology studies were used to clarify why this coating displayed good corrosion prevention on mild steel, even with very low EB loading.

Experimental

EB was prepared according to a patent technique developed by this group(9). Ammonium persulfate in 1N HCl solution was dropped into aniline/water/acetone/1N HCl solution to initiate the polymerization, the resultant precipitate was compensated by ammonia and dried under vacuum to obtain EB.

Liquid organic polyamine like tetraethylene pentaamine(TEPA) was used as

a solvent of polyaniline, at room temperature EB could be dissolved in tetraethylene pentaamine to 20wt% without gelation. The EB/TEPA solution was mixed with epoxy resin where TEPA was stoichiometrically used as hardener of epoxy resin.

The intrinsic viscosity of EB in NMP after the EB/TEPA solution was stored for different time was obtained as follows. The EB/TEPA solution was stored at 20°C under ambient atmosphere, it was then dropped into large quantity of 1M HCl solution. The precipitate was washed with portions of distilled water till neutral, compensated by 0.5M ammonia, and subsequently washed with portions of water, ethanol, and then dried at 40°C under reduced pressure for 48h. The intrinsic viscosity of the dried polyaniline in NMP solution was measured at 30°C using Ubbelohde viscometer.

The corrosion parameters, corrosion voltage($E_{(t=0)}$), corrosion current(I_{corr}) and polarized resistance(R_p), were obtained from related Tafel curves. Electrochemical impedance spectroscopy was recorded on a Solartron 1255 Impedance Analyzer, where the equivalent circuit was automatically given.

UV-vis spectra of various polyanilines in NMP were recorded on a Cary 50 UV-vis Spectrometer at 25°C.

Results and Discussion

Preparation of EB/TEPA Solution and EB/EPR Coating

Calculated amount of EB was dissolved in TEPA, deep blue solution with EB concentration as high as 20wt% was obtained without gelation. As indicated from the significant change in the intrinsic viscosity of EB in NMP, strong interaction between EB and TEPA was confirmed. Table 1 listed the change of intrinsic viscosity of EB after the EB/TEPA solution was stored for different

period. It was 0.49 dl/g at the beginning, and decreased to 0.42dl/g after 240h. It further decreased to 0.21 after 720h. The decrease of the intrinsic viscosity of EB with the increase of storage time clearly indicated that EB was degraded by TEPA during storage.

Table 1. Intrinsic viscosity of EB for different storage time

Storage time(h)	0	120	240	480	720
Intrinsic viscosity(dl/g)	0.49	0.48	0.42	0.37	0.21

NOTE: The intrinsic viscosity was measured at 30°C in NMP solution.

Fortunately, when the EB/TEPA solution was stored at 20°C, the degradation was not significant during the first 120h. Furthermore, the degradation reaction was stopped when the solution was added into epoxy resin, where TEPA acted as hardener of epoxy resin. Therefore, the blending of EB/TEPA solution with epoxy resin was carried out within 24h after the EB/TEPA solution was prepared, which was quite practical a method to avoid the degradation reaction of EB.

When controlled amount of EB/TEPA solution and liquid EPR were blended, TEPA acted as hardener for EPR and reacted with EPR stoichiometrically, no volatile compound evolved during the whole process. Therefore, a “solvent” free method was developed for the EB/EPR coating. Currently, EB/EPR coatings with EB loading from 0 to 2wt% were available by adjusting the molar ratio of EB, TEPA and EPR.

Corrosion Prevention behavior of EB/EPR Coating

The EB/EPR blending solution was cast on a pretreated 5cm x 5cm mild steel panel (first polished by 600 grit polishing paper, followed by thoroughly washing with portions of distilled water, ethanol and acetone, and then dried at 80°C for 4h). The thickness of EB/EPR coating was about 150-180µm. The coating was then pinned to make a hole in 1mm of diameter for electrochemical

test. The corrosion parameters were obtained from corresponding Tafel curves in different media. Table 2 lists some of the important corrosion parameters.

Table 2 Some Important Corrosion Parameters of EB/EPR Coated Mild Steel in 3.5wt% NaCl and 0.1N HCl solution.

EB, wt%	Corrosion potential ($E_{(t=0)}$, V)	corrosion current (I_{corr} , μA)	polarized resistance (R_p , $\text{k}\Omega$)
3.5wt% NaCl			
0	-0.541	0.102	337.8
1.0	-0.387	0.023	1430.0
2.0	-0.562	0.034	1872.0
0.1N HCl			
0	-0.574	29.18	9.86
1.0	-0.655	0.163	259.1
2.0	-0.613	3.06	30.52

Table 2 shows that the corrosion potential increases by several times and the corrosion current decreases by several times upon addition of EB into the epoxy resin, even though the EB content is only about 1wt%. Therefore, the EB/EPR coating is effective in corrosion protection on mild steel both in 3.5wt% NaCl and 0.1N HCl solution even under very low EB loading. Furthermore, when the EB loading in EB/TEPA coating is over 1wt%, the corrosion protection behavior of the coating was not improved, neither in diluted acid solution nor in aqueous NaCl solution. One possible explanation may be from the morphology of the blends. Generally, as a hardener of the epoxy resin, the loading of TEPA in epoxy resin should be below 10wt% to assure good mechanical property of the final coating. Since the maximum concentration of EB/TEPA solution was about 20wt%, the EB loading in the EB/EPR coating was below 2wt%. In fact, defect (coarse film or porous film) was formed in the final EB/EPR coating when higher concentration of EB/TEPA solution was used, which was not beneficial for good corrosion prevention performance.

The surface morphology of EB/EPR coating was studied by SEM technique. Both the film surfaces of epoxy resin and EB/EPR coating (EB loading of 1wt%) were subjected to NMP extracting, the SEM images of the

treated film were shown in Figure 1. There was no significant change on the epoxy resin surface before and after NMP extracting, indicating that epoxy resin could withstand the NMP itching. However, a fibrous network appeared on the EB/EPR coating surface after NMP extracting. Since EB was soluble in NMP, this network was attributed to the EB rich phase in the blends. Such good network was a sound evidence for that EB and EPR was blended homogeneously, which was responsible for the good corrosion protection behavior of the EB/EPR coating even though the EB loading was as low as 1.0 wt%.

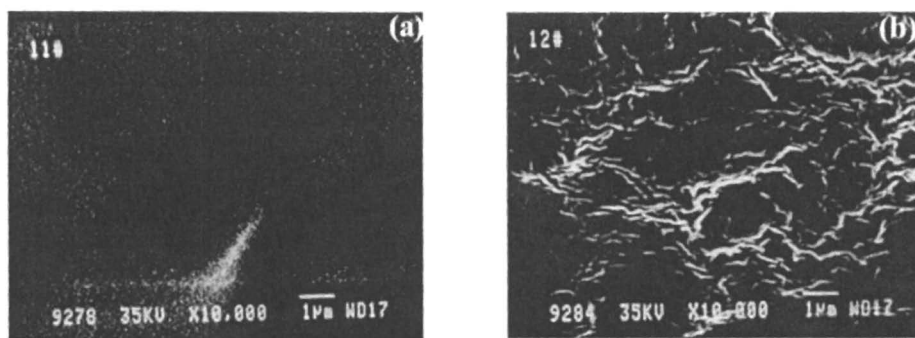


Figure 1. Scanning electron micrograph(SEM) images of the surface of EPR(a) and EB/EPR(1.0wt%)(b), the surface was extracted by NMP prior to SEM experiment.

As shown in Figure 2, Nyquist plots of Epoxy resin and EB/EPR coating from the Electrochemical Impedance Spectroscopy(EIS) were used to evaluate the corrosion prevention property of corresponding coating in 0.1M HCl solution.

The semicircle radius in high and low frequency zone from the Nyquist plots showed great difference between EPR coating and EB/EPR coating. It was about 10^5 and 10^4 for EB/EPR coating for low and high frequency zone, respectively, whereas it was only 10^3 and 10^2 for epoxy resin coating for low and high frequency zone, respectively. The increase of the semicircle radius by several orders of magnitude did indicate that the improvement of corrosion

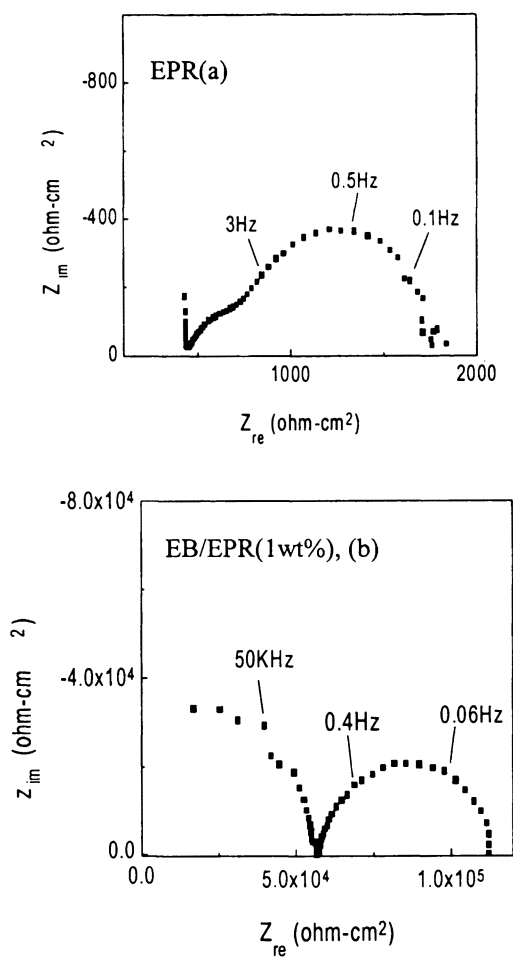


Figure 2. Nyquist plots of EPR and EB/EPR coatings on mild steel in 0.1M HCl for 8 weeks,
(a) EPR coating; (b) EB/EPR coating, EB loading was 1wt%.

prevention effect, since the ion permeation through the coating was reduced with increasing semicircle radius. Moreover, the Z_{\max} of pure EPR coating was only $1.8 \times 10^3 \text{ ohm}\cdot\text{cm}^2$, whereas it increased to $5.0 \times 10^5 \text{ ohm}\cdot\text{cm}^2$ for EB/EPR coating, further indicating that the corrosion prevention property of the EB/EPR coating was greatly improved even in very low EB loading.

The equivalent circuits of the above Nyquist plots are shown in Figure 3. Where C_{ol} was the oxide layer capacitance, R_s was the solution resistance, C_{dl} was the double layer capacitor, Z_w was the Warburg impedance, R_{pore} was the pore resistance of corresponding coating, R_{ol} was the oxide layer resistance, and R_{ct} was the electrochemical charge transfer resistance.

As shown in Figure 3, new elements, oxide layer resistance and oxide layer capacity, exist in the equivalent circuit of EB/EPR coating, which are a clear contrast to the pure EPR coating. These new elements can raise the total impedance of the coating. In fact, compared with the pure EPR coating, the EB/EPR coating with EB loading of about 1.0wt% displayed 2-3 orders of magnitude increase in the impedance. This was another good evidence for the effective corrosion protection behavior of the EB/EPR coating, mainly due to introduction of EB in the coating.

Interaction of polyaniline and iron

The important corrosion parameters from Tafel curves and equivalent circuits from electrochemical impedance spectra have demonstrated that EB/EPR coating was quite effective for corrosion prevention on mild steel, even in very low EB loading. However, the extremely low loading of EB was really amazing. In the following, possible explanation will be given mainly based on the study of interaction between EB and Fe.

Reduced iron powder was stirred with EB(1/10 in mole ratio of EB to Fe) in aqueous solution or 3.5wt% NaCl solution for certain time at room temperature, the oxidation degree of EB was determined by UV-vis spectra in EB/NMP solution. Figure 4 shows the time dependence of the relative intensity of absorption band of 330nm to 630nm. Generally, the absorption band at 630nm is characteristic of quinoid content of polyaniline, whereas that at 330nm is

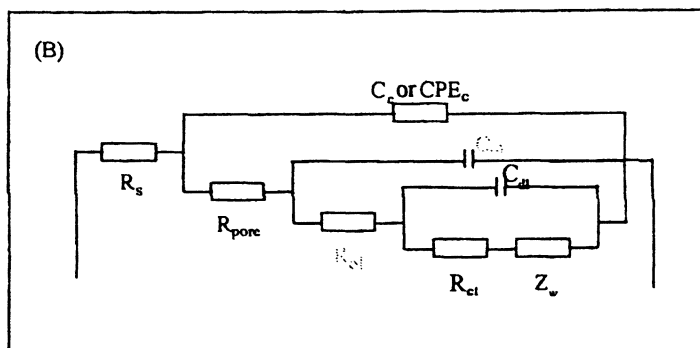
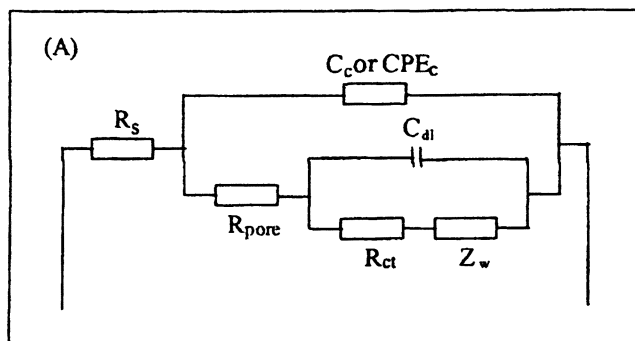


Figure 3. Equivalent circuits of EPR coating(A) and EB/EPR coating(B) coated mild steel in 0.1M HCl aqueous solution.

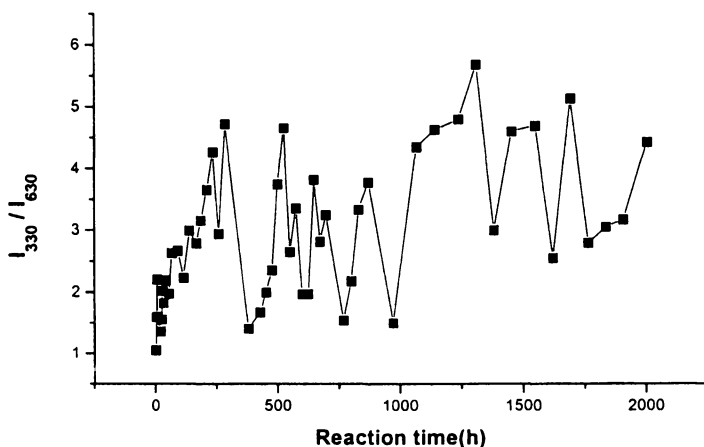


Figure 4. Time dependence of I_{330}/I_{630} in UV-vis spectra, EB/10 Fe in NaCl aq. Solution at room temperature.

characteristic of benzoid unit of polyaniline, and the relative intensity of 330nm to 630nm (I_{330}/I_{630}) may reflect the oxidation change of polyaniline.

During the first 250h, I_{330}/I_{630} increased from 1.1 to 4.8, indicating that the oxidation degree of polyaniline decreased significantly at this stage. However, it was very interesting to observe that I_{330}/I_{630} dropped after 250h, it became 1.3 at 400h, indicating that the oxidation degree of polyaniline increased quickly at this stage. It was more interesting to find that I_{330}/I_{630} started to increase soon, it was 4.7 at 500h. After that, again it dropped to 1.7 at 600h. Generally, a stable reversible change in oxidation degree of polyaniline with a period of about 200-250h was observed after 500h. Therefore, a “quasi-reversible” change of oxidation degree of polyaniline was observed for the first time. This quasi-reversibility of the oxidation degree of polyaniline was very important for the corrosion protection behavior of EB, the reason was that polyaniline may act as “quasi-catalyst” for the irreversible redox reaction of Fe/Fe^{x+}, because the produced Fe^{x+} was transformed to iron oxide quickly. Therefore, very low polyaniline loading may be enough for efficient corrosion prevention on mild steel.

The interaction between EB salt and Fe was also studied, where EB salt (EB·HCl) was used instead of EB for above experiment. It should be noted that dedoping was necessary before the EB salt was subjected to UV-vis spectra. Figure 5 showed the time dependence of I_{330}/I_{630} of polyaniline. Only 10h was needed when I_{330}/I_{630} increased from 1.1 to 2.3. It quickly dropped to 1.4 in 50h, and then increased to 2.2 after 100h. The EB salt showed much faster oxidation change than EB, especially at the first 200h. Though not so regular as EB, the oxidation degree of EB salt also showed certain increase-decrease cycle with the time going. The irregular change of oxidation degree in EB salt indicated that interaction between EB salt and Fe was more complicated than that between EB and Fe. Though further study is necessary in the future to get more information on this subject, it is certain that both EB salt and EB have good corrosion protection behavior.

The oxide layer formed between EB/EPR coating and pure Fe layer was analyzed by XPS technique and shown in Figure 6. There are two different oxide layers, that closed to bare iron mainly consisted of Fe_3O_4 , whereas that closed to EB/EPR coating mainly consisted of Fe_2O_3 . Therefore, the oxide layer between

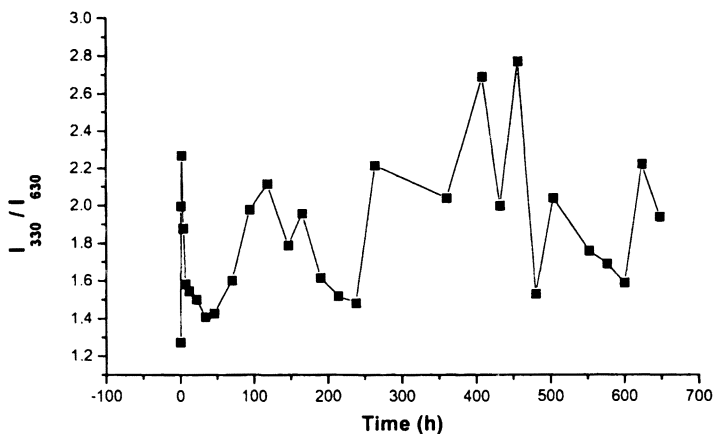


Figure 5. Dependence of I_{330}/I_{630} of polyaniline on reaction time when EB·HCl reacted with iron powder.

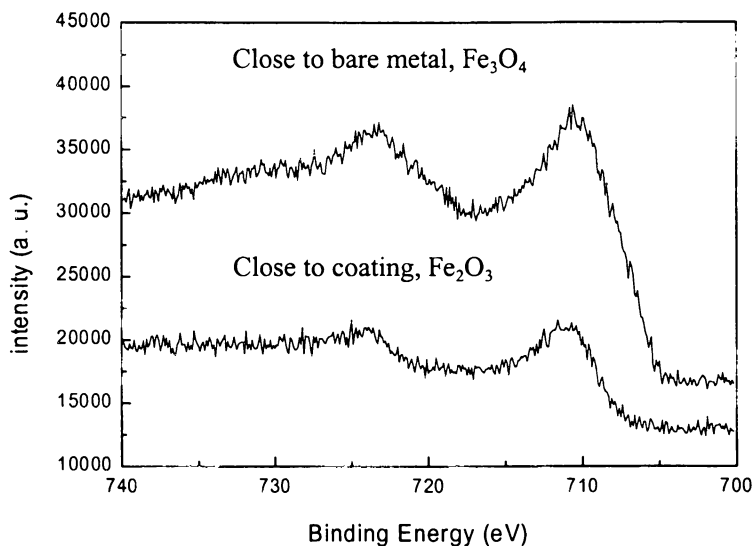


Figure 6. XPS spectra of oxide layer close to bare metal and coating layer.

EB/EPR coating and iron was mixture of iron oxide. This oxide layer was very dense as observed from surface SEM image, which was beneficial for good corrosion prevention performance.

Based on the above experiments and analyses, the interaction between iron and EB was summarized in Figure 7. Where EB was at first reduced by iron to lower oxidation degree of polyaniline (or even LEB), and iron was quickly oxidized to iron oxide (Fe^{2+}). The low oxidation degree of polyaniline was then oxidized by oxygen in the media. Therefore, the change of oxidation degree of polyaniline was somewhat “reversible”, whereas that of iron to iron oxide was irreversible. This difference led to the formation of the dense iron oxide layer, and polyaniline acted as “quasi-catalyst” for the oxidation reaction of iron. Since the redox reaction includes electron transfer process, EB salt may have much quick electron transfer speed than EB, leading to faster reversible change of oxidation for EB salt than for EB.

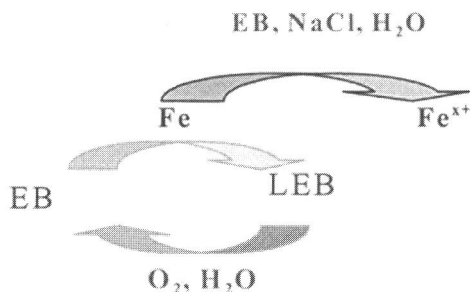


Figure 7. Interaction of iron and EB

Conclusions

A solvent free corrosion prevention coating was developed employing liquid polyamine as solvent for EB as well as hardener for epoxy resin. The corrosion prevention efficiency of EB/EPR coating was significantly improved even with a low EB loading. Equivalent circuit analysis of EIS spectra showed the existence of oxide layer resistance and oxide layer capacity in EB/EPR coating, whereas no such elements were found in pure EPR coating. When EB interacted with iron, a quasi-reversible change in oxidation degree of polyaniline was observed, giving good explanation why low EB loading in the EB/EPR coating showed good corrosion prevention property.

Acknowledgements

Financial support from Natural Science Foundation of China and Chinese Academy of Sciences was gratefully acknowledged.

References

1. Wessling, B. *Adv. Mater.* **1994**, *6*, 226.
2. Lu, W. K.;Elsenbaumer, R. L.; Wessling, B. *Synth. Met.* **1995**, *71*, 2163-2166.
3. McAndrew, T. P. *Trends in Poly. Sci.* **1997**, *5*, 7.
4. Fahlman, M.; Jasty, S.; Epstein, A. J. *Synth. Met.* **1997**, *85*, 1323-1326.
5. Wei, Y.; Wang, J. G.; Jia, X. R.;Yeh, J. M.; Spellane P. *Polymer* **1995**, *36*, 4535-4537.
6. Wei, Y.; Yeh, J. M.; Wang, J. G.; Jia, X. R.;Yang, C. C; Jin, D. L. *Pro. Am. Chem. Soc., Div. Polym. Mater. Sci.*, **1996**, *74*, 202-203.
7. Zhang, J. L.; Li, J.;Wang, X. H.; Jing, X. B.; Wang, F. S. *Chinese Pat. Appl. No.* 98116978.3,1998.
8. Wang, X. H.; Wang, Y. J.; Lu, J. L.; Li, J.; Jing, X. B.; Wang, F. S. *Polym. Prepr.* **2000**, *41(2)*, 1752.
9. Geng, Y. H.; Li, J.; Wang, X. H.; Jing, X. B.; Wang, F. S. *Chinese Pat. Appl. No.* 95108490.9, 1995.

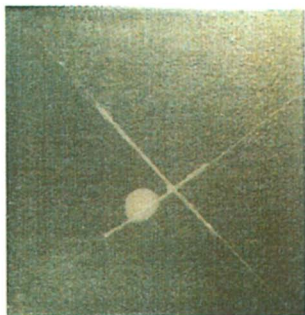


Plate 1. Panel 1. Pure epoxy coating on aluminum substrate.



Plate 2. Panel 2. Pure epoxy coating on aluminum substrate.



Plate 3. Panel 3. 3% BAMPPV/epoxy coating on aluminum substrate.



Plate 4. Panel 4. 3% BAMPPV/epoxy coating on aluminum substrate.

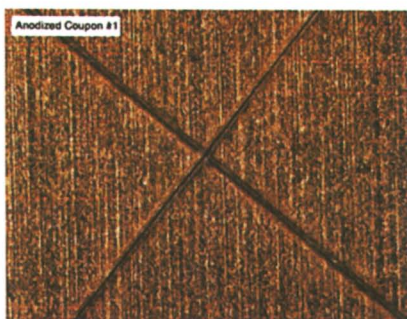


Plate 5. Panel 3. 40X magnification of the scribe lines in the 3% BAMPPV/ epoxy coating. (Reproduced from reference 12.)

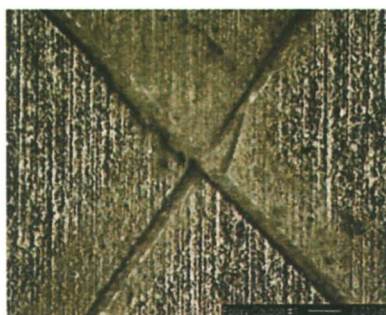


Plate 6. Panel 1. 40X magnification of the scribe lines in the 3% pure epoxy coating. (Reproduced from reference 12.)



Plate 7. Scribed polymer coated Al panel after 616 hours of exposure. (Reproduced from reference 12.)



Plate 8. Scribed conversion coated Al panel after 616 hours of exposure. (Reproduced from reference 12.)



Plate 9. Scribed polymer coated Al panel (1146 hours of exposure). (Reproduced from reference 12.)



Plate 10. Scribed conversion coated Al panel (1146 hours of exposure). (Reproduced from reference 12.)

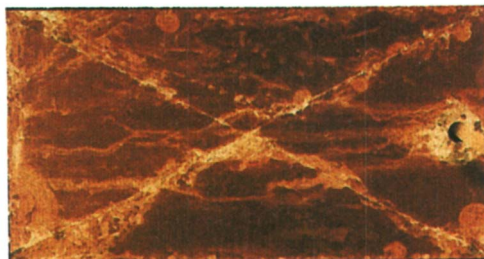


Plate 11. Scribed polymer coated Al panel (3000 hours of exposure). (Reproduced from reference 12.)



Plate 12. Scribed conversion coated Al panel (3000 hours of exposure). (Reproduced from reference 12.)

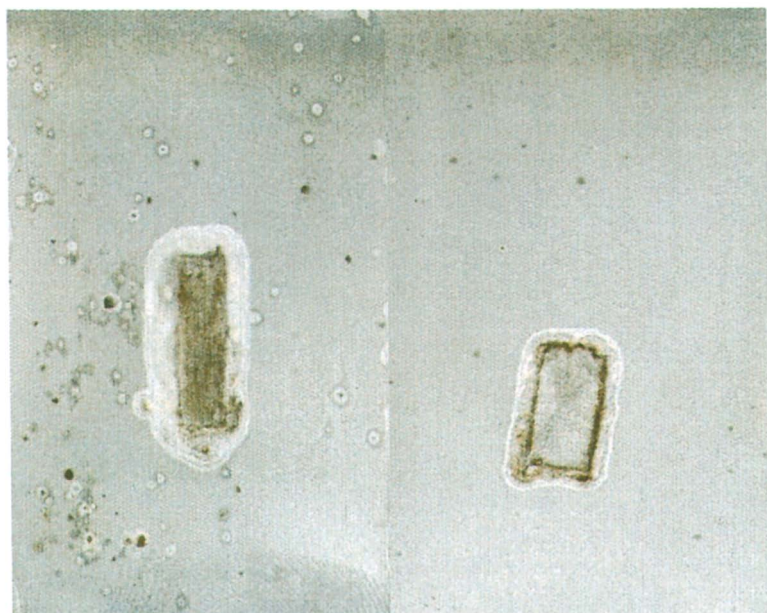


Plate 1. The retardation phenomenon of PCAT. The surface of steel plates were coated with the pure BP lacquer (right) and with the 5%-PCAT-lacquer (left).

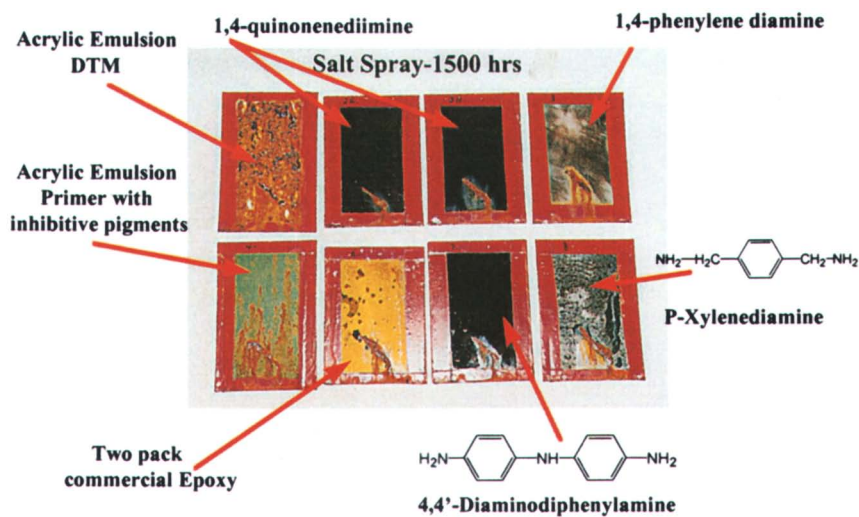


Plate 1. Condition of panels after 1500 hours of salt spray

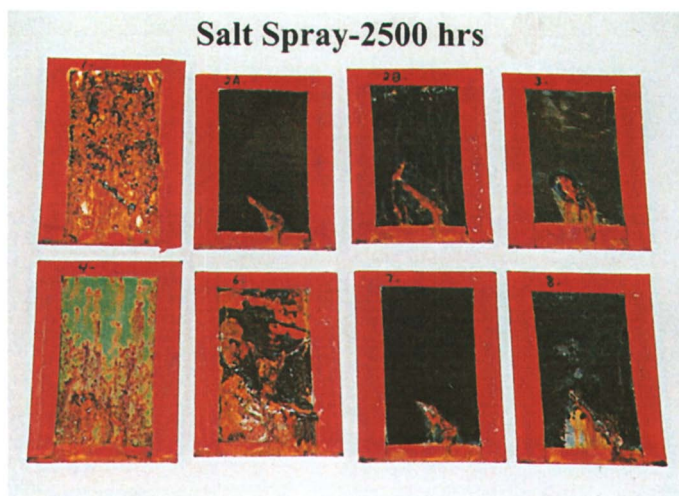


Plate 2. Condition of panels after 2500 hours of salt spray

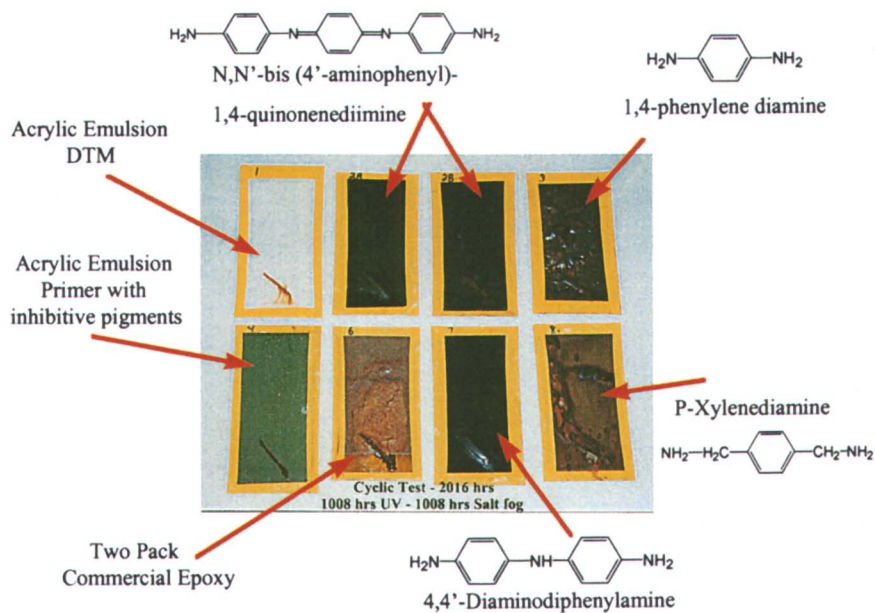


Plate 3 . Condition of panels after 2016 hours of cyclic test

Author Index

- Anderson, Nicole, 140
Benicewicz, Brian C., 18, 126
Berry, B. C., 182
Bie, Huimin, 175
Bierwagen, Gordon P., 228
Brédas, J. L., 76
Brown, R., 196
Chen, Liang, 156
Chen, Ru, 126
Cheng, Shan, 208
Crispin, X., 76
Dominis, Anton, 103
Duong, Thanh, 90
Epstein, A. J., 76
Fahlman, M., 76
Gelling, Victoria Johnston, 228
Guenther, Andrew, 140
Han, Mijeong, 175
He, Jie, 228
Helms, A. Brent, 168
Hu, Yongqi, 168
Irvin, David J., 140
Irvin, Jennifer A., 140
Jamasbi, Homayoun, 208
Jansen, Susan A., 90, 208
Jing, Xiabin, 254
Lazzaroni, R., 76
Li, Ji, 254
Li, Shuxi, 76, 208
Lin, Y., 196
Lu, Jinlong, 254
Mao, Huaping, 156
McClarnon, F., 196
Nikles, David E., 168, 175
Racicot, R., 196
Sein, Lawrence T., Jr., 90, 208
Shaikh, A. U., 182
Sharma, Rahul, 168
Smallfield, J. A. O., 76
Spinks, Geoffrey M., 103
Stenger-Smith, John D., 2, 140
Street, Shane C., 168
Tallman, Dennis E., 103, 228
Thompson, Karen Gebert, 18
Varnum, James M., 90
Viswanathan, T., 182
Wallace, Gordon G., 103, 228
Wang, Ce, 156, 208
Wang, Fosong, 254
Wang, Xianhong, 254
Warren, Garry W., 168, 175
Webber, Cindy, 140
Wei, Yen, 76, 90, 156, 208
Wessling, Bernhard, 34
Yang, Dehua, 168
Yang, S. C., 196
Yu, Youhai, 156
Zarras, Peter, 2, 140
Zhang, Wanjin, 156, 208

Subject Index

A

Acrylamide monomers. *See*

Oligoaniline side chains, polymers with

Acrylate monomers. *See* Oligoaniline side chains, polymers with

Adhesion

poly((*bis*-dialkylamino)phenylene vinylene) (BAM-PPV), 143, 149
study consideration, 20

Aluminum alloys

corrosion, 196

corrosion tests with coatings of inter-polymer complexes, 201–202

polypyrrole on, 106, 112–113, 116

See also Electroactive conducting polymers (ECPs); Inter-polymer complex

Amine–quinone polyimides

Bode plots, 180*f*

composition, 177*t*

corrosion studies, 179

impedance and phase angle as function of frequency, 180*f*

monomer synthesis, 176

structures, 177*f*

tensile properties, 178*t*

thermal and mechanical properties, 178–179

thermal properties, 178*t*

two-step polymerization, 176–178

Amine–quinone polyurethanes

protecting iron from corrosion, 176

synthesis, 168–169, 176

See also Sulfur–quinone polyurethanes

Amino-terminated aniline oligomers

anticorrosion performance, 223, 225

corrosion protection properties, 223

crosslinking agents, 209–210

synthesis, 210–211

See also Epoxy-cured aniline oligomers

Aniline oligomers

aniline capping phenylene diamine, 95

anticorrosion properties, 209

charge transfer agents

tetracyanoquinodimethane

(TCNQ) and tetracyanoethylene

(TCNE), 93

comparison of trimers and

corresponding form of polyaniline (PANI), 95*t*

complexes of aniline trimer, 96–97

computational approach, 93–94

computed ionization potentials and

electron affinities for substituted trimer compounds, 97*t*

conductivity, 91

conformational assessment of

representative trimers, 94*t*

corrosion inhibition, 100

density functional theory (DFT), 93–94

DFT calculations of frontier orbital

levels of charge transfer agents, 96

electronic spectra, 93

electron paramagnetic resonance, 93

emeraldine, 91, 92

emeraldine trimer and

tetrathiafulvalene (TTF), 96

energetics of alkyl substituted

emeraldine trimers, 100*t*

enthalpies of emeraldine base and

salts, 96*t*

experimental, 93–94

frontier energy/donor energy states
for substituted aniline trimers,
97*t*

frontier orbitals of charge transfer
agents and emeraldine trimer,
98*f*

interconversion between redox
forms, 91

leucoemeraldine, 91, 92

magnetic properties of trimers, 96

methods for preparation, 91

optical and electronic chromophore
of PANI, 95

pernigraniline, 91, 92

predicted UV-vis bands vs.
experiment, 101*t*

redox forms of trimer, 92

solid state and solution band gaps,
101

solvation effect, 100

solvent and conformational effects
for substituted trimeric anilines,
100–101

substitution of terminal aniline, 97,
100

synthesis, 93

synthesis methods, 157

trimer as electronic chromophore for
polyaniline, 94–96

UV-vis spectra data vs. DFT
calculations, 94–95

UV-vis spectra of trimeric
emeraldine and TCNE charge
transfer complex, 99*f*

zuirin, 156

See also Epoxy-cured aniline
oligomers; Phenyl-capped
tetraaniline (PCAT)

Anticorrosion

performance test, 159

phenyl-capped tetraaniline, 162,
164

scientific engineering for coatings,
49

B

Band gaps, comparing solid state and
solution, 101

Barrier coatings
corrosion prevention, 9
metal pretreatments, 9–10

Bode plots
amine–quinone polyimides, 180*f*
sulfur–quinone polyurethanes, 171*f*,
172*f*

C

Chemistry, 2000 Nobel Prize, 2

Chromate conversion
coatings, corrosion prevention, 9–10

Classes, electroactive polymers, 3

Climate cycling test (VDA), screening,
64

Composition, electroactive polymers,
3

Conducting polymers
background, 34–35
discovery of organic metal state in
dispersion, 35
polymeric electronics and photonics,
2–3
See also Inherently conducting
polymers (ICP)

Conductivity
aniline oligomers, 91
polymers, 2

Conjugated oligomers, oligoanilines,
127

Conjugation, electroactive polymers, 3

Copper
aging pretreated, vs. sulfuric acid
etched plates, 66–67
experimental, 66
formation of Cu oxide layers vs.
aging time, 68*f*
passivation, 66

- rate constants for CuO formation
with and without organic metal
treatment, 67*t*
- relationship between color and oxide
layer thickness, 67, 68*f*
- scanning electron microscopy (SEM)
image of copper oxidized by
annealing, 69*f*
- SEM image of golden
copper/polyaniline surface, 69*f*
- Corrosion**
aluminum alloys, 196
barrier coatings, 9–10
chromate conversion coatings, 9–10
classifying forms, 9
costs to U.S. economy, 183
definition, 8
difference between, and passivation,
47
environments, 8–9
metal pretreatments, 9–10
processes, 8–10
rusting iron, 9
under coating, 9
- Corrosion inhibition**
alkyl-substituted aniline trimers,
100
polyaniline, 184–185
See also Aniline oligomers;
Inherently conducting polymers
(ICP)
- Corrosion prevention.** *See* Solvent-
free polyaniline coating
- Corrosion protection**
electroactive conducting polymers
(ECPs), 249–251
electroactive polymers, 10–13
first work, 35–36
polyaniline, 126
reaction sequence, 39, 40*f*
See also Amine–quinone polyimides;
Epoxy-cured aniline oligomers;
Organic metal polyaniline; Sulfur–
quinone polyurethanes
- Corrosion-protective coatings**
additional environmental and
physical testing, 27–28
adhesion, 20
corrosion testing process, 21–22
doping polyaniline (PANI), 21
doping studies, 23, 24*t*
effect of additive concentration on
gelation, 28*f*
experimental, 19–22
gelation of PANI solutions, 26*f*
gelation of PANI solutions with
additives, 27*f*
gel permeation chromatography of
PANI, 22*t*
laboratory corrosion testing in
gas/liquid cells, 23, 26
laboratory corrosion testing in HCl
solutions, 25*f*
launch environment needs, 19
outdoor exposure, 28
PANI, 20–21
PANI film doping, 24*t*
PANI synthesis and characterization,
22–23
polymer selection, 19–20
polymers for initial screening, 20*f*
relationship between PANI
molecular weight and gel time, 26
seven months exposure, 29*f*
sixteen months exposure, 30*f*
spray coating, 26–27
twenty-eight months exposure, 31*f*
- Crosslinking.** *See* Epoxy-cured aniline
oligomers
- Crystalline nature, poly((bis-
dialkylamino)phenylene vinylene)
(BAM–PPV), 149**
- Curing.** *See* Epoxy-cured aniline
oligomers
- Cyclic tests**
comparing coatings by time to
failure, 224*f*
epoxy-cured aniline oligomers, 221,
222*t*, 223
panels after 2016 hours, 222

See also Epoxy-cured aniline oligomers

D

Density functional theory (DFT)

comparing UV-vis spectral data for aniline oligomers with DFT calculations, 94–95
interfacial interactions, 79
methods for aniline oligomers, 93–94

2,5-Diamino-1,4-

benzoquinone, corrosion protection, 175–176

4,5-Dihydroxy-1,3-benzenesulfonic acid disodium salt (Tiron®), dopant for polypyrrole, 112–113, 116

Dinonylnaphthalene sulfonic acid (DNNSA)

polyaniline on steel, 109–112
structure, 105

Dispersion

difficulties in paint, 197
discovery of organic metal state in, 35

Dopants

corrosion protection for PANI on steel, 116, 118*f*, 119
degree of doping and oxygen permeability, 119, 121
dinonylnaphthalene sulfonic acid (DNNSA), 105
nature of anion on rate of corrosion, 110, 112

Tiron® (4,5-dihydroxy-1,3-benzenedisulfonic acid disodium salt), 112–113, 116

See also Inherently conducting polymers (ICP)

Doping

electroactive polymers, 3
lignosulfonic acid-doped polyaniline, 12–13
polyaniline film, 23, 24*t*

process for polyaniline coating, 21
protonic acid, 5, 6*f*

E

Electroactive conducting polymers (ECPs)

coated aluminum alloys, 236
corrosion protection, 249–251
corrosion resistant coatings, 229
counterion effects in corrosion control, 242, 245
current density map and optical micrograph for PODP–PCPTS (counterions of perchlorate and paratoluene sulfonate with poly(3-octadecyl pyrrole)) on Al alloy for 12 hours immersion, 237*f*
current density map and optical micrograph for PODP–PCPTS on Al alloy for 13.5 hours immersion, 238*f*
current density map and optical micrograph for PODP–PCPTS on Al alloy for 50 hours immersion, 240*f*
current density map and optical micrograph for polyurethane coating on Al alloy at 6 hours immersion, 247*f*
current density map and optical micrograph for poly(3-octyl pyrrole) (POP) with PC (POP–PC) on Al alloy at 6 and 10.5 hours immersion, 244*f*
current density map and optical micrograph for POP–PCPTS coating with polyurethane topcoat on Al alloy at 6.5 days immersion, 248*f*
current density map and optical micrograph for POP–PTS on Al alloy at 5 minutes, 241*f*

- current density map and optical micrograph for POP-PTS on Al alloy at 76 hours immersion, 243*f*
- cyclic voltammograms of four ECPs, 245*f*
- Fermi energy of electrons, 249
- oxidants towards active metals, 250
- PODP-PCPTS, 236, 239
- POP on cold-rolled steel (CRS), 235–236
- POP-PC and POP-PTS, 239, 242, 245
- POP-PCPTS with polyurethane topcoat, 245–246
- preparation of POP polymers, 232–233
- previous scanning vibrating electrode technique (SVET) studies, 234–236
- reservoir for corrosion inhibiting ions, 250–251
- sample preparation, 232–233
- SVET measurements, 233–234
- See also* Local electrochemical techniques; Scanning vibrating electrode technique (SVET)
- Electroactive polymers (EAPs)
- applications, 3
- classes, 3
- composition, 3
- conjugation, 3
- corrosion protection with, 10–13
- doping process, 3
- lignosulfonic acid-doped polyaniline (ligno-PANI), 12–13
- mechanism of corrosion protection, 11
- PANI, 5, 6*f*
- PANI containing paints for corrosion protection, 10–11
- PANI-layered montmorillonite nanocomposite, 12
- pH dependence of PANI, 11–12
- poly(*bis*-dialkylamino)phenylene vinylene) (BAM-PPV), 12
- polymeric electronics and photonics, 2–3
- poly(3-methylthiophene), 12
- poly(phenylene vinylene) (PPV), 7–8
- polypyrrole, 7
- polypyrrole (PPy), 12
- polythiophene, 7
- processability, 18
- structures and conductivities, 4*t*
- syntheses, 5–8
- synthetic metals, 2
- usefulness, 3
- See also* Corrosion-protective coatings; Lignosulfonic acid-doped polyaniline (LIGNO-PANI™)
- Electroactive primer, water-borne, 199, 201
- Electrocatalytic deposition, polypyrrole, 106, 112–113, 116
- Electrochemical impedance spectroscopy (EIS)
- amine-quinone polyimides, 180*f*
- epoxy resin (EPR) and emeraldine base/EPR coatings, 255, 260*f*
- lignosulfonic acid-doped polyaniline, 186, 189–190
- poly(octyl pyrrole) on aluminum, 116, 117*f*
- predicting coating performance, 62–64
- sulfur-quinone polyurethanes, 170, 171*f*, 172*f*
- Electrochemical techniques. *See* Local electrochemical techniques
- Electron affinities, substituted trimer compounds, 97*t*
- Emeraldine
- energetics of alkyl substituted trimers, 100*t*
- enthalpies of base and salts, 96*t*
- frontier energy/donor energy states for substituted aniline trimers, 97*t*
- predicted UV-vis bands for substituted, 101*t*

- redox form of aniline trimer, 91, 92
- Emeraldine base**
 alternative to emeraldine salt, 183
 polyaniline (PANI), 5, 6*f*
 solvents, 255
See also Solvent-free polyaniline coating
- Emeraldine salt, polyaniline (PANI),**
 5, 6*f*
- Energetics, alkyl substituted**
 emeraldine trimers, 100*t*
- Energy of activation, conformational**
 assessment of aniline trimers, 94*t*
- Ennobling**
 conducting polymer layer, 104
 organic metal, 36, 39
- Enthalpies, emeraldine base and salts,**
 96*t*
- Environmental testing, poly((bis-dialkylamino)phenylene vinylene) (BAM-PPV) films,** 149–150
- Environments, corrosion,** 8–9
- Epoxy-cured aniline oligomers**
 comparison of coatings by time in cyclic test before failure, 224*f*
 comparison of coatings by time in salt spray before failure, 220*f*
 compounds for study, 212
 crosslinking procedure, 212
 cyclic test, 221, 223
 cyclic test results after 2016 hours, 222*t*
 experimental, 210–213, 216
 ingredients in formulations, 214*t*, 215*t*
 panels after 1500 hours salt spray, 217
 panels after 2016 hours of cyclic test, 222
 panels after 2500 hours salt spray, 217
 preparation of coating systems, 211–213
 preparation of substrate and coatings, 213, 216
- salt spray, 216, 219, 221
 salt spray results after 1500 hours exposure, 218*t*
 salt spray results after 2500 hours exposure, 218*t*
 sample matrix and identification, 213*t*
 synthesis of amino-terminated aniline trimer, 211
 synthesis of aniline oligomers, 210–211
- Epoxy resin (EPR)**
 corrosion prevention of emeraldine base (EB)/EPR coating, 257–261
 preparation of EB/EPR, 256–257
 surface morphology of EB/EPR, 258–259
See also Solvent-free polyaniline coating
- Equivalent circuits, epoxy resin (EPR) and emeraldine base/EPR coatings,** 261, 262*f*
- F**
- Fermi energy, electrons, 249
- Filiform corrosion test, inter-polymer complex of polyaniline, 202, 204*f*, 205*f*
- Film formation, processability, 106–107, 109
- Formulation, optimal polyaniline, 48
- G**
- Gas permeation rate (GPR), oxygen, 119, 120*t*
- Gelation**
 effect of additive concentration, 28*f*
 polyaniline molecular weight and, 26
 polyaniline solutions, 26*f*

polyaniline solutions with additive,
27*f*
Gilch polymerization, 146

H

Hydrochloric acid
doping polyaniline, 198
launch environment coating needs,
19
See also Inter-polymer complex

I

Immersion testing
inter-polymer complex of
polyaniline, 202, 203*f*
poly(*bis*-dialkylamino)phenylene
vinylene) (BAM-PPV), 143, 149–
150
Inherently conducting polymers (ICP)
atomic force micrographs of Al
2024-T3 alloy and polypyrrole
films on alloy, 114*f*, 115*f*
concentration of soluble iron in test
solution after immersion for
polyaniline/polyurethane
(PANI/PU) coated steels, 111*f*
concentration of soluble iron in test
solutions after immersion for plain
carbon steel (PCS) coupled to
PANI-emeraldine salt (ES),
111*f*
differences between galvanically
coupled PANI-ES and PCS, 110
dinonylnaphthalene sulfonic acid
(DNNSA) dopant, 105
dopant, 104
dopant dependence of polyaniline
solubility, 106
dopant effects, 116, 119, 121
dopant incorporation into
polyaniline, 106

effect of counterion on tensile
strength, potassium ion flux rate,
and conductivity of membranes,
120*t*
effect of degree of doping on oxygen
permeability, 119, 121
effect of dopant on contact angle of
polypyrroles, 107, 108*t*
effect of dopant on corrosion
protection for PANI.DNNSA,
109–110
electrocatalytic deposition of
polypyrrole, 106
electrochemical impedance
spectroscopy (EIS) for poly(octyl
pyrrole) coatings on Al, 117*f*
ennobling underlying metal,
104
examples, 104
experimental, 105–106
film formation—processibility, 106–
107, 109
full immersion testing, 105–106
gas permeation rate for oxygen, 119,
120*t*
nature of dopant anion and rate of
corrosion, 110, 112
NO₃⁻ use as dopant, 107, 109
oxidation of metal, 118*f*
polyanilines on steel, 109–112
polypyrrole on aluminum alloy 2024-
T3, 112–116
preparation of de-protonation and re-
protonation solutions, 105
proposed mechanism of corrosion
protection by polyaniline coatings
at pinholes, 118*f*
reagents and standard solutions,
105
role of dopant in polymer solubility,
107
schematic of galvanic coupling of
plain carbon steel (PCS) to PANI,
108*f*
structures, 104

- Tiron® (4,5-dihydroxy-1,3-benzenedisulfonic acid) dopant, 112–113, 116
- ways of providing protection, 104
- Interfaces. *See* Iron–polyaniline interfaces
- Inter-polymer complex
- conductive state in marine environment, 198–199
 - filiform corrosion test, 202, 204*f*, 205*f*
 - immersion in sea water, 202, 203*f*
 - polyaniline and poly acid, 197–198, 200*f*
 - salt fog spray test, 201, 203*f*
 - synthesis, 197–198
 - titration curves, 200*f*
 - water-borne electroactive primer, 199, 201
- Iodine, polyacetylene (PA), 34
- Iodine-doped polyacetylene, conductivity, 2
- Ionization potentials, substituted trimer compounds, 97*t*
- Iron
- interaction of polyaniline and iron, 261, 263–265, 266*f*
 - rusting, 9
 - See also* Solvent-free polyaniline coating
- Iron–polyaniline interfaces
- C(*1s*) core level spectrum at low coverage, 82
 - C(*1s*) shake up spectra of thin films, 84–85
 - calculated bond formation energies, 85–86
 - deconvolution of N(*1s*) core level, 78, 84*f*
 - density functional theory (DFT), 79
 - DFT calculations supporting experimental, 85–86
 - DMol program, 79
 - evolution of Fe(*2p*) core level spectra, 82, 83*f*
 - experimental methodology, 77–78
 - extended coverage of Fe on trimer, 83–84
 - Fe *2p* core level evolution during early stages, 80
 - Fermi–Dirac distribution, 80
 - geometrical structures of emeraldine base (EB) and three-ring model molecule of EB (trimer), 78*f*
 - iron peak at low and high levels of coverage, 81
 - N(*1s*) core at high iron coverage, 82
 - N(*1s*) core at low levels of iron coverage, 81–82
 - N(*1s*) core level spectra of pristine EB and EB at high Fe coverage, 81*f*
 - optimized structures of complexes, 86*f*
 - partial electron transfer from iron atoms, 86–87
 - self-consistent field (SCF) procedure, 79
 - steel/EB interface study by sputter-depositing atoms, 80
 - theoretical methodology, 78–80
 - X-ray photoelectron spectroscopy (XPS), 77–78
- Iron protection. *See* Amine–quinone polyimides; Sulfur–quinone polyurethanes
- J**
- John F. Kennedy Space Center (KSC), electroactive polymers for corrosion prevention, 10
- K**
- Kraft process, lignosulfonate, 183–184

L

- Launch environment, Space Shuttle, 19
- Leucoemeraldine
 polyaniline (PANI), 5, 6*f*
 redox form of aniline trimer, 9*i*, 92
- Lignosulfonate
 functionality, 184
 Kraft process, 183–184
 lignin monomer unit after
 sulfomethylation via Kraft, 184*f*
- Lignosulfonic acid polyaniline,
 doping, 12–13
- Lignosulfonic acid-doped polyaniline
 (LIGNO-PANI™)
 coating failure, 190–191
 coating preparation, 185–186
 correction behavior, 190
 cyclic voltammogram of, in water by
 pH, 187*f*
 dispersion, 187
 electrochemical impedance
 spectroscopy (EIS), 186, 189
 electrochemical studies, 186
 experimental, 185–186
 experiments on aluminum, 191–192
 impedance, 190
 inhibition by passivating metal, 187*f*,
 188
 leaching, 190–191
 Nyquist plot for, in water-reducible
 acrylic coating, 190*f*
 Nyquist plot using EIS for coatings,
 189*f*
 preparation, 185
 salt fog studies, 186
 salt fog tests, 192–193
 Tafel plots, 188–189, 191, 192*f*
 water based-acrylic coating with,
 188*f*
- Local electrochemical impedance
 mapping (LEIM), 231–232
- Local electrochemical impedance
 spectroscopy (LEIS), 231–232

- Local electrochemical techniques
 approaches to measuring local
 potential gradient, 231
 local electrochemical impedance
 mapping (LEIM), 231–232
 local electrochemical impedance
 spectroscopy (LEIS), 231–232
 local potential gradient, 230
 measurements of local current,
 230
 measuring sample surface, 230
 scanning vibrating electrode
 technique (SVET), 232
See also Electroactive conducting
 polymers (ECPs)
- Local potential gradient, 230
 approaches to measuring, 231
 equation, 230
- Los Alamos National Laboratory
 (LANL), electroactive polymers for
 corrosion prevention, 10

M

- Magnetic properties, aniline trimers,
 96
- Marine environment, stability of inter-
 polymer complex, 198–199
- Mechanism
 corrosion protection using
 electroactive polymers, 11
 passivation effect, 10–11
 polyaniline protection of steel,
 11
- Metals, conversion to corrosion
 product, 9
- Methacrylamide monomers. *See*
 Oligoaniline side chains, polymers
 with
- Methacrylate monomers. *See*
 Oligoaniline side chains, polymers
 with
- Michael addition, monomers for
 amine–quinone polyimides, 176

N

Nanocomposite, polyaniline-layered montmorillonite, 12

Neutral salt fog test, poly(*bis*-dialkylamino)phenylene vinylene (BAM-PPV), 143, 150

Nobel Prize in Chemistry, 2000, 2

Nyquist plots

epoxy resin (EPR) and emeraldine base/EPR coatings, 259, 260*f*

lignosulfonic acid-doped polyaniline in water-reducible acrylic coating, 190*f*

using electrochemical impedance spectroscopy for coatings, 189*f*

O

Oligoaniline side chains, polymers with

4-(4'-aminophenylamino) diphenylamine, 129

aniline tetramer synthesis, 133

N-(4-anilinophenyl)-acrylamide, 131

4-anilinophenyl acrylate, 131

N-(4-anilinophenyl)-methacrylamide, 131

4-anilinophenyl methacrylate, 131
chemical structures of monomers, 128*f*

conjugated oligomers, 127

experimental, 128–132

homopolymers of oligomeric monomers, 128

materials and instruments, 128–129

monomer syntheses methods, 131–132

monomer synthesis, 134, 135

oligoaniline syntheses methods, 129–131

oligomer synthesis, 132–134

4-[[4-(phenylamino)phenyl]amino]-phenol, 129

polymer characterization, 136–137

polymer synthesis, 134, 136

polymer synthesis method, 132

properties of polymers, 138*t*

schematic of structure, 127*f*

Ullmann condensation, 132–133

UV-vis spectra of polymer M5, 138*f*

Open circuit potential measurement

3D plots of potential development in scratch and under coating, 53*f*, 54*f*

climate cycling test (VDA)/salt spray test, 64

development of deep "W" corrosion potential valley in coating system, 56*f*, 57*f*, 58*f*

development of shallow "w" potential distribution at elevated level in best coating system, 59*f*, 60*f*, 61*f*

electrochemical impedance spectroscopy (EIS), 62–64

function principle of, using Kelvin probe, 52*f*

Ormecon scratch test, 49–50

panel after 300 hours immersion, 51*f*

progress, 64–66

scanning Kelvin potential (SKP) results for coating systems, 55*t*

scanning Volta potential measurements (Kelvin probe), 50, 55, 62

Organic metal polyaniline

aging of pretreated copper vs.

sulfuric acid etched plates, 66–67

corrosion current density-potential curves of metal and polyaniline (PANI) coated, 37*f*

development of primers with new strategy, 48–49

difference between corrosion and passivation, 47

discovery of, state in dispersion, 35

ennobling and passivation, 36, 39

evaluation of passive oxide formation process, 39, 47
 experimental, 66
 formation of Cu oxide layers vs. aging time, 68*f*
 optimal formulation, 48
 passivation of copper, 66
 rate constants for CuO formation with and without, 67*t*
 reaction sequence for passivation and corrosion protection, 39, 40*f*
 relationship between color and oxide layer thickness, 67, 68*f*
 scanning electron micrograph (SEM) image of copper oxidized by annealing, 69*f*
 scientific engineering, 49
 SEM image of golden copper/PANI surface after 2h, 68*f*, 69*f*
 spectral change of PANI on PP film without iron, 45*f*, 46*f*
 spectral change of PANI on PP film with suspended iron (back reaction), 43*f*, 44*f*
 spectral change of PANI on PP film with suspended iron (reduction), 41*f*, 42*f*
 XPS analysis of passive iron oxide layers, 38*f*
See also Open circuit potential measurement
 Ormecon scratch test, open circuit potential, 49–50, 51*f*
 Outdoor exposure
 corrosion-protective coatings, 28
 seven months, 29*f*
 sixteen months, 30*f*
 twenty-eight months, 31*f*
 Oxidation states, polyaniline (PANI), 5, 6*f*
 Oxygen permeability
 degree of doping, 119, 121
 gas permeation rate, 119, 120*t*

P

Paratoluene sulfonate
 poly(octyldecyl pyrrole) with perchlorate and, 236, 239
 poly(octyl pyrrole) with, 232, 239, 242, 245
 Passivation
 copper, 66
 difference between corrosion and, 47
 organic metal, 36, 39
 reaction sequence, 39, 40*f*
 Passivation effect, dispersed polyaniline, 10–11
 Passive oxide formation
 evaluation of process, 39, 47
 spectral change of PANI (polyaniline) on polypropylene (PP) film with suspended iron, 41*f*, 42*f*
 spectral change of PANI on PP film without iron, 45*f*, 46*f*
 spectral change of PANI on PP film with suspended iron (back reaction), 43*f*, 44*f*
 Perchlorate
 poly(octyl pyrrole) with, 232, 239, 242, 245
 poly(octyldecyl pyrrole) with paratoluene sulfonate and, 236, 239
 Pernigraniline
 polyaniline (PANI), 5, 6*f*
 redox form of aniline trimer, 91, 92
 Phenyl-capped tetraaniline (PCAT)
 anticorrosive performance of coating with, 162, 164
 formation, 159–161
 instrumentation, 158
 mass spectrum of, by pseudo-high-dilution technique, 162*f*
 mass spectrum of, from *p*-phenylenediamine and diphenylamine, 161*f*

- materials, 157–158
- phenomenon of removing rust, 164*f*
- phenomenon of throwing power, 163*f*
- possible formation mechanism, 161
- preparation of PCAT, 158–159
- preparation of Schiff-base a, 158
- pseudo-high-dilution technique, 159, 161, 164
- retardation phenomenon, 163
- schematic of synthesis, 160
- synthesis, 158–159
- synthetic methods, 156–157
- test of anticorrosion performance, 159
- Plain carbon steel (PCS)
 - PANI-dopant coating system protecting, 109–110
 - schematic of galvanic coupling of, to polyaniline, 108*f*
 - See also* Inherently conducting polymers (ICP)
- Poly(3,4-ethylenedioxythiophene) (PEDOT), structure and conductivity, 4*t*
- Poly(3-alkylthiophene)s, synthesis, 7
- Poly(3-methylthiophene), corrosion studies, 12
- Polyacetylene (PA)
 - conductivity of iodine-doped, 2
 - discovery of organic metal state in dispersion, 35
 - first dispersion, 34–35
 - polyheterocycles, 5
 - reaction of iodine with, 34
 - structure and conductivity, 4*t*
- Polyaniline (PANI)
 - additives as chain initiators, 209
 - advantages, 5
 - applications, 126
 - corrosion inhibition, 184–185
 - corrosion prevention study, 10
 - development of primers with new strategy, 48–49
 - dopant dependence of solubility, 106
 - doping, 3
 - doping procedure, 21
 - doping studies, 23, 24*t*
 - environmental and physical testing, 27–28
 - exposure to HCl solution, 24, 25*f*
 - film doping, 24*t*
 - film formation—processability, 106–107, 109
 - first dispersed PANI, 35–36
 - four forms, 6*f*
 - gelation, 26–27
 - gel permeation chromatography (GPC), 22*t*
 - inter-polymer complex, 197–198, 200*f*
 - laboratory corrosion testing, 23, 26
 - lignosulfonic acid-doped, 12–13
 - mechanism for steel protection, 11
 - molecular weight and gelation, 26–27
 - montmorillonite nanocomposite, 12
 - optimal formulation, 48
 - outdoor testing, 126–127
 - PANI on steel, 109–112
 - pH dependence, 11–12
 - polyheterocycles, 5
 - preparation, 5, 20
 - processability, 127, 183
 - processing difficulties, 91
 - protonic acid doping, 6*f*
 - retarding carbon steel corrosion, 11
 - schematic of galvanic coupling to plain carbon steel, 108*f*
 - solubility, 91
 - spray coating, 26–27
 - structure, 20*f*
 - synthesis and characterization, 22–23
 - thermal and chemical stability of conventional, 196–197
 - trimer as electronic chromophore for, 94–96
 - See also* Aniline oligomers; Corrosion-protective coatings; Epoxy-cured aniline oligomers;

- Inherently conducting polymers (ICP); Inter-polymer complex; Iron-polyaniline interfaces; Lignosulfonic acid-doped polyaniline (LIGNO-PANI™); Oligoaniline side chains, polymers with; Organic metal polyaniline; Phenyl-capped tetraaniline (PCAT); Solvent-free polyaniline coating
- Poly(*bis*-dialkylamino)phenylene vinylene (BAM-PPV)
 adhesion testing, 143, 149
 alternate synthetic routes, 146
 characterization of BAMPPV polymers, 147–149
 chromate conversion coated panels, 150, 152, 153
 differential scanning calorimetry (DSC) heating curves, 148*f*
 epoxy only panels, 151
 experimental, 141, 143
 immersion testing, 143, 149–150
 improved synthesis of BAMPPV, 143–145
 magnification of scribe lines on panels, 151
 materials and methods, 141, 143
 neutral salt fog test, 143, 150, 152, 153
 optimization of literature method, 145–146
 panels with BAMPPV/epoxy coating, 151
 polymerization, 145
 retarding corrosion, 12
 scribed panels after salt-fog exposure, 152, 153
 semicrystalline nature, 149
 synthetic strategies, 141, 142
 thermal and physical analysis, 147
 weight loss vs. temperature curve, 147*f*
- Polymers, conductivity, 2
- Poly(octyl pyrrole)
 electrochemical impedance spectroscopy (EIS) of, on Al, 116, 117*f*
 sample preparation, 232–233
 scanning vibrating electrode technique (SVET) of, with perchlorate and *p*-toluene sulfonate, 239, 242, 245
- Poly(octyldecyl pyrrole)
 sample preparation, 232–233
 scanning vibrating electrode technique (SVET) of, with perchlorate and *p*-toluene sulfonate, 236, 239
- Poly(*para*-phenylene) (PPP)
 polyheterocycles, 5
 structure and conductivity, 4*t*
- Poly(*para*-phenylene vinylene) (PPV)
 polyheterocycles, 5
 structure and conductivity, 4*t*
- Poly(phenylene vinylene) (PPV)
 poly(*bis*-dialkylamino)phenylene vinylene (BAM-PPV), 12
 precursor route, 8
 synthesis, 7–8
- Poly(pyrrole) (PPy)
 atomic force micrographs of Al 2024-T3 and PPy on alloy, 114*f*, 115*f*
 corrosion studies, 12
 dopant Tiron® (4,5-dihydroxy-1,3-benzenedisulfonic acid disodium salt), 112–113, 116
 doping, 7
 effect of counterion on tensile strength, potassium ion flux rate, and conductivity of membranes, 120*t*
 electrocatalytic deposition, 106
 electrochemical impedance spectroscopy (EIS) for poly(octyl pyrrole) on aluminum, 117*f*
 long term corrosion experiments on Al, 116
 poly(3-octyl pyrrole), 12

PPy on Al alloy 2024-T3, 112–116
 preparation, 7
 structure and conductivity, 4*t*
 substrate material influencing surface properties, 109
See also Inherently conducting polymers (ICP)

Poly(thiophene) (PT)
 corrosion studies, 12
 doping, 7
 poly(3-methylthiophene), 12
 polyheterocycles, 5
 preparation, 7
 structure and conductivity, 4*t*
 structures of substituted, 20*f*
See also Inherently conducting polymers (ICP)

Polyurethanes
 poly(octyl pyrrole) and counterions with, topcoat, 245–246
See also Sulfur–quinone polyurethanes

Pretreatments, extending barrier coatings, 9–10

Processability
 electroactive polymers, 18
 film formation, 106–107, 109
 polyaniline, 127, 183

Processing, polyaniline, 91

Protonic acid doping, polyaniline, 5, 6*f*

Pseudo-high-dilution technique
 mass spectrum of PCAT by, 162*f*
 phenyl-capped tetraaniline (PCAT), 159, 161, 164

Pyrrole, heterocyclic monomer, 7

R

Reflectance infrared, sulfur–quinone polyurethanes, 170, 173*f*

Removing rust. phenyl-capped tetraaniline, 164

Retardation, phenyl-capped tetraaniline, 162, 163

Rust
 composition, 47
 removing, by phenyl-capped tetraaniline, 164

Rusting iron, 9

S

Salt fog studies
 inter-polymer complex of polyaniline, 201, 203*f*
 lignosulfonic acid-doped polyaniline, 186, 192–193

Salt fog test, poly(*bis*-dialkylamino)phenylene vinylene (BAM–PPV), 143, 150

Salt spray
 comparing coating systems by time before failure, 220*f*
 epoxy-cured aniline oligomers, 216, 218*t*, 219, 221
 panels after 1500 hours, 217
 panels after 2500 hours, 217
See also Epoxy-cured aniline oligomers

Scanning Kelvin potential (SKP)
 function principle, 52*f*
 scientific engineering, 49
 SKP results for various coatings, 55*t*
 Volta potential with Kelvin sensor, 50
See also Open circuit potential measurement

Scanning vibrating electrode technique (SVET)
 early studies of electroactive conducting polymers (ECPs), 234–236
 local electrochemical technique, 232
 measurements, 233–234
 poly(3-octyl pyrrole) (POP) with perchlorate (PC) and POP with

- paratoluene sulfonate (PTS), 239, 242, 245
- poly(3-octyldecyl pyrrole) (PODP) with PC and PTS, 236, 239
- Scanning Volta potential measurements, open circuit potential, 50, 55, 62
- Scientific engineering anti-corrosion coatings, 49
- climate cycling test, 64
- electrochemical impedance spectroscopy (EIS), 62–64
- Ormecon scratch test, 49–50
- scanning Volta potential measurements, 50, 55, 62
- Self-consistent field (SCF), interfacial interactions, 79–80
- Semicrystalline nature, poly(*bis*-dialkylamino)phenylene vinylene) (BAM–PPV), 149
- Side chains. *See* Oligoaniline side chains, polymers with
- Solubility, polyaniline, 91
- Solvation, frontier levels in solution, 100
- Solvent-free polyaniline coating corrosion parameters of emeraldine base (EB)/epoxy resin (EPR) coated mild steel in NaCl and HCl solutions, 258*t*
- corrosion prevention of EB/EPR coating, 257–261
- dependence of relative intensity of absorption bands of 330 to 630 nm (I_{330}/I_{630}) of polyaniline on reaction time, 264*f*
- EB preparation, 255
- equivalent circuits of EPR and EB/EPR coated mild steel in HCl solution, 261, 262*f*
- experimental, 255–256
- interaction of EB salt and iron, 264
- interaction of polyaniline and iron, 261, 263–265, 266*f*
- intrinsic viscosity of EB for different storage time, 257*t*
- liquid organic polyamine tetraethylene pentaamine (TEPA), 255–256
- Nyquist plots of EPR and EB/EPR coating, 259, 260*f*
- oxide layer analysis by X-ray photoelectron spectroscopy (XPS), 264–265
- preparation of EB/TEPA and EB/EPA coating, 256–257
- scanning electron micrograph (SEM) images of EPR and EB/EPR surfaces, 259*f*
- semicircle radius in high and low frequency zone from Nyquist plots, 259, 261
- surface morphology of EB/EPR, 258–259
- time dependence of I_{330}/I_{630} in UV-vis spectra, 263*f*
- Solvents, emeraldine base, 255
- Space Shuttle, launch environment, 19
- Space Transportation System Orbiter, launch environment, 19
- Stability inter-polymer complex in marine environment, 198–199
- thermal and chemical, of conventional polyaniline, 196–197
- Steel electroactive polymers for corrosion prevention, 10–11
- See also* Inherently conducting polymers (ICP)
- Sulfur–quinone polyurethanes amine–quinone polyurethanes, 168–169
- Bode plots, 171*f*, 172*f*
- electrochemical impedance spectroscopy (EIS), 169
- experimental, 169–170
- functional groups confounding X-ray photoelectron spectra, 170, 172*f*

- grazing incidence reflectance
infrared spectra, 170, 173*f*
impedance and phase angle as
function of frequency, 171*f*, 172*f*
investigating corrosion inhibition for
iron, 170
materials, 169
replacing amine with thioether group,
169
surface spectroscopy, 169–170
X-ray photoelectron spectroscopy
(XPS), 172*f*
Synthetic metals, development, 2
- T**
- Tetraaniline. *See* Phenyl-capped
tetraaniline (PCAT)
Tetracyanoethylene (TCNE)
charge transfer agent, 93
density functional theory (DFT)
calculations, 96–97
frontier orbital levels, 98*f*
UV-vis spectra of trimeric
emeraldine and TCNE charge
transfer complex, 99*f*
Tetracyanoquinodimethane (TCNQ)
charge transfer agent, 93
density functional theory (DFT)
calculations, 96–97
frontier orbital levels, 98*f*
Tetraethylene pentaamine (TEPA).
See Solvent-free polyaniline coating
Tetrathiafulvalene (TTF)
emeraldine trimer and, 96
frontier orbital levels, 98*f*
negative carriers, 91
Theoretical modeling, interfacial
interactions, 78–80
Thiophenes, heterocyclic monomer, 7
Throwing power, phenyl-capped
tetraaniline, 163*f*, 164
- p*-Toluene sulfonate
poly(octyl pyrrole) with, 232, 239,
242, 245
poly(octyldecyl pyrrole) with
perchlorate and, 236, 239
Trimers. *See* Aniline oligomers
- U**
- Under coating corrosion, organic
coatings, 9
- V**
- Volta potential, Kelvin sensor, 50, 55,
62
- W**
- Water-borne electroactive primer,
inter-polymer complexes, 199, 201
- X**
- X-ray photoelectron spectroscopy
(XPS)
sulfur-quinone polyurethanes, 170,
172*f*
See also Iron–polyaniline interfaces
- Z**
- Zuirin
first oligoaniline, 156
See also Phenyl-capped tetraaniline
(PCAT)